

Role of Ribosomal RNA Methyltransferase NSUN5 in Glioblastoma

by

Jiesi Zhou

A thesis submitted in partial fulfillment of the requirements for the degree of

Doctor of Philosophy

in

Cancer Sciences

Department of Oncology  
University of Alberta

© Jiesi Zhou, 2022

## Abstract

### Background:

Glioblastoma is the most common and aggressive malignant primary brain tumor. Despite aggressive standard treatment including surgery, radiation and chemotherapy, the median overall survival for patients with glioblastoma is only about 14 to 16 months. Using a glioblastoma TCGA dataset from 2013, we found that high *NSUN5* mRNA expression is strongly associated with poor survival in glioblastoma patients. *NSUN5* is a member of the Nop1/Nop2/Sun (*NSUN*) family of methyltransferases. It was first characterized in yeast where it was found to methylate 25S ribosomal RNA (rRNA). Moreover, *NSUN5* functions to modulate protein synthesis in yeast, as its deletion leads to alterations in the rRNA structure, consequently leading to the favoured translation of oxidative response mRNAs. However, the function of *NSUN5* in humans, as well as its role in cancer remains obscure. Since protein synthesis is a major mechanism by which cancer cells adapt to their environment and enhance their proliferation and survival, elevated *NSUN5* expression and the consequent rRNA methylation could alter the structure and/or activity of ribosomes to modulate the proteome and to drive tumorigenic phenotypes in glioblastoma.

### Hypothesis and objectives:

Our hypothesis is that elevated *NSUN5* alters the structure and/or activity of ribosomes by regulating the pattern of rRNA methylation, which leads to pro-tumorigenic translational reprogramming thereby promoting glioblastoma progression. We will address our hypothesis by: (1) investigating whether *NSUN5* methylates rRNAs, (2) determining whether *NSUN5* regulates protein synthesis in glioblastoma cells, (3) determining the functional role of *NSUN5* in glioblastoma, and (4) characterizing the *NSUN5*-regulated proteome in glioblastoma cells.

**Results:**

In this study, we demonstrate that: (1) NSUN5 indeed methylates cytosine 3782 of human 28S rRNA; (2) NSUN5 regulates protein synthesis in glioblastoma cells; and (3) NSUN5 promotes the tumorigenic phenotypes of glioblastoma *in vitro* and *in vivo*. In Chapter 3, we demonstrate that NSUN5 is expressed in glioblastoma cells and patient tissues and that NSUN5 methylates cytosine 3782 of human 28S rRNA. Furthermore, we identify cysteines 308 and 359 as the key cysteines required for RNA methyltransferase activity of NSUN5. In Chapter 4, we show that NSUN5 promotes proliferation, sphere formation, resistance to temozolomide, and tumor formation/progression of glioblastoma cells in mice. In Chapter 5, we demonstrate that NSUN5 promotes protein synthesis and regulates the proteome of glioblastoma cells, modulating the expression of STAT3 and NSUN2.

**Significance:**

In this study, we determine that NSUN5 plays a pro-tumorigenic role in glioblastoma. Since RNA methyltransferases have been shown to be readily targetable, our study suggests that NSUN5 is a potential novel therapeutic target for glioblastoma. Moreover, this project will help us to determine whether rRNA cytosine modification regulates translation, and whether it favors the translation of cancer-associated genes in glioblastoma.

**Keywords:**

Glioblastoma, glioblastoma stem cells, NSUN5, NSUN proteins, rRNA cytosine methyltransferase, C3782, 28S rRNA, ribosome biogenesis, ribosomal control in cancer, translational control in cancer, STAT3, NSUN2

## Preface

This project was supervised by Dr. YangXin Fu and co-supervised by Dr. Roseline Godbout and Dr. Lynne Postovit. This project was conducted mainly by Jiesi Zhou with the assistance of people noted below. A manuscript by Zhou et al., which is mainly based on this thesis, entitled “RNA cytosine methyltransferase NSUN5 promotes protein synthesis and tumorigenic phenotypes in glioblastoma” has been submitted for publication. I am the co-first author of the paper.

Jiesi Zhou conducted the cell culture, RNA extraction, cDNA synthesis, quantitative real-time PCR, protein extraction, Western blotting, DNA extraction, plasmid extraction, regular and viral plasmid transfections, the generation of new cell lines (overexpression, knockout, knockdown), genomic DNA sequencing, RNA bisulfite sequencing, immunofluorescence staining, site-directed mutagenesis, neutral red uptake growth assay, sphere formation assays, temozolomide treatment, mice intracranial xenograft model, puromycin protein synthesis assays. Dr. Krista Vincent generated the first NSUN5 survival curve, and Jiesi Zhou generated the subsequent survival curves. Dr. Scott Findlay designed NSUN5 knockout gRNA and the plasmid construct. Dr. Dylan Dieters performed Liquid chromatography–mass spectrometry and data analysis. Western blotting and PCR were conducted by Jiesi Zhou with the assistance of Dr. Xiaowei Huang, Yanshu Kong, and Zhihua Xu. The intracranial xenograft model work in mouse was performed by Jiesi Zhou, with the assistance of Dan McGinn, Cheryl Santos, Daniel Choi, and Dr. Xiaowei Huang. The IVIS bioluminescence imaging was conducted by Amirali Bukhari with the assistance of Jiesi Zhou. Immunohistochemistry work was conducted by Darryl Glubrecht with the assistance of Jiesi Zhou. Experiments using T98 cell lines were conducted by Yanshu Kong.

**A publication in ovarian cancer is included to the thesis as appendix I.**

In the first two years of my PhD studies, before I started NSUN5 project in glioblastoma, I had worked on the Notch signaling pathway in both glioblastoma and ovarian cancer. Unfortunately, the glioblastoma project did not work out. Therefore, I switched to the NSUN5 project to complete my PhD studies. The ovarian cancer project resulted in a first-author publication, which is included to the thesis as an appendix.

Jiesi Zhou, Saket Jain, Abul K Azad, Xia Xu, Hai Chuan Yu, Zhihua Xu, Roseline Godbout, YangXin Fu. Notch and TGF $\beta$  form a positive regulatory loop and regulate EMT in epithelial ovarian cancer cells. *Cellular Signalling*, Volume 28, Issue 8, August 2016, Pages 838-849. Jiesi Zhou was the first author of this article. This project was conducted mainly by Jiesi Zhou with the assistance of people noted bellow. Jiesi Zhou performed the cell culture and treatment, preparation of whole cell lysates and cytosolic and nuclear fractions, Western blotting, immunocytochemistry, and scratch assay. Saket Jain and Xia Xu performed the migration assay. Abul K Azad, and Hai Chuan Yu generated new cell lines, and performed Western blotting. Zhihua Xu performed RT-qPCR. The final version of the manuscript was written by Dr. YangXin Fu. Dr. Roseline Godbout participated in the editing of the manuscript.

## **Acknowledgments**

I would like to express my sincere gratitude to my supervisor Dr. YangXin Fu who taught me how to do research, how to design experiments, and how to think and solve critically. He showed me how much effort we need to put in research, and, with his endeavours and attitude to scientific research, is a great model to me in my future career. He has always been kindly helping me in the research I have been working on in the past seven years and encouraging me when I was self-doubted and in stressful panic. I would like to extend my thanks to my co-supervisor Dr. Roseline Godbout who gave me the opportunity to study in Edmonton and greatly supported me in the glioblastoma projects. She also spent lots of time in supervising this project and helping me in writing. I would also like to thank my committee member Dr. Lynne Postovit who strongly suggested me to keep on working on this project. She is very knowledgeable and intelligent and gave me lots of valuable insights in this project, besides generously supported the research financially and my fifth-year stipends. I also thank Dr. David Eisenstat for collaboration and providing partial stipend to me for the fifth year of my PhD study.

My sincere thanks also go to the people who dedicated to this project: Dr. Krista Vincent who was the first to show us the association between NSUN5 expression and the poor survival of glioblastoma patients, Dr. Dylan Dieters who performed mass spectrometry analysis, Dr. Scott Findlay who designed NSUN5 knockout gRNA, Dr. Xiaowei Huang and Zhihua Xu who helped in the Western blotting and PCR experiments, Amirali Bukhari and Daniel Choi who helped with the mice work, Darryl Glubrecht for the immunohistochemistry work, Yanshu Kong for the help in hypoxia, temozolomide, and radiation treatments, Dr. Anne Galloway for the help in cell sorting, Cheryl from Molecular Biology Services Unit for the Sanger sequencing. I would like to thank all

the other colleagues: colleagues in Dr. Fu's lab, in Dr. Postovit's lab especially Dr. Micheal Jewel, Laura Lee, Dr. Olena Bilyk, in Dr. Godbout's Lab especially Saket Jain, in Dr. Lai's Lab especially Moinul Haque, as well as Dan McGinn and Cheryl Santos at the Cross Cancer Institute Vivarium.

I would like to thank the Li Ka Shing Foundation for the four-year scholarship in University of Alberta. I would like to thank all my friends, especially Dr. Pengfei Wang, Shuoyi Xie, Dr. Srijan Raha, for friendship and making my life in Edmonton more enjoyable. I would like to thank my parents and my wife for always being supportive and keeping faith in me.

## Table of Contents

<b>List of Figures</b> .....	<b>xii</b>
<b>List of Tables</b> .....	<b>xvi</b>
<b>List of Abbreviations</b> .....	<b>xvii</b>
<b>Chapter 1 Introduction</b> .....	<b>1</b>
<b>1.1 Glioblastoma</b> .....	<b>2</b>
1.1.1 Epidemiology and classification of glioblastoma .....	2
1.1.2 Treatment for glioblastoma .....	6
1.1.3 Mechanisms of treatment resistance in glioblastoma .....	9
<b>1.2 mRNA translation and translational control in cancer</b> .....	<b>17</b>
1.2.1 Translation processes .....	17
1.2.2 Translational control in cancer .....	21
<b>1.3 Ribosome biogenesis and ribosomal regulation in cancer</b> .....	<b>29</b>
1.3.1 Ribosomal DNAs (rDNAs), rRNA modifications, and ribosome biogenesis.....	29
1.3.2 Ribosomal regulation in cancer .....	37
<b>1.4 RNA modifications, RNA cytosine methylation, and NSUN proteins</b> .....	<b>44</b>
1.4.1 RNA modifications and enzymes.....	44
1.4.2 RNA cytosine methyltransferase NSUN proteins.....	48
1.4.3 NSUN5 and its cytosine targets on rRNA .....	56
<b>1.5 Hypothesis of the project</b> .....	<b>60</b>
<b>Chapter 2 Materials and Methods</b> .....	<b>61</b>
<b>2.1 TCGA glioblastoma datasets analysis</b> .....	<b>62</b>
<b>2.2 Cell culture</b> .....	<b>62</b>
<b>2.3 Total RNA extraction and complementary DNA (cDNA) synthesis</b> .....	<b>63</b>
<b>2.4 Quantitative real-time PCR</b> .....	<b>64</b>

<b>2.5 Protein extraction.....</b>	<b>64</b>
<b>2.6 Western blotting.....</b>	<b>65</b>
<b>2.7 NSUN5 CRISPR guide RNA design and plasmid production .....</b>	<b>65</b>
<b>2.8 NSUN5 CRISPR knockout.....</b>	<b>67</b>
<b>2.9 Genomic DNA sequencing for indels induced by CRISPR in <i>NSUN5</i> gene .....</b>	<b>67</b>
<b>2.10 NSUN5 knockdown and CaCl<sub>2</sub> mediated transfection .....</b>	<b>68</b>
<b>2.11 RNA bisulfite sequencing.....</b>	<b>70</b>
<b>2.12 Immunofluorescence staining .....</b>	<b>71</b>
<b>2.13 Site-directed mutagenesis.....</b>	<b>72</b>
<b>2.14 Neutral red uptake assay .....</b>	<b>73</b>
<b>2.15 Clonogenic survival assay .....</b>	<b>74</b>
<b>2.16 Sphere formation assay .....</b>	<b>75</b>
<b>2.17 Mice intracranial xenograft model.....</b>	<b>75</b>
<b>2.18 IVIS bioluminescence imaging.....</b>	<b>76</b>
<b>2.19 Immunohistochemistry of the xenografted tumors .....</b>	<b>77</b>
<b>2.20 Puromycin protein synthesis assay.....</b>	<b>78</b>
<b>2.21 Liquid chromatography–mass spectrometry (LC-MS/MS).....</b>	<b>78</b>
<b>Chapter 3 NSUN5 Expression and RNA Methyltransferase Activity in Glioblastoma Cells .....</b>	<b>80</b>
<b>3.1 <i>NSUN5</i> expression is strongly associated with poor outcome in glioblastoma patients ..</b>	<b>81</b>
<b>3.2 NSUN5 is expressed in glioblastoma cells and mainly located in the nucleus.....</b>	<b>88</b>
<b>3.3 NSUN5 methylates C3782 of 28S rRNA in HEK293T and glioblastoma cells .....</b>	<b>94</b>
<b>3.4 Catalytic cysteines (C308 and C359) of NSUN5 are required for the methylation of C3782 in U87 28S rRNA.....</b>	<b>109</b>
<b>Chapter 4 Characterization of the biological function of NSUN5 in glioblastoma.....</b>	<b>116</b>

<b>4.1 NSUN5 regulates proliferation and stem cell phenotype in glioblastoma cells .....</b>	<b>117</b>
4.1.1 NSUN5 regulates proliferation of glioblastoma cells.....	117
4.1.2 NSUN5 regulates the sphere forming ability of glioblastoma cells. ....	124
<b>4.2 Knockdown of NSUN5 renders U251 and T98 cells more sensitive to temozolomide ...</b>	<b>131</b>
<b>4.3 Knockdown of NSUN5 prolonged survival of mice bearing U251 intracranial tumors.</b>	<b>140</b>
<b>Chapter 5 Regulation of global protein synthesis and proteome by NSUN5 in glioblastoma</b>	<b>150</b>
<b>5.1 NSUN5 regulates global protein synthesis in glioblastoma cells.....</b>	<b>151</b>
5.1.1 Knockdown of NSUN5 decreases the global protein synthesis rate in U251 cells. ....	151
5.1.2 Overexpression of NSUN5 increases the global protein synthesis rate of glioblastoma cells.	153
<b>5.2 NSUN5 regulates the proteome of glioblastoma cells. ....</b>	<b>157</b>
<b>Chapter 6 Discussion, Future directions, and Conclusions.....</b>	<b>178</b>
<b>6.1 Discussion.....</b>	<b>179</b>
6.1.1 NSUN5 expression in glioblastoma and the key cysteines of NSUN5 .....	180
6.1.2 Methylation target(s) of NSUN5 in glioblastoma cells .....	182
6.1.3 NSUN5 regulates the behaviour of glioblastoma cells <i>in vitro</i> .....	184
6.1.4 NSUN5 regulates the behaviour of glioblastoma cells <i>in vivo</i> .....	186
6.1.5 NSUN5 increases protein synthesis in glioblastoma cells.....	188
6.1.6 NSUN5 alters the proteome of glioblastoma cells.....	191
<b>6.2 Future directions .....</b>	<b>194</b>
6.2.1 To determine whether NSUN5 reprograms the translome in glioblastoma cells.....	194
6.2.2 To determine whether NSUN5 regulates the composition of ribosomal proteins in glioblastoma cells.....	196

6.2.3 To determine whether NSUN5 has other RNA targets and whether <i>STAT3</i> and <i>NSUN2</i> are the targets of NSUN5 .....	197
<b>6.3 Conclusions.....</b>	<b>199</b>
<b>References .....</b>	<b>200</b>
<b>Appendix I: Notch and TGF<math>\beta</math> form a positive regulatory loop and regulate EMT in epithelial ovarian cancer cells</b>	

## List of Figures

Figure 1.1 The proportion of glioma subtypes. ....	3
Figure 1.2 The most common pathological features of glioblastoma. ....	13
Figure 1.3 GSCs are resistant to treatment and form resistant recurring tumors. ....	15
Figure 1.4 The formation of the 80S pre-initiation complex. ....	19
Figure 1.5 Regulation of mRNA translation by the oncogenic signaling pathways. ....	24
Figure 1.6 The structure of a rDNA repeat. ....	30
Figure 1.7 Transcription initiation and the binding of its key factors. ....	31
Figure 1.8 Ribosome biogenesis. ....	34
Figure 1.9 Ribosomal regulation in cancer. ....	38
Figure 1.10 Cytosine methylation by NSUN proteins. ....	53
Figure 1.11 The conserved sequences and cysteines in the NSUN proteins. ....	55
Figure 1.12 The C3782 methylation site in human 28S rRNA is located in a region with a similar secondary structure to that of the C2278 methylation site in yeast 25S rRNA. ....	57
Figure 1.13 Diagram depicting the central hypothesis of this project. ....	60
Figure 3.1 High <i>NSUN5</i> expression is strongly associated with poor overall survival of glioblastoma patients. ....	83
Figure 3.2 High <i>NSUN5</i> expression is strongly associated with poor overall survival of glioma patients. ....	85
Figure 3.3 DNA copy number amplification of the <i>NSUN5</i> gene of the <i>NSUN5</i> gene was associated with the survival of glioblastoma patients. ....	86
Figure 3.4 DNA methylation of the <i>NSUN5</i> gene promoter is associated with survival of glioblastoma patients. ....	87
Figure 3.5 <i>NSUN5</i> expression in glioblastoma cell lines and glioblastoma patient-derived neurosphere cultures. ....	90
Figure 3.6 Endogenous <i>NSUN5</i> in U251 cells is localized in the nucleus and is found mainly in the nucleolus. ....	91

<b>Figure 3.7 Overexpressed NSUN5 in U87 cells localizes to the nucleus and is found mainly in the nucleolus. ....</b>	<b>92</b>
<b>Figure 3.8 Immunostaining of NSUN5 in two human glioma tissues.....</b>	<b>93</b>
<b>Figure 3.9 NSUN5 expression in 44 CRISPR clones of HEK293T cells. ....</b>	<b>95</b>
<b>Figure 3.10 Genomic DNA sequencing results for indels induced by CRISPR in the <i>NSUN5</i> gene of HEK293T CRISPR clones.....</b>	<b>97</b>
<b>Figure 3.11 NSUN5 is responsible for methylation of C3782 in 293T 28S rRNA. ....</b>	<b>99</b>
<b>Figure 3.12 NSUN5 knockout does not change methylation of C4447 in 293T 28S rRNA.</b>	<b>100</b>
<b>Figure 3.13 NSUN5 expression in U251 CRISPR clones.....</b>	<b>101</b>
<b>Figure 3.14 Genomic DNA sequencing results for indels induced by CRISPR in the <i>NSUN5</i> gene of U251 CRISPR clones. ....</b>	<b>102</b>
<b>Figure 3.15 NSUN5 is responsible for methylation of C3782 in U251 28S rRNA.....</b>	<b>103</b>
<b>Figure 3.16 NSUN5 knockout does not change methylation of C4447 in U251 28S rRNA.</b>	<b>104</b>
<b>Figure 3.17 Overexpression of NSUN5 in U87 cells.....</b>	<b>106</b>
<b>Figure 3.18 Overexpressed NSUN5 induces methylation of C3782 in U87 28S rRNA.....</b>	<b>107</b>
<b>Figure 3.19 Overexpressed NSUN5 does not change methylation of C4447 in U87 28S rRNA. ....</b>	<b>108</b>
<b>Figure 3.20 The amino acid sequences alignment of yeast Rcm1 and human NSUN5. ....</b>	<b>110</b>
<b>Figure 3.21 DNA sequence alignment of pLenti-NSUN5 plasmids carrying mutated codons for cysteine 308 or/and cysteine 359 after site directed mutagenesis. ....</b>	<b>111</b>
<b>Figure 3.22 Overexpression of wild-type and mutant NSUN5 in U87 cells. ....</b>	<b>113</b>
<b>Figure 3.23 NSUN5 C308A, NSUN5 C359A, and NSUN5 C308A/C359A fail to induce methylation of C3782 of 28S rRNA in U87 cells. ....</b>	<b>114</b>
<b>Figure 4.1 Effect of NSUN5 knockout on proliferation of U251 cells. ....</b>	<b>118</b>
<b>Figure 4.2 NSUN5 knockdown decreased cell growth in U251 cells. ....</b>	<b>121</b>
<b>Figure 4.3 NSUN5 knockdown in T98 cells decreased cell growth. ....</b>	<b>122</b>
<b>Figure 4.4 NSUN5 overexpression did not increase the proliferation of U87 cells. ....</b>	<b>123</b>

<b>Figure 4.5 Knockdown of NSUN5 decreases sphere formation in U251 cells. ....</b>	<b>126</b>
<b>Figure 4.6 Knockdown of NSUN5 decreases sphere formation in A4-012 cells.....</b>	<b>127</b>
<b>Figure 4.7 Overexpression of NSUN5 increases sphere formation in U87 cells.....</b>	<b>129</b>
<b>Figure 4.8 Overexpression of NSUN5 increases sphere formation in 50M cells. ....</b>	<b>130</b>
<b>Figure 4.9 NSUN5 knockdown sensitizes U251 cells to temozolomide treatment.....</b>	<b>133</b>
<b>Figure 4.10 Combination of NSUN5 knockdown with temozolomide treatment markedly decreases cell viability of U251 cells.....</b>	<b>134</b>
<b>Figure 4.11 NSUN5 knockdown sensitizes T98 cells to temozolomide treatment. ....</b>	<b>134</b>
<b>Figure 4.12 NSUN5 knockdown renders U251 cells more sensitive to temozolomide treatment. ....</b>	<b>137</b>
<b>Figure 4.13 NSUN5 knockdown renders T98 cells more sensitive to temozolomide treatment. ....</b>	<b>139</b>
<b>Figure 4.14 Knockdown of NSUN5 in U251 cells prolongs the survival time of mice bearing U251 tumors. ....</b>	<b>143</b>
<b>Figure 4.15 Immunostaining of NSUN5 and tumor cells in U251 xenografts. ....</b>	<b>146</b>
<b>Figure 4.16 Knockdown of NSUN5 reduces spinal metastasis of intracranial U251 tumors. ....</b>	<b>147</b>
<b>Figure 5.1 NSUN5 knockdown decreases protein synthesis rate in U251 cells. ....</b>	<b>152</b>
<b>Figure 5.2 NSUN5 overexpression increases protein synthesis in U87 cells. ....</b>	<b>154</b>
<b>Figure 5.3 NSUN5 overexpression increases protein synthesis in 50M cells. ....</b>	<b>155</b>
<b>Figure 5.4 Heat map showing differences in global protein expression patterns in U251/shRandom vs. U251/shNSUN5 #4.....</b>	<b>159</b>
<b>Figure 5.5 Volcano plot highlighting proteins whose levels are increased or decreased as the result of NSUN5 knockdown in U251 cells. ....</b>	<b>165</b>
<b>Figure 5.6 Global protein expression in 50M/pLenti-Vector is different from that of 50M/pLenti-NSUN5 cells.....</b>	<b>167</b>
<b>Figure 5.7 Volcano plot highlighting proteins whose levels are either increased or decreased by more than 2-fold when NSUN5 is overexpressed in 50M cells. ....</b>	<b>171</b>

**Figure 5.8 Knockdown of NSUN5 decreases STAT3 and NSUN2 protein levels in U251 cells.**  
..... 173

**Figure 5.9 Knockdown of NSUN5 decreases *STAT3* and *NSUN2* mRNA levels in U251 cells.**  
..... 174

**Figure 5.10 Knockdown of NSUN5 decreases STAT3 and NSUN2 protein levels in T98 cells.**  
..... 175

**Figure 5.11 Knockdown of NSUN5 decreases *STAT3* and *NSUN2* mRNA levels in T98 cells.**  
..... 176

## List of Tables

<b>Table 4.1 The survival times of mice intracranially injected with U251 cells and the time of appearance of spinal metastasis.....</b>	<b>148</b>
<b>Table 5.1 Proteins that are downregulated in U251/shNSUN5 cells.....</b>	<b>159</b>
<b>Table 5.2 Proteins that are upregulated in U251/shNSUN5#4 cells.....</b>	<b>162</b>
<b>Table 5.3 Proteins that are upregulated in 50M/pLenti-NSUN5 cells.....</b>	<b>168</b>
<b>Table 5.4 Proteins that are downregulated in 50M/pLenti-NSUN5 cells. ....</b>	<b>169</b>

## List of Abbreviations

aa-tRNA	Aminoacyl-tRNA
AIM-2	Absent in melanoma 2
AKT	Protein Kinase B (PKB)
ATM	Serine/Threonine Kinase
BCRP	Breast Cancer Resistance <i>Protein</i>
CBTRUS	Central Brain Tumor Registry of the United States
CDK4/6	Cyclin-dependent kinase 4/6
CDX-110	Rindopepimut; vaccine targeting EGFRvIII
Chk	Checkpoint kinase
DFC	Dense fibrillary component
DKC1	Dyskerin 1
4EBP	eIF4E-binding protein
eEF	Eukaryotic elongation factor
EGFR	Epidermal growth factor receptor
eIF	Eukaryotic initiation factor
EMT	Epithelial-to-mesenchymal transition
eRF	Eukaryotic release factor
ETS	External transcribed spacer
FBL	Fibrillarin
FC	Fibrillary centers

GBM	Glioblastoma
GC	Granular component
GM-CSF	Granulocyte-macrophage colony stimulating factor
GSCs	Glioblastoma stem cells
HER-2	Human epidermal growth factor receptor 2
IDH1	Isocitrate dehydrogenase 1
IGS	Intergenic spacer
IHC	Immunohistochemistry
IL-13RA2	Interleukin 13 receptor subunit alpha 2
IRES	Internal ribosome entry site
LSU	Large 60S ribosomal subunit
ITS	Internal transcribed spacer
Mage-1	Melanoma-associated antigen 1
Met-tRNA	Methionine-transfer RNA
MGMT	O (6)-methylguanine-DNA methyltransferase
mRNA	Messenger ribonucleic acid
mTOR	Mammalian target of rapamycin
MultAlin	Multiple sequence alignment
NCCN	National Comprehensive Cancer Network
NF1	Neurofibromatosis type 1
NOR	Nucleolus organizer region
PD-1	Programmed cell death 1

PDGFRA	Platelet derived growth factor receptor alpha
PD-L1	Programmed death-ligand 1
PTEN	Phosphatase and tensin homolog
RB1	Retinoblastoma 1
Rcm1	25S rRNA (cytosine (2278)-C (5))-methyltransferase
rDNA	Ribosomal DNA
rRNA	Ribosomal RNA
S6K	S6 kinase
SAH	S-adenosylhomocysteine
SAM	S-adenosyl methionine
SL1	Selective factor 1
snoRNAs	Small nucleolar RNAs
SSU	Small 40S ribosomal subunit
STAT3	Signal transducer and activator of transcription 3
TAAAs	Tumor associated antigens
TCGA	The Cancer Genome Atlas
TGF $\beta$	Transforming growth factor- $\beta$
tRNA	Transfer ribonucleic acid
TRP-2	Tyrosinase related protein 2
TSAAs	Tumor-specific antigens
UCE	Upstream control elements
WHO	World Health Organization

**Chapter 1 Introduction**

## 1.1 Glioblastoma

### 1.1.1 Epidemiology and classification of glioblastoma

Glioblastoma is the most common and aggressive malignant primary brain tumor. According to the 2021 report of the Central Brain Tumor Registry of the United States (CBTRUS), glioblastoma accounts for 49.1% of all the primary malignant brain tumors and 14.3% of all the primary brain tumors. The incidence rate is 3.2 case per 100,000 people in North America [1]. According to the American Brain Tumor Association, there is an estimated 13,000 newly diagnosed glioblastoma cases per year in the United States. Despite aggressive standard treatments including surgery, radiation and chemotherapy, the median overall survival for patients with glioblastoma is only about 14 to 16 months [2-4].

Based on the 2007 WHO Classification of tumors of the central nervous system, glioblastoma is classified as grade IV astrocytoma [5, 6]. In this classification, glioma is divided into several major types (astrocytoma, ependymoma, oligodendroglioma, and oligoastrocytoma) based on the histological tumor cell types and four grades based on the degree of anaplasia of the tumor cells [5, 6]. Astrocytoma, accounting for about 75% of gliomas, are composed of pilocytic astrocytoma (grade I, 5.0% of all gliomas), diffuse astrocytoma (grade II, 7.3%), anaplastic astrocytoma (grade III, 6.8%), and glioblastoma (grade IV, 58.4%) (**Figure 1.1**) [7]. In the 2016 WHO Classification of tumors of the central nervous system, the tumor molecular genetic features (including *IDH* mutation, *MGMT* promoter methylation, 1p/19q-co-deletion, *EGFR*, *PTEN*, and *TP53*) are included in the classification of glioma [8]. The incorporation of pathological features with molecular genetics has improved diagnosis and provided clues for the development of targeted therapies.

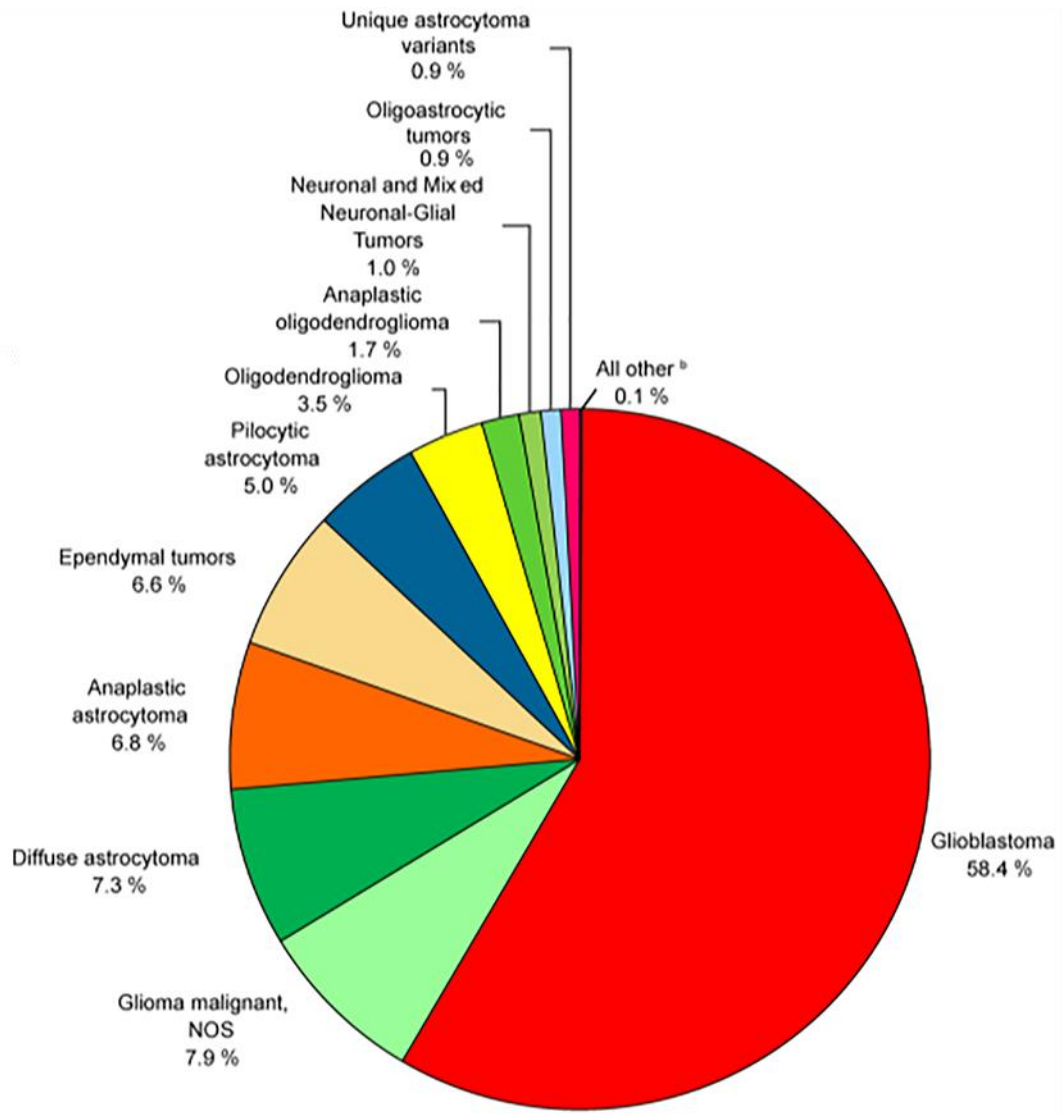


**Figure 1.1 The proportion of glioma subtypes.**

Data are from 105,729 glioma patients from 2014 to 2018. This figure has been reused with permission from Oxford University Press (Neuro-Oncology), License Number: 5172500364531,2021, Quinn T. Ostrom et al. [7, 9]

Using The Cancer Genome Atlas (TCGA) Research Network of glioblastoma in 2008, researchers found core pathogenesis pathways and key mutated or high amplified genes in glioblastoma, including *EGFR*, *TP53*, *PTEN*, *NF1*, *IDH1*, *PDGFRA*, *PTEN*, and *RBI* [10]. A more

detailed analysis revealed that amplification or mutational activation of receptor tyrosine kinase (RTK)/Ras signaling/RTK-PI3K signaling pathways were found in approximately 90% of glioblastoma samples [11]. Mutations in *EGFR*, *PTEN*, *PI3K*, *NF1*, and *PDGFRA* were found in 57%, 41%, 25%, 10%, and 10% of glioblastoma samples, respectively [11]. Inactivation of the p53 and RB tumor suppressor signaling pathways was found in 86% and 79% of glioblastoma samples, respectively [11]. Mutations in *CDKN2A/B*, *TP53*, *MDM2/4*, *CDK4*, and *RBI* were found in 61%, 28%, 14.8%, 14%, and 7.6% of glioblastoma samples, respectively [11]. Based on these genomic abnormalities, glioblastoma is now classified into three main molecular subtypes: Classical, Proneural, and Mesenchymal [10, 12].

The Classical subtype is characterized by amplification of *EGFR* (95%), expression of point-mutated *EGFR* or *EGFRvIII* (55%), and expression of wild-type *TP53* (100%) [10]. *EGFR* is an important member of the receptor tyrosine kinase family. *EGFR* signaling is one of the key players for cell proliferation, growth, development, and survival. It is activated by extracellular epidermal growth factor (and other ligands) and delivers signals from the Ras, PI3K and STAT3 signaling pathways to the nucleus to regulate cell proliferation, survival, and cell growth. *EGFR* amplification and/or mutations occur in about 60% of GBM, which results in persistent activation of the signaling networks that promote malignancy. The most common *EGFR* mutation leads to the formation of *EGFRvIII* that has no ligand binding sites but is a constitutive self-activated receptor.

The Proneural subtype is characterized by amplification of *PDGFRA* (35%) and expression of mutated *IDH1* (30%) and mutated *TP53* (54%) [10]. Interestingly, *IDH1* mutations were only found in 12 cases out of the total 116 samples tested and 11 of the 12 cases were of the Proneural subtype. *IDH1* is an isocitrate dehydrogenase that catalyzes the reversible conversion of isocitrate

to  $\alpha$ -ketoglutarate ( $\alpha$ -KG) in glucose metabolism. *IDH1* mutations are mostly found at arginine 132 (mainly R132H) [13, 14]. IDH1 R132H loses the ability to produce  $\alpha$ -KG but increases the conversion of  $\alpha$ -KG to 2-hydroxyglutarate (2-HG) [13]. 2-HG inhibits  $\alpha$ -KG-dependent dioxygenases, including histone demethylase and TET2 DNA hydroxylase. Therefore, the accumulation of 2-HG causes the widespread abnormal methylation or hypermethylation of DNAs and histones, contributing to tumorigenesis [13]. More than 73% of all grade II and III gliomas (of all types) have been found to have *IDH1* mutated at R132 [14]. About 80% of secondary glioblastomas have mutated *IDH1* at R132, are believed to have progressed from grade II and III gliomas [14]. More interestingly, 2-HG can be detected by magnetic resonance spectroscopy and this detection can be used in the diagnosis and prognosis of IDH-mutated glioma patients [15].

The Mesenchymal subtype is characterized by deletion mutation of *NF1* (37%), point mutation of *PTEN* (32%), and high levels of expression of mesenchymal markers *CHI3L1* and *CD44* [10]. As two important suppressors of the AKT-mTOR signaling pathway, low expression of NF1 and PTEN increases the effects of AKT signaling which promotes the proliferation, migration, and invasion of tumor cells. CHI3L1 is a secreted glycoprotein that is associated with angiogenesis and invasion of glioblastoma [16]. Knockdown of *CHI3L1* decreases, whereas overexpression of *CHI3L1* increases, migration and invasion of glioblastoma cell lines *in vitro* [16]. Knockdown of *CHI3L1* also inhibits the angiogenesis and tumorigenesis of glioblastoma xenografts *in vivo* [17]. *CHI3L1* is the direct target of STAT3 in the regulation of invasion and differentiation of glioma cells [16, 17].

The Classical and Mesenchymal subtypes have better outcomes with temozolomide treatment, whereas the Proneural subtype does not respond to temozolomide treatment [10]. In addition, for

the prediction of prognosis and treatment outcome, glioblastoma can simply be classified as *IDHI*-mutated vs. *IDHI*-wild-type or *MGMT* promoter-methylated vs. *MGMT* promoter-unmethylated subtypes [14, 18, 19]. *IDHI*-mutated glioblastomas are more common in younger patients and have a much better median survival (27 to 31 months) compared to *IDHI*-wild-type glioblastoma (11 to 15 months) [14, 19]. *MGMT* promoter-methylated glioblastomas have a better response to radiotherapy and/or temozolomide treatment compared to glioblastomas without *MGMT* promoter methylation [18]. With combined radiotherapy and chemotherapy, the median survival of *MGMT* promoter-methylated glioblastoma is 21.7 months compared to 12.7 months in *MGMT* promoter-unmethylated glioblastoma [18]. While *IDHI* mutation is a feature of the Proneural subtype, *MGMT* promoter methylation is observed in all glioblastoma subtypes [10].

### **1.1.2 Treatment for glioblastoma**

Without treatment, the median survival for glioblastoma patients is only 2 to 3 months [20, 21]. Even though complete surgical resection has better outcome than biopsies only [22, 23], the median overall survival is still only about 4 months [24]. Compared with surgery, radiotherapy is a much more effective treatment for glioblastoma. With 60 Gy of radiation treatment, the median survival for glioblastoma patients increases to 10 to 12 months [2, 24]. Radiation mainly damages the DNA of tumor cells, leading to activation of DNA repair pathways, cell cycle arrest and apoptosis. p53 signalling plays a key role in the regulation of these cell damage processes. However, inactivation of p53 signalling is found in about 86% of glioblastoma patient samples, resulting in enhanced survival of tumor cells exposed to radiation [11].

Chemotherapy is also commonly used for the treatment of glioblastoma patients and the first line chemotherapy drug is temozolomide [25]. Temozolomide is an alkylating agent that induces

cytotoxicity by methylating the O<sup>6</sup> position of guanine, resulting in DNA damage [26]. Cancer cells proliferate faster but have less capacity for DNA repair. Therefore, DNA chains are easier to be cross linked with alkylating agent through addition of alkyl groups into the guanine bases and causing a cytotoxic reaction. However, some glioblastoma cells express O-6-Methylguanine-DNA Methyltransferase (MGMT) which removes the guanine methylation and allows the cells to survive after temozolomide treatment [18].

Since 2006, the combination of surgery, radiotherapy and temozolomide has become the standard treatment for glioblastoma. Specifically, glioblastoma patients are treated with surgery and standard radiotherapy concurrent with temozolomide treatment for 6 weeks, followed by adjuvant temozolomide treatment for 6 months. Despite this aggressive treatment, the median overall survival is still only about 14 to 16 months [2-4]. There is a great need to develop novel therapeutic strategies to improve patient outcomes. Targeted therapy, alternating electric field therapy, and glioblastoma immunotherapy are among the novel approaches that have been developed in the past two decades.

Targeted therapy is defined as treatment that targets specific mutated/abnormal molecules in the tumor or on the surface of the tumor and is a more personalized form of treatment. With significant discoveries made in 2008 and 2013 following analyses of glioblastoma patient datasets from TCGA research network, the molecular mechanisms of glioblastoma pathophysiology are increasingly being understood [11, 27]. Using these datasets, several new molecular therapeutic targets were identified [27]. For instance, *EGFR* amplification and/or mutations occur in more than 60% of glioblastomas, which results in persistent activation of the signaling networks that promote malignancy. The most common *EGFR* mutation is the EGFRvIII (variant III, deletion of exons 2–7) [28, 29]. EGFR inhibitors (such as erlotinib and gefitinib) have been used in the clinic for the

treatment of some *EGFR*-mutated glioblastomas. However, combination treatment with erlotinib or gefitinib only increased progression-free survival time, with no effect on overall survival time [30]. After treatment with EGFR inhibitors, surviving glioblastoma cells accumulate different types of gene mutations and become resistant to the inhibitors [30]. Nowadays, some researchers are trying to combine EGFR inhibitors with inhibitors that target different proteins, including Palbociclib which targets cyclin-dependent kinase 4/6 (CDK4/6) and/or Crizotinib, a c-Met pathway inhibitor [31, 32]. However, tumor cell heterogeneity is still a big challenge for the development of targeted therapy.

Alternating electric field therapy consists of applying low intensity alternating electromagnetic field to the brain to interfere with the mitosis of tumor cells. In a multicenter Phase III trial with 695 patients, alternating electric field therapy increased the median overall survival for patients with glioblastoma to 20.5 months [3]. Alternating electric field therapy has been recommended as the standard of care for glioblastoma patients by the American National Comprehensive Cancer Network (NCCN). However, this treatment is still controversial, and there are some skepticism about this treatment [33]. More accurate and precise clinical trials are needed to confirm the Phase III trial results, and a better understanding of the mechanisms of this treatment is also necessary before it can be used in the clinic as standard therapy.

Immunotherapy for glioblastoma primarily focuses on the intrinsic recognition of tumor antigen targets, including tumor associated antigens (TAAs), viral antigens (CMV-pp65), and tumor-specific antigens (TSAs) [34-36]. There is increasing evidence supporting immunotherapy as an attractive additional treatment for glioblastoma to improve patient survival [37-39]. For example, glioblastoma patients additionally treated with dendritic cells pulsed with mixed TAAs (AIM-2, Mage-1, TRP-2, GP 100, HER-2, and IL-13RA2) showed an increase in median overall

survival to more than 30 months [38] TSAs are widely generated because of the existence of tumor-specific mutations. In this regard, one study showed that administration of EGFRvIII vaccines resulted in an overall survival of 26 months for newly diagnosed glioblastoma patients and prolonged the survival time of recurrent EGFRvIII-positive glioblastoma patients by more than 3 months [39]. Similarly, glioblastoma patients who received the EGFRvIII vaccine (CDX-110 + GM-CSF) achieved a median survival of 23.2 months [40]. Immunotherapy can also focus on the checkpoint pathways that activate or inhibit T-cell activity. Programmed death-ligand 1 (PD-1) and its ligand 1 (PD-L1) mediate the inhibition of antitumor immune response, a main mechanism by which tumor cells avoid immune detection. Two PD-1 inhibitors have been approved for use in the clinic for melanoma and non-small cell lung cancer [41, 42]. PD-L1 is expressed in more than 70% of human glioblastoma, and the administration of pembrolizumab (PD-1 monoclonal antibody) before surgery improved the overall survival of glioblastoma patients by 6 months compared to control group [43, 44]. However, in a large-scale phase III clinical trial, addition of anti-PD-1 therapy (nivolumab) to standard therapy failed to increase the survival of glioblastoma patients treated by standard therapy [45]. There are still some challenges in the development of novel therapeutic approaches for glioblastoma. There is no doubt that we need to better understand the detailed molecular mechanisms of both resistance to treatment and therapeutic approaches to improve the overall survival for glioblastoma patients [46, 47].

### **1.1.3 Mechanisms of treatment resistance in glioblastoma**

There are two main reasons for treatment failure in glioblastoma. One is the invasive feature, and the other is the stemness feature [48]. The invasive feature of glioblastoma helps the tumor cells escape treatment, while the stemness feature promotes resistance to treatment [48].

### **1.1.3.1 The invasive feature of glioblastoma**

First, because of the infiltrating growth of glioblastoma, tumor cells invade into the surrounding brain tissue at early stages [49]. As a result, surgery and radiotherapy cannot fully eradicate all the tumor cells [49]. Thus, the invasive phenotype is associated with poorer patient survival [10, 50, 51]. The mechanism whereby glioblastoma cells invade the surrounding brain is not very clear. To date, research has focused on two possible mechanisms of infiltration. One is related to the substrates in the extracellular matrix (ECM) including attractants produced by the ECM itself and secretion of specific substrates produced by glioblastoma cells. The binding of glioblastoma cells to these substrates promotes their movement and invasion. The second mechanism is related to hypoxia whereby invasion of glioblastoma is associated with the oxygen content and other nutrients in the surrounding microenvironment.

Brain parenchyma contains neurons, glial cells (including astrocytes, oligodendrocytes, and microglia), and interstitial spaces. The interstitial spaces are filled with interstitial fluid and ECM substrates [52]. The ECM is composed of a variety of proteoglycans, hyaluronic acid chain, tenascins (such as tenascin R, tenascin C, tenascin W), link proteins, and protein ligands [53, 54]. Proteoglycans consist mainly of chondroitin sulfate proteoglycans such as neurocan, versican, aggrecan, brevican, and phosphacan. Link proteins promote the binding of proteoglycans onto the hyaluronic acid chain [54]. Tenascins allow accumulation of proteoglycans in the ECM [54]. Protein ligands including chemokines, growth factors, axon guidance molecules bind onto the glycosaminoglycan chains of proteoglycans and are stored in the ECM [54]. All these components in the ECM form a network that supports the nutrition, metabolism, communication, growth, and movement of cells.

Cell adhesion molecules (CAMs) on the surface of cells are responsible for interaction between cells and/or binding to the ECM. CAMs are usually transmembrane receptors and have an intracellular domain, a transmembrane domain, and an extracellular domain that binds with other cells or to the ECM. There are mainly four types of CAMs, namely cadherins, immunoglobulin-like CAMs, selectins, and integrins. The first three types of CAMs are responsible for interactions between cells, while integrins are mainly responsible for binding to ECM components. By comparing the transmembrane CAMs in the normal brain tissue and glioblastoma, researchers found that normal brain tissue expresses higher levels of integrin  $\alpha3\beta1$ , neural CAM, and CD44, whereas glioblastoma cells highly express a variety of integrins (such as  $\alpha v\beta3$ ,  $\alpha v\beta5$ ,  $\alpha2\beta1$ ,  $\alpha3\beta1$ ,  $\alpha5\beta1$ ,  $\alpha6\beta1$ ), ICAM1, CD58, CD44, and P75NTR [48, 55]. Integrins such as  $\alpha v\beta3$  and  $\alpha v\beta5$  play important roles in the angiogenesis and migration of cancer cells [56-58]. The expression of integrins is induced by growth factors and chemokines such as vascular endothelial growth factor (VEGF), basic fibroblast growth factor, and tumor necrosis factor-alpha [57, 59]. Integrin binds to the ECM and activate signaling pathways such as Erk and Akt signaling pathways [60, 61].

Besides CAMs, glioblastoma cells secrete high levels of many specific proteoglycans into the ECM to help the adhesion with its own receptors., brevican and tenascin W, all abundantly secreted by glioblastoma cells, increase tumor invasiveness [62-66]. For instance, high levels of Tenascin C are associated with severe peritumoral edema and inflammation reaction based on patient MR imaging, and poor glioblastoma patient survival [67]. Tenascin C promotes the expression of matrix metalloproteinase MMPs and contributes to migration and invasion of glioblastoma [68, 69]. Moreover, tenascin C binds with integrin  $\alpha2\beta1$  and promotes the stemness of glioblastoma through the activation of the Notch signalling pathway [69]. Interestingly,

activation of Notch, MAPK, and AKT signaling pathways further promotes the expression of tenascin C in glioblastoma [70-72]. The regulation is amplified in a positive feedback loop.

Hypoxia also plays a role in the invasion of glioblastoma in the surrounding microenvironment. The most common pathological features of glioblastoma from the most internal to the most external regions of the tumor include a central necrotic core, a hypoxic intermediate region, malformed and malfunctioning blood vessels on the tumor surface, and a surrounding region of severe edema (**Figure 1.2**) [73-77]. The microenvironment of tumor tissue is complex. The hypoxic condition in the intermediate region of glioblastoma tumors is a source of stress for the cells, resulting in increased invasion of tumors to the surrounding brain tissue [74, 78, 79]. Hypoxic conditions promote migration of tumor cells toward the blood vessels on the tumor surface and secretion of angiogenesis factors to generate more blood vessels [74, 78, 79]. However, because the newly generated blood vessels are malformed and malfunctioning, these vessels cannot offer normal blood supply but increase the hydrostatic pressure to cause edema. Invasive tumor cells are found in the edema area of brain tissue [49]. This pathological microenvironment induces tumor cell heterogeneity including generation of GSCs and also promotes the infiltrating growth of glioblastoma [80].

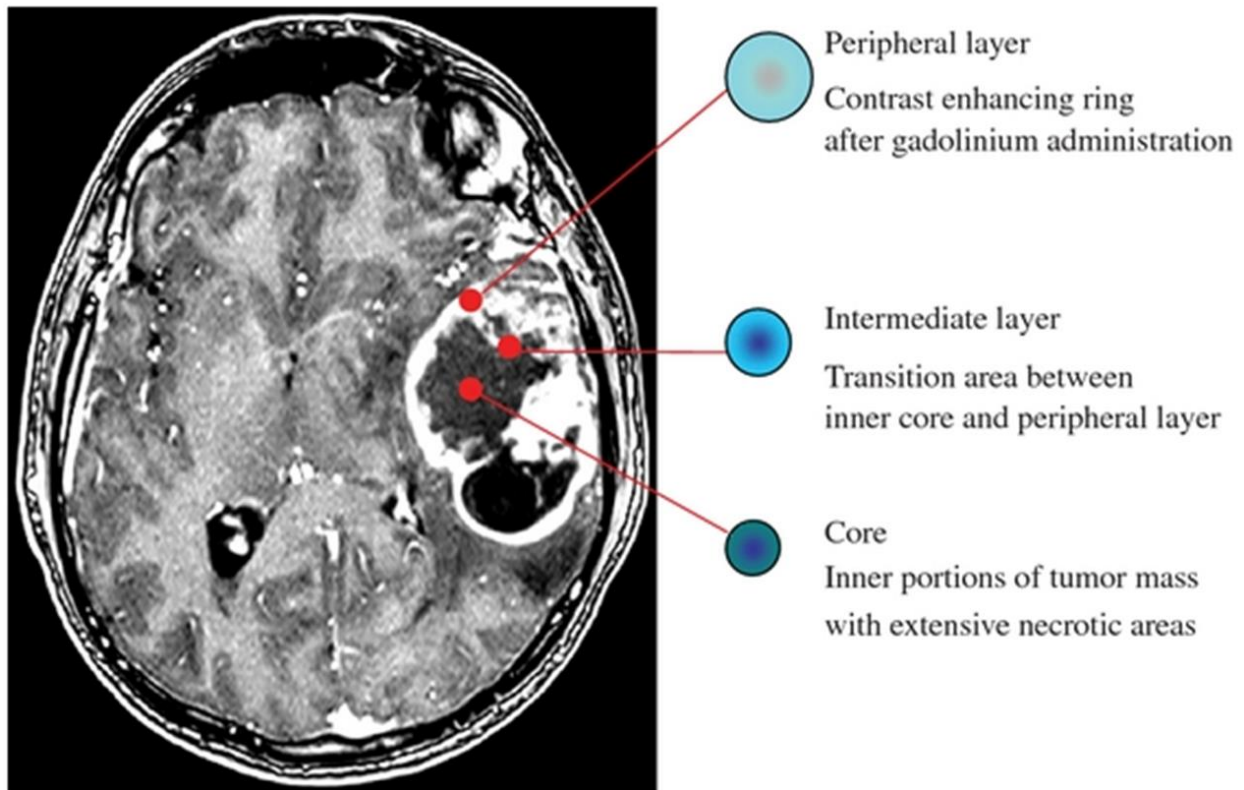


**Figure 1.2 The most common pathological features of glioblastoma.**

The tumor includes a central necrotic core, a hypoxic intermediate region, malformed and malfunctioning blood vessels on the tumor surface, and a surrounding region of severe edema. This figure has been reused with permission from The Scientific World Journal, Creative Commons Attribution License, Luca Persano et al. [81].

In addition to extracellular environment alterations, intracellular changes are also important for the invasion of glioblastoma cells. Epithelial-to-mesenchymal transition (EMT) is an important process for cancer cells to migrate and invade, and EMT-like processes also occur in glioblastoma cells [82]. Elevated expression of mesenchymal markers such as Twist, Snail, Slug, fibronectin, alpha-SMA is found in glioblastoma cells [82-85]. EMT-like transition can result from the intrinsic genetic alterations found in glioblastoma cells causing the dysregulation of signaling pathways,

such as abnormal activation of EFGR, Notch, and Wnt signaling [86-91], and by the factors from the microenvironment, such as TGF- $\beta$ , fibronectin from microglial and vascular cells, and hypoxic conditions [85, 86, 92]. EMT-like processes lead to cytoskeleton transformation of glioblastoma cells, rendering the cells more mesenchymal and motile, with increased expression of matrix metalloproteinases (MMPs) and ADAMTS proteases that degrade different ECM components and detach the cells from the ECM [93].

### 1.1.3.2 The stemness feature of glioblastoma

Because of tumor cell heterogeneity, some specific tumor cells are more resistant to radiotherapy, temozolomide treatment or other novel treatments. These surviving cells develop into new glioblastoma tumors, leading to recurrence after treatment. Glioblastoma stem cells (GSCs) were identified by Canadian scientists in 2003 and 2004 as a small subpopulation of CD133+ cells that can self-renew and differentiate into different lineages [94, 95]. GSCs are also considered to be the glioblastoma-initiating cells [95]. More importantly, GSCs play a key role in treatment resistance in glioblastoma (**Figure 1.2**) [18, 96-99]. First, GSCs are more resistant to radiotherapy [96]. After radiation treatment, GSCs can increase the phosphorylation of checkpoint proteins (e.g. Chk1, Chk2, and ATM) and activate the checkpoint response to DNA damage, which allows more damaged DNA to be repaired [96]. Second, GSCs have been shown to be more resistant to temozolomide treatment, because they express a higher level of MGMT that removes the guanine methylation (DNA damage) caused by temozolomide [18, 99]. *MGMT* promoter methylation, which leads to silencing of MGMT expression, is an important indicator of positive temozolomide treatment response [18]. Moreover, GSCs also express higher levels of BCRP1 (an ATP-binding cassette transporter) that pumps out chemotherapeutic drugs (e.g., carboplatin and

paclitaxel) [99]. Third, GSCs can remain in the quiescent state to avoid the damage caused by radiation and chemotherapeutic drugs. As a result, the GSCs that survive treatment can self-renew and differentiate into different lineages, and these newly differentiated cells show increased resistance to previous treatments.

In addition, some specific conditions (e.g., chemotherapy, radiotherapy, and hypoxia) induce the dedifferentiation of non-GSCs to GSCs, resulting in an increase in the GSC population (**Figure 1.3**) [97, 99, 100]. This dedifferentiation can be activated through EMT and the activation of stem cell-associated signaling pathways, such as Notch, Wnt, STAT3, and hedgehog signaling pathways [101-107]. As mentioned previously, EMT is also associated with invasiveness and can be initiated by factors from the microenvironment, hypoxic conditions, and/or dysregulation of signaling pathways [85, 86, 92]. Therefore, the mechanisms of glioblastoma treatment resistance are not through a single factor but are multifactorial.

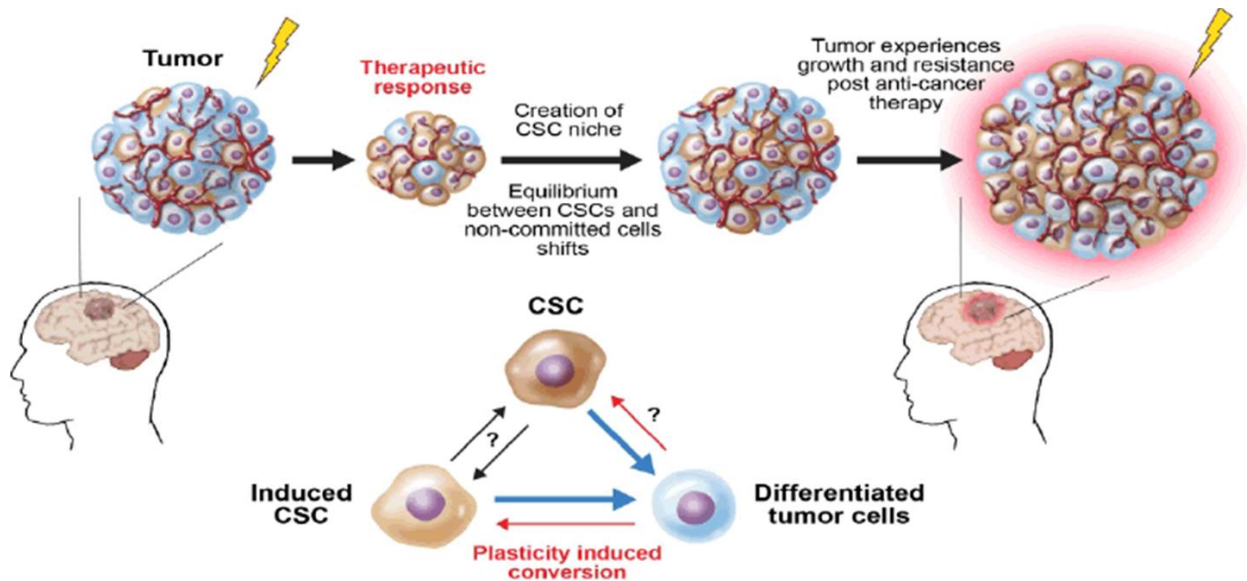


**Figure 1.3 GSCs are resistant to treatment and form resistant recurring tumors.**

Radiation or chemotherapy kill most differentiated tumor cells but induce the generation of more GSCs. After treatment, the remaining GSCs can differentiate into more resistant cells. Finally, the recurrent tumor cells become more malignant and contain a larger population of GSCs. This figure has been reused with permission from Journal of Stem Cell Research and Therapy, Creative Commons Attribution License, Gina Lee et al. [80].

## **1.2 mRNA translation and translational control in cancer**

Cancer cells have different mRNA translation and protein synthesis from normal cells. They usually increase the global protein synthesis or specifically increase the expression of a series of proteins to benefit tumor development and progression, as well as enhance resistance to treatments [108]. It is essential to know the regulation of all the components and steps involved in mRNA translation in cancer. In this section, I will discuss mRNA translation and translational control in cancer.

### **1.2.1 Translation processes**

Translation is the process by which genetic information stored in mRNA is translated into proteins. More specifically, it is a process whereby different tRNAs that carry specific amino acids are paired onto a mRNA template one by one to form the amino acid sequences at the protein synthetic machinery ribosome [109]. To correctly assemble mRNA, tRNAs and ribosome subunits, and to regulate translation, a large number of translation-associated factors are also needed [109]. The process of translation is divided into three sub-processes including initiation, elongation, and termination.

Translation initiation is well studied and considered to be associated with protein synthesis rate [108, 110, 111]. The canonical translation initiation for eukaryotic mRNAs is cap dependent translation initiation. First, the eukaryotic Initiation Factor 2 (eIF2) binds with Initiator Met-tRNA and a GTP to form a ternary complex. This ternary complex binds to the 40S ribosome subunit, eIF1, eIF1A, eIF3, and eIF5 to form a 43S preinitiation complex. Second, eIF4E, eIF4G, and eIF4A bind together to form the eIF4F complex. eIF4E (as part of the eIF4F complex) binds to the modified guanosine cap structure at the 5' end of a mRNA, and further recruits the binding of

eIF4B and 43S complex to the cap to form a 48S complex (**Figure 1.4A**). Third, this 48S complex unwinds the secondary structures and moves through the untranslated region to the start codon (AUG). When the Initiator Met-tRNA pairs with the start codon, eIF5 catalyzes the hydrolysis of GTP in the eIF2 ternary complex and promotes the release of eIF2-GDP. After that, the 60S ribosome subunit is recruited to form a complete ribosome 80S, and other initiation factors are released from this 80S complex (**Figure 1.4B**) [109, 110, 112]. In addition, about 10-15% of mRNAs have an alternative translation initiation process, whereby the 43S ternary complex binds directly to the secondary structure or tertiary structure at the 5' untranslated region (5' UTR) and initiates the translation, termed cap-independent translation initiation or internal ribosome entry site (IRES) dependent translation initiation [112, 113]. IRES was first found in poliovirus and other RNA viruses [114]. The RNA virus inhibits the cap-dependent translation of its host and promotes viral IRES-dependent translation [114]. Translation initiation of IRES structures does not need the cap-binding initiation factors eIF4E, but still needs the assistance of a few initiation factors depending on the type of IRES structure [115]. The binding of the 43S complex to IRES structures also needs the assistance of a group of specific RNA binding proteins, termed IRES-transacting factors (ITAFs) [116]. The canonical translation initiation manner is mainly associated with the development of cells, while IRES-dependent initiation is increased in response to environmental stresses including starvation, extremes in temperature, hypoxia, and DNA damage [112, 117].

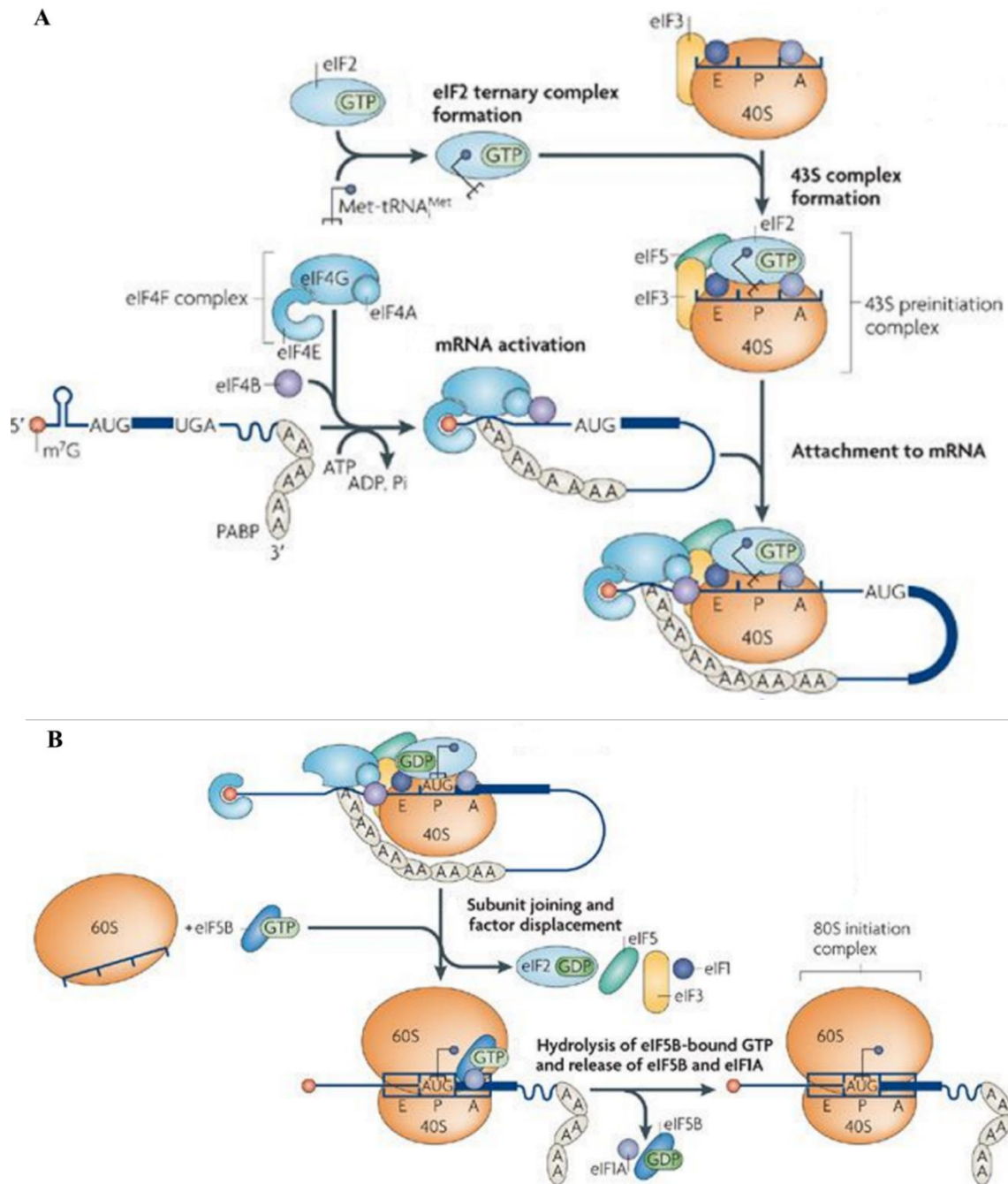


**Figure 1.4 The formation of the 80S pre-initiation complex.**

(A) eIF2 binds with Initiator Met-tRNA and a GTP to form a ternary complex. This ternary complex binds with 40S ribosome subunit, eIF1, eIF1A, eIF3, and eIF5 to form a 43S preinitiation complex. Next, eIF4E, eIF4G, and eIF4A bind together to form the eIF4F complex. eIF4E (as part of the eIF4F complex) binds to the G cap structure at the 5' end of a mRNA, and further recruits

the binding of eIF4B and 43S complex to the cap to form a 48S complex. **(B)** 48S complex unwinds secondary structures and moves through the untranslated region to the start codon (AUG). When the Initiator Met-tRNA pairs with the start codon, eIF5 catalyzes the hydrolysis of GTP in the eIF2 ternary complex and promotes the release of eIF2-GDP. After that, the 60S ribosome subunit is recruited to form a complete ribosome 80S. Initiation factors are then released from this 80S complex. This figure has been reused with permission from Springer Nature (Nature Reviews Molecular Cell Biology) License Number: 4630060730450, Richard Jackson et al. [118]

Translation elongation is the process of peptide chain synthesis, involving pairing of tRNAs on the mRNA template, peptide bond formation and elongation, and ribosome translocation on the mRNA template. Eukaryotic Elongation Factor 1A (eEF1A), eEF1B, and eEF2 are the three main factors in the regulation of translation elongation. A complete elongation cycle can be divided into three steps. First, eEF1A binds with an aminoacyl-tRNA (aa-tRNA) and a GTP to form a ternary complex and carries the aa-tRNA to the A site of a ribosome. When the anti-codon on the aa-tRNA correctly matches with a codon on the mRNA, the GTP is hydrolyzed to GDP, and then the eEF1A-GDP is released. Next, rRNA, acting as the ribosomal peptidyl-transferase, catalyzes aa-tRNA and peptidyl-tRNA to form a new peptide bond. The peptidyl-tRNA at the P site is deacylated, and the peptidyl chain is moved to aa-tRNA to form a new peptidyl-tRNA at the A site. Third, eEF2 catalyzes the translocation of the new peptidyl-tRNA from the A site to the P site. With completion of an elongation cycle, eEF1A-GDP is reactivated to eEF1A-GTP by eEF1B. In addition, eEF2 is a GTP-dependent protein and can be inactivated when it is phosphorylated by the EF-2 kinase. Studies have shown that the PI3K/AKT/mTOR signaling pathway can regulate the phosphorylation of eEF2 through the regulation of EF-2 kinase [119]. Moreover, the TGF $\beta$  signaling pathway can also regulate the phosphorylation of eEF2 through the inhibition of EF-2

kinase [120]. These data provide strong evidence that signaling pathways regulate the ribosome translocation (elongation) process.

Translation termination is the step that releases factors bound to the stop codon in the ribosome and catalyze the release of the peptide chain from ribosome. When the translating ribosome reaches the stop codon (including UAA, UAG, and UGA), eukaryotic release factor 1 (eRF1) binds to the A site of the ribosome and triggers the release of the peptide chain [121]. The ribosome is further disassembled, and the components are recycled for the next round translation [121].

## **1.2.2 Translational control in cancer**

Theoretically, the dysregulation of any of the translation components, including translation associated factors, mRNA structures, ribosomes, and tRNAs will cause the dysregulation of translation. Dysregulation of translation is commonly associated with the development and progression of cancers [108]. The dysregulation of translation associated factors, secondary mRNA structures and specific motifs on the mRNA, as well as modifications of tRNAs in cancer will be reviewed in this section. Ribosome biogenesis and modifications of rRNAs, which is the focus of this project, will be discussed in the next section (section 1.3).

### **1.2.2.1 Dysregulation of translation associated factors in cancer**

To date most research on translational control in cancer has focused on the dysregulation of translation associated factors [108, 110, 111]. Among all the translation associated factors, eIF4E in the eIF4F complex is the best-studied factor in the dysregulation of translation initiation in cancer (**Figure 1.5**). eIF4E binds to the cap structure at the 5' end of a mRNA and recruits eIF4B and the 43S complex to form a 48S initiation complex, which is the rate limiting step for translation initiation [122]. In quiescent cells, eIF4E is inactivated by binding to its binding partner 4EBP, as

4EBP binding prevents interaction between eIF4E and eIF4G to form the eIF4F complex [123, 124]. However, during mitosis or in stress conditions, 4EBP is phosphorylated, leading to release of eIF4E [124]. eIF4E is further phosphorylated at serine 209, which increases the binding affinity with the cap structure at the 5' end of a mRNA more than 3 fold and accelerates the protein synthesis rate [125]. eIF4E is phosphorylated by a mitogen and stress activated kinase Mnk1, a downstream effector of the MAPK and P38 MAPK signaling pathways [124, 126, 127]. Mnk1 has been shown to be hyperactivated in various cancers as the result of dysregulation of the MAPK signaling pathways [127-131]. Functionally, phosphorylation of eIF4E promotes the invasion and metastasis of prostate and breast cancers through the regulation of metastasis associated genes including MMP3, MMP9, VEGF, and Snail [128, 130, 132-134]. In addition to post-translational modifications, eIF4E is also regulated at the transcriptional level. In this regard, the *eIF4E* gene promoter has E-box sequences and *eIF4E* is a direct target gene of c-Myc, an oncogene that is implicated in many cancers [135-137]. *eIF4E* mRNA levels are increased by the dysregulation of the c-Myc signaling pathways in cancer [108, 135]. In addition, mTOR directly binds to 4EBP and phosphorylates 4EBP, leading to release and activation of eIF4E [138, 139]. Thus, dysregulation of the PI3K/Akt/mTOR signaling pathway increases the function of eIF4E through inactivation of 4EBP (**Figure 1.5**) [110, 138-141].

The function and regulation of eIF4A and eIF4B are also well studied. eIF4A is an ATP-dependent helicase that unwinds the secondary structure of mRNAs [142]. eIF4B is a cofactor of eIF4A; binding of eIF4B to eIF4A increases the ATP binding affinity of eIF4A by ~10-fold and increases translation rates [142, 143]. eIF4A is also a direct target of c-Myc and its expression is affected by the c-Myc signaling pathways [137]. eIF4B is phosphorylated at Serine 422 by ribosomal protein S6 kinase (S6K) and p90 ribosomal S6 kinase (RSK), which increases its

binding to mRNAs and increases translation rates [144, 145]. The phosphorylation and activation of eIF4B through S6K and RSK is regulated by the PI3K/Akt/mTOR and RAS/MAPK signaling pathways [144, 145]. More interestingly, eIF4A expression is associated with cap-independent translation. In this regard, eIF4A has been shown to be required for the unwinding of G-quadruplex structures at the 5' UTR of mRNAs for IRES-mediated translation of many oncogenes such as *Notch1*, *BCL2*, *RUNX1*, *CCND3*, *c-Myc*, *Myb*, *MDM2*, and *LEF-1* in leukemia [146, 147].

eEF2 is an important factor being studied in the translation elongation step. eEF2, which promotes the translocation of ribosomes, can be phosphorylated and thus completely inactivated by the eEF2 kinase [148]. eEF2 kinase is phosphorylated and inactivated by S6 kinase, cdc2-cyclin B and cdk2-cyclin A complexes [148-150]. Therefore, the PI3K/Akt/mTOR signaling pathways or direct cell cycle signals increase eEF2 activity and thus promote the translocation of ribosomes **(Figure 1.5) [148-150]**. Importantly, overexpression of eEF2 kinase can also inhibit global mRNA translation, and has been found to be associated with resistance and survival of cancer cells under nutrition deprivation conditions [151].

In addition, c-myc also binds to the promoters of the *eIF2 $\alpha$* , *eIF4E* and *eIF4G* genes and the expression of these factors is increased by the dysregulation of the c-Myc signaling pathways [135-137]. eIF2 $\alpha$  activity is essential for the formation of the ternary complex in translation initiation. However, eIF2 $\alpha$  can be phosphorylated at Ser 51 by GCN2 (amino acid deprivation activated genes), HCR (haem-controlled repressor) and PKR (Protein kinase R) to inhibit the protein synthesis under stress conditions such as heat shock and virus infection [152, 153]. The phosphorylation of eIF2 $\alpha$  plays a role in the inhibitory regulation of cap-dependent translation initiation [152, 153]. The overexpression of other translation-associated factors, such as eIF2 $\alpha$ ,

eIF3, eIF5A, and eIF6, has been shown to be associated with the poor survival of patients with different types of cancer [108, 110]

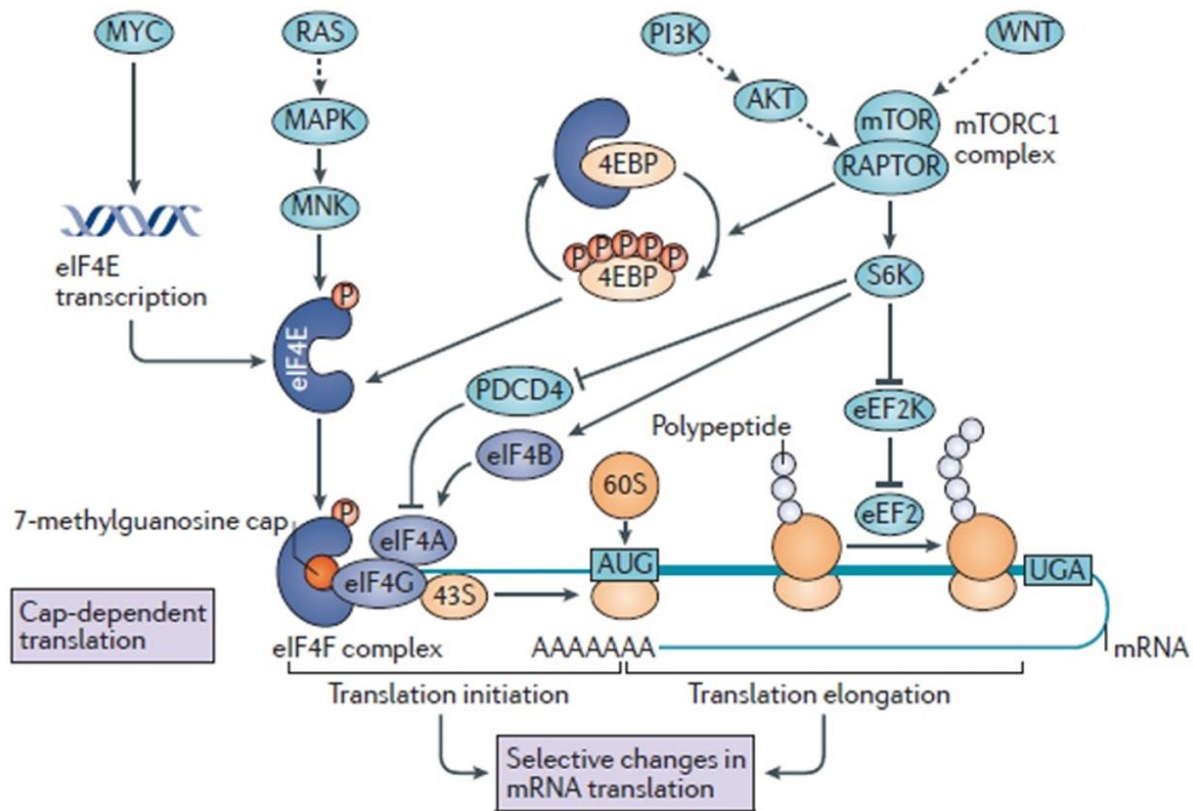


**Figure 1.5 Regulation of mRNA translation by the oncogenic signaling pathways.**

eIF4E expression is up-regulated through the c-Myc signaling pathways. eIF4E is hyperactivated when phosphorylated via the Ras and AKT signaling pathways. The AKT signaling pathway can also inactivate 4EBP which is an inhibitor of eIF4E, thereby increasing the function of eIF4E. In addition, both eIF4B and eEF2 can also be regulated by the PI3K/AKT/mTOR signaling pathways through the activation of ribosomal protein S6 kinase (S6K). This figure has been reused with permission from Springer Nature (Nature Reviews Cancer) License Number: 4627990695708, Morgan Truitt et al. [110]

### 1.2.2.2 Structures and modifications of mRNA in cancer

The secondary structures at the 5' UTR of mRNAs such as the IRES and G-quadruplex structures, as well as mRNA modifications, are gaining increasing attention in translational control.

IRES sequences that are associated with cap-independent translation were found at the 5' UTR of 10% to 15% of all mRNAs, including proto-oncogene mRNAs, such as *c-Myc*, *HIF-1 $\alpha$* , *EGFR*, and *VEGF* [154, 155]. For instance, c-Myc is highly expressed in HeLa cells and liver cancer cells, and the IRES translation initiation but not cap-dependent initiation of *c-Myc* is highly active in these cancer cells [156]. When *c-Myc* IRES sequences were inserted into a luciferase gene reporter vector and transfected into these two types of cancer cells, the translation rate of IRES-regulated gene expression increased by more than 50 fold [156]. Moreover, mutations in *c-Myc* IRES sequences have also been shown to be associated with c-Myc dysregulation and tumorigenesis in multiple myeloma [157, 158]. For example, a “C” to “T” mutation in *c-Myc* IRES sequences was found in 42% of multiple myeloma patients, contributing to the increased expression of c-Myc [158]. When this mutated *c-Myc* IRES sequence was transfected into multiple myeloma cells, the translation rate of luciferase reporter enzyme increased by ~6-fold compared to wild type IRES [159]. In addition, IRES-dependent initiation is increased in response to environmental stresses, including nutrient deprivation, heat shock, hypoxia, and DNA damage. [112, 117]. For instance, while global protein expression was inhibited under stress conditions such as hypoxic and serum starvation, the expression of c-Myc, VEGF, and HIF-1 $\alpha$  was maintained via the IRES-mediated translation initiation in HeLa cells [160].

G-quadruplex, a guanine-rich four-stranded structure at the 5' UTR of some mRNAs, has been shown to affect the translation of oncogenes, such as *NRAS*, *c-Myc*, *EGFR*, and *BCL2*. G-quadruplexes were first found to act as repressors in *NRAS* mRNA translation. Deletion or

mutation of G-quadruplex structures in *NRAS* mRNA increases translation of NRAS by more than 3.5-fold [161]. Similarly, deletion of G-quadruplex structures in *BCL2* mRNA increased translation by 3.5 fold [162]. It has been shown that eIF4A (RNA helicase) unwinds G-quadruplex structures. For example, inhibition of eIF4A did not alter *c-Myc* and *CyclinD3* RNA levels but inhibited MYC and Cyclin D3 protein levels because translation was obstructed by the G-quadruplex structure when eIF4A was inhibited [146]. Similarly, the unwinding of G-quadruplex by eIF4A is required for VEGF IRES cap-independent translation initiation under stress conditions [163, 164].

N<sup>6</sup>-methyladenosine (m<sup>6</sup>A), the most abundant modification in mRNAs, is catalyzed by the methyltransferase like 3 (METTL3) complex [165-167]. The m<sup>6</sup>A at the 3' UTR of *SOX2* recruits the mRNA stabilizer human antigen R (HuR) and is required for the stability of *SOX2* in glioblastoma cells [168]. Knockdown of METTL3 in glioblastoma stem cells decreased SOX2 protein levels and inhibited the radiation resistance associated with glioblastoma stem cells, an effect that could be rescued by the overexpression of 3'UTR-less *SOX2* [168]. Moreover, knockdown of METTL3 decreased the expression of 2110 m<sup>6</sup>A associated genes including 261 apoptosis and cellular stress response genes, and reduced the viability of HeLa cells [169]. In contrast to the stability aspect, m<sup>6</sup>A can also be bound by m<sup>6</sup>A reader proteins such as YTHDF2 which marks mRNAs for degradation in processing bodies [170]. m<sup>6</sup>A can be demethylated by demethylases, such as fat mass and obesity associated (FTO) and  $\alpha$ -ketoglutarate-dependent dioxygenase ALKB homologue 5 (ALKBH5) [171, 172]. Demethylation of m<sup>6</sup>A prevents mRNA degradation in developing spermatogenic cells [173]. FTO has been shown to demethylate the m<sup>6</sup>A of mRNAs such as *PD-1* and *SOX10* and prevent the binding of YTHDF2 and degradation of mRNAs in processing bodies [174]. High levels of FTO promotes proliferation and inhibits

treatment response in melanoma cells [174]. Similarly, knockdown of ALKBH5 decreased the expression of specific mRNAs including *FOXMI* and *BCL2* and inhibited the proliferation of glioblastoma cells [172]. High levels of ALKBH5 are associated with poor survival of glioblastoma patients [172].

In addition, many mRNAs have upstream open reading frames (uORFs) at the 5' UTR [175, 176]. The function of uORFs is not clear. Normally, uORFs suppress translation by blocking the 48S pre-initiation complex or contains premature stop codons to produce non-sense peptides [175-178]. However, under stress conditions (hypoxia or starvation conditions), the 48S pre-initiation complex shows a preference for scanning through uORFs to the main ORF, resulting in increased expression of genes with uORFs such as GCN4, ATF4, and ATF5 [177].

### **1.2.2.3 tRNAs in the translation of cancer**

Alterations in tRNA, tRNA synthetases, and tRNA modifications are also implicated in cancer. For instance, tRNA expression has been shown to be globally increased by more than 3-fold in breast cancer cells compared to normal breast cells, and by more than 10-fold in breast cancer tissue compared to normal breast tissue [179]. The high expression of specific tRNAs such as tRNA<sup>Arg</sup> isoacceptors is associated with the elevated expression of many cell cycle genes (such as cyclin D1) and transcription factors (such as c-Myc) [179]. Moreover, multi-tRNA synthetases such as methionyl-tRNA, threonyl-tRNA, leucyl-tRNA, tryptophanyl-tRNA synthetases are overexpressed in multiple cancers, and are considered to be poor prognosis markers [180]. Interestingly, many tRNAs are enzymatically cleaved under stress-induced conditions, and this plays a role in translation regulation [181]. These tRNA-derived halves bind to the 3' UTRs of multiple oncogenic mRNAs, such as eIF4G, eIF3B, AKT, and HMGA1, in breast cancer cells and inhibit the translation of these mRNAs. The tRNA-derived halves are increased under stress

conditions such as hypoxia or starvation, thereby suppressing the proliferation and invasion of cancer cells [182]. In this regard, RNA methyltransferase NSUN2-mediated cytosine methylation at the variable loop of tRNAs prevents the cleavage and degradation of tRNAs by the endonuclease angiogenin [183]. NSUN2 is upregulated by the oncogene c-Myc in various cancer tissues, and knockdown of NSUN2 increases the tRNA-derived halves and thus inhibits global protein synthesis in cancer cells [184].

### **1.3 Ribosome biogenesis and ribosomal regulation in cancer**

As ribosomes are the site of mRNA translation and protein synthesis, the level of ribosome synthesis and modifications of ribosomal RNAs and proteins can directly affect translation in cancer cells. Therefore, ribosomal regulation is also an important mechanism of translational control and dysregulation of this regulation is implicated in cancer. In this section, I will review rRNA synthesis and modifications and ribosome biogenesis in normal biology and in cancer.

#### **1.3.1 Ribosomal DNAs (rDNAs), rRNA modifications, and ribosome biogenesis**

##### **1.3.1.1 Structure of nucleoli and rDNAs**

Human rDNAs are located on the short arms of 5 pairs of acrocentric chromosomes, including chromosomes 13, 14, 15, 20, and 21 [185]. Each chromosome has around 30 to 40 copies of rDNAs that are clustered together, and there are totally around 300 to 400 copies of rDNAs in human cells [186-188]. These tandem repeated rDNA sequences form numerous nucleolus organizer regions (NORs), which form the core of the nucleolus [189].

Under the electron microscope, three types of components in the nucleolus can be recognized: the fibrillary center (FC), the dense fibrillary component (DFC) area, and the granular component (GC). The NORs are recognized as the FCs of the nucleolus where rDNAs accumulate and are transcribed. At the outer edge of FCs, there is an irregular dense fibrillary area (known as the DFC) which contains transcribing rDNAs, transcription factors, splicing factors, and modifying enzymes. rDNA transcription, precursor-rRNA processing and modifications occur in these DFC regions [189]. After splicing and modifications, the rRNAs are assembled with ribosomal proteins to form ribosome subunits, a process that occurs mostly in the GC area of the nucleolus [189]. There are more than 700 proteins in the nucleolus that are involved in ribosome biogenesis [190].

The length of each rDNA is around 43 kb, including an ~30 kb of intergenic spacer (IGS) region and a ~13 kb transcribed region (**Figure 1.6**) [191]. The IGS contains enhancers, spacer promoter, upstream control elements (UCE), and core elements (e.g. promoter), and is involved in the regulation of rDNA transcription (**Figure 1.6**) [192, 193]. From the 5' end to 3' end, the gene sequences of the transcribed region are composed of a 5' external transcribed spacer (5'ETS), 18S rRNA sequences, internal transcribed spacer 1 (ITS1), 5.8S rRNA sequences, internal transcribed spacer 2 (ITS2), 28S rRNA sequences, and 3' external transcribed spacer (3'ETS) (**Figure 1.6**) [192, 193].

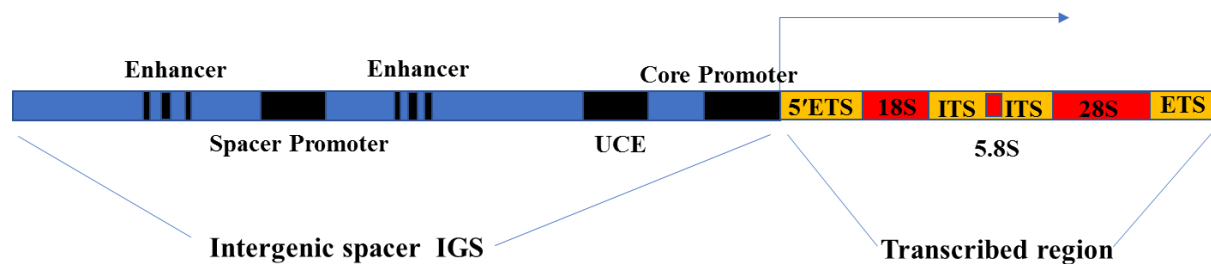


**Figure 1.6 The structure of a rDNA repeat.**

rDNA consists of an intergenic spacer (IGS) and a transcribed region. The IGS includes enhancers, spacer promoter, UCE, and core promoter. From the 5' end to 3' end, the transcribed region is composed of the 5'ETS, 18S rRNA sequences, ITS1, 5.8S rRNA sequences, ITS2, 28S rRNA sequences, and 3'ETS. This figure has been modified with permission from ANNUAL REVIEWS, License number: 4630641084964, Lawrence J. Weider, et. al.

### 1.3.1.2 rDNA transcription

rDNAs are transcribed into the precursor rRNA (47S rRNA) by rRNA polymerase I. rRNA Polymerase I is a large molecular complex of 580 kDa that contains 14 protein subunits with different functions in the synthesis of precursor rRNA. The initiation of rDNA transcription involves a series of transcription factors. The two most well-studied transcription initiation factors

are Selective Factor 1 (SL1) and Upstream Binding Factor (UBF) (**Figure 1.7**) [194-201]. Two UBFs are recruited and bind to the UCE region as a dimer. The UBF dimer bends and unwinds the upstream region of rDNA, which allows the binding of other transcription initiation factors and RNA Polymerase I [202]. Specifically, the UBF dimer recruits SL1 to bind to the promoter area of rDNAs, and then SL1 recruits RNA Polymerase I and other transcription initiation factors such as TIF-1B to initiate transcription [194-197]. Unlike 47 rRNA, 5S rRNA is transcribed by RNA Polymerase III.

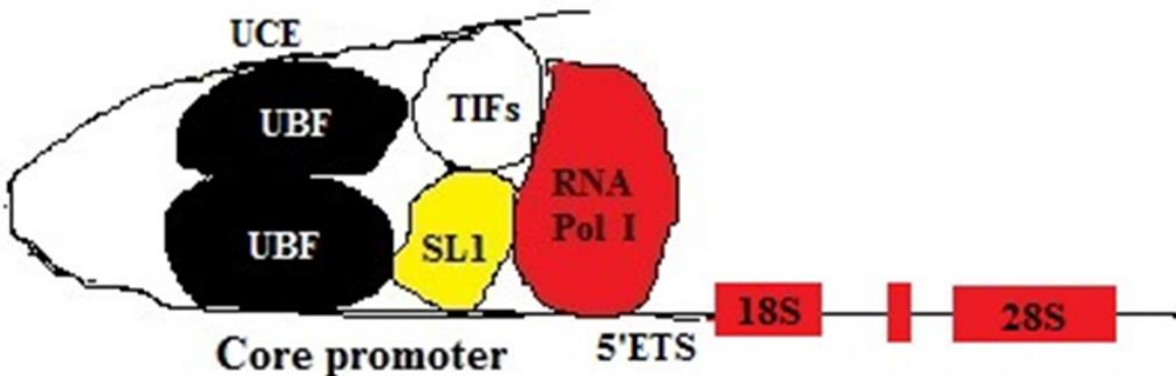


**Figure 1.7 Transcription initiation and the binding of its key factors.**

Two UBFs are recruited to the UCE region, forming a dimer that binds to the UCE. The UBF dimer bends and unwinds the upstream region of rDNA, and recruits the binding of SL1, other transcription initiation factors, and RNA Polymerase I to initiate transcription.

rDNA transcription is regulated by a few signalling pathways through activation of the transcription factors. For instance, UBF is phosphorylated through the PI3K/Akt/mTOR and Ras/Raf/Mek/Erk signalling pathways [198-201]. After UBF phosphorylation, SL1 is recruited and stably bound to UBF. However, the binding of SL1 can be dissociated by the regulation of the

phosphatase PTEN [196, 197, 203]. In addition, c-Myc that is upregulated by multiple signalling pathways, including the PI3K/Akt/mTOR and Ras/Raf/Mek/Erk signalling pathways directly binds to the promoter area of rDNA and stimulates its transcription [204-208]. Normally, the regulation of rDNA transcription is associated with nutrients, such as glucose and amino acids, and growth factors. However, the abnormal activation of these pathways and key regulating proteins, which is commonly observed in rapidly proliferating cancer cells, also promotes abnormally active ribosomal biogenesis [209-211].

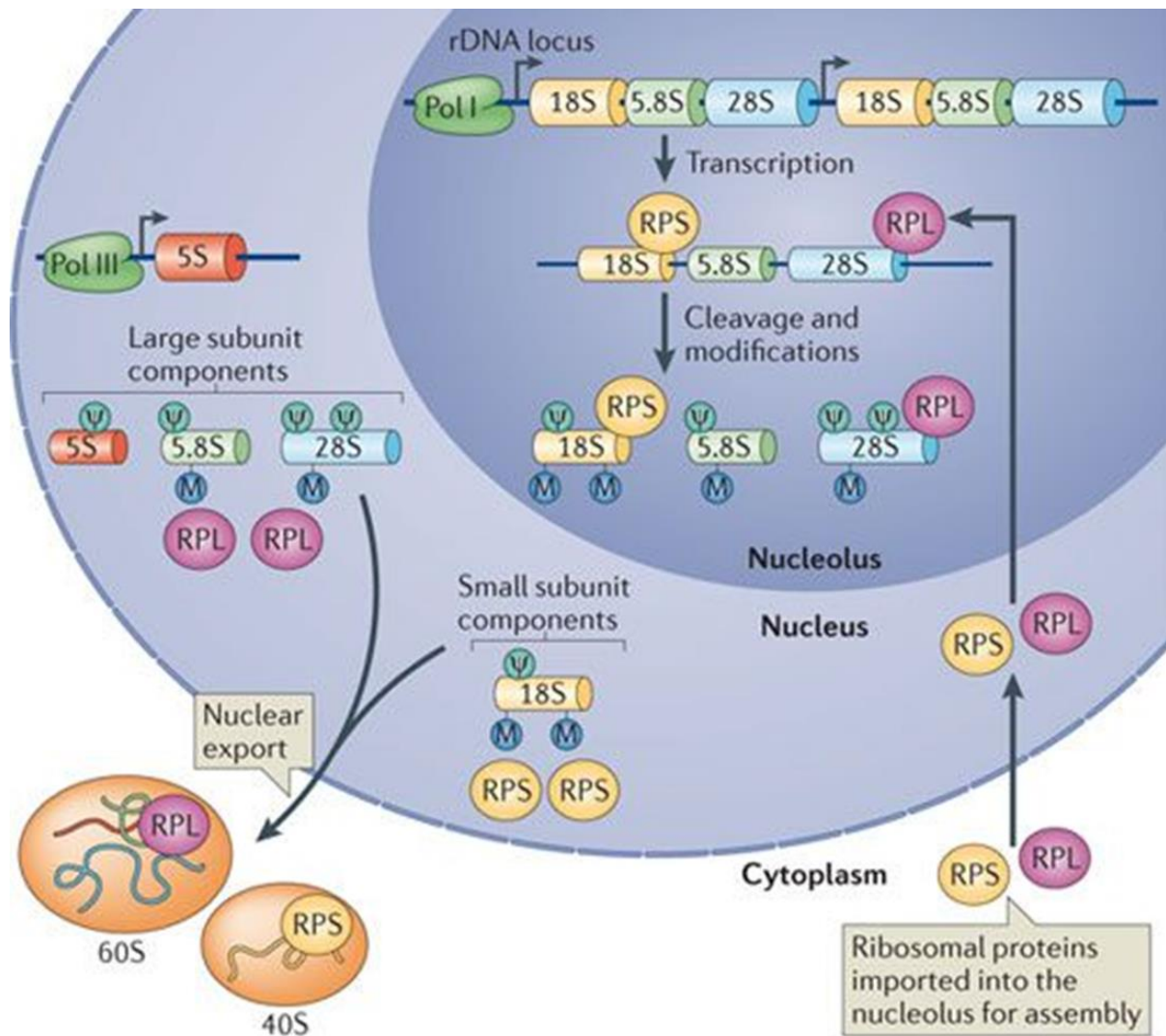
### **1.3.1.3 Ribosome synthesis**

Ribosome synthesis mainly involves the processing of precursor rRNAs, modification of rRNAs, and the assembly of rRNAs with ribosomal proteins. During the splicing process, 47S rRNA is spliced into 18S rRNA, 5.8S rRNA, and 28S rRNA. Small nucleolar RNAs (snoRNAs) play an important role in the rRNA splicing process. SnoRNAs have conserved antisense sequences (10-20 nucleotides) to match with their target sites on 47S rRNA [212-217]. A number of small nucleolar RNAs (e.g., U3, U8, U14 and U22 snoRNA) bind to the ETS or ITS region, and guide the endonucleases and exonucleases to conduct the cleavage of the two flanking ETS, ITS1 and ITS2 [212-217].

18S rRNA, 5.8S rRNA, and 28S rRNA have three types of modifications including methylation of the hydroxyl group at carbon 2 of ribose (2'-O methylation), uridine pseudouridylation, and base modifications. In human rRNAs, totally 228 modification sites have been identified: 112 2'-O methylation sites, 104 pseudouridylation sites (pseudouridine,  $\Psi$ ), and 12 base methylation sites (including 2 sites for  $m^5C$ ,  $m^6A$ ,  $m^6_2A$ , and  $ac^4C$ , and 1 site for  $m^1A$ ,  $m^7G$ ,  $m^3U$  and  $m^1acp^3\Psi$ ) [218-220]. SnoRNAs guide the enzymes (methyltransferases and pseudouridine synthases) to the

rRNAs for the modification process [221-224]. Generally, C/D box snoRNAs are associated with 2'-O methylation, whereas H/ACA box snoRNAs are associated with pseudouridylation [221-224]. Studies in yeast and bacteria have shown that the modification sites are predominantly located at the functional center of rRNAs [218].

The assembly of rRNAs with ribosomal proteins takes place at the same time as precursor rRNA splicing and modification (**Figure 1.8**). Ribosomal proteins are synthesized in the cytoplasm and are transported into the nucleus through the nuclear pore. In human, 18S rRNA is assembled with 33 ribosomal proteins to form the small 40S ribosomal subunit (SSU) [225]. The 5S, 5.8S and 28S rRNAs are assembled together with 46 ribosomal proteins to form the large 60S ribosomal subunit (LSU) [225]. The 40S SSU and 60S LSU are exported to the cytoplasm where they attach to the endoplasmic reticulum or exist free in the cytoplasm. For translation, SSU and LSU are assembled to form an 80S ribosome.



Nature Reviews | Molecular Cell Biology

**Figure 1.8 Ribosome biogenesis.**

28S, 18S, 5.8S rRNA are transcribed and modified in the nucleolus. 5S is transcribed in the nucleus, and ribosomal proteins are synthesized in the cytoplasm and transported into the nucleolus. The LSU and SSU are exported to the cytoplasm. This figure has been reused with permission from Springer Nature (Nature Reviews Molecular Cell Biology), License Number: 4630681247127, Shifeng Xue et al. [109]

#### **1.3.1.4 The functions of ribosomal structures and rRNA modifications**

The ribosome is the site of mRNA translation and protein synthesis. rRNAs have two main functions. The first one is to support the pairing, decoding, and proofreading of tRNA and mRNA at the decoding center (also called tRNA-mRNA binding center). The decoding center has three tRNA binding sites: aminoacyl-tRNA binding site (A site), peptidyl-tRNA binding site (P site) and tRNA exit site (E site). The second function is to act as a peptidyltransferase that catalyzes the peptide-bond formation at the peptidyl transferase center (PTC). The decoding center is mainly formed by the 18S rRNA, while the PTC is formed by the 28S rRNA. Between the decoding center and PTC, there are many sites and loops for interactions with tRNAs. The interaction between 18S rRNA and 28S rRNA forms the intersubunit bridge. At the secondary structure level, 28S rRNA is divided into six domains and 99 helices, while 18S rRNA is divided into 4 domains and 45 helices. PTC is located at helices 90 to 93 in domain V of 28S rRNA. The tRNA-mRNA binding center is associated with helices 23, 24, 26, 28, 34, and 44 in the central, 3' major, and 3' minor domains of 18S rRNAs. Helices 69 to 71 are located at the intersubunit bridge B2A and B3, respectively. Because bridge B2A and B3 are between the decoding center and PTC, helices 69 to 71 are responsible for ribosome assembly, translation initiation and translation rate [226-228]. Deletion of helix 69 leads to a defect in the association between 50S and 30S subunits in bacteria cells [228]. Helix 69 is required for the release of initiation factor 3 and the start codon selection; deletion of helix 69 decreases the rate of translation initiation by 20-fold in bacteria cells [229]. The rRNA modifications are mainly located at PTC, decoding center, tRNA binding sites, and the intersubunit bridge B2A and B3 areas [230].

Pseudouridine modifications occur at higher frequencies in the more complex eukaryotes [231]. There are 11 pseudouridine sites in *E. coli*, 44 sites in yeast, and 91 sites in human [231]. Generally,

when uridine is pseudouridylated to become reactive pseudouridine, it will have an additional hydrogen bond donor that helps stabilize interactions between RNAs [226]. More specifically, pseudouridine modifications in rRNAs are involved in the regulation of pre-rRNA processing, protein synthesis, and ribosome stabilization [230, 232]. For example, deletion of three pseudouridine modifications at the decoding center slowed down the processing of pre-rRNA, reduced the cleavage of 18S rRNA and the composition of 40S subunit, resulting in a decreased growth rate in yeast [232]. Importantly, lack of a single pseudouridine ( $\Psi$  1191) at the P site of the decoding center inhibited 40S subunit formation, protein synthesis, and cell growth [232]. In another study, deletion of the six pseudouridine modifications at the central loop of PTC altered the structure of 25S, decreased the total number of translating ribosomes, inhibited protein synthesis by ~45%, and decreased growth rate in yeast [230]. Importantly, lack of a single key pseudouridine ( $\Psi$  2919) out of the six pseudouridine in the PTC was enough to decrease protein synthesis by ~20%, and decreased cell growth rate [230].

Generally, 2'-O methylation makes the nucleotides more hydrophobic, which could benefit interactions with other bases [233]. At the decoding center of bacterial 23S rRNA, 2'-O-methylated Gm2251 binds to the C75 at the acceptor stem of tRNA at the P site, and the methyl group binds to the base of U2449 and the ribose of C2065 at the peptidyl tRNA binding loop (P loop) of the 23S rRNA [234]. Moreover, the methyl group of Um2552 interacts with G2553 at the aminoacyl tRNA binding loop (A loop), and the G2553 binds to C75 at the acceptor stem of tRNA at the A site [234]. At the intersubunit bridge, the 2'-O methylation contributes to the interaction and stability of the association. The methyl group of Gm1920 at helix 69 of 23S rRNA interacts with C1496 of 16S rRNA, and the association makes the ribosome more stable at high temperatures [234]. In yeast, deletion of methylation at G1572 in 18S rRNA as the result of mutation of snR57

decreased growth rate by about 20% [235]. However, deletion of methylation of U2347 in 25S rRNA by mutated snR65 increased growth rate by about 20% [235]. Usually, absence of 2'-O methylation at a single nucleotide in 18S rRNA and 25S rRNA would not cause severe growth defect but would lead to increased sensitivity to ribosome specific antibiotics [235].

In addition, the adenine methylation site m<sup>6</sup>A1832 is located at the P site of the decoding center, and absence of A1832 methylation resulting from mutation of its catalyzing enzyme methyltransferase-like 5 (METTL5) decreased protein synthesis rate and impaired the stemness of mouse embryonic stem cells [236, 237]. The cytosine methylation site m<sup>5</sup>C2278 in yeast is located at helices 69 to 71, and m<sup>5</sup>C2780 is located at the PTC center [238]. The C2780 methylation is the focus of this project and will be further reviewed in the following sections.

### **1.3.2 Ribosomal regulation in cancer**

Dysregulation of ribosome biogenesis, which collectively includes increased global ribosome synthesis, abnormal rRNA modifications, overexpression of specific ribosomal proteins, alterations in protein synthesis rates, and increased selective translation of cancer-associated mRNAs, plays an important role in cancer progression (**Figure 1.9**) [239]. In this section, I will discuss the role of dysregulation of rDNA transcription regulation, rRNA modifications, and ribosomal proteins in cancer.

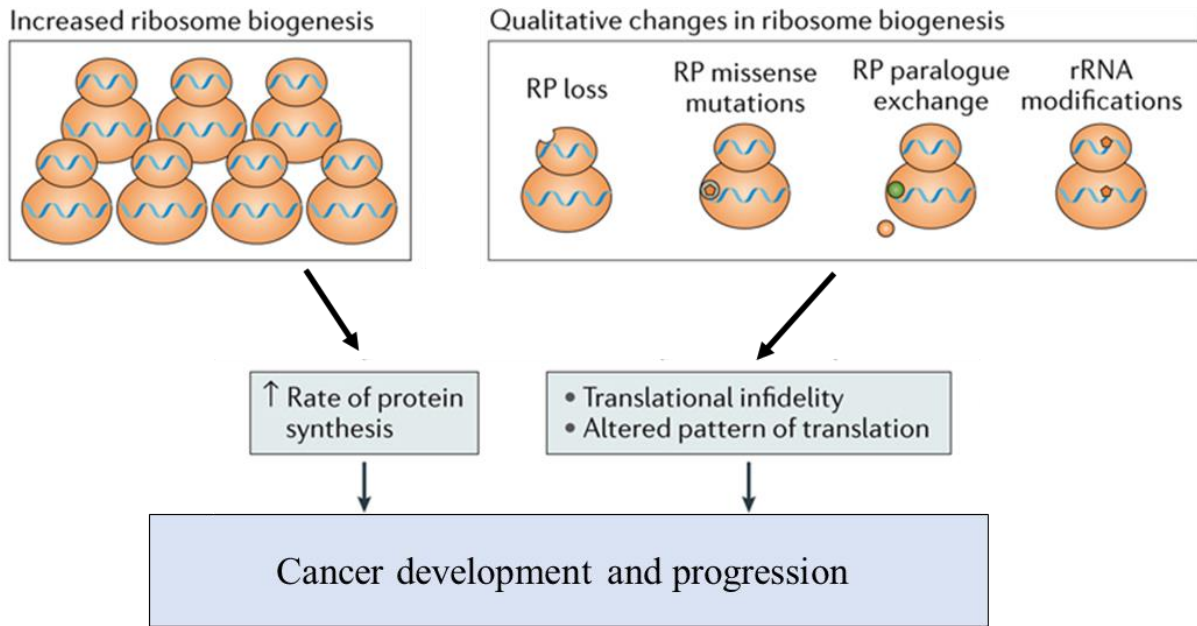


**Figure 1.9 Ribosomal regulation in cancer.**

Dysregulation of ribosome biogenesis, including increased ribosome synthesis, abnormal rRNA modifications, and overexpression of specific ribosomal proteins, alters protein synthesis rates or increases the selective translation of cancer-associated mRNAs, thereby promoting cancer development and progression. This figure has been modified with permission from Springer Nature (Nature Reviews Cancer) License Number: 4627980815061 [239].

### 1.3.2.1 rDNA transcription regulation in cancer

rDNA transcription is mainly regulated by cell cycle associated kinases and the MAP kinase signaling pathways. Elevated rDNA transcription is one of the steps in the dysregulation of cell cycle associated kinases and the MAP kinase signaling pathways associated with the progression of various cancers. Through the regulation of the main component RNA polymerase I, transcription initiation factors (e.g., UBF, SL1, TIF-IA) and c-Myc, rDNA transcription is rapidly increased more than 5-fold upon serum or growth factor treatment conditions, but gradually inhibited under nutrient starvation and stress conditions [240, 241].

Transcription of rDNA is activated at the interphase of the cell cycle, mainly through regulation of the interaction between UBF and RNA polymerase I. UBF is directly phosphorylated and activated by cell cycle-associated kinase complexes in G1, S, and G2 phases [242]. In G1 phase, UBF is phosphorylated at serine 484 by CDK4–Cyclin D1 and CDK2–Cyclin E, which is required for binding to RNA polymerase I [242]. Replacement of serine 484 with alanine severely decreases transcription of rDNA and inhibits cell growth by about 30% [242]. In S and G2 phases, serine 388 of UBF is phosphorylated by CDK2–Cyclin A and CDK2–Cyclin E, which is further required for binding to RNA polymerase I [243]. Conversion of serine 388 to glycine (S388G) impairs the binding of UBF to RNA polymerase I and thus inhibits the transcription of rDNA [243]. Overexpression of wild type UBF increases the activity of a reporter plasmid containing a rDNA gene by about 3-fold in NIH 3T3 cells, whereas overexpression of UBF S388G fails to induce rDNA transcription [243]. Importantly, the release of transcription components from the rDNA promoter is the limiting step in the transcription rate, and the phosphorylation of UBF at threonine 117 and threonine 201 is required for UBF release from the rDNA promoter [200, 244]. ERK directly binds and phosphorylates UBF at threonine 117 and threonine 201, increasing rDNA transcription by about 3-fold [200]. Since Cyclin D1, CDKs and ERK are frequently dysregulated and abnormally activated in various cancers, UBF phosphorylation and rDNA transcription are associated with the progression of these cancers. For instance, upregulation of UBF was found in more than 70% of hepatocellular carcinomas obtained from patients [210]. Inhibition of UBF expression was shown to strongly inhibit the growth of hepatoma cells and even kill the cells *in vitro*, while overexpression of UBF in human fibroblasts increased the proliferation rate by about 1.5-fold [210].

TIF-1A is another key transcription initiation factor involved in activation of rDNA transcription. Phosphorylation of TIF-1A is required for binding to SL1 and RNA polymerase I, which is regulated by ERK signaling and RSK activation [241]. In serum-treated cells, ERK and RSK directly interact with and phosphorylate TIF-1A at serine 633 and serine 649 [241]. Replacement of these two sites with other amino acids impairs rDNA transcription and cell proliferation [241]. In addition, c-Myc was found to directly bind to the E-box located within the promoter region of the rDNA genes and activation of c-Myc was required for rDNA transcription [208, 245]. Meanwhile, c-Myc was also found to bind to the promoter of UBF, and increase the expression of UBF to induce rDNA transcription [211]. The increase in rDNA transcription was an important mechanism for c-Myc driven cancers [246, 247].

rDNA transcription is shut down during mitosis phase, mainly through dissociation of SL1 and UBF. Threonine 852 of TAFI110 (one of the subunits of SL1) is phosphorylated by Cdc2-Cyclin B during M phase, which prevents binding of SL1 to UBF and inhibits rDNA transcription [240, 248]. Moreover, rDNA transcription is also repressed by p53 activity. It has been shown that p53 directly binds to TBP (one of the subunits of SL1) to inhibit the further binding of SL1 to UBF, thereby repressing rDNA transcription. Inhibition of rDNA transcription is lost when p53 is mutated at histidine 175 (His175) [249]. Inhibition of p53 increases, whereas overexpression of p53 inhibits, pre-rRNA synthesis in cancer cells [250-252]. p53 expression is reversely associated with rRNA synthesis and the nucleolar size in human breast carcinoma [73].

### **1.3.2.2 rRNA modifications in cancer**

A total of 112 sites of 2'-O methylation sites and 104 sites of pseudouridylation have been identified in human rRNAs [218-220]. 2'-O methylation of rRNA is conducted by a specific

snoRNP complex consisting of a group of C/D box snoRNAs, rRNA 2'-O methyltransferase fibrillarin (FBL), NOP56 and NOP58. FBL methylates the ribose of the 2' hydroxyl group. Pseudouridylation of rRNA is carried out by a specific snoRNP complex consisting of a group of H/ACA box snoRNAs, Dyskerin (DKC1), NHP2, NOP10, and GAR1. H/ACA box snoRNAs guide the complex to target its complementary sequence on rRNAs. DKC1 is a pseudouridine synthase that catalyzes the isomerization of uridine. Modifications of rRNAs by FBL and DKC1 are associated with tumor progression.

FBL is overexpressed in breast cancer and prostate cancer tissues compared with the matched normal tissues [253]. The expression of FBL is associated with the poorer survival of patients with breast cancer, prostate cancer, and squamous cell cervical carcinoma [253-256]. High levels of FBL increase the methylation status of most of its target sites in the ribosomes of breast cancer cells, especially those at the decoding center of 18S rRNA [256]. The newly synthesized ribosomes in cells with high FBL expression promote IRES-mediated translation of oncogenes, such as IGF1R, FGF1, and EMCV [256, 257]. Moreover, FBL overexpression decreases translational fidelity, resulting in a surplus of premature stop codons and amino acid misincorporations [256]. Knockdown of FBL or its C/D box snoRNP complex components (NOP56 and NOP58) markedly inhibits the expression of snoRNAs and thus ribosome biogenesis [253].

The expression of FBL is regulated by c-Myc and p53 [253, 256]. Overexpression of c-Myc increases, whereas knockdown of c-Myc decreases, the expression of FBL [253]. p53 binds to the first intron of the *FBL* gene to inhibit its transcription; thus, FBL is expressed at low levels in wild type p53 cancer cells, but is highly expressed in p53 mutated or inactivated cells [253, 256]. Interestingly, knockdown of FBL increases p53 expression by increasing IRES translation of p53 mRNA and by stabilizing p53 protein through increased levels of RPL5 and RPL11 in the

cytoplasm. The latter form a complex with p53 which prevents its degradation. p53 and FBL regulate each other, forming a negative feedback loop [253, 256]. FBL knockdown inhibits, whereas FBL overexpression increases, tumorigenesis of breast cancer [253, 256].

Overexpression of DKC1 is associated with the progression of colorectal, hepatocellular, and prostate cancers [258, 259]. DKC1 is more highly expressed in colorectal cancer and glioma tissues compared to matched normal para-tumor tissues [259, 260]. In the *DKC1* mutation mouse, ribosomal RNA pseudouridylation sites are decreased by about 25% [261, 262]. The newly synthesized ribosomes with lower rRNA pseudouridylation decrease tRNA binding and translation fidelity, and more importantly, fail to translate mRNAs with IRES elements, including HIF-1 $\alpha$ , VEGF, p53, p27, Bcl-xL, and XIAP [261, 262]. For instance, DKC1 knockdown inhibits, whereas DKC1 overexpression increases the expression of HIF-1 $\alpha$  and VEGF in colorectal cancer cells, and thus regulates the angiogenesis and metastasis of colorectal cancer [259]. Inhibition of DKC1 in glioblastoma cells causes cell cycle arrest and inhibits the proliferation and migration of glioblastoma cells [260]. The expression of HIF-1 $\alpha$  and MMP2 is decreased when DKC1 is knocked down in glioma cells [260]. Activation of IRES-dependent translation of p53 mRNA is impaired in DKC1-depleted human breast cancer cells treated with deferoxamine [263].

Like FBL, DKC1 is also a direct target of c-Myc [264]. c-Myc directly binds to the promoter and the first intron of the *DKC1* gene to regulate its expression [264]. Lack of DKC1 slows down rRNA processing, decreases the total number of 80S ribosomes and inhibits the expression of FBL in the nucleoli of hepatocytes [265]. Moreover, lack of DKC1 induces the expression of p53 and p21, resulting in complete inhibition of the cell cycle and proliferation [265]. Knockdown of DKC1 increased degradation of incomplete ribosomes, and increased free RPL5 and RPL11 in the cytoplasm to prevent p53 protein degradation [253, 256].

### **1.3.2.3 Ribosomal protein regulation in cancer**

The dysregulation of ribosomal proteins has also been shown to be associated with cancer [266-271]. For instance, overexpression of RPL13, RPL15 and RPL19 is associated with the progression of gastric and intestinal cancers [268-270], while the expression of RPL22 is decreased in lung cancer [267]. Ribosomal protein composition heterogeneity was found in different tissues and even in cell lines. For instance, RPL10A, RPL38, RPS7, and RPS25 are found in significantly lower levels in the ribosomes of mouse embryonic stem cells [272]. RPL10A and RPS25 are located next to the mRNA exit tunnel of ribosome, and loss of RPL10A or RPS25 in ribosomes selectively increases or decreases the translation of certain specific subgroups of mRNAs in mouse embryonic stem cells [272]. Interestingly, RPL10A is involved in IRES translation: loss of RPL10A impairs the translation of viral IRES elements such as Cripavirus and HCV IRES elements and decreases cap-independent translation of *Igf2*, *App*, and *Chmp2* mRNAs in mouse embryonic stem cells [272]. Moreover, when the ribosome is damaged or degraded by physical or cytotoxic factors, ribosomal proteins play a role in the stress response [273]. For instance, RPL5 and RPL11 released from nucleoli bind to MDM2, which prevents the interaction of MDM2 with p53 and thereby inhibits the ubiquitination and degradation of p53 [273, 274].

In addition, the composition of ribosomal proteins in the whole ribosome is also associated with the modification of rRNAs. For instance, loss of the methylation at 3 bases located in helix 70 and helix 71 of yeast 25S rRNA (cytosine methylation of C2278 and 2'-O methylation at G2288 and A2281) led to ribosome instability, and more importantly, caused the loss of many ribosomal proteins in the 60S subunit (Rpl9, Rpl23, Rpl24, Rpl31, and Rpl38) [275]. These results indicate that the methylation status of rRNA can affect the binding of ribosomal proteins, and thus the conformation of ribosomes [275].

## **1.4 RNA modifications, RNA cytosine methylation, and NSUN proteins**

### **1.4.1 RNA modifications and enzymes**

According to Modomics (a database of RNA modification), there are more than 160 types of RNA modifications and 340 functional enzymes and co-factors involved in RNA modification across all species [276]. RNA modifications at selective sites regulate the biology and function of all RNAs, including splicing, nuclear export, stability, and translation of mRNAs, as well as the expression, structure and functions of non-coding RNAs (e.g., tRNAs and rRNA), thereby altering both mRNA levels and translation [277-279]. This regulatory mechanism via RNA modifications has been referred to as epitranscriptomics or RNA epigenetics [277, 280].

#### **1.4.1.1 tRNA modifications and enzymes**

tRNAs have the most extensive nucleotide modifications among the RNAs, as there is an average of 13 modifications out of a total of 76 nucleotides in most tRNAs [281]. More than 42 types of modifications have been found in eukaryotic tRNAs [282]. The modifications include  $\Psi$ , 2'-O-methylation,  $m^5C$ ,  $m^6A$ ,  $m^1A$ ,  $m^7G$ ,  $m^2G$ , base thiolation, inosine modification, and some more complex modifications ( $acp^3U$ ,  $mnm^5U$ ,  $ms^2i^6A$ ). Modifications are mainly located at the anticodon loop, D loop, T loop and variable loop.

The modifications at the anticodon loop are directly associated with base pairing during the translation process [281]. Modifications at the wobble position (position 34) of the anticodon loop ensure correct and diverse codon recognition in mRNA decoding, and increases the fidelity and efficiency of translation [283-285]. Many adenosines at position 34 are modified by adenosine deaminase acting RNA (ADAR) to form inosine (I), and inosine at the wobble position can pair with cytosine, adenine, and uracil. Inosine pairing increases translation efficiency and is required

for cell cycle progression [285]. The thiolation and methoxycarbonyl methylation of Uridine 34 ( $mcm^5s^2U$ ) increases the binding rate of lysine tRNA (UUU) to the ribosomal A site and promotes translation efficiency [283]. The cytosine 34 of mitochondrial methionine tRNA is methylated and dioxygenated by NSUN3 and ABH1, respectively [284]. Modification at C34 is required for protein synthesis and mitochondrial activity [284]. The isopentenyladenosine ( $i^6A37$ ) modification at position 37 of the anticodon loop prevents frameshifting during decoding [286]. Cytosine at position 38 of many tRNAs is methylated by DNA methyltransferase homologue (DNMT2), and  $m^5C$  modification prevents the codon mistranslation and fragmentation of tRNAs [287].

Modifications in the body of tRNAs such as at the T, D or variable loops, are mainly associated with the stability and functional folding of the cloverleaf-like secondary structure of tRNAs. For instance, pseudouridine synthase 1 (PUS1) catalyzes the pseudouridylation at positions 27, 34, 36, and 67 of the isoleucine tRNA, thereby stabilizing the tRNA structure, a requirement for the nuclear export of tRNAs [288-290]. PUS4 catalyzes the pseudouridylation at position 55 in the variable loop [290]. Deletion of PUS1 or PUS4 results in destabilization of the tRNA 3-dimensional structure, leading to cell death [288, 290].  $m^5C$  at position 48, 49, or 50 in the variable loop is methylated by NSUN2 [183], with methylation preventing the degradation of tRNAs. Loss of NSUN2 increases the cleavage of tRNAs and decreases protein synthesis rates [183].

#### **1.4.1.2 mRNA modifications and enzymes**

mRNAs, serving as templates for protein synthesis, have multiple types of RNA modifications including  $m^6A$ ,  $m^5C$ ,  $\Psi$ , 2'-O-methylation,  $m^1A$ ,  $m^6Am$  [165, 291-294].  $m^6A$  is the most abundant modification, with an average of three  $m^6A$  sites in every mRNA [165-167].  $m^6A$  sites are found in the 3' UTR (57%), CDS (35%), 5' UTR (8%) of the mRNAs, but are mostly enriched near the

stop codon [295]. m<sup>6</sup>A is methylated by methyltransferase like 3 (METTL3) with the assistance of many interaction proteins such as METTL14, METTL16, Wilms' tumor 1-associating protein (WTAP), and RNA-binding motif protein 15 (RBM15) [169, 296, 297]. The m<sup>6</sup>A methylation is a marker of translation or turnover of mRNAs.

m<sup>6</sup>A methylation is recognized and bound by YTH domain family proteins including YTHDF1, YTHDF2, YTHDC1, YTHDC2, and these proteins are termed 'reader proteins of m<sup>6</sup>A' [170, 295, 298]. YTHDF1 specifically binds to the m<sup>6</sup>A sites of its target mRNAs and promotes the translation efficiency of these mRNAs through further interactions with initiation factors and the ribosomal subunits [298]. In contrast, YTHDF2, when specifically bound to the m<sup>6</sup>A sites of its target mRNAs, transports them to decay sites, and causes their degradation through further binding to degradation processing bodies [170]. 50% of the target mRNAs of YTHDF1 and YTHDF2 are the same [298]. Similarly, YTHDC2 binds to m<sup>6</sup>A sites at the coding region of its target mRNAs, and promotes protein synthesis through interaction with small ribosomal subunits [295, 299]. YTHDC1 mediates transcriptional silencing and translation repression by binding with RNA X-inactive specific transcripts [297]. In addition, m<sup>6</sup>A can be demethylated by the fat mass and obesity associated (FTO) or  $\alpha$ -ketoglutarate-dependent dioxygenase AlkB homologue 5 (ALKBH5), with FTO and ALKBH5 termed 'eraser proteins of m<sup>6</sup>A' [171, 172]. The demethylation of m<sup>6</sup>A sites located at the 3' UTR prevents the degradation of the target mRNAs [173].

There are thousands of mRNAs with m<sup>5</sup>C sites in different mouse tissues and HeLa cells [292]. Each of these mRNAs has two to three m<sup>5</sup>C sites located in the CDS (45%), intron (20%), 5' UTR (19%), or 3' UTR (16%) [292]. The average methylation rate at each site is about 20% (mostly

varying between 10% and 40%) [292]. An m<sup>5</sup>C site is found in ~4000 mRNAs, with 1,158 mRNAs catalyzed by NSUN2, an mRNA m<sup>5</sup>C writer protein [292, 300]. Knockdown of NSUN2 decreased by about 40%, while overexpression of NSUN2 increased by about 3-fold, total m<sup>5</sup>C methylation levels [292]. m<sup>5</sup>C sites are required for the recognition and binding by ALYREF (mRNA m<sup>5</sup>C reader protein) [292]. Once bound to ALYREF, the m<sup>5</sup>C mRNAs are exported from the nucleus to the cytoplasm [292]. Moreover, the m<sup>5</sup>C sites in mRNAs have been found to be associated with the stability of mRNAs [301]. m<sup>5</sup>C sites in mRNAs are recognised by the Y-box binding protein 1 (YBX1), with YBX1 further recruiting embryonic lethal abnormal vision like 1 (ELAVL1, or HuR) that stabilizes and promotes the translation of mRNAs [300, 301]. m<sup>5</sup>C in mRNAs is required for YBX1 and ELAVL1 to promote tumorigenesis in multiple cancers [301, 302].

There are 260 Ψ modification sites in 238 yeast mRNAs, and 96 Ψ modification sites in 89 human mRNAs [291]. The human Ψ modification sites are located in CDS (64.6%), 3' UTR (31.2%), or 5' UTR (4.2%) [291]. The majority of Ψ sites are catalyzed by PUS proteins including PUS1, PUS2, PUS3, PUS4, PUS7, but not DKC1 [291]. Unlike the DKC1 complex, PUS proteins recognize and target distinct RNA sequences and catalyze target RNAs independently. The total number and modification levels of Ψ sites are increased upon nutrient deprivation or heat shock in yeast, and serum starvation in human cells [291, 303]. For instance, yeast cells in log growth phase have only 58% of the total Ψ sites found in yeast cells in post-diauxic growth phase, with 41% of the Ψ sites in log growth phase having only half of the modification of yeast cells in the post-diauxic growth phase [291]. Knockdown of pseudouridine synthases decreases mRNA levels upon heat shock [303]. These observations might suggest Ψ modifications are increased to protect the stability of mRNAs under nutrient deprivation, serum starvation or heat shock [303].

### 1.4.1.3 rRNA modifications and enzymes

rRNA makes up about 80% of total RNA, and there are 228 modification sites with at least 10 types of RNA modifications in human rRNA including 104  $\Psi$  sites, 112 2'-O-methylation sites, 2  $m^5C$ ,  $m^6A$ ,  $m^6_2A$ ,  $ac^4C$  sites, each, and 1  $m^1A$ ,  $m^7G$ ,  $m^3U$  and  $m^1acp^3\Psi$  site, each [220]. Two main modifications (pseudouridylation and 2'-O-methylation) are associated with the stability of the rRNA structure, and interaction with tRNA and translational factors. In addition to DKC1 and FBL which regulate these two modifications as previously described, some studies have focused on  $m^6A$  and  $m^5C$  modifications in rRNA. For instance,  $m^6A1832$  is located at the decoding center of mouse 18S rRNA and is methylated by METTL5. Deletion of A1832 methylation decreases protein synthesis rate and impairs the stemness of mouse embryonic stem cells [236, 237]. Similarly,  $m^6A4220$  is located at the PTC of human 28S rRNA and is methylated by Zinc Finger CCHC-Type Containing 4 (ZCCHC4) [237, 304]. Knockout of ZCCHC4 decreases global protein synthesis and proliferation of hepatocellular carcinoma cells [304]. The cytosine methylation site  $m^5C2278$  in yeast is located at helices 69 to 71, and  $m^5C2780$  is located at the PTC center [238].  $m^5C2278$  is methylated by NSUN5, whereas  $m^5C2780$  is methylated by NSUN1 [238].

### 1.4.2 RNA cytosine methyltransferase NSUN proteins

RNA modifications such as  $\Psi$ , 2'-O-methylation,  $m^6A$ ,  $m^5C$ , and their related enzymes such as DKC1, PUSs, FBL, METTL3, NSUN2, DNMT2 have been discussed in previous sections. Many studies have focused on  $m^6A$  and its associated enzymes [305]. However, in recent years, the role of RNA 5-methylcytosine ( $m^5C$ ), which is mediated by a family of Nol1/Nop2/SUN domain (NSUN) RNA methyltransferases and DNA methyltransferase homologue DNMT2 (TRDMT1), in regulating the structure, biology, and function of RNAs has been gaining

significant interest [238, 284, 306-313]. Importantly, dysregulation of m<sup>5</sup>C and NSUN proteins have been implicated in diseases, including cancer [314-316].

#### **1.4.2.1 The function of NSUN proteins and their cytosine targets**

There are seven members of the NSUN family (NSUN1-7). These proteins are responsible for methylation of cytosines at different sites in RNAs including tRNAs, rRNAs, mRNAs, mitochondrial tRNAs, and mitochondrial rRNAs [317]. Among all the NSUN proteins, NSUN2 is the most well-studied. Only limited research has been carried out with the other NSUN proteins so far.

NSUN2 is traditionally thought to mainly methylate tRNAs; however, recent studies show that NSUN2 also methylates mRNAs and regulates mRNA stability and translation. NSUN2 methylates cytosine 48 or 49 at the variable loop of 80% of tRNAs in mouse and human skin fibroblasts [183]. The methylation of tRNA by NSUN2 prevents the binding, cleavage, and degradation of tRNAs by the endonuclease angiogenin [183]. The absence of NSUN2 increases the amount of cleaved tRNA fragments in the cells, which increases cellular stress and decreases global protein synthesis [183, 184]. In 2017, NSUN2 was found to catalyze the m<sup>5</sup>C site on 1,158 mRNAs [292]. Knockdown of NSUN2 decreased by about 40%, while overexpression of NSUN2 increased by about 3-fold, total m<sup>5</sup>C methylation levels [292]. Interestingly, NSUN2 methylates cell cycle-associated mRNAs, including CDK1, p27, and p16 [318-320]. NSUN2 levels increase in the presence of serum, and NSUN2 is highly expressed during the S phase of cell cycle [319]. NSUN2 methylates C1733 at the 3' UTR of CDK1 mRNA, which is required for the stability of CDK1 in the S and G2/M phases of the cell cycle [319]. Overexpression of NUSN2 induces the expression of CDK1 and thus promotes cell cycle progression [319]. In contrast, NSUN2 methylates cytosine 64 at the 5' UTR of p27 mRNA in HeLa cells, but the methylation of p27

mRNA inhibits p27 expression at the translational level [318]. However, how methylation of p27 leads to a decrease in translation is unknown [318].

Compared with the low expression of NSUN2 in normal tissues, NSUN2 is highly expressed in many tumor tissues including prostate, breast, oral, colorectal, stomach, and liver cancers [184, 321]. The elevated levels of NSUN2 shown by immunohistochemistry (IHC) staining are accompanied by elevated levels of Ki-67, giving rise to the idea that NSUN2 is a proliferative marker in cancers [321]. NSUN2 is a direct target of c-Myc and is required for c-Myc-induced proliferation and progression in keratinocytes [184]. The expression of NSUN2 is upregulated by c-Myc in various cancer tissues, and knockdown of NSUN2 reduces growth of squamous cell carcinoma xenografts [184, 322]. Knockdown of NSUN2 also inhibits hepatocellular carcinoma cell proliferation and invasion through the impairment of the cell cycle. HepG2 hepatocellular carcinoma cells are retained in the G2 phase of the cell cycle, which could be due to decreased expression of CDK1 as a result of NSUN2 knockdown [323, 324]. Moreover, knockdown of NSUN2 resulted in abnormal spindle structure formation during mitosis, with normal mitosis being decreased by more than 50% in HCC1954 blood lymphocytes and breast cancer cell lines [325]. Interestingly, the spindle impairment caused by NSUN2 knockdown can be rescued by NSUN2 with mutations at the catalytic cysteines [325]. This result suggests that the function of NSUN2 in spindle assembly is independent of functions associated with methylated NSUN2 [325].

NSUN1 (also called NOP2) is responsible for the methylation of cytosine 2870 (C2870) in yeast 25S rRNA, and *NSUN1* knockdown leads to severe defects in yeast pre-rRNA processing [238]. In human, NSUN1 is predicted to methylate C4447 in 28S rRNA [238]. Human NSUN1 is associated with the maintenance of ribosomes and has been shown to be a proliferation marker [326, 327]. The expression of NSUN1 is associated with the progression of hepatocellular

carcinoma [328]. However, the detailed role of NSUN1 in cancer is still unknown. In addition, NSUN1 has also been found to inhibit the transcription of the HIV-1 virus in human immune cells [329]. NSUN1 binds to and methylates a cytosine in HIV-1 TAR RNA. This methylation prevents binding of the HIV-1 protein Tat to TAR RNA and promotes viral latency [329].

NSUN3 has been shown to be localized in the mitochondria and methylates cytosine 34 at the first nucleotide (wobble position) of the anticodon loop in methionine mitochondrial tRNAs [284]. 5-methylcytosine is further oxidized by dioxygenase ABH1 to form 5-formylcytosine. Both methylation and oxidation of cytosine 34 are required for the recognition of different methionine codons and the encoding of methionine in mitochondria [308, 313]. NSUN3 knockout decreases protein synthesis in mitochondria, and inhibits mitochondrial activity [284]. Reduced modification of cytosine 34 by NSUN3 causes the inhibition of cell growth, the deregulation of embryonic stem cell differentiation, and is also associated with many mitochondrial diseases, including early-onset mitochondrial encephalomyopathy and seizures [313, 330, 331].

NSUN4 has dual functions in mitochondrial rRNA biogenesis [332-335]. It contributes to the methylation of cytosine 911 in mouse mitochondrial SSU 12S rRNA and forms a tight complex with mitochondrial transcription termination factor 4 (MTERF4) which plays an essential role in LSU and SSU assembly to form monosomes. The methylation of cytosine 911 by NSUN4 is independent of interaction with MTERF4 [334]. NSUN4 knockout strongly inhibits protein synthesis in mitochondria, and deletion of NSUN4 causes embryonic lethality in the mouse [334]. However, the function of methylated cytosine 911 at mitochondrial SSU rRNA is unknown.

NSUN6 has been shown to be localized in the cytoplasm, and methylates cytosine 72 at the acceptor stem of threonine and cysteine tRNAs in human embryonic kidney 293T (HEK293T) cells [307]. However, a well folded structure including the CCA tail structure at the 3' end and

base pairings of tRNAs are required for the binding of NSUN6 to the tRNAs and their methylation by NSUN6, suggesting that the cytosine 72 methylation modification happens at a late step of tRNA biogenesis [336, 337]. Moreover, cysteine 373 of NSUN6 has been predicted to be the catalytic cysteine and is required for the methylation of cytosine 72 [307].

*NSUN7* mutations including mutations in exon 4 and exon 7 are found in mice with sperm motility defects as well as in human asthenospermia [338-341]. NSUN7 methylates m<sup>5</sup>C of an enhancer RNA termed the peroxisome proliferator-activated receptor-gamma coactivator 1 $\alpha$  (PGC-1 $\alpha$ ). Deletion of NSUN7 causes instability of PGC-1 $\alpha$  and decreases the expression of PGC-1 $\alpha$  targeted genes such as *Pfkl*, *Sirt5*, *Idh3b*, and *Hmox2*.

NSUN5 is the focus of this project, the detailed information about NSUN5 will be introduced in 1.4.3.

#### **1.4.2.2 The two functional cysteines of NSUN proteins**

All NSUN proteins have a similar catalytic domain that contains two conserved cysteines and an S-Adenosyl methionine (SAM)-binding pocket [314, 317, 342]. NSUN proteins use SAM as a substrate for methyl groups and add the methyl group to the carbon 5 position of cytosine to form m<sup>5</sup>C (**Figure 1.10**). The methylation process by NSUN proteins is not required for interaction with other proteins or cofactors [307, 318]. SAM becomes S-Adenosylhomocysteine (SAH) after the methylation reaction. The two cysteines of NSUN proteins have different functions in RNA methylation. The first cysteine is also called the catalytic cysteine, which forms a covalent link with carbon 6 of its target cytosine, and activates carbon 5 to receive the methyl group from SAM [314, 317, 342]. The second cysteine is also called the releasing cysteine, which releases the covalent binding, thereby releasing the target RNA [314, 317, 342].

## Cytosine methylation ( $m^5C$ ) :

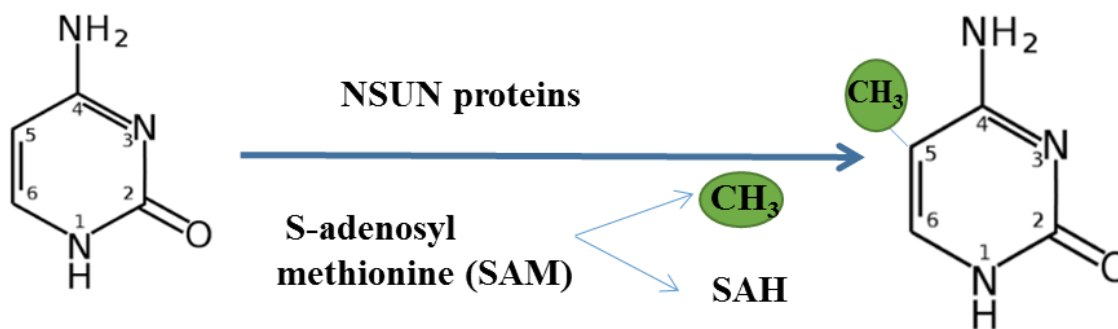


**Figure 1.10 Cytosine methylation by NSUN proteins.**

NSUN proteins use SAM as a substrate for methyl groups and add the methyl group to the carbon 5 position of cytosine to form  $m^5C$ . SAM becomes S-Adenosylhomocysteine (SAH) after the methylation reaction. This figure has been modified with permission from Genetics Research International, Creative Commons Attribution License, Mehrdad Ghavifekr Fakhr et al.

So far, the two functional cysteines of NSUN proteins have mainly been studied in yeast. The location of these two cysteines in yeast NSUN1 (NOP2) has been determined: the first cysteine (cysteine 478) is in motif IV and catalyzes the methylation of target cytosines, whereas the second cysteine (cysteine 424) is in motif VI and helps to release NSUN1 from target RNAs after methylation [238]. Similarly, the functions of these two cysteines in yeast NSUN2 have also been reported: the first cysteine (cysteine 321) in motif IV catalyzes the methylation of target cytosines, whereas the second cysteine (cysteine 271) in motif VI helps to release NSUN2 from its target RNAs after methylation [292, 320, 343-345]. Consistently, a study of the two cysteines of Rcm1 (the yeast NSUN5) showed the same results: the catalytic cysteine (cysteine 404) is in motif IV, and the releasing cysteine (cysteine 330) is in motif VI [238]. However, the locations of these two cysteines in human NSUN5 have not been studied.

Alignment of the amino acid sequences of NSUN proteins (NSUN1 to NSUN6) revealed three main conserved amino acid sequences: ILDMCAAPGK, DRILLDAPCS, and GGYLVYSTCS (**Figure 1.11**). There are totally three conserved cysteines in these NSUN proteins (each of these conserved sequences has a conserved cysteine) (**Figure 1.11**). NSUN1 (NCBI Reference Sequence: NP\_006161.2) has C388, C459, and C513. NSUN2 (NCBI Reference Sequence: NP\_001180384.1) has C149, C236, and C286. NSUN3 (NCBI Reference Sequence: NP\_071355.1) has C139, C214, and C265. NSUN4 (NCBI Reference Sequence: NP\_950245.2) has C181, C258, and C310. NSUN5 (NCBI Reference Sequence: NP\_683759.1) has C234, C308, and C359. NSUN6 (NCBI Reference Sequence: NP\_872349.1) has C242, C326, and C373. In addition, the location of these three cysteines in human NSUN5 can also be identified upon comparison of the amino acid sequences of the yeast homolog with the human homolog (**Figure 3.20**). However, the functions of these cysteines in human NSUN5 need to be further studied.

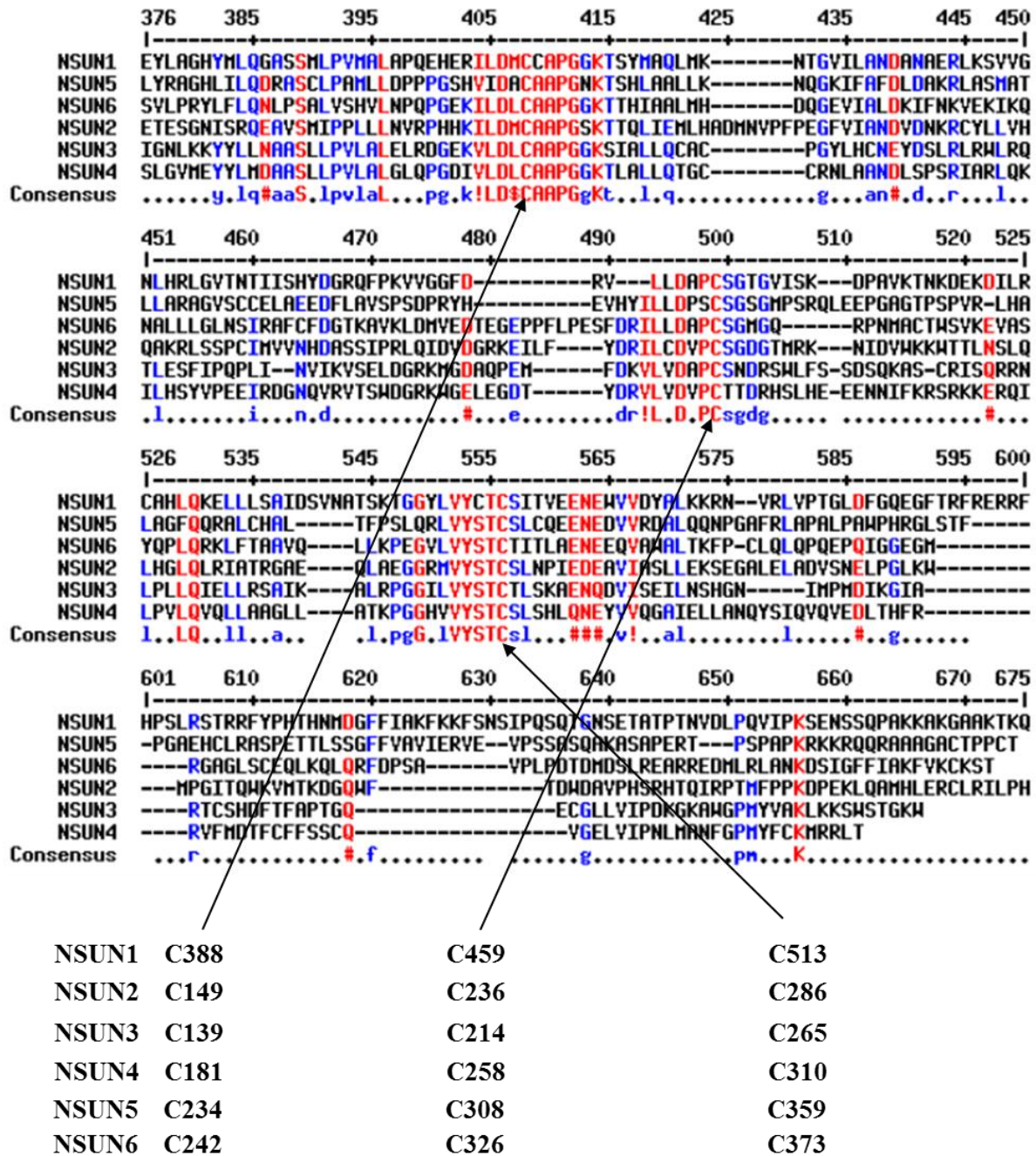


Figure 1.11 The conserved sequences and cysteines in the NSUN proteins.

The amino acid sequences of human NSUN proteins (NSUN1 to NSUN6) were downloaded from NCBI Protein and aligned with MultAlin (Multiple sequence alignment with hierarchical clustering). There are three main conserved sequences among the NSUN proteins:

ILDMMCCAPGKT, DRILLDAPCS, and GGYLVYCTCS. All the NSUN proteins have three conserved cysteine as described above.

### 1.4.3 NSUN5 and its cytosine targets on rRNA

Using a glioblastoma TCGA dataset from 2013 (540 glioblastoma samples), we found that high *NSUN5* mRNA expression is strongly associated with poor survival in glioblastoma patients (**Figure 3.1**). In addition, when glioblastomas in TCGA (273 patients) and GSE4290 datasets (86 patients) were divided into 3 groups based on 42 probes [346], *NSUN5* was found to be deleted or downregulated in the group with the best outcome (with survival time being more than twice as long as that of the other two groups) [346]. *NSUN5* is one of the 26 deleted genes on chromosome 7 associated with a human neurodevelopmental disease named Williams-Beuren syndrome [347]. However, the biological function of *NSUN5* in human cells and in glioblastoma needs to be carefully investigated.

In mouse hippocampus and corpus callosum, *NSUN5* is specifically expressed in oligodendrocytes and oligodendrocyte precursors, but not in neurons or astrocytes [348, 349]. *NSUN5* is required for the proliferation of oligodendrocyte lineage cells that play a role in the long-term potentiation of hippocampal ability and the myelin sheath growth of neuronal axons [348, 349]. *Nsun5* knockout mice suffer from impairment of memory and cognition, and hypotrophy of the corpus callosum [348, 349]. Interestingly, *NSUN5* knockout decreases CDK1 and CDK2 protein levels by 30% to 40%, but does not affect *CDK1* and *CDK2* mRNA levels [349]. However, how *NSUN5* affects the translation of CDK1 and CDK2 is unknown.

In yeast, Rcm1 (the yeast homologue of *NSUN5*) is a rRNA cytosine methyltransferase [238, 312]. Rcm1 is responsible for the methylation of C2278 in 25S rRNA of yeast [238, 275, 312].

Deletion of Rcm1 alters the rRNA structure that favors the translation of oxidative stress-responsive mRNAs, leading to increased stress response and lifespan [312]. More importantly, similar to yeast 25S rRNA that has only two cytosine methylation sites (C2278 and C2870), human 28S rRNA (total length of 5028 nucleotides) also has only two cytosine methylation sites at C3782 and C4447 [238, 310, 350]. Yeast 25S rRNA and human 28S rRNA have similar secondary structures in helix 71 of rRNA domain IV containing the C2278 (or C3782) methylation site. Therefore, NSUN5 is predicted to be responsible for the methylation of C3782 in human 28S rRNA (Figure 1.12) [238].

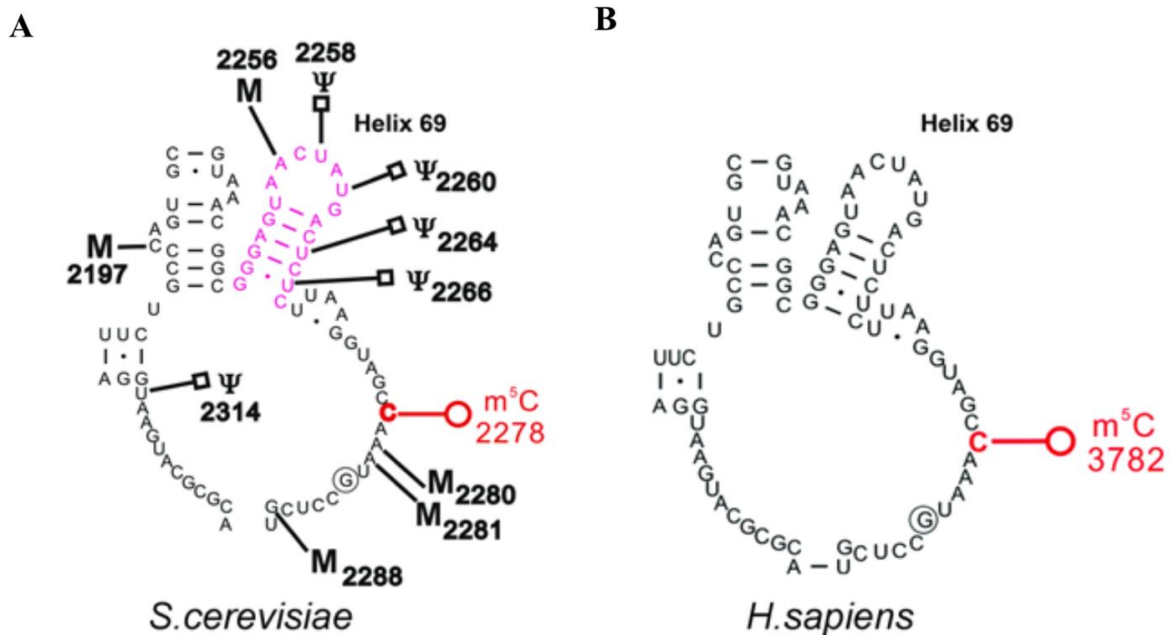


**Figure 1.12** The C3782 methylation site in human 28S rRNA is located in a region with a similar secondary structure to that of the C2278 methylation site in yeast 25S rRNA.

Yeast and human have a similar secondary structure in helix 68 to helix 71 of 25S (or 28S) rRNA domain IV containing methylated C2278 and C3782. This figure has been reused with permission from Oxford University Press (Neuro-Oncology), License Number: 4627360701453, Sunny Sharma et al. [238].

C3782, the target of NSUN5, is located in the middle of helix 69 and helix 71 of domain IV of 28S rRNA, which is at the intersubunit bridge and the aminoacyl tRNA binding loop between the decoding center and the peptidyl transferase center of the ribosome [226-228]. Both helix 69 and helix 71 of the 25S rRNA (or 28S rRNA) are conserved intersubunit bridge structures (B2a and B3, respectively) among prokaryotic and eukaryotic ribosomes [351]. Deletion of helix 69 leads to defective association between 50S and 30S subunits in bacterial cells [228]. Moreover, the loop of helix 69 interacts with the tRNA at the A site and the stem of helix 69 interacts with the tRNA at the P site, and helps the correct binding of tRNAs at the peptidyl transferase activity site [352]. Helix 69 is also required for the release of initiation factor 3 and start codon selection, with deletion of helix 69 decreasing the rate of translation initiation by 20-fold [229].

According to the maps shown in the SnoRna-LBME database, about 24 nucleotides (~14% of total nucleotides from A3670 to A3840) are modified at helices 67 to 71 in the intersubunit and decoding center of human 28S rRNA, including 10 2'-O methylation sites and 14 pseudouridine sites. Base methylation modification of C3782 at helix 70 is in the middle of this sequence. The functional impact of modifications in helix 69 to helix 71 has been studied. First, when 3 to 5 modifications in helix 69 of 25S rRNAs in bacteria are deleted, the 25S rRNAs are instable [227]. Consequently, protein synthesis rates and cell growth are dramatically decreased, and the cells are more sensitive to temperature and neomycin (which binds to helix 44 and helix 69, and inhibits translation) [227, 353]. Second, loss of methylation at 3 bases of helix 70 to helix 71 in yeast (cytosine methylation of C2278 and 2'-O methylation at G2288 and A2281) leads to the instability of the 60S ribosome subunit and the whole ribosome. The cells grow more slowly than wild type cells in competition assays, and are more sensitive to anisomycin (which binds to the A site and

inhibits translation) [275]. In addition, the methyl group of m<sup>5</sup>C1942 in bacteria (C3782 in human) interacts with tRNA at the A site [234]. However, the function of m<sup>5</sup>C1942 is unknown.

From studies in yeast and mouse, we know that: (a) NSUN5 is an RNA cytosine methyltransferase and is predicted to methylate C3782 in human 28S rRNA; (b) NSUN5 is specifically expressed in human oligodendrocyte lineage cells and is associated with the survival of glioblastoma patients; and (c) NSUN5 regulates protein expression (e.g., CDK1 and CDK2) at the translational level through alteration of the rRNA structure. In addition, based on the biological functions of cytosine targets, and the conserved catalytic cysteines of the NSUN proteins, we can deduce that NSUN5 may affect the function of ribosomes through the methylation of C3782 in human 28S rRNA and that NSUN5 could have other mRNA targets and methylation independent functions as well. Increasing evidence indicates that NSUN proteins are implicated in cancer. However, the role of NSUN5 in cancer needs to be thoroughly or carefully investigated.

## 1.5 Hypothesis of the project

My thesis centers on glioblastoma, translation control in cancer, ribosomal regulation in cancer, and the function of RNA cytosine methyltransferase NSUN proteins. The central question that I am asking is whether rRNA cytosine methylation by NSUN5 regulates ribosome conformation, the subsequent mRNA translation, and the resulting translome in glioblastoma cells. I hypothesize that elevated NSUN5 alters the structure and/or activity of ribosomes by regulating the pattern of rRNA methylation, which leads to pro-tumorigenic translational reprogramming and thereby promotes the progression of glioblastoma. (Figure 1.13).

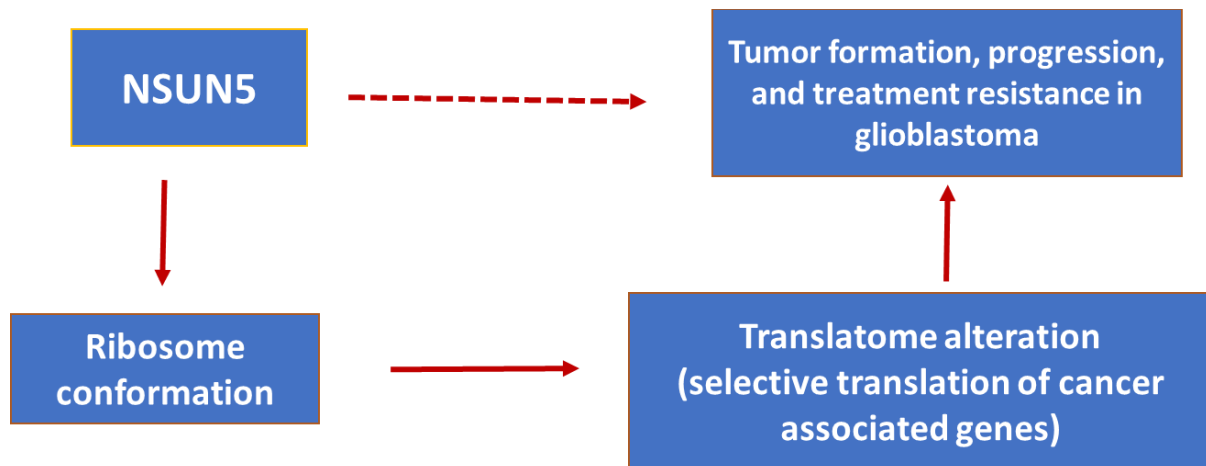


**Figure 1.13** Diagram depicting the central hypothesis of this project.

NSUN5 promotes tumor formation and progression of glioblastoma through the regulation of ribosome conformation in ribosomal biogenesis that reprograms the translome.

## **Chapter 2 Materials and Methods**

## **2.1 TCGA glioblastoma datasets analysis**

Analysis of TCGA glioblastoma (GBM) datasets including DNA copy number variation, somatic mutation, DNA methylation, exon expression RNAseq, gene expression AffyU133a array, gene expression RNAseq were performed using the UCSC Xena platform. The correlation between genes in TCGA datasets and GBM patient survival was determined using Kaplan-Meier survival analysis according to the guidelines offered by UCSC Xena. Specifically, only primary glioblastoma tumors were selected, and the survival curves were generated automatically at the median cut-off site with statistical analysis also generated automatically. Images were downloaded from the platform.

The R2 Genomics Analysis and Visualization platform was used to analyze NSUN5 expression as a function of overall survival and progression-free survival in glioblastoma patients and all grades of glioma patients [354]. The Kaplan Meier Scanner and Tumor Glioblastoma-TCGA-540 dataset was selected for analysis. NSUN5 was analyzed using both overall survival and progression-free survival datasets. Survival curves were generated automatically at the cut-off site where high mRNA expression samples compared against the low mRNA expression samples had the lowest P-values. The Tumor Glioma-French-284 Dataset from the Erasmus University Medical Center including 276 all grades of glioma samples from 1989 to 2005 was also used in the analysis [354]. NSUN5 was scanned automatically with overall survival dataset, and the Kaplan Meier curve with the lowest P-value was generated.

## **2.2 Cell culture**

Nine glioblastoma cell lines (A172, CLA, T98, U87, M021, M016, M049, M103, and U251) were obtained from Dr. Roseline Godbout, and the cell lines were described in publications from

their lab [355-357]. The mainly used cell lines including U251, U87, and T98 cells were authenticated by their STR codes. Seven glioblastoma patient-derived neurosphere cultures were established by Dr. Godbout (A4-003, A4-004, A4-007, A4-010, A4-012) or Dr. Kenn Petruk (ED511 and ED512) from the University of Alberta. Five patient-derived neurosphere cultures (12EF, 48EF, 25M, 50M, 53M) were obtained from Dr. Mary Hitt and established by Dr. Samuel Weiss from the University of Calgary, and these neurosphere cultures have been described in two publications [358, 359]. Glioblastoma cell lines were cultured in Dulbecco's Modified Eagle Medium (DMEM) low glucose with 10% fetal bovine serum (Gibco, Thermo Fisher), 100 U/ml penicillin and 100 µg/ml streptomycin (Gibco, Thermo Fisher). Glioblastoma patient-derived primary cells were cultured in DMEM/F12 with 20 ng/ml EGF (Gibco, Thermo Fisher), 20 ng/ml basic FGF (Gibco, Thermo Fisher), and 1X B27 supplement (Gibco, Thermo Fisher). Both glioblastoma cell lines and glioblastoma patient-derived primary cells were frozen and stored in DMEM low glucose medium with 20% fetal bovine serum and 10% DMSO. HEK293T cells were cultured in DMEM high glucose with 10% fetal bovine serum and 100 U/ml penicillin and 100 µg/ml streptomycin (Gibco, ThermoFisher).

### **2.3 Total RNA extraction and complementary DNA (cDNA) synthesis**

Total RNA extraction and cDNA synthesis were performed as described in our previous publication [360]. Total RNA was extracted using the TRIzol reagent (Ambion, Life Technologies) following the manufacturer's instructions. The RNA concentration was measured by DU 730 Life science UV/Vis spectrophotometer at 260 nm wavelength. The cDNAs were synthesized using Reverse Transcriptase (SuperScript II Reverse Transcriptase, Invitrogen) following the

manufacturer's instructions. The RNase inhibitor (RNaseOUT Recombinant Ribonuclease Inhibitor, Invitrogen) was used to inhibit RNA degradation.

## **2.4 Quantitative real-time PCR**

Quantitative real-time PCR were performed as described in our previous publication [360]. PCR primer sequences for NSUN5, NSUN2, STAT3, and GAPDH were designed as follows: hNSUN5 Forward (For): 5'-CTT CTG AAG AAC CAA GGG AAG A-3', hNSUN5 Reverse (Rev): 5'-AGC CAG TTC ACA GCA AGA G-3'; NSUN2 For: 5'-GTG GAA TAA ACG TCA GCC AAA-3', NSUN2 Rev: 5'-CTT AGA GGG ATC TGT GGG TTTC-3'; STAT3 For: 5'- GAG AAG GAC ATC AGC GGT AAG-3', STAT3 Rev: 5'-CGA TGG AGA CAC CAG GAT ATT-3'; hGAPDH For: 5'-GGA CCT GAC CTG CCG TCT AGA A-3', hGAPDH Rev: 5'-GGT GTC GCT GTT GAA GTC AGA G-3'. These primers were purchased from Integrated DNA Technologies (IDT). Power SYBR Green PCR master mix which contains SYBR™ Green 1 Fluorescence Dye, DNA Polymerase, dNTPs, and reaction buffer (Applied Biosystems), was used for quantitative real-time PCR following the manufacturer's instructions. Threshold cycle (CT) values of fluorescence signals were compared amongst the samples. Threshold cycle (CT) values of all the samples were exported and analyzed. The CT value of GAPDH was used as the internal control for each sample.

## **2.5 Protein extraction**

Cultured cells were lysed with RIPA buffer containing Complete Protease Inhibitor cocktail (Roche) and phosphatase inhibitors as described previously [360]. RIPA buffer is composed of 1.0% Triton X-100, 0.1% SDS, 50 mM Tris-Cl pH 8.0, 1 mM EDTA, 150 mM NaCl, 1.0% DOC

(sodium deoxycholate), 1X Protease Inhibitor cocktail, 10 mM NaP<sub>2</sub>O<sub>7</sub>, 10 mM NaF, 1 mM Na<sub>3</sub>VO<sub>4</sub>. The cell lysates were sonicated, and centrifuged at 13,000g for 15 minutes at 4°C. After centrifugation, cell debris was pelleted, and the supernatant was transferred to a new tube. Protein concentration in the supernatant was measured using the DC Protein Assay Kit (Bio-Rad) following the manufacturer's instructions and quantified using a FLUOstar Omega reader.

## **2.6 Western blotting**

Western blotting was performed as described in our previous publication [360]. Briefly, 30 µg to 50 µg proteins were loaded in an SDS-PAGE gel and separated by electrophoresis. Following electrophoresis, proteins were transferred from the gel to nitrocellulose membranes (Bio-Rad) at constant voltage. The membranes were blocked with 5% dry milk powder in TBST and incubated with primary antibodies in 5% BSA in TBST overnight. The membranes were then incubated with secondary antibodies in 5% dry milk powder in TBST for 1 hour. The blots were scanned using a Li-Cor Odyssey Infrared imaging system. Processing of the images and densitometry analyses were performed using Li-Cor Odyssey imager software. The following primary antibodies were used at 1:1000 dilution: NSUN5 (H-10), mouse monoclonal antibody (#K1411, Santa Cruz Biotechnology); NSUN2, rabbit polyclonal antibody (#20854-1-AP, Proteintech); STAT3 (124H6), mouse monoclonal antibody (#9193, Cell Signaling); and β-Actin, mouse monoclonal antibody (#A5441, Sigma-Aldrich). The following secondary antibodies were used at 1:50000 dilution: IR Dye 800CW, Donkey anti-Rabbit (#C70918-03, Li-Cor), and IR Dye 800CW, Donkey anti-Mouse (#C50422-04, Li-Cor)

## **2.7 NSUN5 CRISPR guide RNA design and plasmid production**

To knockout NSUN5 in glioblastoma cells, NSUN5 knockout plasmids were generated using the method described in the publication from Dr. Lynne Postovit's lab [361]. Two NSUN5 CRISPR guide RNA target sequences were designed by Dr. Scott Findlay from Dr. Postovit's lab. The all-in-one CRISPR/Cas9 sequences are as follows: Human NSUN5 gRNA target sequence 1: GCGCCGGCCTCCTCCGTG (Exon II, sense) and human NSUN5 gRNA target sequence 2: GAGCTTCTTCTCCGCACGG (Exon II, antisense). The NSUN5 gRNA target sequences were each integrated into the guide RNA template at the site indicated by X's:

GTGACGTAGAAAGTAATAATTCTTGGGTAGTTTGCAGTTTTAAAATTATGTTTTAAA  
ATGGACTATCATATGCTTACCGTAACTTGAAAGTATTTTCGATTTCTTGGGTTTATATA  
TCTTGTGGAAAGGACGAAACACCXXXXXXXXXXXXXXXXXXXXGTTTTAGAGCTAGA  
AATAGCAAGTTAAAATAAGGCTAGTCCGTTATCAACTTGAAAAAGTGGCACCGAGT  
CGGTGCTTTTTTCTAGACACAATTGCATGAAGAATCTGCTTAGGGTTAGGCGTTTTGC  
GCTGCTTCGCGATGTACGGGCCAGATATACGCGTTGACATTGATTATTGACTAGTTA  
TTAATAGTAATCAATTACGGGGTCATTAGTTCATAGCCCATATATGGAGTTCCGCGT  
TACATAACTTACGGTAAA. The oligos of NSUN5 guide RNA sequences were purchased from IDT and ligated into the CRISPR/Cas9 plasmid using T4 DNA Ligase following the manufacturer's directions (Invitrogen).

After ligation, the plasmids were transformed into One Shot TOP10 Competent E. coli cells (Thermo Fisher) following the manufacturer's directions. Following blue/white selection, the plasmids from six white colonies (indicating successful uptake of plasmid) were purified using QIAprep Spin Miniprep Kit (QIAGEN) following the manufacturer's instructions. Insertion of the NSUN5 CRISPR guide RNA was verified by sequencing.

## 2.8 NSUN5 CRISPR knockout

To investigate whether C3782 of 28S rRNA is the methylation target of NSUN5, NSUN5 was knocked out in HEK293T and U251 cells which express endogenous NSUN5. The CRISPR knockout method is described in the publication from Dr. Postovit's lab [361]. Briefly, 5 µg of NSUN5 CRISPR knockout plasmid DNA was mixed with 15 µl of Lipofectamine 2000 (Invitrogen), topped up with calcium-free Dulbecco's PBS (Gibco, Thermo Fisher) to 150 µl, and distributed evenly to each HEK293T or U251 plate with cells at 50% confluency in a 10 cm dish). 72 hours post-transfection, the cells were sorted by flow cytometry using m-Cherry which is included in the plasmid into the 96-well plates with each well containing a single cell. The single cell clones were expanded and screened for NSUN5 expression by Western blotting. The clones that express NSUN5 were defined as NSUN5 wild-type and those that have lost NSUN5 expression were defined as NSUN5 knockout. The NSUN5 wild-type and knockout clones were further confirmed by genomic DNA sequencing as described below.

## 2.9 Genomic DNA sequencing for indels induced by CRISPR in *NSUN5* gene

To determine whether mutations in *NSUN5* DNA were induced by CRISPR in HEK293T and glioblastoma cells, genomic DNA sequencing was conducted. The protocol is described in the application note "Using Sanger sequencing to facilitate CRISPR and TALEN-mediated genome editing workflows" by Thermo Fisher Scientific. Total DNA from 293T/wild-type (clone #37), 293T/NSUN5 knockout cells (clone #22), U251/wild-type, and U251/NSUN5 knockout cells was extracted using the PureLink Genomic DNA Mini Kit (Invitrogen) following the manufacturer's instructions. Primers were designed to amplify the CRISPR NSUN5 guide RNA target sequences, with the following sequences: NSUN5 CRISPR Forward Primer: 5'-GCG ACT TGC TCC AGT

CC-3', and NSUN5 CRISPR Reverse Primer: 5'-AGA ACG TGA AGC AGC TGT-3'. PCR was carried out to amplify the CRISPR NSUN5 guide RNA target sequences using AmpliTaq Gold 360 Master Mix (Applied Biosystems) following the manufacturer's instructions using an annealing temperature of 50°C. Amplified PCR DNA products were electrophoresed through 2% agarose gel in TAE buffer (UltraPure™ TAE Buffer, Thermo Fisher) and visualized by staining with ethidium bromide. TOPO cloning and transformation were further conducted using TOPO TA Cloning Kit (Thermo Fisher). Briefly, PCR products were ligated into TOPO TA vector and transformed into One Shot TOP10 Competent E. coli. The successfully transformed bacterial colonies were selected via blue/white selection, and their plasmids were extracted using QIAprep Spin Miniprep Kit (QIAGEN) following the manufacturer's instructions. Agarose gel electrophoresis (0.8% agarose in TEA buffer) was performed to confirm the presence of plasmid DNA, and the concentration of plasmid DNAs was measured using a DU 730 Life science UV/Vis spectrophotometer. 575 ng of each plasmid DNA was mixed with 0.25 µM TOPO vector specific M13 forward primer in a final volume of 10 µl and the plasmids were sent to Molecular Biology Service Unit in the University of Alberta for Sanger sequencing. The sequencing data were compared with NSUN5 wild type DNA sequence using multiple sequence alignment on Multalin online platform [362].

Based on the NSUN5 expression and genomic sequencing results, the following colonies were selected for experiments: 293T/wild-type (clone #37), 293T/NSUN5 knockout cells (clone #22), U251/wild-type (clone A1), and U251/NSUN5 knockout (clone B1).

## **2.10 NSUN5 knockdown and CaCl<sub>2</sub> mediated transfection**

NSUN5 was knocked down with shRNA in U251 and T98 cells and A4-012 patient-derived neurospheres, which express endogenous NSUN5 (based on Western blotting results). The NSUN5 shRNA Kit (Origene Biotechnology company, Catalogue: TL302876) was used which includes four unique human NSUN5 shRNA constructs in the lentiviral GFP vector and one scrambled negative control non-effective shRNA in lentiviral GFP vector. The sequences of the four unique 29-mer NSUN5 shRNAs are as follows:

1. TTGGTGTACTCCAGCAACTTCCAGAACGT,
2. ACCAGTCACTTGGCTGCTCTTCTGAAGAA,
3. AGACCACACTCAGCAGTGGCTTCTTCGTT,
4. GGCCAAGGTGCTAGTGTATGAGTTGTTGT.

The plasmids were transfected using the CaCl<sub>2</sub>-mediated third-generation lentivirus transfection method as previously described by Sambrook et al. [363]. Briefly, 5 µg of plasmid was mixed with 5 µg of the packaging plasmids (RRE, REV, and VSVG), and water (Biotech Grade, Fisher BioReagents) was added to reach 450 µl, and mixed by vortexing. 50 µl of 2.5M CaCl<sub>2</sub> was added to the mixture, followed by 500 µl 2X HBS (HEPES-Buffered Saline, pH 7.05, Fisher Scientific) to allow binding of plasmids to cell membranes. The mixture was incubated for five minutes at room temperature and distributed evenly onto HEK293T cells cultured in 9 ml fresh medium in a 10 cm dish. The next day, the medium was replaced with 7 ml fresh medium to help concentrate the virus. On the third day, the HEK293T culture medium containing the infectious viral particles was used to infect U251 cells or A4-012 neurospheres (the latter were first digested with StemPro Accutase (Gibco) into single cells prior to infection), and 48 hours post-infection, the cells were collected and cultured in fresh or sphere culture medium. Using this method, U251/shRandom, U251/shNSUN5 #1, U251/shNSUN5 #2, U251/shNSUN5 #3, U251/shNSUN5 #4, A4-

012/shRandom, A4-012/shNSUN5 #1, A4-012/shNSUN5 #2, A4-012/shNSUN5 #3, and A4-012/shNSUN5 #4, T98/shRandom, T98/shNSUN5 #3, T98/shNSUN5 #4 cells were generated. The infection efficiency of the cells was determined by fluorescence microscopy as the plasmids contain the marker GFP. Thus, fluorescence-activated cell sorting (FACS) analysis was conducted when necessary.

The CaCl<sub>2</sub>-mediated third-generation lentivirus transfection system was also used for the overexpression of pLenti-NSUN5 in U87 cells and 50M patient-derived neurospheres, which do not express endogenous NSUN5. The plasmids, pLenti-Vector-Myc-DDK and pLenti-NSUN5-Myc-DDK, were purchased from Origene Biotechnology company (Catalogue: RC200144L3). Through this method, the U87/pLenti-Vector, U87/pLenti-NSUN5, 50M/pLenti-Vector, and 50M/pLenti-NSUN5 cells were generated.

## **2.11 RNA bisulfite sequencing**

RNA bisulfite sequencing was used to determine the methylation status of cytosine 3782 and cytosine 4447 of 28S rRNA in HEK293T and glioblastoma cells. This method was previously described in the Rcm1 (the yeast homolog of NSUN5) study [312]. First, total RNA from 293T/wild-type (clone #37), 293T/NSUN5 knockout cells (clone #22), U251/wild-type, U251/NSUN5 knockout cells, U87/CMV-Vector, U87/CMV-NSUN5 and U87/CMV-NSUN5 single clone #2 was extracted as described in the RNA extraction section (add the section number here). Second, 500 ng total RNA from each sample was used to conduct bisulfite conversion using EZ RNA Methylation Kit (ZYMO Research) by following the protocol provide in the kit [312]. Unmethylated cytosines were converted to uracil through sulphonation, hydrolytic deamination, and alkali desulphonation, while methylated cytosines remained unchanged. Third, the RNA from

the bisulfite conversion step was reverse transcribed into cDNA as described in section 2.3. Fourth, the following primers were designed to anneal to the converted C3782 and C4447-containing sequences; 28S rRNA 3782 For: 5'- TGT GGG TAA ATG GTG GGA GTA-3'; 28S rRNA 3782 Rev: 5'-AAC ACC AAA AAC CTC CCA CCT A-3'; 28S rRNA 4447 For: 5'-GAT TGT GAA AGT GGG GTT TTA TG-3'; 28S rRNA 4447 Rev: 5'-AAA CCC AAC TCA CAT TCC CTA TT-3'. These primers were used for PCR to amplify two potential methylation sites (C3782, C4447) on human 28S rRNA using AmpliTaq Gold 360 Master Mix Kit (Applied Biosystems). The annealing temperature was 50°C for the two sets of primers. 2% agarose gel electrophoresis was used to confirm the amplification of C3782 and C4447-containing sequences. Fifth, TOPO cloning and transformation were further conducted using TOPO TA Cloning Kit (Thermo Fisher) as described in section 2.9. Sixth, 12 plasmids extracted from the positive colonies were applied to Sanger sequencing and sequencing analysis as described above [362]. The sequencing data were compared with unconverted 28S rRNA sequence using multiple sequence alignment on Multalin online platform [362] to determine the methylation status of C3782 and C4447.

## **2.12 Immunofluorescence staining**

To determine the localization of NSUN5 in glioblastoma cells, immunofluorescence staining was conducted as described in a publication from Dr. Godbout's lab [364]. First, cells were seeded on coverslips placed in 24-well plates. After cells reached 50% confluence, immunostaining was performed directly in the well. Cells were washed with PBS, fixed with 4% paraformaldehyde in PBS (Santa Cruz Biotechnology), and permeabilized with 0.2% Triton X-100 (Sigma) in PBS. NSUN5 mouse monoclonal primary antibody (#K1411, Santa Cruz Biotechnology) was diluted 1 to 100 in the 0.2% Triton X-100 permeabilization buffer. After 2 hours of incubation with primary

antibody, the cells were washed with 0.2% Triton X-100 and incubated with Alexa-Fluor 488-conjugated anti-mouse secondary antibody (Cell Signaling) for 1 hour (1:200 dilution), followed by incubation in DAPI (1 µg/ml in PBS) for 5 minutes. Coverslips were mounted onto slides. The images were taken using confocal microscope and AMG EVOS FL microscope.

### 2.13 Site-directed mutagenesis

To determine the function of catalytic cysteines of NSUN5, site-directed mutagenesis was conducted to create pLenti-NSUN5 C308A, pLenti-NSUN5 C359A, and pLenti-NSUN5 C308A/C359A plasmids where cytosine (C)308 and/or C359 were converted into alanine (A) using QuikChange Lightning Site-Directed Mutagenesis Kit (Agilent). First, two sets of mutagenic primers targeting NSUN5 cysteine 308 and cysteine 359 were designed using Quick Change Primer Design system, in which cysteine (UGC) was mutated to alanine (GCC). The NSUN5 cysteine 308 mutagenic primers were:

Forward: 5'-CTGCTGGATCCTTCCGCCAGTGGCTCGGGTAT-3',

Reverse: 5'-ATACCCGAGCCACTGGCGGAAGGATCCAGCAG-3', and the NSUN5 cysteine 359 mutagenic primers were:

Forward: 5'-TCGTCTACTCCACGGCCTCCCTCTGCCAGG-3',

Reverse: 5'-CCTGGCAGAGGGAGGCCGTGGAGTAGACGA-3'. Second, pLenti-NSUN5 plasmid served as a template for site-directed mutagenesis using QuikChange Lightning Site-Directed Mutagenesis Kit (Agilent). Briefly, pLenti-NSUN5 plasmid, the two sets of primers listed above, and QuikChange Lightning kit components (enzyme, dNTPs, and reaction buffer) were used in PCR reactions to generate mutated NSUN5. After PCR, Dpn I enzyme (provided in the kit) was added to the reaction mixtures to digest the parental pLenti-NSUN5 plasmid template, and the

newly synthesized cysteine-mutated pLenti-NSUN5 plasmid was transformed and amplified using XL10-Gold ultracompetent cells (provided in the kit). pLenti-NSUN5 C308A and pLenti-NSUN5 C359A were both generated using this approach. Sanger sequencing was performed to confirm the presence of the mutated residues in pLenti-NSUN5 plasmid as described in section 2.9. To generate the double mutant, site-directed mutagenesis was further conducted using pLenti-NSUN5 C308A to generate the pLenti-NSUN5 C308A/C359A plasmid.

#### **2.14 Neutral red uptake assay**

Cell viability with or without temozolomide (TMZ) treatment was measured using the neutral red uptake assay, following the protocol provided by Repetto et al. [365, 366]. The neutral red uptake assay is based on the absorption of the neutral red dye in the lysosomes of viable cells, and cell numbers are quantitatively estimated by the absorbance intensity of the dye at the wavelength of 580 nm.

To detect change in the number of viable cells over time, glioblastoma cells were seeded into multiple 96-well plates with 500 or 1000 cells per well. Cell viability was measured on day 1, day 3, and day 5 as follows. The culture medium was replaced with fresh medium containing 33 µg/ml of neutral red dye (Sigma) and cells were incubated for 3 hours. The cells were then washed with PBS twice to remove the dye in medium, and the dye absorbed by the cells was extracted using 100 µl of dye extraction solution (50% ethanol and 1% acetic acid). The plate was gently shaken to ensure even distribution of dye. The intensity of the dye was measured using FLUOstar Omega microplate reader. The neutral red absorbance intensities were standardized to day 1 for each cell line.

The sensitivity of cells to temozolomide, the first-line chemotherapeutic agent for glioblastoma, was measured using the neutral red assay [2]. Temozolomide is an alkylating agent that methylates the O<sup>6</sup> position of guanine, subsequently leading to DNA damage and apoptosis [2]. U251/shRandom, U251/shNSUN5 #3, and U251/shNSUN5 #4, T98/shRandom, T98/shNSUN5 #3, T98/shNSUN5 #4 cells were seeded into 96-well plates with 1000 cells per well. The next day, the culture medium was replaced with fresh medium, and cells treated with increasing concentrations of temozolomide (untreated, 62.5, 150, 250, and 500  $\mu$ M) for 96 hours. Cell viability was measured using the neutral red uptake assay described above. The intensity of the dye was measured using a FLUOstar Omega microplate reader. The survival curves and the half maximal inhibitory concentrations (IC<sub>50</sub>) for temozolomide treatment were obtained using GraphPad Prism 6 software.

### **2.15 Clonogenic survival assay**

To determine the sensitivity of single cells to temozolomide, the clonogenic assay was used. The clonogenic assay measures the ability of single cells to grow into colonies upon treatment with drugs, and the method has been described in previous publications [367-370]. U251/shRandom, U251/shNSUN5 #3, and U251/shNSUN5 #4, T98/shRandom, T98/shNSUN5 #3, T98/shNSUN5 #4 cells were seeded at 300, 300, 600, 1200, 2400, and 4800 cells per well in 6-well plates. The next day, the cells with 300, 300, 600, 1200, 2400, and 4800 cells per well were treated with 0, 6.25, 12.5, 25, 50, and 100  $\mu$ M temozolomide, respectively, for 48 hours. Cells were allowed to proliferate until colonies (defined as >50 cells) formed. To quantify the colonies, the cells were washed with PBS, fixed with 4% paraformaldehyde, and stained with 0.5% crystal violet (Sigma-Aldrich) in 70% ethanol for an hour at room temperature. The colonies were counted both

manually and automatically. The plating efficiency (PE) is the number of colonies divided by the number of seeded cells in the 0  $\mu$ M temozolomide-treated well. The survival fraction (SF) is the number of colonies divided by the number of plated cells and PE (SF = number of colonies/ (number of seeding cells\*PE). The survival curves and the IC<sub>50</sub> of temozolomide treatment were obtained using GraphPad Prism 6 software.

### **2.16 Sphere formation assay**

To determine whether NSUN5 regulates the stem cell phenotype, sphere formation assays were performed in glioblastoma cells as previously described [371]. Briefly, cells were washed with modified Hank's Balanced Salt Solution (HBSS) and resuspended in DMEM/F12 sphere culture medium, which contains 20 ng/ml EGF (Gibco, Thermo Fisher), 20 ng/ml basic FGF (Gibco, Thermo Fisher), and 1X B27 supplement (Gibco, Thermo Fisher). Specific numbers of cells (100 cells, 200 cells, or 500 cells in 100  $\mu$ l) were seeded in ultralow attachment 96-well plates. After culturing cells for 7 to 14 days, sphere numbers were counted. Images of the spheres were taken using AMG EVOS FL microscope and 10X or 20X lens.

For sphere formation assay of patient-derived primary glioblastoma cultures, cells were seeded in regular 96-well plates. For limiting dilution sphere formation assay, the following numbers of cells per well were seeded into 96 well plates in a volume of 100  $\mu$ l: 1024, 512, 256, 128, 64, 32, 16, 8, 4, 2, 1, and 0.5 cells. Eight wells were seeded for each cell concentration in two replicate plates.

### **2.17 Mice intracranial xenograft model**

To determine whether NSUN5 regulates the growth of glioblastoma tumors *in vivo*, control and NSUN5-depleted glioblastoma cells were xenografted into the brains of non-obese diabetic, severe combined immunodeficient, and IL2 receptor gamma chain complete mutation (NSG) mice. U251 cells were used in this orthotopic mouse model as the cell line was already known to form tumors in mice [372]. Specifically, U251/shRandom-luciferase-tdTomato vs U251/shNSUN5 #4-luciferase-tdTomato cells were utilized. The procedure was performed following the method published by Bauman et al. and described in publications from Dr. Donna Senger's lab [373-375]. Briefly, glioblastoma cells were harvested, counted, and resuspended in serum-free medium to achieve the concentration of 10,000 cells/ $\mu$ l or 50,000 cells/ $\mu$ l for U251 cells. Mice were subjected to 3% isoflurane in oxygen as anesthesia and they were positioned on a stereotactic platform for injection. The respiration and body temperature of the mice were monitored throughout the process. A 1 cm sagittal incision over the parietal bone was made, and a burrhole 2 mm to the right of the midline and 1 mm posterior to the bregma (coronal suture) was drilled [373-375]. 50,000 cells (or 250,000 cells in 5  $\mu$ l of serum-free media) were injected by syringe injector at a rate of 1  $\mu$ l/min into the skull at 3 mm depth followed by stapling of the scalp [373-375]. The mice were weighted weekly and euthanized when the weight lost surpassed 20% of its highest body weight. GraphPad Prism 6 was used to generate mice survival curves.

## **2.18 IVIS bioluminescence imaging**

To monitor the growth of xenografted glioblastoma tumors, the mice injected with cells carrying the luciferase gene were imaged weekly using the IVIS bioluminescence imaging system. Briefly, mice were anesthetized with 3% isoflurane in oxygen. After anesthesia, 500  $\mu$ l of D-Luciferin, Potassium Salt (GoldBio) in PBS solution was intraperitoneally injected. Mice were

transferred to the scanner and scanned using the living image software. Bioluminescence imaging was conducted weekly, and tumor growth and survival were analyzed.

### **2.19 Immunohistochemistry of the xenografted tumors**

Upon euthanasia, mouse brains containing tumors were paraffin-embedded and sectioned. Tissue sections were used for Hematoxylin and Eosin (H&E) staining and IHC. U251 tumors were detected and expression of NSUN5 in the tumors was determined by IHC using an antibody that specifically recognizes a human mitochondrial protein (anti-mitochondria, Chemicon MAB1273, clone 113-1 at 1:1500 dilution) and an NSUN5-specific antibody (#K1411, Santa Cruz Biotechnology, at 1:400), respectively. H&E staining and IHC protocols, performed by Darryl Glubrecht in Dr. Roseline Godbout's lab, have been previously described [357, 376]. Briefly, paraffin-embedded tissue sections were heated to 60°C for 10 minutes, and deparaffinized with xylene 3 times for 10 minutes each. Tissue sections were then hydrated in 100%, 100%, 100%, 100%, 80%, and 50% ethanol solution by dipping 20 times, followed by ddH<sub>2</sub>O and then TBS. The antigens on the sections were exposed with antigen retrieval solution containing citraconic anhydride, 98% (Aldrich 125318-100g) diluted in ddH<sub>2</sub>O to 0.05%, pH 7.4. Tissue sections were then placed in a Nordic Ware Tender Cooker pressure cooker, and heated at 750W for 6 minutes, then cooled for 15 minutes. Endogenous peroxidases were blocked with 0.5% fish gelatin in TBST (0.05% Tween 20) for 30 minutes. Tissue sections were incubated with primary antibodies diluted in Dako antibody diluent overnight at 4°C in a sealed humidified chamber. To block endogenous peroxidases, the slides were treated with 3% H<sub>2</sub>O<sub>2</sub> in TBS for 15 minutes and washed 2 times in TBST (0.05% Tween 20) for 5 minutes. Secondary antibody (Dakocytomation Envision+ System Labelled Polymer HRP anti-mouse) was then added for 60 minutes. Dako Liquid DAB+ Substrate

Chromagen System was added, and the slides were monitored under a microscope to achieve an appropriate signal strength. The reaction was terminated by rinsing with water. The stained sections were dipped in Harris hematoxylin for 10 seconds for counterstaining and washed with running water for 3 minutes. Sections were dehydrated and mounted with coverslips.

## **2.20 Puromycin protein synthesis assay**

To determine the effect of NSUN5 on protein synthesis rates in glioblastoma cells, the puromycin protein synthesis assay was performed. Puromycin mimics the 3' end of the aminoacylated tRNA and is incorporated into the nascent peptide chain, which causes the termination of translation and the release of this puromycin-containing premature translating peptide [377, 378]. After puromycin treatment, the nascent synthesized peptide chains containing puromycin can be visualized by Western blotting using an anti-puromycin antibody as described by Grewal et al. [377, 378]. Briefly, glioblastoma cells were treated with 10 µg/ml Puromycin Hydrochloride (Sigma) for 15 minutes. The cells were washed with PBS and cell lysates were prepared as described in section 2.6. The protein lysates were run on SDS-PAGE gels and transferred to nitrocellulose membranes for puromycin detection via anti-puromycin antibody (clone 12D10 Millipore, Sigma). Ponceau S acid (Sigma-Aldrich) staining was used to confirm even loading. IR Dye 800CW, Donkey anti-Mouse (#C50422-04, Li-Cor) was used as the secondary antibody.

## **2.21 Liquid chromatography–mass spectrometry (LC-MS/MS)**

To examine differential protein expression in glioblastoma cells with NSUN5 knockdown or overexpression, three cell lysate replicates (R1, R2, R3) from each of U251/shRandom and

U251/shNSUN5#4 cells, as well as from 50M/pLenti-Vector and 50M/pLenti-NSUN5 cells were prepared and analysed by LC-MS/MS. The experiment was performed and analyzed by Dr. Dylan Dieters in Dr. Postovit's lab as previously described [379]. Briefly, cells were cultured to 80% confluence and pelleted. Whole cell lysates were prepared using lysis buffer (8 M urea, 10 mM DTT, 50 mM ABC (Ammonium Bicarbonate, Thermo Fisher Scientific), and 2% SDS). Proteins from 25 µg of cell lysate were precipitated with chloroform/methanol following Wessel and Flügge's method [380]. Next, On-pellet in-solution digestion was conducted as described by Duan et al. [381]. Briefly, 100 µL of 50 mM ABC (pH 8) was added to the precipitated protein to resuspend the protein, followed by LysC (Wako Chemicals, USA) at a 1:100 ratio and mass spectrometry grade trypsin/LysC mix (Promega, Madison, WI, USA) at a 1:50 ratio. The mixture was incubated at 37°C overnight with constant mixing (300 rpm). The next day, additional trypsin/LysC at a 1:100 ratio was added and mixed at 1400 rpm for 4 hours. Ten µl of 10% formic acid (FA) was added to acidify the digests. The digests were analyzed by LC-MS/MS and MS data were analysed in MaxQuant of the Human Uniprot database [382, 383]. The data were further analyzed to generate heat maps, volcano plot maps, and tables for comparison of U251/shRandom vs. U251/shNSUN5#4 cells, and 50M/pLenti-Vector vs. 50M/pLenti-NSUN5 cells.

## **Chapter 3 NSUN5 Expression and RNA Methyltransferase Activity in Glioblastoma Cells**

### 3.1 *NSUN5* expression is strongly associated with poor outcome in glioblastoma patients

Since The Cancer Genome Atlas (TCGA) research network established the first genomic sequencing dataset of glioblastoma patients in 2008, gene expression profiling of glioblastoma has been increasingly used to better understand this cancer [11]. In 2013, glioblastoma TCGA datasets increased to include a total of 543 glioblastoma samples, with more comprehensive genomic sequencing data provided for these samples [27]. TCGA analysis resulted in the identification of key mutated or high amplified genes in glioblastoma, including *EGFR*, *TP53*, *PTEN*, *NF1*, *MGMT*, *IDH1*, *PDGFRA*, *PTEN*, and *RBI*, resulting in the discovery of core pathogenesis pathways allowing the classification of glioblastoma into different molecular subtypes [10, 11, 27].

The newest RNA Sequencing datasets (20,500 mRNAs in 153 glioblastoma samples) were generated by the University of North Carolina TCGA genome characterization center in 2013, whereas the Broad Institute of MIT and Harvard University cancer genomic characterization center generated the AffyU133a array dataset (13,500 mRNAs in 540 glioblastoma samples) in 2013. We have analyzed the relationship between *NSUN5* mRNA expression and survival of glioblastoma patients using both datasets. Analyzing the RNA sequencing exon expression dataset on the UCSC Xena platform, we found that *NSUN5* was strongly associated with poor overall survival of glioblastoma patients ( $p = 3.5e-04$ ) (**Figure 3.1 A**). The p value was generated upon comparison of high versus low *NSUN5* expression, with the cut-off for high versus low *NSUN5* RNA levels set at the median point. Consistently, analyzing the Glioblastoma-TCGA-Affymetrix U133A microarray dataset using the R2 Genomics Analysis and Visualization platform, we found that high *NSUN5* expression is strongly associated with poor overall survival in glioblastoma patients (**Figure 3.1 B**). In this analysis, the overall survival curve was automatically generated based on low ( $n = 130$ ) versus high levels ( $n = 374$ ) *NSUN5* mRNA, with a p value of  $3.4e-05$ . We also

analyzed the Glioblastoma-TCGA-Affymetrix U133A mRNA expression profiling for association between NSUN5 expression and progression-free survival of glioblastoma patients. Consistent with overall survival, high NSUN5 mRNA levels were also associated with shorter progression-free survival in glioblastoma patients (**Figure 3.1 C**). When a progression-free survival curve was automatically generated based on low (n = 149) versus high (n = 355) NSUN5 mRNA levels, the p value was 6.4e-04. This suggests that glioblastomas with high levels of NSUN5 mRNA recur much earlier than glioblastomas with low NSUN5 mRNA levels.

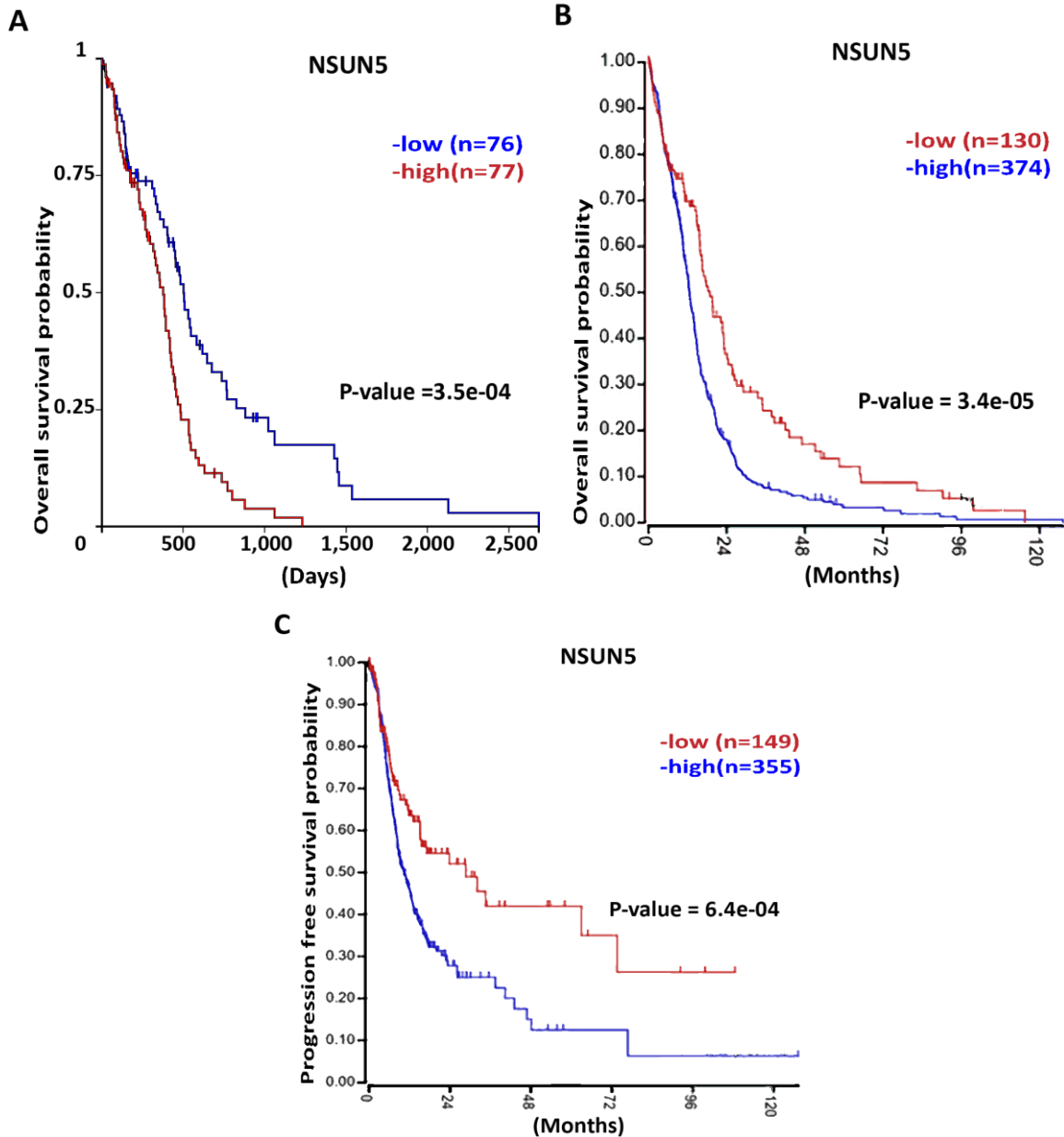


**Figure 3.1 High *NSUN5* expression is strongly associated with poor overall survival of glioblastoma patients.**

(A) The exon expression RNAseq profile of TCGA Glioblastoma dataset containing 153 patients were analysed on the UCSC Xena platform. Kaplan Meier survival analysis showed that glioblastoma patients with high *NSUN5* mRNA levels had shorter overall survival than those with low *NSUN5* mRNA levels. The cut-off for low versus high *NSUN5* RNA levels represents the median position. P value obtained upon comparing high *NSUN5* expression group (n = 77) and

low *NSUN5* expression group (n = 76) was 3.5e-04, Log-rank test statistics was 12.78. **(B and C)** The Affymetrix U133A mRNA expression profiling of Glioblastoma-TCGA-2013 dataset containing 540 patients (504 with survival information) was analysed on the R2 Genomics Analysis and Visualization Platform. The survival curve was automatically generated at scan cut-off site (where the P value was the lowest). **(B)** Kaplan Meier survival analysis showed that glioblastoma patients with high *NSUN5* mRNA expression (n = 374) had shorter overall survival than those with low *NSUN5* mRNA expression (n = 130). The P value was 3.4e-05, and Bonferroni correction test statistics was 0.017. **(C)** Glioblastoma patients with high *NSUN5* mRNA levels (n = 355) had shorter progression-free survival than those with lower *NSUN5* RNA levels (n = 149). The P value was 6.4e-04, and Bonferroni correction test statistics was 0.313.

To confirm the results from the TCGA datasets, we also analyzed another glioma datasets (French 284 dataset Affymetrix HU133) that contains 276 samples from the Erasmus University Medical Center from 1989 to 2005 including 244 high grade gliomas and 32 low grade gliomas patients [354]. Consistent with the results from TCGA datasets, the analysis showed that high *NSUN5* mRNA levels were strongly associated with poor overall survival in these glioma patients. In this analysis, the overall survival curve was automatically generated, resulting in 156 gliomas with low *NSUN5* and 117 gliomas with high *NSUN5* mRNA levels, with a p value of 3.2e-07 **(Figure 3.2)**.

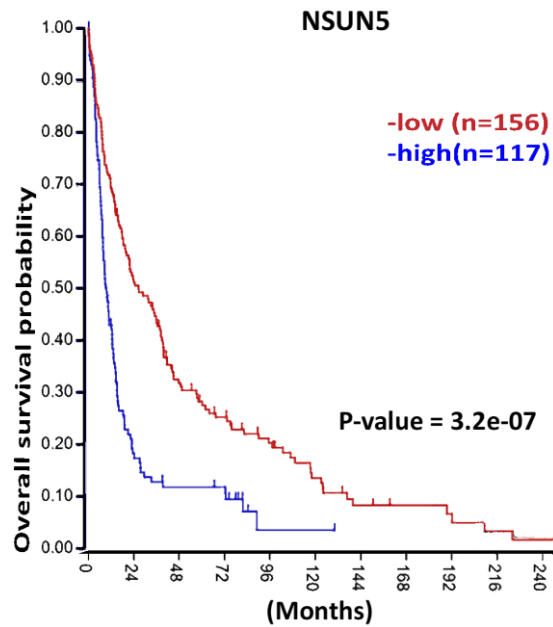


**Figure 3.2 High *NSUN5* expression is strongly associated with poor overall survival of glioma patients.**

Analysis of Tumor Glioma-French-284 dataset of glioma patients showed that patients with high *NSUN5* mRNA levels had shorter overall survival. Kaplan Meier survival analysis showed that glioma patients with high *NSUN5* mRNA expression (n=117) had shorter overall survival than those with low *NSUN5* mRNA expression (n=156). The p value was 3.2e-07, and Bonferroni correction test statistics was 8.2e-05.

Moreover, we also investigated the somatic DNA copy number status of the *NSUN5* gene and DNA methylation status of the *NSUN5* gene promoter, as well as their associations with glioblastoma survival. Analysis of the TCGA-GBM copy number gistic2 thresholded dataset (n = 577) and somatic mutation (SNP and INDEL) dataset (n = 314) on the UCSC Xena platform showed that more than 80% of glioblastoma samples (469 in 573 samples) had *NSUN5* copy number amplification (more than two copies), but only about 1% of glioblastoma samples (4 in 311 samples) had *NSUN5* somatic mutations (including single-nucleotide polymorphisms and small insertion/deletion mutation variants). Somatic copy number alterations were associated with

glioblastoma global survival and progression free survival ( $P = 1.2e-04$  and  $4.7e-04$ , respectively) (**Figure 3.3**). Analysis of the TCGA-GBM DNA methylation 27k dataset ( $n=288$ ) on the UCSC Xena platform showed that lower *NSUN5* CpG islands methylation was associated with shorter glioblastoma global survival and progression free survival ( $P = 3.7e-02$  and  $8.1e-05$ , respectively) (**Figure 3.4**), which is consistent with our finding that high *NSUN5* expression is associated with the shorter survival of glioblastoma patients (**Figure 3.1**). This is because promoter methylation represses gene expression and therefore lower methylation of the *NSUN5* promoter is associated with higher expression of *NSUN5* in the glioblastoma.

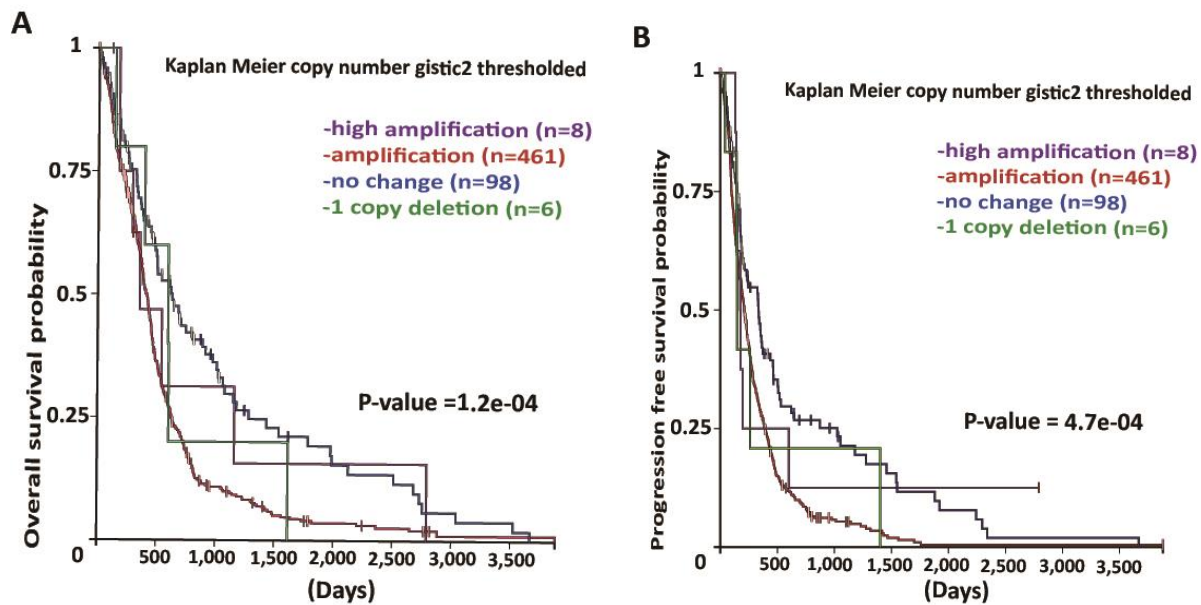


**Figure 3.3 DNA copy number amplification of the *NSUN5* gene was associated with the survival of glioblastoma patients.**

The TCGA-GBM copy number gistic2 thresholded dataset ( $n = 577$ ) was analysed on the UCSC Xena platform. (**A and B**) Kaplan Meier survival analysis showed that glioblastoma patients with *NSUN5* copy number amplification ( $n = 461$ ) had shorter overall survival and progression-free survival than those with no DNA copy number change ( $n = 98$ ). The P value for overall survival

and progression-free survival was  $1.2 \times 10^{-4}$  and  $4.7 \times 10^{-4}$ , respectively. The Log-rank test statistics was 20.75 and 17.82, respectively. Amplification = 3 copies, high amplification  $\geq 4$  copies.

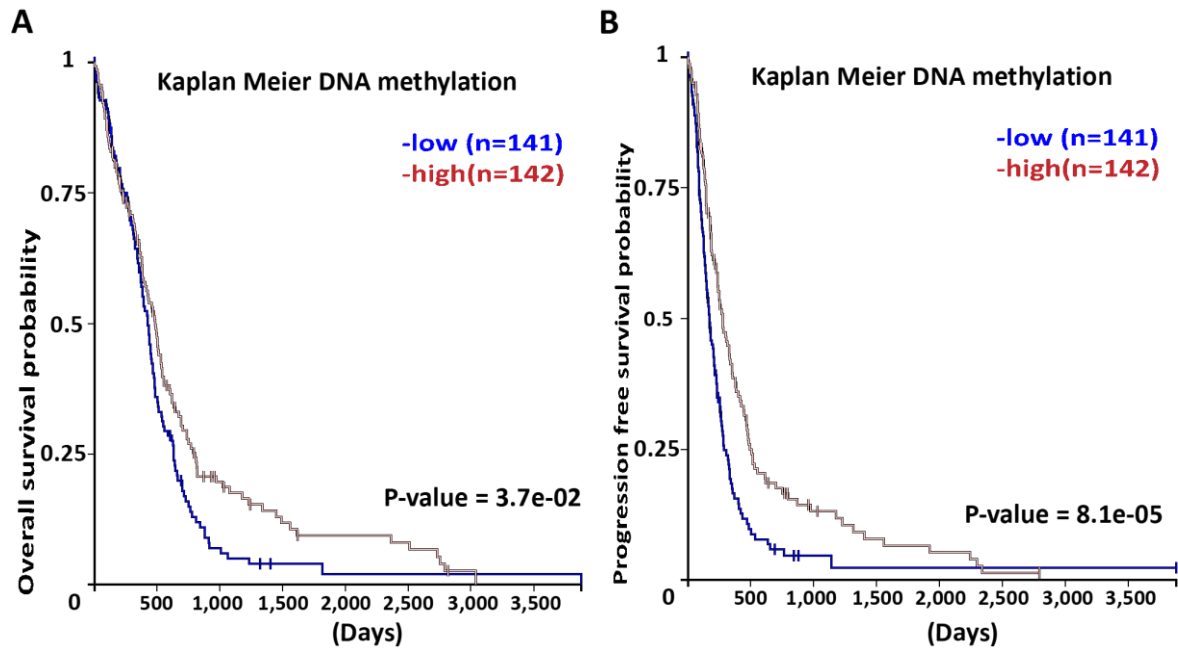


**Figure 3.4 DNA methylation of the *NSUN5* gene promoter is associated with survival of glioblastoma patients.**

The TCGA-GBM DNA methylation 27k dataset ( $n = 288$ ) was analysed on the UCSC Xena platform. Kaplan Meier survival analysis showed that glioblastoma patients with low CpG islands methylation of the *NSUN5* gene promoter ( $n = 141$ ) had shorter overall survival (**A**) and progression-free survival (**B**) than those with high *NSUN5* CpG islands methylation ( $n = 142$ ). The P value for overall survival and progression-free survival was  $3.7 \times 10^{-2}$  and  $8.1 \times 10^{-5}$ , respectively, and the Log-rank test statistics was 4.331 and 15.54, respectively.

In summary, our analysis of TCGA and other datasets indicate that high *NSUN5* expression is associated with shorter overall and progression-free survival for high-grade gliomas including grade III gliomas and glioblastoma. Thus, *NSUN5* is a potential prognostic marker for poor prognosis in high grade glioma patients.

### 3.2 NSUN5 is expressed in glioblastoma cells and mainly located in the nucleus

Our analysis of TCGA and other datasets revealed that high *NSUN5* mRNA levels are strongly associated with poor survival in glioblastoma patients. To determine whether NSUN5 contributes to the formation and/or progression of glioblastoma, we first examined the expression of NSUN5 in human glioblastoma cell lines and patient-derived neurosphere cultures. Nine glioblastoma cell lines (A172, CLA, T98, U87, M021, M016, M049, M103, and U251) were obtained from Dr. Roseline Godbout's lab. These cell lines have been described in many publications [355-357]. Seven glioblastoma patient-derived neurosphere cultures established by Dr. Godbout's lab (A4-003, A4-004, A4-007, A4-010, A4-012) and Dr. Kenneth Petruk's lab (ED511 and ED512) were also examined. In addition, we obtained five patient-derived neurosphere cultures (12EF, 48EF, 25M, 50M, 53M) from Dr. Mary Hitt's lab who obtained them directly from Dr. Godbout's lab. The latter five neurosphere cultures were established by Dr. Samuel Weiss' lab at the University of Calgary, and described in the following publications [358, 359].

Quantitative RT-PCR (RT-qPCR) showed that *NSUN5* was expressed at variable levels in glioblastoma cell lines (**Figure 3.5A**). Western blotting revealed NSUN5 protein in 7 out of 9 glioblastoma cell lines, which is consistent with the mRNA data (**Figure 3.5B**). Because patient-derived glioblastoma cells maintained as neurospheres more closely represent the genotype and phenotype of primary tumors compared to glioblastoma cell lines established under standard growth conditions [384, 385], we also examined NSUN5 protein levels in patient-derived neurosphere cultures. Western blotting showed that NSUN5 was expressed in 8 out of 12 patient-derived primary glioblastoma neurosphere cultures (**Figure 3.5C**). The NSUN5 antibody we used for this study is specific because it detects a single protein band of the right size (47 kDa) and the

band disappeared when NSUN5 was knocked out via CRISPR (see Figure 3.16) or was dramatically decreased when NSUN5 was knocked down via shRNAs (see Figure 4.2). Moreover, this antibody detects ectopically expressed NSUN5 in transfected cell lines (see Figure 4.3). This antibody has also been used by others to detect NSUN5 [386, 387]. Based on our Western blotting data, we selected U87, 50M, 25M cells that do not express endogenous NSUN5 for NSUN5 overexpression and U251, T98, A4-012 cells that express high levels of NSUN5 for NSUN5 knockout or knockdown experiments.

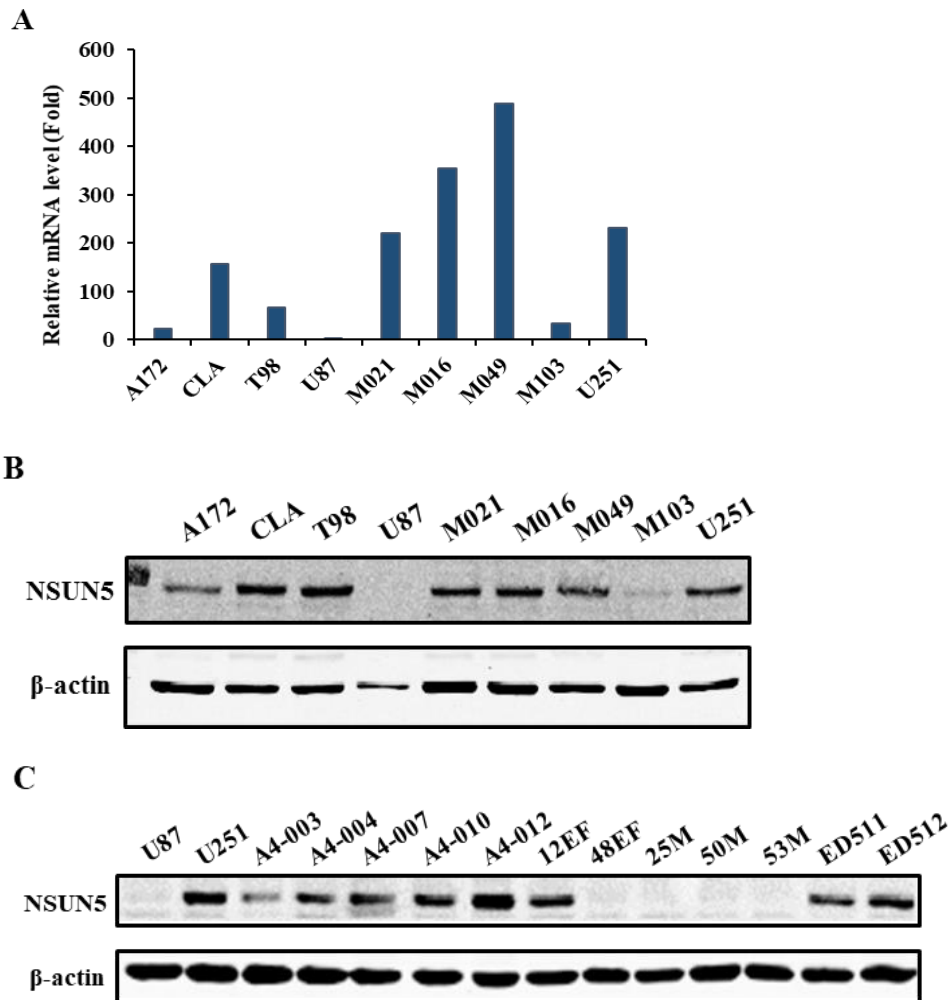


**Figure 3.5 NSUN5 expression in glioblastoma cell lines and glioblastoma patient-derived neurosphere cultures.**

(A) *NSUN5* mRNA levels were examined by RT-qPCR in 9 glioblastoma cell lines. The expression of *NSUN5* is normalized against GAPDH (the internal control) and presented as fold change relative to that of U87 cells that expresses the lowest levels of *NSUN5* mRNA. The result is from one experiment. (B) *NSUN5* protein levels in 9 glioblastoma cell lines were examined by Western blotting.  $\beta$ -actin was the loading control. (C) *NSUN5* protein levels in 12 patient-derived primary glioblastoma cultures were examined by Western blotting.  $\beta$ -actin was the loading control. U87 and U251 are the negative and positive control, respectively.

As *NSUN5* is predicted to be an rRNA cytosine methyltransferase and modification of rRNAs (a predominant step of ribosome biogenesis) takes place in the nucleus (mainly in the nucleolus) [388, 389], we examined the subcellular localization of *NSUN5* in glioblastoma cells. To do this, we performed immunocytochemistry in U251 cells that express endogenous *NSUN5* and U87 cells that were stably transfected with a CMV-*NSUN5* expression construct. As shown in **Figures 3.6 and 3.7**, both endogenous *NSUN5* in U251 cells and overexpressed *NSUN5* in U87 cells were localized to the nucleus and found mainly in the nucleolus. Additionally, the localization of *NSUN5* was also examined in two glioblastoma patient tissues (A4-009 glioblastoma and A4-001 grade III astrocytoma) using IHC. We found that *NSUN5* was differentially expressed in the two tissues and located in the nucleus of most of the cells in A4-009 tissue, but only a few cells in A4-001 tissue (**Figure 3.8**). Therefore, our combined results show that *NSUN5* is located in the nucleus and mainly in the nucleolus of glioblastoma cells, which is consistent with the prediction that *NSUN5* is an RNA cytosine methyltransferase that plays a role in ribosome modification [312].

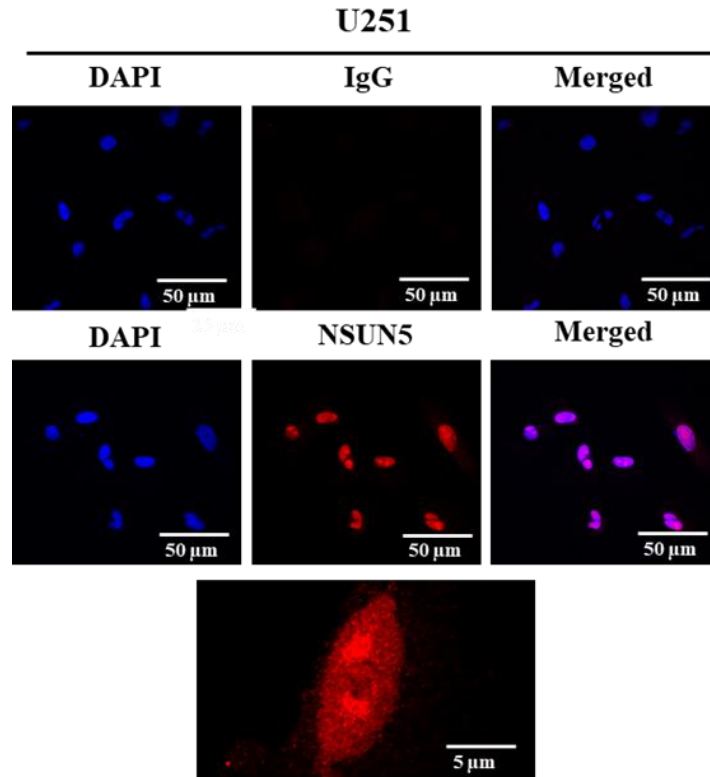


**Figure 3.6 Endogenous NSUN5 in U251 cells is localized in the nucleus and is found mainly in the nucleolus.**

Immunocytochemistry was performed to examine the subcellular localization of NSUN5 in U251 cells using an anti-NSUN5 antibody. IgG was the negative control. DAPI was used to stain the nucleus. A single cell immunostained with NSUN5 antibody is shown at a higher magnification in the bottom panel. The results show that endogenous NSUN5 in U251 cells is localized in the nucleus and highly present in the nucleolus. Merged images of DAPI and NSUN5 show that NSUN5 is expressed in all U251 cells. Immunofluorescence images were captured with a confocal microscope using a 20X objective. Scale bar = 50  $\mu\text{m}$ .

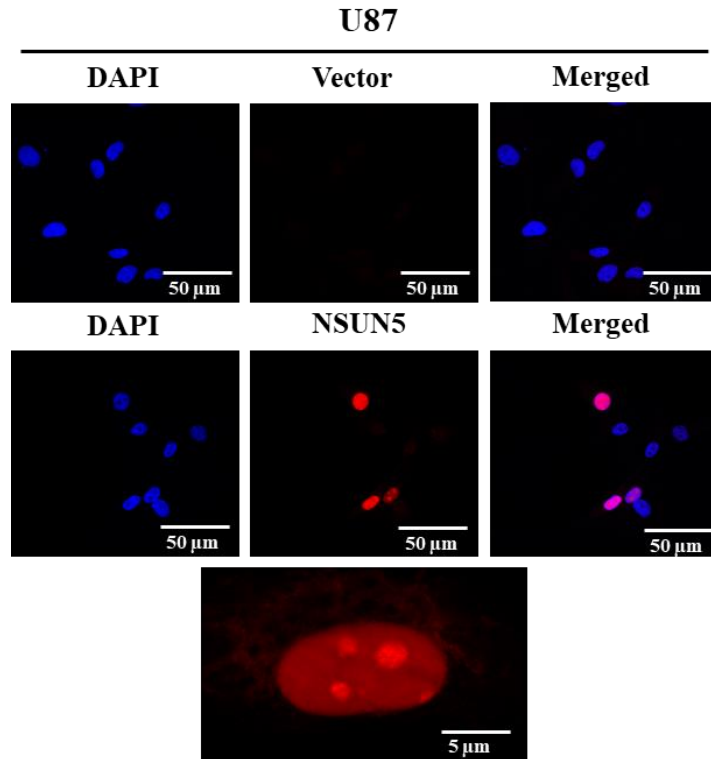


**Figure 3.7 Overexpressed NSUN5 in U87 cells localizes to the nucleus and is found mainly in the nucleolus.**

Immunocytochemistry was performed to detect overexpressed NSUN5 in U87 CMV-NSUN5 cells using an anti-NSUN5 antibody. U87 cells transfected with empty vector were included as the negative control. DAPI was used to stain the nucleus. A single cell immunostained with NSUN5 antibody is shown in the bottom panel. The results show that NSUN5 is not detected in U87 cells transfected with empty vector and that overexpressed NSUN5 in U87 cells localizes to the nucleus and is primarily found in the nucleolus. Merged images of DAPI and NSUN5 staining showed that 3 in 7 cells were positive for NSUN5, suggesting a transfection efficiency of ~40% for the CMV-NSUN5 vector. Immunofluorescence images were captured using a confocal microscope with a 20X objective. Scale bar = 50  $\mu\text{m}$ .

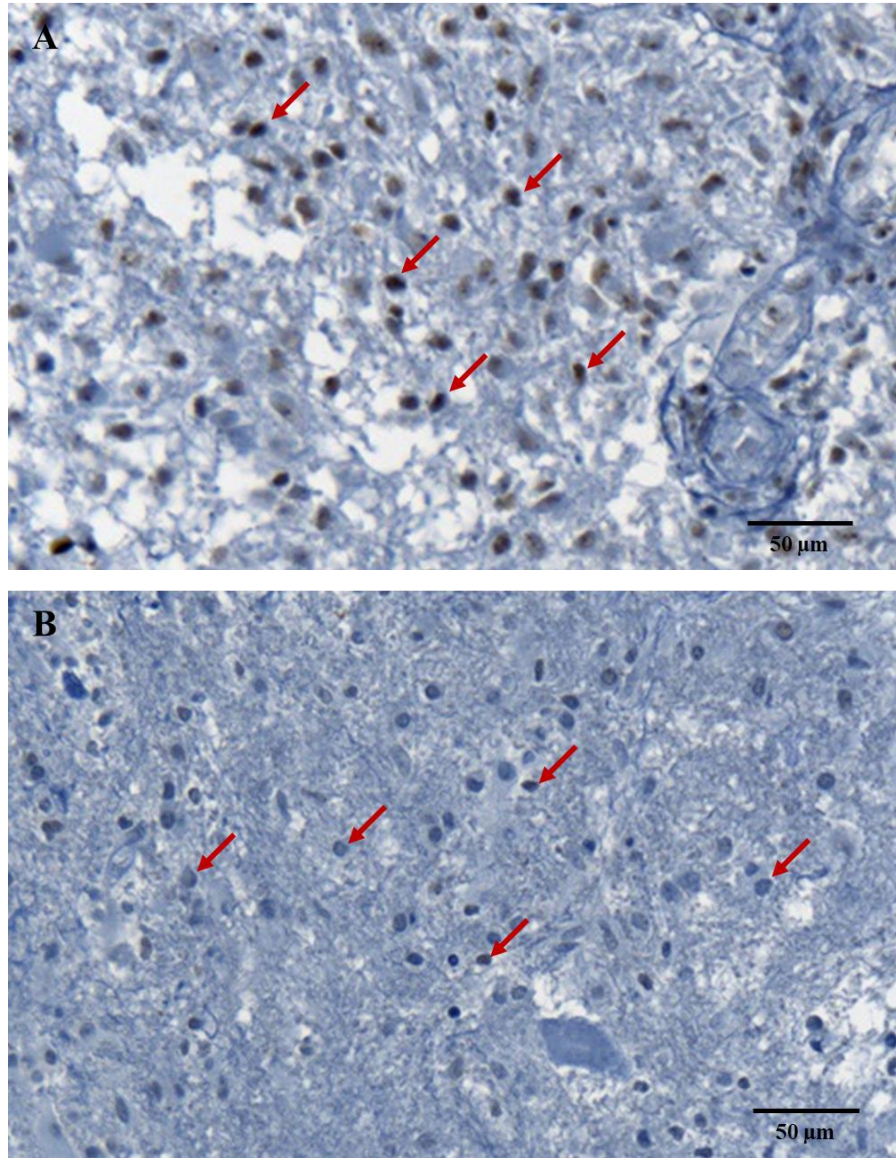


**Figure 3.8 Immunostaining of NSUN5 in two human glioma tissues.**

(A) IHC staining shows high levels of NSUN5 expression in A4-009 glioblastoma tissue. The brown stain represents positive signals (red arrows), with most of the immunostaining found in the nuclei of tumor cells. (B) IHC staining shows low expression of NSUN5 in the A4-001 grade III astrocytoma tissue. Nuclei were counterstained with hematoxylin. All the images were taken with a 20X objective.

### 3.3 NSUN5 methylates C3782 of 28S rRNA in HEK293T and glioblastoma cells

There are three types of rRNA modifications: pseudouridylation, 2'-O methylation of ribose and base modifications [219]. Technological advances have resulted in improved mapping of these rRNA modifications in yeast and human [219, 238, 390]. Most modified sites are at the functional center of the rRNA structure in both yeast and human. In yeast rRNAs, there are 113 modified sites: 55 2'-O methylations of ribose, 47 pseudouridines, and 10 base methylations. Among the base methylations, there are only two cytosine methylation sites: cytosine 2278 (C2278) and cytosine 2870 (C2870) of 25S rRNA in yeast [219, 238, 390]. Rcm1 (the yeast homologue of NSUN5) and Nop2 (the yeast homologue of NSUN1) are responsible for methylating C2278 and C2870, respectively [238]. In human rRNAs, there are 212 modified sites in rRNAs: 106 2'-O methylations of ribose, 95 pseudouridines, and 10 base methylations. Similarly, there are only two cytosine methylation sites: C3782 and C4447 of 28S rRNA [219, 225]. Because of the similarity between human 28S and yeast 25S rRNA secondary structures at the two cytosine methylation sites (Figure 1.4), NSUN5 and NSUN1 are predicted to methylate C3782 and C4447 of human 28S rRNA, respectively [238]. However, whether NSUN5 indeed methylates C3782 in mammalian cells was unknown when we started the project. To address this question, we knocked out the expression of NSUN5 in HEK293T and U251 cells, and overexpressed NSUN5 in U87 cells that does not express endogenous NSUN5. We measured the change in C3782 methylation status in response to NSUN5 expression using RNA bisulfite sequencing.

HEK293T cells are easy to transfect and express endogenous NSUN5. We therefore first used 293T cells to determine whether NSUN5 is responsible for C3782 methylation of human 28S rRNA. We used CRISPR/Cas9 technology to knock out NSUN5 expression in 293T cells. Briefly, 293T cells were transfected with CRISPR/Cas9 NSUN5 knockout plasmids and sorted by FACS

into 96-well plates with one single cell per well (positively transfected cells express mCherry red fluorescent protein). The single cells were then expanded and NSUN5 expression in these clonal populations was examined by Western blotting. Among the successfully propagated 44 clones that we examined, two clones (#12 and #22) lost NSUN5 expression, and two clones (#4 and #38) had reduced NSUN5 protein levels (**Figure 3.9A**). Clone #37 (normal NSUN5 expression), clones #4 and #38 (reduced NSUN5), as well as clone #12 and clone #22 (loss of NSUN5) were propagated further and NSUN5 expression status in these clones was confirmed by Western blotting (**Figure 3.9B**).

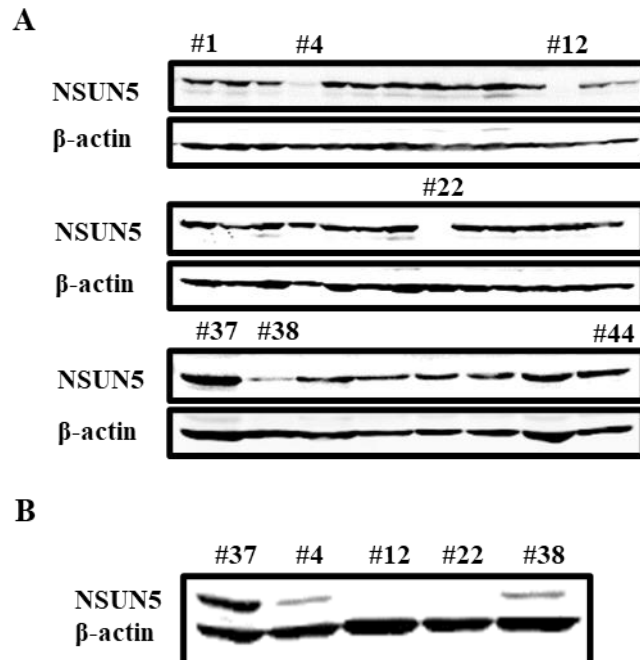


**Figure 3.9 NSUN5 expression in 44 CRISPR clones of HEK293T cells.**

(A) NSUN5 protein levels in 44 CRISPR clones were examined by Western blotting. Clones #12 and #22 lost NSUN5 expression. Clones #4 and #38 displayed a reduced level of NSUN5.  $\beta$ -actin was the loading control. (B) Clones #37, #4, #12, #22, and #38 were further propagated for longer-term studies and NSUN5 expression in these cells was examined by Western blotting.  $\beta$ -actin was the loading control.

Next, we performed genomic DNA sequencing to confirm that lost or reduced expression of NSUN5 in the HEK293T clones in **Figure 3.9B** was due to indels (insertions/deletions) in exon 2 of the *NSUN5* gene induced by the NSUN5 CRISPR knockout plasmid. Briefly, genomic DNA was isolated from clones #37, #4, #12, #22, and #38. DNA sequences at CRISPR guide RNA target sites of exon II of the *NSUN5* gene were amplified by PCR and cloned into Topo cloning plasmids. The plasmids were transformed into bacteria and plasmid DNA was isolated from multiple bacterial colonies (2 for #37 and 6 each for #4, #12, #22 and #38) for sequencing. As expected, clone #37 had wild type DNA sequence at the *NSUN5* guide RNA target site (**Figure 3.10**). Clones #12 and #22 each had two different types of frameshift DNA mutations (deletion of 8 nucleotides and insertion of one nucleotide in clone #12 and deletion of 4 nucleotides and insertion of 8 nucleotides in clone #22), which explained the loss of NSUN5 protein expression in these clones (**Figure 3.10**). Both clones #4 and #38 had one deletion of 8 nucleotides and wild type DNA (**Figure 3.10**). Because somatic human genes have two alleles, it is not surprising that the two alleles have different types of mutations after CRISPR/Cas9 knockout and DNA double strand break repair. The presence of the wild type allele in clones #4 and #38 explained why NSUN5 expression was reduced, but not lost in these two clones (**Figure 3.10**). Our sequencing results thus confirmed that appropriate frame-shift mutations were induced in clones #12 and #22, which caused loss of NSUN5 protein expression.

**NSUN5 DNA sequence at CRISPR guide RNA target site**

<b>Original</b>		CGGCCTCCTC	CGTGCGGAGA	AGAAGCTGCG	GCCGCACCTG	GCCAAGG
<b>Clone #37</b>	Sample 1	CGGCCTCCTC	CGTGCGGAGA	AGAAGCTGCG	GCCGCACCTG	GCCAAGG
	Sample 2	CGGCCTCCTC	CGTGCGGAGA	AGAAGCTGCG	GCCGCACCTG	GCCAAGG
	Sample 3	CGGCCTCCTC	CGTGCGGAGA	AGAAGCTGCG	GCCGCACCTG	GCCAAGG
	Sample 4	CGGCCTCCTC	CGTGCGGAGA	AGAAGCTGCG	GCCGCACCTG	GCCAAGG
<b>Clone #4</b>	Sample 1	CGGCCTCCTC	AGTGCG----- A	AGAAGCTGCA	GCCGCACCTG	GCCAAGG
	Sample 2	CGGCCTCCTC	AGTGCG----- A	AGAAGCTGCA	GCCGCACCTG	GCCAAGG
	Sample 3	CGGCCTCCTC	AGTGCG----- A	AGAAGCTGCA	GCCGCACCTG	GCCAAGG
	Sample 4	CGGCCTCCTC	AGTGCG----- A	AGAAGCTGCA	GCCGCACCTG	GCCAAGG
	Sample 5	CGGCCTCCTC	CGTGCGGAGA	AGAAGCTGCG	GCCGCACCTG	GCCAAGG
	Sample 6	CGGCCTCCTC	CGTGCGGAGA	AGAAGCTGCG	GCCGCACCTG	GCCAAGG
<b>Clone #12</b>	Sample 1	CGGCCTCCTC	AGT-GCG-----A	AGAAGCTGCA	GCCGCACCTG	GCCAAGG
	Sample 2	CGGCCTCCTC	AGT-GCG-----A	AGAAGCTGCA	GCCGCACCTG	GCCAAGG
	Sample 3	CGGCCTCCTC	AGT-GCG-----A	AGAAGCTGCA	GCCGCACCTG	GCCAAGG
	Sample 4	CGGCCTCCTC	AGT-GCG-----A	AGAAGCTGCA	GCCGCACCTG	GCCAAGG
	Sample 5	CGGCCTCCTC	CGTTGCGGAGA	AGAAGCTGCG	GCCGCACCTG	GCCAAGG
	Sample 6	CGGCCTCCTC	CGTTGCGGAGA	ANAAGCTGCG	GCCGCACCTG	GCCAAGG
<b>Clone #22</b>	Sample 1	CGGCCTCCT	---- GCGGAGA	AGAAGCTGCG	GCCGCACCTG	GCCAAGG
	Sample 2	CGGCCTCCT	---- GCGGAGA	AGAAGCTGCG	GCCGCACCTG	GCCAAGG
	Sample 3	CGGCCTCCT	---- GCGGAGA	AGAAGCTGCG	GCCGCACCTG	GCCAAGG
	Sample 4	CGGCCTCCT	---- GCGGAGA	AGAAGCTGCG	GCCGCACCTG	GCCAAGG
	Sample 5	CGGCCTCCTC	AGTGCG----- A	AGAAACTGCA	GCCGCACCTG	GCCAAGG
	Sample 6	CGGCCTCCTC	AGTGCG----- A	AGAAGCTGCA	GCCGCACCTG	GCCAAGG
<b>Clone #38</b>	Sample 1	CGGCCTCCTC	AGTGCG----- A	AGAAGCTGCA	GCCGCACCTG	GCCAAGG
	Sample 2	CGGCCTCCTC	AGTGCG----- A	AGAAGCTGCG	GCCGCACCTG	GCCAAGG
	Sample 3	CGGCCTCCTC	CGTGCGGAGA	AGAAGCTGCG	GCCGCACCTG	GCCAAGG
	Sample 4	CGGCCTCCTC	CGTGCGGAGA	AGAAGCTGCG	GCCGCACCTG	GCCAAGG
	Sample 5	CGGCCTCCTC	CGTGCGGAGA	AGAAGCTGCG	GCCGCACCTG	GCCAAGG

**Figure 3.10 Genomic DNA sequencing results for indels induced by CRISPR in the *NSUN5* gene of HEK293T CRISPR clones.**

The *NSUN5* DNA at the CRISPR guide RNA target site in 293T clones #37, #4, #12, #22, and #38 cells was sequenced by Sanger sequencing. The results show that clone #37 still has the wild type sequence; clone #12 has two different types of mutations (deletion of 8 nucleotides and insertion of one nucleotide); clone #22 has two different types of mutation (deletion of 4 nucleotides and deletion of 8 nucleotides); both clone #4 and clone #38 have one type of mutation (deletion of 8 nucleotides) and wild type sequence.

Bisulfite treatment converts unmethylated cytosines in RNAs into uracils that would be converted to thymines in the RT-PCR step of bisulfite sequencing. Methylated cytosines are not affected by bisulfite treatment. Bisulfite sequencing has been widely used to determine the cytosine

methylation status in genomic DNA or RNA. To determine whether NSUN5 is responsible for methylation of C3782 of human 28S rRNA, we isolated RNA from the HEK293T CRISPR clones described above and performed RNA bisulfite sequencing. Total RNA was isolated from one wild type (clone #37) and two NSUN5 knockout 293T clones (#12 and #22). The RNA samples were treated with bisulfite and reverse transcribed to cDNA as described in the Material and Methods chapter (Figure 2.11). The regions of 28S rRNA containing C3782 or C4447 were amplified by PCR and cloned into the TOPO vector. After transformation and white/blue colony screening, plasmid DNA was isolated from white colonies and subject to sequencing analysis.

The sequencing results showed that most cytosines (C) in the 28S rRNA sequences were converted into thymines (T) by bisulfite treatment, with a conversion efficiency > 99%. C3782 was not converted to thymine by bisulfite treatment in the wild-type clone (#37), indicating that C3782 is methylated in wild type 293T cells. In contrast, C3782 was converted into thymine in the two NSUN5 knockout clones (#12 and #22), indicating that NSUN5 knockout led to loss of C3782 methylation (**Figure 3.11**). These results confirm that NSUN5 is responsible for the methylation of C3782 on 28S rRNA in 293T cells.

		↙ C3782
<b>Original C3782 sequence</b>		AGTAACTATG ACTCTCTTAAGGTAGCCAAATGCCCTCGTCATCTAATTAGT GACGCGCATG
<b>Clone #37</b>	Sample 1	AGTAATTATG ATTTTTTTAA GGTAGTCAA TGTTTTGTTA TTTAATTAGT GATGTGTATG
	Sample 2	AGTAATTATG ACTTTTTTAA GGTAGTCAA TGTTTTGTTA TTTAATTAGT GATGTGTATG
	Sample 3	AGTAATTATG ANTTTTTTAA GGTAGTCAA TGTTTTGTTA TTTAATTAGT GATGTGTATG
	Sample 4	AGTAATTATG ATTTTTTTAA GGTAGTCAA TGTTTTGTTA TTTAATTAGT GATGTGTATG
	Sample 5	AGTAATTATG ATTTTTTTAA GGTAGTCAA TGTTTTGTTA TTTAATTAGT GATGTGTATG
	Sample 6	AGTAATTATG ATTTTTTTAA GGTAGTCAA TGTTTTGTTA TTTAATTAGT GATGTGTATG
	Sample 7	AGTAATTATG ATTTTTTTAA GGTAGTCAA TGTTTTGTTA TTTAATTAGT GATGTGTATG
	Sample 8	AGTAATTATG ATTTTTTTAA GGTAGTCAA TGTTTTGTTA TTTAATTAGT GATGTGTATG
	Sample 9	AGTAACTATG ATTTTTTTAA GGTAGTCAA TGTTTTGTTA TTTAATTAGT GATGTGTATG
	Sample 10	AGTAATTATG ATTTTTTTAA GGTAGTCAA TGTTTTGTTA TTTAATTAGT GATGTGTATG
	Sample 11	AGTAATTATG ATTTTTTTAA GGTAGTCAA TGTTTTGTTA TTTAATTAGT GATGTGTATG
<b>Clone #12</b>	Sample 1	AGTAATTATG ATTTTTTTAA GGTAGTTAAA TGTTTTGTTA TTTAATTAGT GATGTGTATG
	Sample 2	AGTAATTATG ATTTTTTTAA GGTAGTTAAA TGTTTTGTTA TTTAATTAGT GATGTGTATG
	Sample 3	AGTAATTATG ATTTTTTTAA GGTAGTTAAA TGTTTTGTTA TTTAATTAGT GATGTGTATG
	Sample 4	AGTAATTATG ATTTTTTTAA GGTAGTTAAA TGTTTTGTTA TTTAATTAGT GATGTGTATG
	Sample 5	AGTAATTATG ATTTTTTTAA GGTAGTTAAA TGTTTTGTTA TTTAATTAGT GATGTGTATG
	Sample 6	AGTAATTATG ATTTTTTTAA GGTAGTTAAA TGTTTTGTTA TTTAATTAGT GATGTGTATG
	Sample 7	AGTAATTATG ATTTTTTTAA GGTAGTTAAA TGTTTTGTTA TTTAATTAGT GATGTGTATG
	Sample 8	AGTAATTATG ATTTTTTTAA GGTAGTTAAA TGTTTTGTTA TTTAATTAGT GATGTGTATG
	Sample 9	AGTAATTATG ATTTTTTTAA GGTAGTTAAA TGTTTTGTTA TTTAATTAGT GATGTGTATG
	Sample 10	AGTAATTATG ATTTTTTTAA GGTAGTTAAA TGTTTTGTTA TTTAATTAGT GATGTGTATG
	Sample 11	AGTAATTATG ATTTTTTTAA GGTAGTTAAA TGTTTTGTTA TTTAATTAGT GATGTGTATG
	Sample 12	AGTAATTATG ATTTTTTTAA GGTAGTTAAA TGTTTTGTTA TTTAATTAGT GATGTGTATG
<b>Clone #22</b>	Sample 1	AGTAATTATG ATTTTTTTAA GGTAGTTAAA TGTTTTGTTA TTTAATTAGT GATGCGTATG
	Sample 2	AGTAATTATG ATTTTTTTAA GGTAGTTAAA TGTTTTGTTA TTTAATTAGT GATGTGTATG
	Sample 3	AGTAATTATG ATTTTTTTAA GGTAGTTAAA TGTTTTGTTA TTTAATTAGT GATGTGTATG
	Sample 4	AGTAATTATG ATTTTTTTAA GGTAGTTAAA TGTTTTGTTA TTTAATTAGT GATGTGTATG
	Sample 5	AGTAATTATG ATTTTTTTAA GGTAGTTAAA TGTTTTGTTA TTTAATTAGT GATGTGTATG
	Sample 6	AGTAATTATG ATTTTTTTAA GGTAGTTAAA TGTTTTGTTA TTTAATTAGT GATGTGTATG
	Sample 7	AGTAATTATG ATTTTTTTAA GGTAGTTAAA TGTTTTGTTA TTTAATTAGT GATGTGTATG
	Sample 8	AGTAATTATG ATTTTTTTAA GGTAGTTAAA TGTTTTGTTA TTTAATTAGT GATGTGTATG
	Sample 9	AGTAATTATG ATTTTTTTAA GGTAGTTAAA TGTTTTGTTA TTTAATTAGT GATGTGTATG
	Sample 10	AGTAATTATG ATTTTTTTAA GGTAGTTAAA TGTTTTGTTA TTTAATTAGT GATGTGTATG
	Sample 11	AGTAATTATG ATTTTTTTAA GGTAGTTAAA TGTTTTGTTA TTTAATTAGT GATGTGTATG

**Figure 3.11 NSUN5 is responsible for methylation of C3782 in 293T 28S rRNA.**

RNA from the 293T clones (#37 for wild-type and #12 and 22 for NSUN5 knockout) were analyzed by bisulfite sequencing to determine the methylation status of C3782 in 28S rRNA. Compared with the original sequence, > 99% of cytosines (C) were converted into thymines (T), indicating the success of the experiments. C3782 in wild-type clone #37 (n = 11) remained unconverted, while C3782 in NSUN5 knockout clones #12 (n = 12) and 22 (n = 11) was converted to thymine, indicating that C3782 methylation was lost in the NSUN5 knockout clones. The results confirm that NSUN5 is responsible for the methylation of C3782 in 293T 28S rRNA.

Another 28s rRNA cytosine methylation site, C4447, has been predicted to be the target of NSUN1, but not NSUN5 [238]. As a negative control for C3782, we also measured the methylation

status of C4447 in the 293T clones. As expected, sequencing results showed that C4447 remained methylated in both NSUN5 wild-type and knockout 293T clones (**Figure 3.12**), confirming that C4447 in 28S rRNA is not the target of NSUN5 [238].

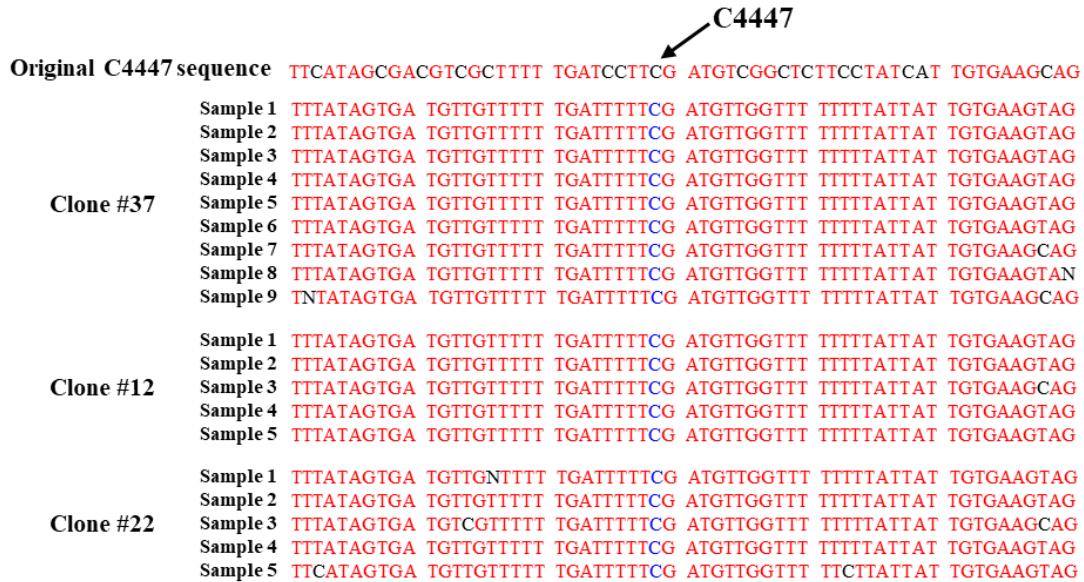


**Figure 3.12 NSUN5 knockout does not change methylation of C4447 in 293T 28S rRNA.**

RNA from the 293T clones (#37 for wild-type and #12 and #22 for NSUN5 knockout) were analyzed by bisulfite sequencing to determine the methylation status of C4447 in 28S rRNA. Compared with the original sequence, more than 99% of cytosines (C) were converted into thymines (T). C4447 was not converted to thymine in the NSUN5 wild-type (#37, n = 9) and two NSUN5 knockout 293T cell clones (#12, n = 5 and #22, n = 5), indicating that C4447 remains methylated with or without NSUN5. Thus, C4447 in 28S rRNA is not the target of NSUN5 in 293T cells.

After determining that NSUN5 is required for the methylation of C3782 in 28S rRNA of 293T cells, we wanted to ensure that NSUN5 is also responsible for methylation of C3782 in 28S rRNA in glioblastoma cells. Using the same CRISPR/Cas9 NSUN5 knockout plasmids described for 293T cells, we generated NSUN5 knockout clones in U251 cells (**Figure 3.13**). Unlike 293T cells,

we got only 8 CRISPR clones after single cell seeding in two 96-well plates. Plate A had two clones that expressed NSUN5, and plate B had 6 clones (two clones expressed NSUN5 and 4 clones either did not express NSUN5 or expressed considerably reduced levels of NSUN5) (**Fig. 3.13**).

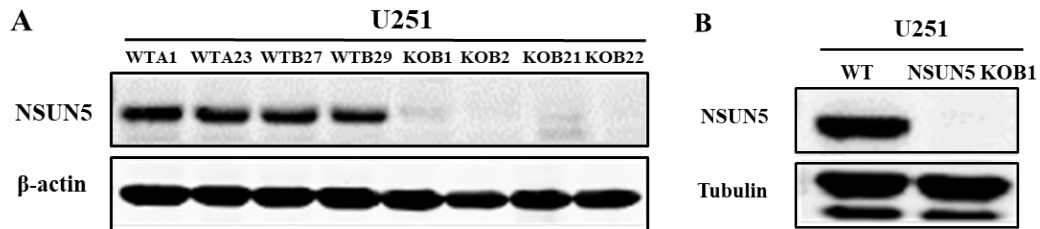


**Figure 3.13 NSUN5 expression in U251 CRISPR clones.**

(A) NSUN5 protein levels in 8 CRISPR clones of U251 cells were examined by Western blotting. Results show that NSUN5 is expressed at 4 wild-type clones (WTA1, WTA23, WTB27, and WTB29), but not in 3 knockout clones (KOB1, KOB2, and KOB22). Clone KO21 expresses a very weak and slightly smaller form of NSUN5. (B) As we suspected that there was leak-through between the WTB29 and KOB1 wells, we repeated the Western blotting using wild-type U251 and knockout clone KOB1 and confirmed loss of NSUN5 expression in KOB1.  $\beta$ -actin and Tubulin were the loading control.

We then selected one clone that expressed NSUN5 (WTA1) and 3 clones that had lost NSUN5 expression (KOB1, KOB21 and KOB22) for genomic sequencing to examine the mutations at the CRISPR guide RNA target site of the *NSUN5* gene as described for 293T cells. Genomic DNA sequencing results showed that clone WTA1 had a wild type NSUN5 sequence at the CRISPR guide RNA target site, whereas all three clones without NSUN5 expression had three different types of DNA mutations, suggesting that U251 has three copies of the *NSUN5* gene (**Figure 3.14**). This is consistent with our finding that the *NSUN5* gene is found at high copy numbers in more than 80% of glioblastoma samples (**Figure 3.3**). Mutations identified in KOB1 (1-nucleotide

insertion, 1-nucleotide deletion, and 8-nucleotide deletion) and in KOB22 (1-nucleotide insertion, 2-nucleotide deletion, and 8-nucleotide deletion) were frameshift mutations, which explains loss of NSUN5 protein expression in these clones. KOB21 had 1-nucleotide insertion, 4-nucleotide deletion, and 18-nucleotide deletion. Although an 18-nucleotide deletion will not cause a frameshift mutation, it will generate a deletion of 6 amino acids in the NSUN5 protein, which is consistent with the presence of a weak and smaller band of NSUN5 as determined by Western blotting (Figure 3.13).

		NSUN5 DNA sequence at CRISPR guide RNA target site			
<b>Original</b>		CGGCCTCCTC	CGTGCGGAGA	AGAAGCTGCG	GCCGCACCTG GCCAAGG
<b>Clone WTA1</b>	Sample 1	CGGCCTCCTC	CGTGCGGAGA	AGAAGCTGCG	GCCGCACCTG GCCAAGG
	Sample 2	CGGCCTCCTC	CGTGCGGAGA	AGAAGCTGCG	GCCGCACCTG GCCAAGG
	Sample 3	CGGCCTCCTC	CGTGCGGAGA	AGAAGCTGCG	GCCGCACCTG GCCAAGG
<b>Clone KOB1</b>	Sample 1	CGGCCTCCTC	CGTTGCGGAGA	AGAAGCTGCG	GCCGCACCTG GCCAAGG
	Sample 2	CGGCCTCCTC	C --- ----- A	AGAAGCTGCG	GCCGCACCTG GCCAAGG
	Sample 3	CGGCCTCCTC	C --- ----- A	AGAAGCTGCG	GCCGCACCTG GCCAAGG
	Sample 4	CGGCCTCCTC	--GTGCGGAGA	AGAAGCTGCG	GCCGCACCTG GCCAAGG
	Sample 5	CGGCCTCCTC	--GTGCGGAGA	AGAAGCTGCG	GCCGCACCTG GCCAAGG
	Sample 6	CGGCCTCCTC	--GTGCGGAGA	AGAAGCTGCG	GCCGCACCTG GCCAAGG
<b>Clone KOB21</b>	Sample 1	CGGCCTCCTC	CGTTGCGGAGA	AGAAGCTGCG	GCCGCACCTG GCCAAGG
	Sample 2	CGGCCTCCTC	CGTTGCGGAGA	AGAAGCTGCG	GCCGCACCTG GCCAAGG
	Sample 3	CGGCCTCCTC	CGTTGCGGAGA	AGAAGCTGCG	GCCGCACCTG GCCAAGG
	Sample 4	CGGCCTCCTC	CG -----	-----	GCCGCACCTG GCCAAGG
	Sample 5	CGGCCTCCTC	CG -----	-----	GCCGCACCTG GCCAAGG
	Sample 6	CGGCCTCCTC	AGTGCG-----A	AGAAGCTGCA	GCCGCACCTG GCCAAGG
<b>Clone KOB22</b>	Sample 1	CGGCCTCCTC	CGTTGCGGAGA	AGAAGCTGCG	GCCGCACCTG GCCAAGG
	Sample 2	CGGCCTCCTC	CGTTGCGGAGA	AGAAGCTGCG	GCCGCACCTG GCCAAGG
	Sample 3	CGGCCTCCTC	----TGCGGAGA	AGAAGCTGCG	GCCGCACCTG GCCAAGG
	Sample 4	CGGCCTCCTC	AGTGCG-----A	AGAAGCTGCA	GCCGCACCTG GCCAAGG
	Sample 5	CGGCCTCCTC	AGTGCG-----A	AGAAGCTGCA	GCCGCACCTG GCCAAGG
	Sample 6	CGGCCTCCTC	AGTGCG-----A	AGAAGCTGCA	GCCGCACCTG GCCAAGG

**Figure 3.14 Genomic DNA sequencing results for indels induced by CRISPR in the *NSUN5* gene of U251 CRISPR clones.**

DNA sequences at the CRISPR guide RNA target site of the NSUN5 gene in U251 WTA1, KOB1, KOB21, and KOB22 clones were obtained by Sanger sequencing. The results show that clone WTA1 has wild type *NSUN5* DNA sequence. However, all the other clones had three different types of DNA mutations. Clone KOB1 had 1-nucleotide insertion mutation, 1-nucleotide deletion

mutation, and 8-nucleotide deletion mutation. Clone KOB22 had 1-nucleotide insertion mutation, 2-nucleotide deletion mutation, and 8-nucleotide deletion mutation. Clone KOB21 had 1-nucleotide insertion mutation, 4-nucleotide deletion mutation, and 18-nucleotide deletion mutation.

After NSUN5 knockout in U251 cells was confirmed as described above, we selected WTA1 (wild type) and KOB1 (NSUN5 knockout) clones for bisulfite sequencing analysis to determine whether NSUN5 is responsible for methylation of C3782 in 28S rRNA in U251 cells. Indeed, the sequencing results showed that C3782 was methylated in WTA1, but not in KOB1 cells (**Figure 3.15**), confirming that NSUN5 is responsible for methylation of C3782 in glioblastoma cells. Similarly, as observed in 293T cells, NSUN5 knockout did not change C4447 methylation in U251 cells (**Figure 3.16**).

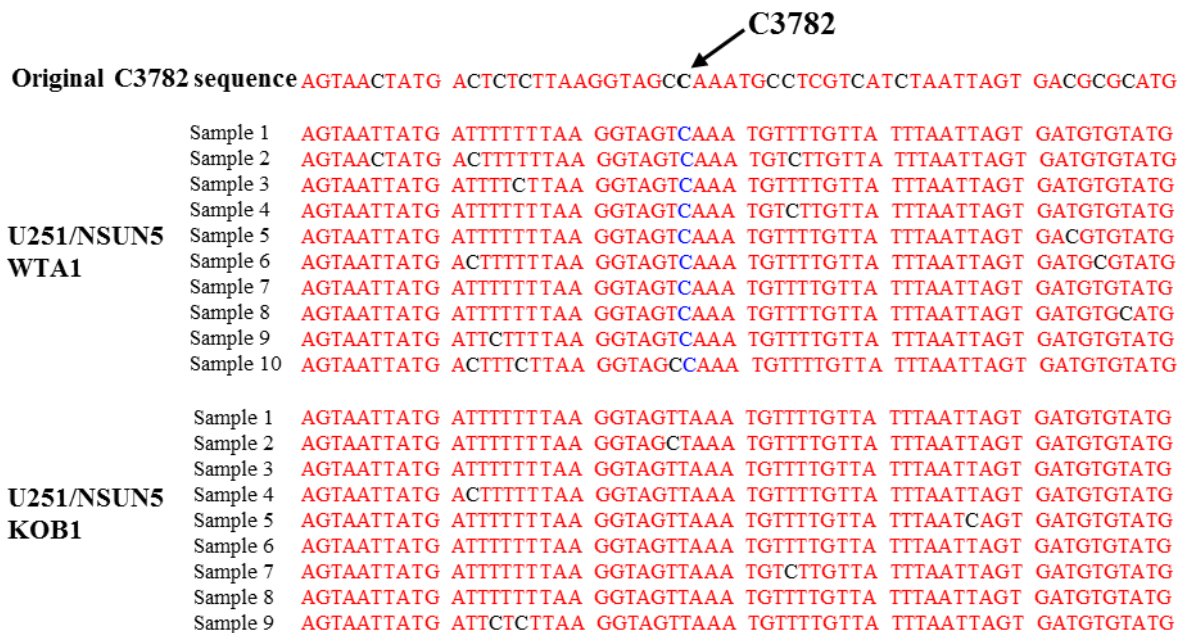


**Figure 3.15 NSUN5 is responsible for methylation of C3782 in U251 28S rRNA.**

RNA from the U251 clones (WTA1 for wild-type and KOB1 for NSUN5 knockout) were analyzed by bisulfite sequencing to determine the methylation status of C3782 in 28S rRNA. Compared with the original sequence, > 99% of cytosines (C) were converted into thymines (T), indicating the success of the experiments. C3782 in wild-type clone WTA1 (n = 10) remained unconverted,

while C3782 in knockout clone KOB1 (n = 9) was converted to thymine, indicating that C3782 methylation was lost in NSUN5 knockout clones. The results confirmed that NSUN5 is responsible for the methylation of C3782 in U251 28S rRNA.

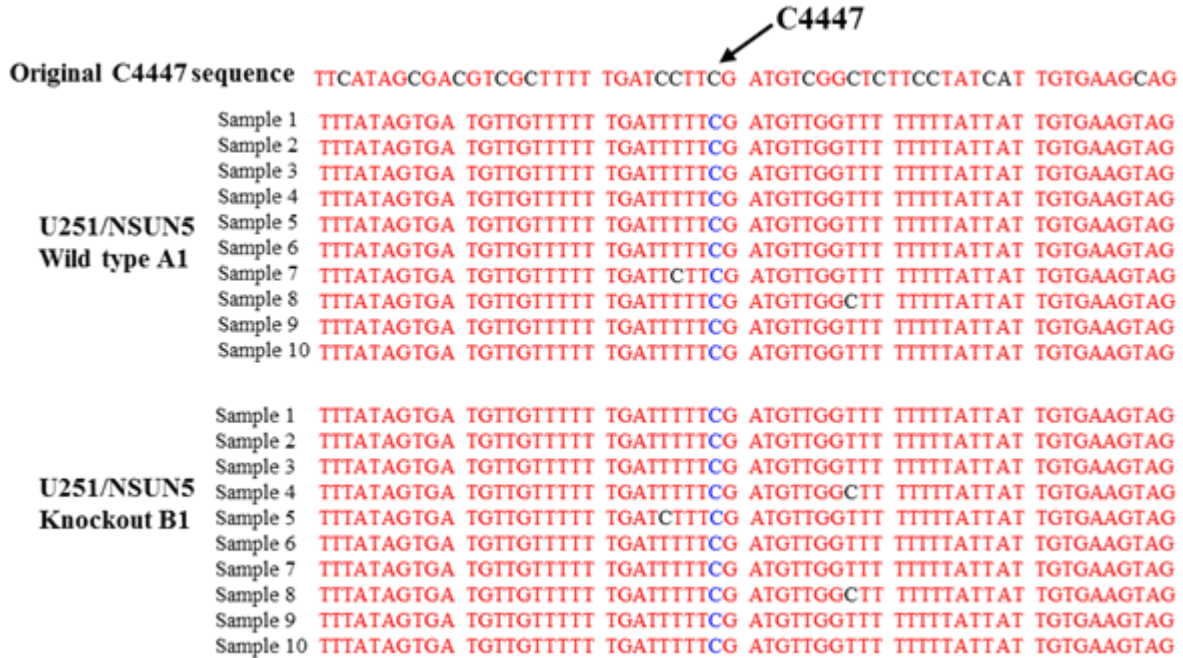
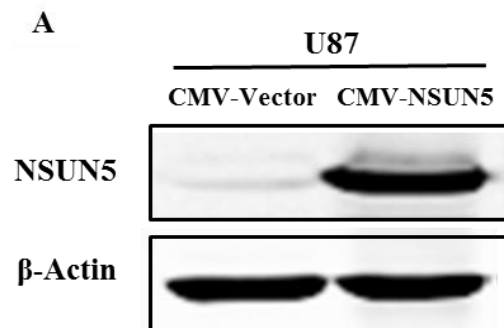


**Figure 3.16 NSUN5 knockout does not change methylation of C4447 in U251 28S rRNA.**

RNA from the U251 clones (WTA1 for wild-type and KOB1 for NSUN5 knockout) were analyzed by bisulfite sequencing to determine the methylation status of C4447 in 28S rRNA. Compared with the original sequence, > 99% of cytosines (C) were converted into thymines (T). C4447 was not converted to thymine in NSUN5 wild type (WTA1, n = 10) and NSUN5 knockout clone (KOB1, n=10), indicating that C4447 remained methylated even though NSUN5 expression was knocked out. The results suggest that C4447 in 28S rRNA is not the target of NSUN5 in U251 cells.

Next, we examined whether overexpressed NSUN5 was able to induce methylation of C3782 in 28S rRNA of glioblastoma cells that do not normally express NSUN5. U87 cells that do not express endogenous NSUN5 (**Figure 3.5B**) were stably transfected with an empty CMV vector or a CMV-NSUN5 expression construct. The expression of NSUN5 was confirmed by Western

blotting (**Figure 3.17A**). RNA bisulfite sequencing showed that C3782 was not methylated in U87 CMV-Vector cells (**the first block in Figure 3.18**) but was methylated in 3 out of 9 samples of U87 CMV-NSUN5 cells (**the second block in Figure 3.18**). The partial methylation of C3782 in NSUN5-overexpressing U87 cells prompted us to determine the transfection efficiency using immunocytochemistry. Our results showed that approximately 40% of the CMV-NSUN5 transfected U87 cells expressed NSUN5 (**the second column in Figure 3.17B**). To select NSUN5-expressing cells, we used cloning rings to obtain clones derived from the pooled NSUN5-transfected U87 cells. We propagated 5 clones and examined NSUN5 expression using immunocytochemistry in these clones. Results showed that all cells in clone #2 (clone N2) expressed NSUN5 (**the third column in Figure 3.17B**). Consistent with the expression of NSUN5 in all the cells of U87 CMV-NSUN5 clone N2, RNA bisulfite sequencing showed that C3782 was methylated in all the samples from these cells (**the third block in Figure 3.18**). These results demonstrate that NSUN5 is necessary and sufficient for methylation of C3782 in 28S rRNA in glioblastoma cells.



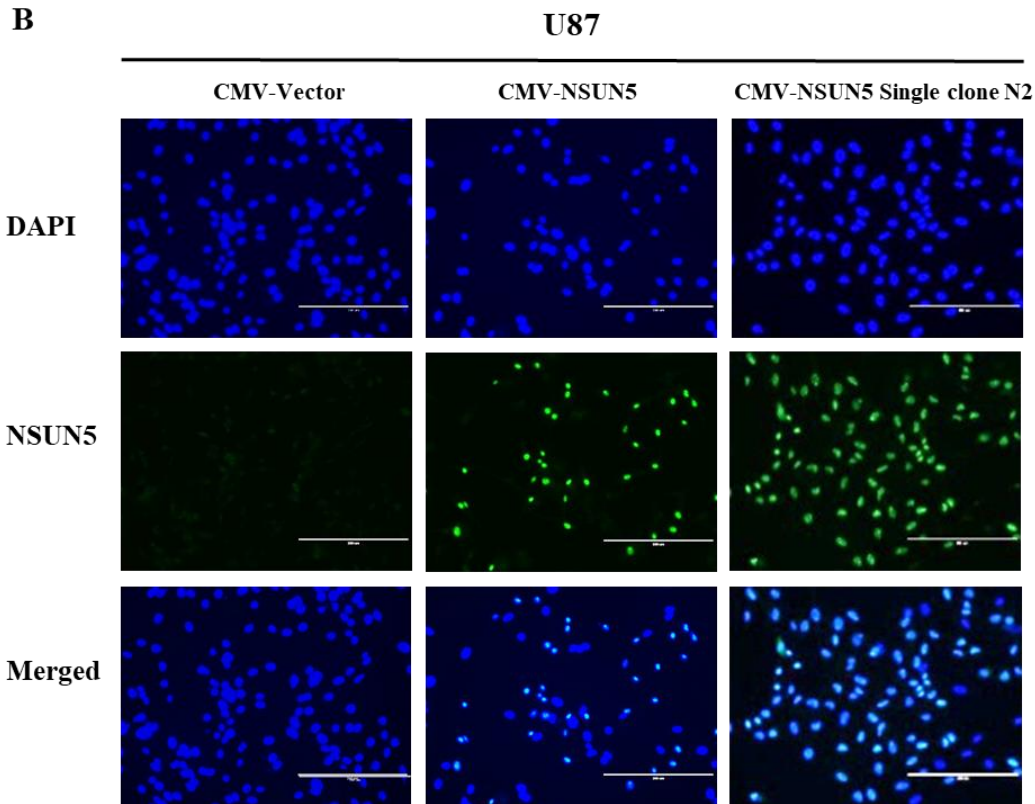


**Figure 3.17 Overexpression of NSUN5 in U87 cells.**

(A) Western blotting confirmed that NSUN5 was expressed in U87 CMV-NSUN5 cells, but not in U87 CMV-Vector cells.  $\beta$ -Actin was the loading control. (B) Immunofluorescence images of U87/CMV-Vector, U87/CMV-NSUN5, and U87/CMV-NSUN5 clone N2 were captured under a fluorescence microscope. DAPI was used to stain the nucleus and anti-NSUN5 antibody was used to immunostain NSUN5. Results show that the U87/CMV-Vector does not express NSUN5, whereas overexpressed NSUN5 in U87/CMV-NSUN5 and U87/CMV-NSUN5 clone N2 cells was localized to the nucleus. Merged DAPI/NSUN5 images showed that about 40% of U87/CMV-NSUN5 cells (second column) and approximately 100% of U87/CMV-NSUN5 clone N2 expressed NSUN5 (third column). The scale bar = 200  $\mu$ m.

C3782

**Original C3782 sequence** AGTAACTATG ACTCTCTTAAGGTAGCCAAATGCCCTCGTCATCTAATTAGT GACGCGCATG

Sample 1	AGTAATTATG	ATTTTTTTAA	GGTAGTAAA	TGTTTGTTA	TTTAATTAGT	GATGTGTATG
Sample 2	AGTAATTATG	ATTTTTTTAA	GGTAGTAAA	TGTTTGTTA	TTTAATTAGT	GATGTGTATG
Sample 3	AGTAATTATG	ATTTTTTTAA	GGTAGTAAA	TGTTTGTTA	TTTAATTAGT	GATGTGTATG
U87/ CMV-Vector	Sample 4	AGTAATTATG	ATTTTTTTAA	GGTAGTAAA	TGTTTGTTA	TTTAATTAGT GATGTGTATG
	Sample 5	AGTAATTATG	ATTTTTTTAA	GGTAGCTAAA	TGTTTGTTA	TTTAATTAGT GATGTGTATG
	Sample 6	AGTAATTATG	ATTTTTTTAA	GGTAGTAAA	TGTTTGTTA	TTTAATTAGT GATGTGTATG
	Sample 7	AGTAATTATG	ATTTTTTTAA	GGTAGTAAA	TGTTTGTTA	TTTAATTAGT GATGTGTATG
	Sample 8	AGTAATTATG	ATTTTTTTAA	GGTAGTAAA	TGTTTGTTA	TTTAATTAGT GATGTGTATG
	Sample 9	AGTAATTATG	ATTTTTTTAA	GGTAGTAAA	TGTTTGTTA	TTTAATTAGT GATGTGTATG
	Sample 10	AGTAATTATG	ATTTTTTTAA	GGTAGTAAA	TGTTTGTTA	TTTAATTAGT GATGTGTATG
	Sample 1	AGTAATTATG	ATTTTTTTAA	GGTAGTAAA	TGTTTGTTA	TTTAATTAGT GATGTGTATG
	Sample 2	AGTAATTATG	ACTTTTTTAA	GGTAGTAAA	TGTTTCGTTA	TTTAATTAGT GATGTGCATG
	Sample 3	AGTAACTATG	ATTTTTTTAA	GGTAGTAAA	TGTTTGTTA	TTTAATTAGT GATGCGTATG
U87/ CMV-NSUN5	Sample 4	AGTAATTATG	ATTTTTTTAA	GGTAGTCAA	TGTTTGTTA	TTTAATTAGT GATGTGTATG
	Sample 5	AGTAATTATG	ATTTTTTTAA	GGTAGTAAA	TGTTTGTTA	TTTAATTAGT GATGTGTATG
	Sample 6	AGTAATTATG	ATTTTTTTAA	GGTAGCTAAA	TGCTTGTTA	TTTAATTAGT GATGTGTATG
	Sample 7	AGTAATTATG	ATTTTTTTAA	GGTAGTCAA	TGTTTGTTA	TTTAATTAGT GATGTGTATG
	Sample 8	AGTAATTATG	ATTTTTTTAA	GGTAGTCAA	TGTTTGTTA	TTTAATTAGT GATGTGTATG
	Sample 9	AGTAACTATG	ATTTTTTTAA	GGTAGTAAA	TGTTTGTTA	TTTAATTAGT GATGTGTATG
	Sample 1	AGTAATTATG	ATTTTTTTAA	GGTAGTCAA	TGTTTGTTA	TTTAATTAGT GATGTGTATG
	Sample 2	AGTAATTATG	ATTTTTTTAA	GGTAGTCAA	TGTTTGTTA	TTTAATTAGT GATGTGTATG
	Sample 3	AGTAATTATG	ATTTTTTTAA	GGTAGTCAA	TGTTTGTTA	TTTAATTAGT GATGTGTATG
U87/ CMV-NSUN5 Single clone N2	Sample 4	AGTAATTATG	ATTTTTTTAA	GGTAGTCAA	TGTTTGTTA	TTTAATTAGT GATGTGTATG
	Sample 5	AGTAATTATG	ATTTTTTTAA	GGTAGTCAA	TGTTTGTTA	TTTAATTAGT GATGTGTATG
	Sample 6	AGTAATTATG	ATTTTTTTAA	GGTAGTCAA	TGTTTGTTA	TTTAATTAGT GATGTGTATG
	Sample 7	AGTAATTATG	ATTTTTTTAA	GGTAGTCAA	TGTTTGTTA	TTTAATTAGT GATGTGTATG
	Sample 8	AGTAATTATG	ATTTTTTTAA	GGTAGTCAA	TGTTTGTTA	TTTAATTAGT GATGTGTATG
	Sample 9	AGTAATTATG	ATTTTTTTAA	GGTAGTCAA	TGTTTGTTA	TTTAATTAGT GATGTGTATG
	Sample 10	AGTAATTATG	ATTTTTTTAA	GGTAGTCAA	TGTTTGTTA	TTTAATTAGT GATGTGTATG
	Sample 11	AGTAATTATG	ATTTTTTTAA	GGTAGTCAA	TGTTTGTTA	TTTAATTAGT GATGTGTATG
	Sample 12	AGTAATTATG	ACTTTTTTAA	GGTAGTCAA	TGTTTGTTA	TTTAATTAGT GATGTGTATG

**Figure 3.18 Overexpressed NSUN5 induces methylation of C3782 in U87 28S rRNA.**

RNA from U87/CMV-Vector, U87/CMV-NSUN5 and U87/CMV-NSUN5 clone N2 was analyzed by bisulfite sequencing to determine the methylation status of C3782 in 28S rRNA. Compared with the original sequence, >99% of cytosines (C) were converted to thymines (T). C3782 in U87/CMV-Vector cells (n = 10) was converted to thymine (top block), indicating that C3782 is unmethylated in these cells. In the case of U87 CMV-NSUN5 cells, C3782 in 3 out of 9 samples were not converted to cytosine (middle block), suggesting partial methylation of C3782 in these transfected cells. C3782 in U87/CMV-NSUN5 clone N2 cells (n = 12) was not converted to thymine (low block), suggesting that all the cytosines were methylated in this clonal population. These results confirm that NSUN5 overexpression is sufficient to induce methylation of C3782 in 28S rRNA in U87 cells.

Consistent with the results in 293T cells and U251 cells, C4447 was methylated regardless of NSUN5 expression status, indicating that NSUN5 is not responsible for methylation of C4447 in 28S rRNA in U87 cells (**Figure 3.19**). Taken together, our RNA bisulfite sequencing results indicate that NSUN5 is necessary and sufficient for methylation of C3782 in 28S rRNA of human 293T and glioblastoma cells.



**Figure 3.19 Overexpressed NSUN5 does not change methylation of C4447 in U87 28S rRNA.**

RNA from U87/CMV-Vector, U87/CMV-NSUN5 and U87/CMV-NSUN5 clone N2 were analyzed by bisulfite sequencing to determine the methylation status of C3782 in 28S rRNA. Compared with the original sequence, > 99% of cytosines (C) were converted into thymines (T). C4447 was not converted (methylated) to thymines in all of the cells analysed regardless of NSUN5 expression, suggesting that C4447 of 28S rRNA is not the target of NSUN5 in U87 cells.

### **3.4 Catalytic cysteines (C308 and C359) of NSUN5 are required for the methylation of C3782 in U87 28S rRNA.**

All NSUN proteins have a similar enzyme domain that contains two conserved cysteine and an s-adenosyl methionine (SAM)-binding pocket. So far, the two functional cysteines of NSUN proteins have mainly been studied in yeast. The catalytic cysteine (cysteine 478) in motif IV of Nop2 (the yeast NSUN1) catalyzes the methylation of its target cytosines, whereas the cysteine (cysteine 424) in motif VI helps to release Nop1 from its target RNA after methylation [238]. Similarly, the catalytic cysteine (cysteine 321) in motif IV of yeast NSun2 catalyzes the methylation of its target cytosines, whereas the cysteine (cysteine 271) in motif VI helps to release NSun2 from its target RNA after methylation [292, 320, 343-345]. Consistently, a study on Rcm1 (the yeast NSUN5) showed similar results: the catalytic cysteine 404 catalyzes the methylation of its target cytosines, whereas the cysteine 330 helps to release the Rcm1 from its target RNA after methylation [238]. Rcm1 contains 490 amino acids (NCBI NP\_014376), while human NSUN5 has 470 amino acids (NCBINP\_001161819.1). As homologs, Rcm1 and NSUN5 have highly conserved regions (**Figure 3.20**). By comparing Rcm1 and NSUN5 amino acid sequences, we identified two potential functional cysteines in NSUN5: cysteines 308 and 359, corresponding to cysteines 330 and 404 in Rcm1, respectively (**Figure 3.20**).

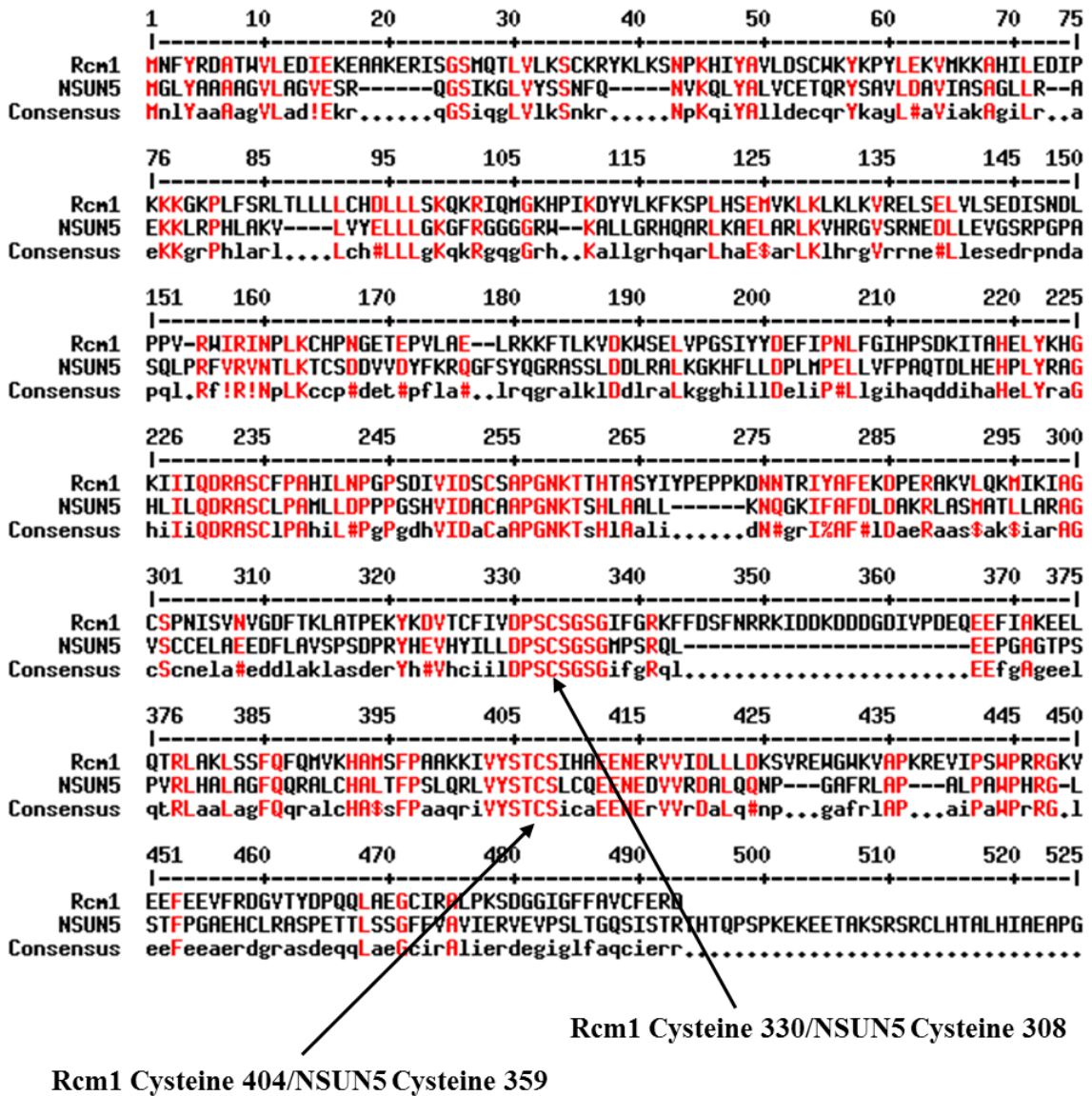


**Figure 3.20** The amino acid sequences alignment of yeast Rcm1 and human NSUN5.

Yeast Rcm1 has 490 amino acids (NCBI NP\_014376), whereas human NSUN5 has 470 amino acids (NCBI NP\_001161819.1). As homologs, Rcm1 and NSUN5 have some highly conserved sequences (indicated in red). The two functional cysteines of Rcm1 are cysteine 330 and cysteine 404. Comparison of NSUN5 and Rcm1 amino acid sequences revealed two potential functional cysteines in NSUN5: cysteines 308 and 359.

To determine whether these two cysteines are indeed responsible for the enzymatic function of NSUN5, we introduced point mutations at these two sites and examined the methylating activity of the resulting mutants. Using site-directed mutagenesis, we mutated either cysteine 308 or cysteine 359, or both cysteines, into alanine residues and generated pLenti-NSUN5 constructs that express mutated NSUN5: C308A, C359A and C308A/C359A (double mutations). Two bacterial colonies for each construct were selected for plasmid preparation and sequencing. The sequencing results confirmed the successful mutation of C308A, C359A and C308A/C359A, with the cysteine codon (UGC) mutated to alanine codon (GCC) in these plasmids (**Figure 3.21**). Thus, three new pLentivirus constructs expressing NSUN5 mutants (C308A, C359A, and C308A/C359A) were successfully generated.

**Plasmid sequencing results after site directed mutagenesis**

	Cysteine 308			Cysteine 359		
Wild type NSUN5	GCTGGATCCT	TCCTGCAGTG	GCTCGGGTAT	GCTCGTCTAC	TCCACGTGCT	CCCTCTGCCA
NSUN5 C308A mutant 1	GCTGGATCCT	TCCGCCAGTG	GCTCGGGTAT	GCTCGTCTAC	TCCACGTGCT	CCCTCTGCCA
NSUN5 C308A mutant 2	GCTGGATCCT	TCCGCCAGTG	GCTCGGGTAT	GCTCGTCTAC	TCCACGTGCT	CCCTCTGCCA
NSUN5 C359A mutant 1	GCTGGATCCT	TCCTGCAGTG	GCTCGGGTAT	GCTCGTCTAC	TCCACGGCCT	CCCTCTGCCA
NSUN5 C359A mutant 2	GCTGGATCCT	TCCTGCAGTG	GCTCGGGTAT	GCTCGTCTAC	TCCACGGCCT	CCCTCTGCCA
NSUN5 C308A and C359A mutant 1	GCTGGATCCT	TCCGCCAGTG	GCTCGGGTAT	GCTCGTCTAC	TCCACGGCCT	CCCTCTGCCA
NSUN5 C308A and C359A mutant 2	GCTGGATCCT	TCCGCCAGTG	GCTCGGGTAT	GCTCGTCTAC	TCCACGGCCT	CCCTCTGCCA

**Figure 3.21 DNA sequence alignment of pLenti-NSUN5 plasmids carrying mutated codons for cysteine 308 or/and cysteine 359 after site directed mutagenesis.**

pLenti-NSUN5 C308A, C359A, and C308A/C359A plasmids from two bacterial colonies were isolated and sequenced. Sequencing confirmed that the cysteine codons (UGC) of C308 and C359 were changed to alanine codons (GCC) in all the samples. These sequencing results confirmed that three pLentiviral constructs expressing mutant NSUN5 (C308A, C359A, C308A/C359A) were successfully generated.

To determine whether these mutants can methylate C3782 of 28S rRNA in glioblastoma cells, we transduced U87 cells with empty pLenti-vector, pLenti-NSUN5 wild-type, pLenti-

NUSN5C308A, pLenti-NUSN5C359A, and pLenti-NUSN5C308AC359A. Immunofluorescence staining showed that U87 cells transduced pLenti-Vector cells did not express NSUN5, while U87 cells transduced with the pLenti-NSUN5 (wild type and mutants) expressed NSUN5 that was localized in the nucleus. The transfection efficiency of wild-type pLenti-NSUN5 and the three mutant pLenti-NSUN5 plasmids was almost 100% (**Figure 3.22**).

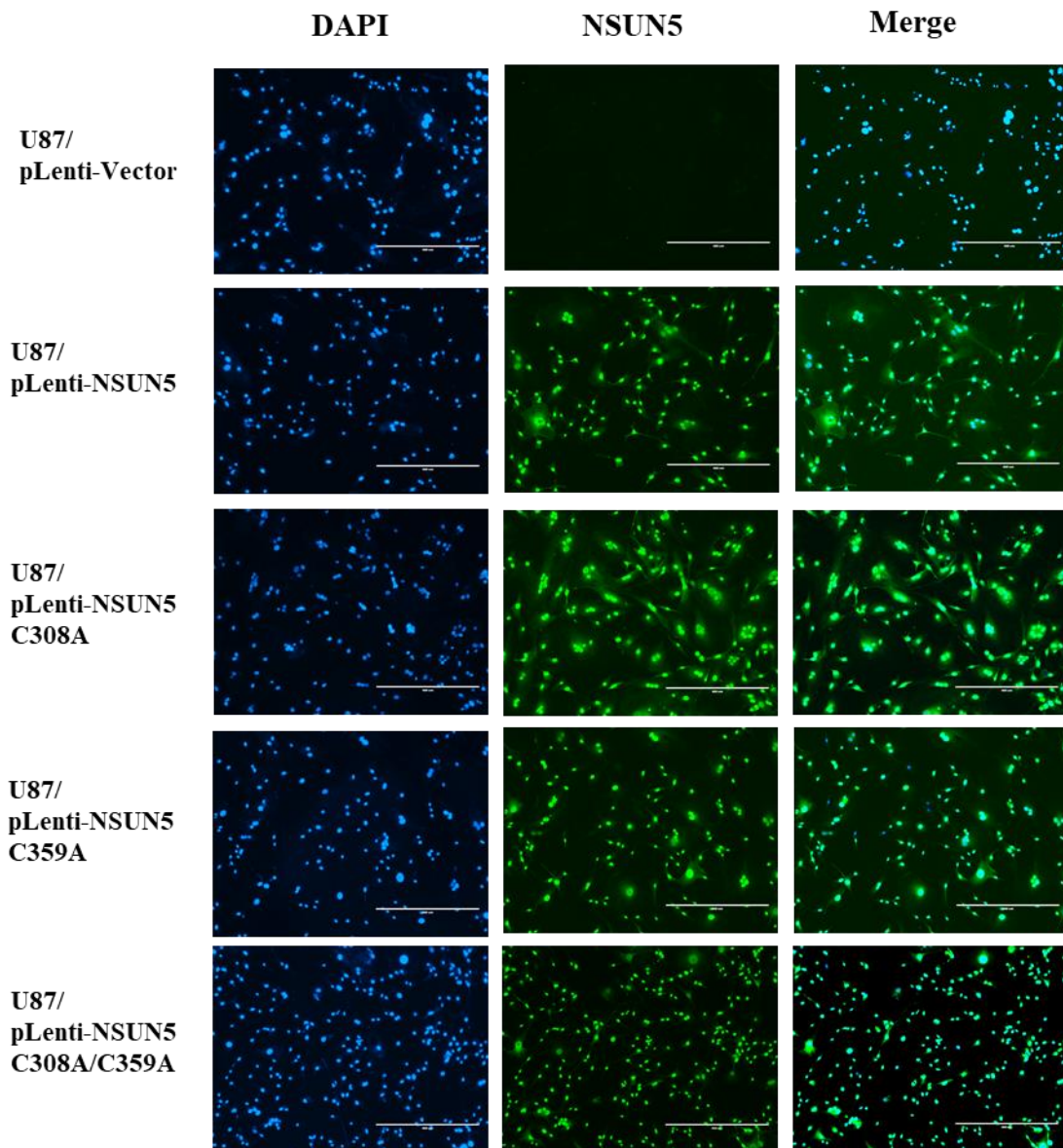


**Figure 3.22 Overexpression of wild-type and mutant NSUN5 in U87 cells.**

Expression of NSUN5 in U87 cells transduced with pLenti-Vector, pLenti-NSUN5, pLenti-NSUN5 C308A, pLenti-NSUN5 C359A, and pLenti-NSUN5 C308AC359A was determined by immunocytochemistry. Images were captured using a fluorescence microscope. DAPI was used to stain the nucleus and an anti-NSUN5 antibody was used to immunostain NSUN5. Results show that the U87 pLenti-Vector cells do not express NSUN5, whereas all the pLenti-NSUN5 vectors (wild type and mutants) expressed NSUN5 that is localized to the nucleus. Merged DAPI/NSUN5 show that the transfection efficiency of all the NSUN5-expressing vectors was almost 100%. Scale bar = 400  $\mu$ m.

RNA bisulfite sequencing results show that C3782 in all the samples of U87 cells transduced with pLenti-NSUN5C308A, pLenti-NSUN5C359A, and/or pLenti-NSUN5C308A/C359A was converted to thymine, which means that C3782 was unmethylated in the cells that express mutated NSUN5 (**Figure 3.23**). This is in a sharp contrast to the methylation induced by overexpression of wild-type NSUN5 (**Figure 3.19**). The results suggest that both catalytic cysteines (C308 and C359) in NSUN5 are required for the methylation of C3782 in U87 28S rRNA.

			C3782 ↙
<b>Original C3782 sequence</b>		AGTAACTATG	ACTCTCTTAAGGTAGCCAAATGCCCTCGTCATCTAATTAGT GACGCGCATG
<b>U87/ pLenti-NSUN5 C308A</b>	Sample 1	AGTAATTATG	ATTTTTTAA GGTAGTAAA TGTTTGTTA TTTAATTAGT GATGTGTATG
	Sample 2	AGTAATTATG	ATTTTTTAA GGTAGTAAA TGTTTGTTA TTTAATTAGT GATGTGTATG
	Sample 3	AGTAATTATG	ATTTTTTAA GGTAGTAAA TGTTTGTTA TTTAATTAGT GATGTGTATG
	Sample 4	AGTAACTATG	ATTTTTTAA GGTAGTAAA TGTTTGTTA TTTAATTAGT GATGTGTATG
	Sample 5	AGTAATTATG	ATTTTTTAA GGTAGTAAA TGTTTGTTA TTTAATTAGT GATGTGTATG
	Sample 6	AGTAATTATG	ATTTTTTAA GGTAGTAAA TGTTTGTTA TTTAATTAGT GATGTGTATG
<b>U87/ pLenti-NSUN5 C359A</b>	Sample 1	AGTAATTATG	ATTTTTTAA GGTAGTAAA TGTTTGTTA TTTAATTAGT GATGTGTATG
	Sample 2	AGTAATTATG	ATTTTTTAA GGTAGTAAA TGTTTGTTA TTTAATTAGT GATGTGTATG
	Sample 3	AGTAATTATG	ATTTTTTAA GGTAGTAAA TGTTTGTTA TTTAATTAGT GATGTGTATG
	Sample 4	AGTAATTATG	ATTTTTTAA GGTAGTAAA TGTTTGTTA TTTAATTAGT GATGTGTATG
	Sample 5	AGTAATTATG	ATTTTTTAA GGTAGTAAA TGTTTGTTA TTTAATTAGT GACGTGTATG
	Sample 6	AGTAATTATG	ATTTTTTAA GGTAGTAAA TGTTTGTTA TTTAATTAGT GATGTGTATG
	Sample 7	AGTAATTATG	ATTTTTTAA GGTAGTAAA TGTTTGTTA TTTAATTAGT GATGTGTATG
	Sample 8	AGTAATTATG	ATTTTTTAA GGTAGTAAA TGTTTGTTA TTTAATTAGT GATGTGTATG
<b>U87/ pLenti-NSUN5 C308A/C359A</b>	Sample 1	AGTAATTATG	ATTTTTTAA GGTAGTAAA TGTTTGTTA TTTAATTAGT GATGTGTATG
	Sample 2	AGTAATTATG	ANTNTTTTTAA GGTAGTAAA TGTTTGTTA TTTAATTAGT GATGTGTATG
	Sample 3	AGTAATTATG	ATTTTTTAA GGTAGTAAA TGTTTGTTA TTTAATTAGT GATGTGTATG
	Sample 4	AGTAATTATG	ATTTTTTAA GGTAGTAAA TGTTTGTTA TTTAATTAGT GATGTGTATG
	Sample 5	AGTAATTATG	ATTTTTTAA GGTAGTAAA TGTTTGTTA TTTAATTAGT GATGTGTATG
	Sample 6	AGTAATTATG	ATTTTTTAA GGTAGTAAA TGTTTGTTA TTTAATTAGT GATGTGTATG
	Sample 7	AGTAATTATG	ATTTTTTAA GGTAGTAAA TGTTTGTTA TTTAATTAGT GATGTGTATG

**Figure 3.23 NSUN5 C308A, NSUN5 C359A, and NSUN5 C308A/C359A fail to induce methylation of C3782 of 28S rRNA in U87 cells.**

RNAs prepared from U87/pLenti-NSUN5 C308A, U87/pLenti-NSUN5 C359A, and U87/pLenti-NSUN5 C308A/C359A cells were analyzed by bisulfite sequencing to determine the methylation status of C3782 in 28S rRNA. Compared with the original sequence, more than 99% of cytosines (T) were converted into thymines (T). C3782 in U87/pLenti-NSUN5 C308A, U87/pLenti-NSUN5 C359A, and U87/pLenti-NSUN5 C308A/C359A cells was uniformly converted to thymine, indicating that C3782 was unmethylated in cells expressing these mutant NSUN5 constructs. These results suggest that both catalytic cysteines (C308 and C359) in NSUN5 are required for the methylation of C3782 in U87 28S rRNA.

Interestingly, it appears that U87 cells transduced with pLenti-NSUN5 C308A were arrested at mitosis (some cells had two or multiple nuclei) and died gradually one-week post-transduction. U87 cells transduced with pLenti-NSUN5 wild-type, C359A or C308A/C359A were viable, which is consistent with the study in yeast where mutations involving Rcm1 C330 (equivalent to C308

in human NSUN5) were lethal, whereas mutations involving C404 (equivalent to C359 in human NSUN5) were compatible with cell survival [312]. The reason could be that NSUN5 with mutated cysteine 308 fails to be released from its target sites after binding, causing cell division defect, whereas NSUN5 with mutated cysteine 359 and the double mutated cysteines could not bind with the targets thus avoiding the most lethal effects. In this regard, it is likely that stable binding of NSUN5 to 28S rRNA disrupts assembly of the ribosome, causing the failure of cytokinesis and cell death. However, because this effect may not be specific to NSUN5, we did not pursue this direction.

## **Chapter 4 Characterization of the biological function of NSUN5 in glioblastoma**

## **4.1 NSUN5 regulates proliferation and stem cell phenotype in glioblastoma cells**

We have determined that: (i) high NSUN5 expression is associated with the poor survival of patients with glioblastoma and (ii) NSUN5 methylates C3782 of 28S rRNA in glioblastoma cells. However, it is unknown whether NSUN5 contributes to tumorigenesis and/or treatment resistance of glioblastoma. rRNAs are critical components of the ribosome and their methylation alters the structure and activity of the ribosome, thereby altering mRNA translation [312]. Recent studies implicate RNA methylation in normal development and various diseases including cancer [284, 307, 308, 319, 320, 331, 333-336, 391, 392]. Therefore, high levels of NSUN5 are likely to change mRNA translation and contribute to formation and/or progression, as well as treatment resistance, of glioblastoma. In this chapter, we investigated the biological functions of NSUN5 in glioblastoma using *in vitro* and *in vivo* models.

### **4.1.1 NSUN5 regulates proliferation of glioblastoma cells.**

Continuous and invasive proliferation is one of the most important characteristics of glioblastoma. Tumor cells invade the surrounding brain tissue, causing severe edema and damage to the brain. Without treatment, the median survival of glioblastoma patients is less than five months [393]. Unlimited proliferation is a hallmark of cancer [394, 395]. Excessive and autonomous growth signals, insensitivity to antigrowth signals, and inactivation of apoptosis signaling pathways are the three main reasons for unlimited growth of cancer cells [394, 395]. We hypothesized that NSUN5, as an rRNA cytosine methyltransferase, alters the structure of ribosomes and thus favors the mRNA translation of the genes associated with glioblastoma proliferation.

#### 4.1.1.1 Knockdown of NSUN5 decreases proliferation in U251 and T98 cells.

We first examined the effect of NSUN5 knockout on U251 cell proliferation with the NSUN5 knockout clones described in Figure 3.16 using the neutral red uptake assay. The neutral red uptake assay is based on the take-up of neutral red dye in the lysosomes of viable cells, and cell numbers are estimated based on the absorbance intensity of the dye at a wavelength of 580 nm [365, 366]. The neutral red uptake assay showed that the proliferation of individual wild-type and NSUN5 knockout clones was highly variable, making it impossible to reach any conclusion regarding the effect of NSUN5 knockout on U251 cell proliferation (**Figure 4.1**). Moreover, we found that the morphology of two of the clones, WTA23 and KOB21, was different from that of other clones, and both clones expressed a higher level of the stem cell marker SOX2 and formed more than twice the number of spheres on sphere formation assay, when compared to other clones (data not shown). This may be because each of the knockout cell lines was generated from a single cell, and the cellular heterogeneity between the individual clones likely underlies the observed variability.

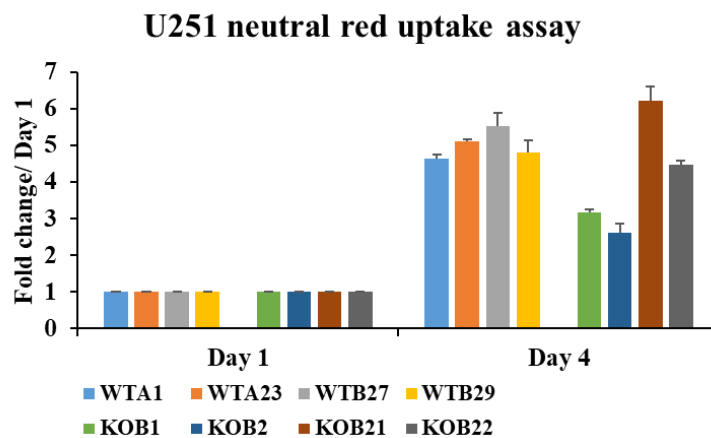
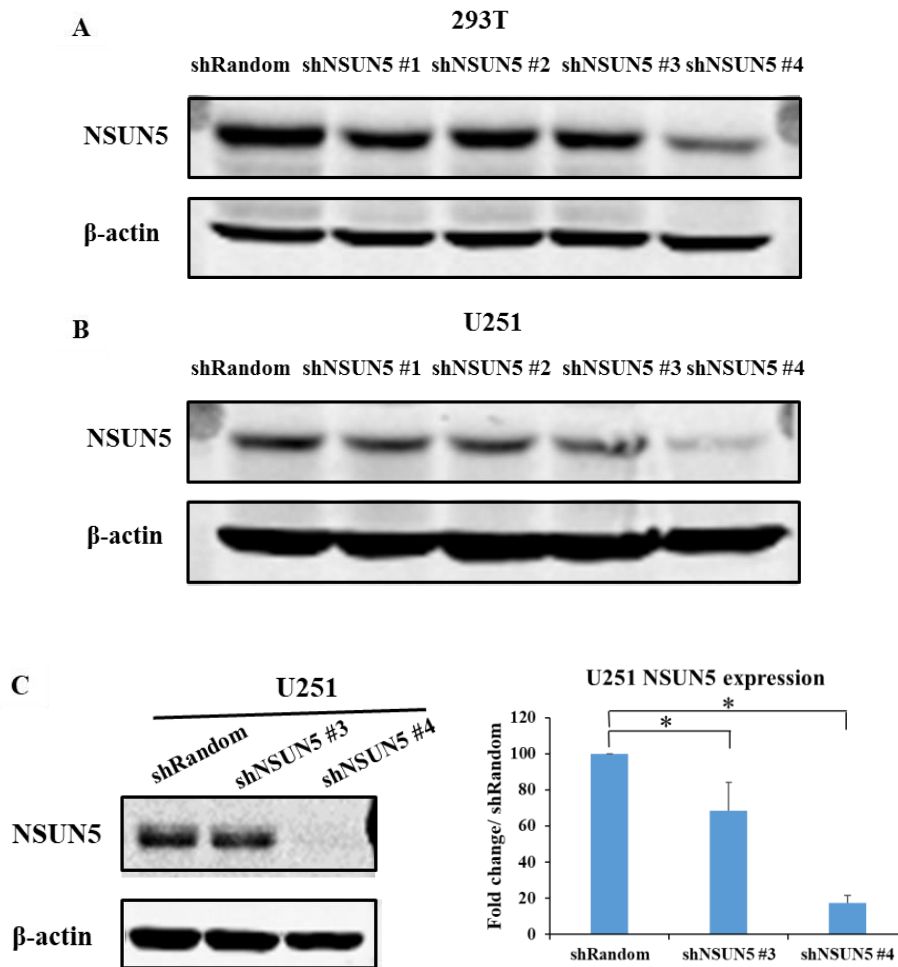


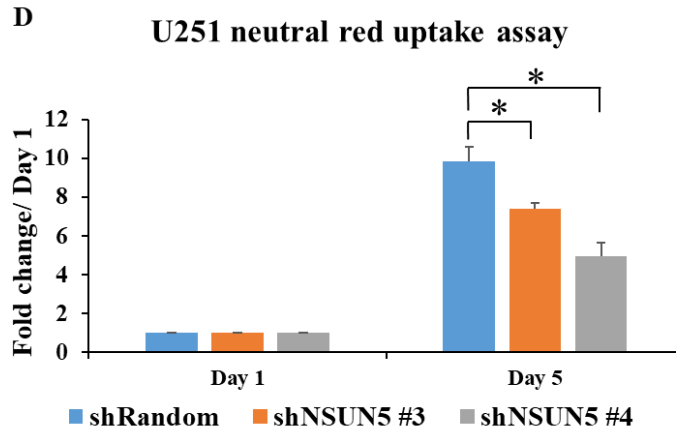
**Figure 4.1** Effect of NSUN5 knockout on proliferation of U251 cells.

The neutral red uptake assay was used to examine the proliferation of the four U251 wild type and four U251 NSUN5 knockout clones. Because of the variability in the results obtained for the different clones, we were not able to assess the effect of NSUN5 on proliferation. Data are from two independent experiments carried out in triplicates.

However, in the knockdown model using lentiviral-shRNA constructs, a pooled population of cells, not single cell clones, were used for experiments, which mitigated the effect of cellular heterogeneity. All subsequent experiments were therefore carried out with the pooled NSUN5 knockdown model. To knock down NSUN5, we transfected 293T cells with four lentiviral shRNA constructs targeting four different NSUN5 sequences (pLenti-shNSUN5-GFP#1-4) or a control shRNA (pLenti-shRandom-GFP), collected medium that contains lentiviral particles and used them to infect U251 cells. Cell lysates were prepared from both 293T and U251 cells and NSUN5 expression was determined by Western blotting. Of the four shRNAs targeting NSUN5, pLenti-shNSUN5 #4 has the best knockdown efficiency, while pLenti-shNSUN5-GFP #1-3 showed weak knockdown of NSUN5 (**Figures 4.2A and 4.2B**). We expanded U251/shRandom, U251/shNSUN5 #3, and U251/shNSUN5 #4 cells for our experiments. The NSUN5 protein levels in U251/shNSUN5 #3 and U251/shNSUN5 #4 cells were about 69% and 17% of that in U251/shRandom, respectively (**Figure 4.2C**). Next, the neutral red uptake assay was performed to determine whether NSUN5 knockdown will affect the proliferation of U251 cells. In keeping with the extent of NSUN5 knockdown, the growth of U251/shNSUN5 #3 and U251/shNSUN5 #4 cells was decreased by 25% and 49%, respectively, when compared to U251/shRandom cells (**Figure 4.2D**). Similarly, NSUN5 was knocked down in T98 cells using pLenti-shNSUN5 #3 and pLenti-shNSUN5 #4. The NSUN5 levels in T98/shRandom, T98/shNSUN5 #3, and T98/shNSUN5 #4 cells were about 71% and 21% of that in T98/shRandom, respectively (**Figure**

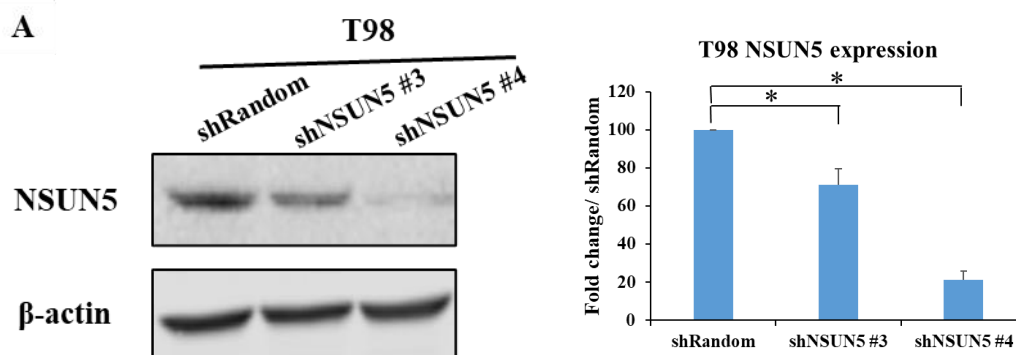
**4.3A).** Consistent with the findings in U251 cells, the growth of T98/shNSUN5 #3 and T98/shNSUN5 #4 cells was decreased by 49% and 53%, respectively, when compared to T98/shRandom cells (**Figure 4.3B**). Our results thus suggest that NSUN5 promotes proliferation in U251 and T98 cells.





**Figure 4.2 NSUN5 knockdown decreased cell growth in U251 cells.**

(A, B) Knockdown efficiency of NSUN5 by the four lentivirus shRNA constructs targeting NSUN5 in 293T cells and U251 cells was examined by Western blotting. (C) NSUN5 knockdown in U251/shRandom, U251/shNSUN5 #3 and U251/shNSUN5 #4 cells was further confirmed by Western blotting. P values for U251/shRandom versus U251/shNSUN5 #3, and U251/shRandom versus U251/shNSUN5 #4 are 1.0e-3 and 6.7e-13, respectively.  $\beta$ -actin was the loading control for all the Western blots. Data are mean  $\pm$  SE of three independent experiments. (D) Growth of U251/shRandom, U251/shNSUN5 #3 and U251/shNSUN5 #4 cells was examined using the neutral red uptake assay. Data are mean  $\pm$  SE of four independent experiments, with P values of 0.037 for shRandom vs. shNSUN5 #3 and 0.0053 for shRandom vs. shNSUN5 #4.



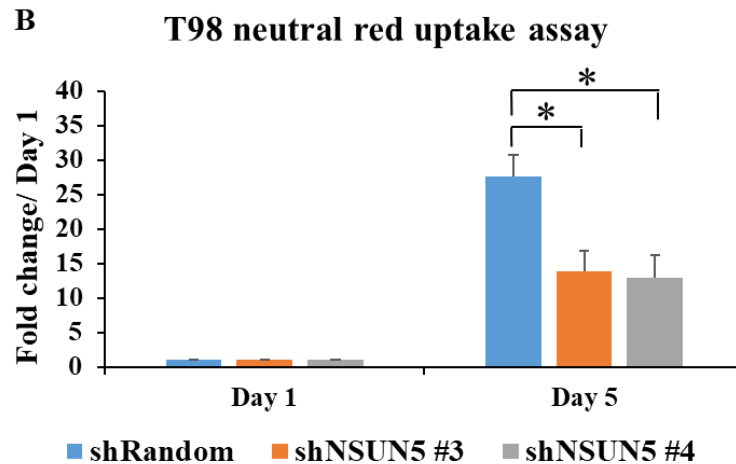


**Figure 4.3 NSUN5 knockdown in T98 cells decreased cell growth.**

(A) NSUN5 was knocked down in T98 cells, and the expression of NSUN5 in T98/shRandom, T98/shNSUN5 #3 and T98/shNSUN5 #4 cells was determined by Western blotting. The P values for T98/shRandom versus T98/shNSUN5 #3, and T98/shRandom versus T98/shNSUN5 #4 were 0.024 and 8.0e-05, respectively. (B) Growth of T98/shRandom, T98/shNSUN5 #3, and T98/shNSUN5 #4 cells was examined using the neutral red uptake assay. Data are mean  $\pm$  SE of four independent experiments, with P values of 0.011 for shRandom vs. shNSUN5 #3 and 0.01 for shRandom vs. shNSUN5 #4.

#### 4.1.1.2 Overexpression of NSUN5 does not change proliferation of U87 cells.

We next determined whether NSUN5 overexpression affects the proliferation of U251 cells. Initially, we compared the growth of U87/CMV-NSUN5 cells and U87/CMV-Vector cells and found that there was no difference in cell growth between the two types of cells as determined by the neutral red uptake assay (**Figure 4.4A**). Because only ~40% of U87/CMV-NSUN5 cells were NSUN5 positive as determined by immunocytochemistry (**Figure 3.10**), we generated U87 cells transduced with lentivirus vector pLenti-NSUN5 (U87/pLenti-NSUN5) (**Figure 4.4B**) that were ~100% NSUN5 positive as determined by immunocytochemistry (**Figure 3.23**). The neutral red

uptake assay showed that U87/pLenti-NSUN5 had a similar proliferation rate as the U87 cells transduced with the empty pLenti-Vector (U87/pLenti-Vector) (**Figure 4.4C**).

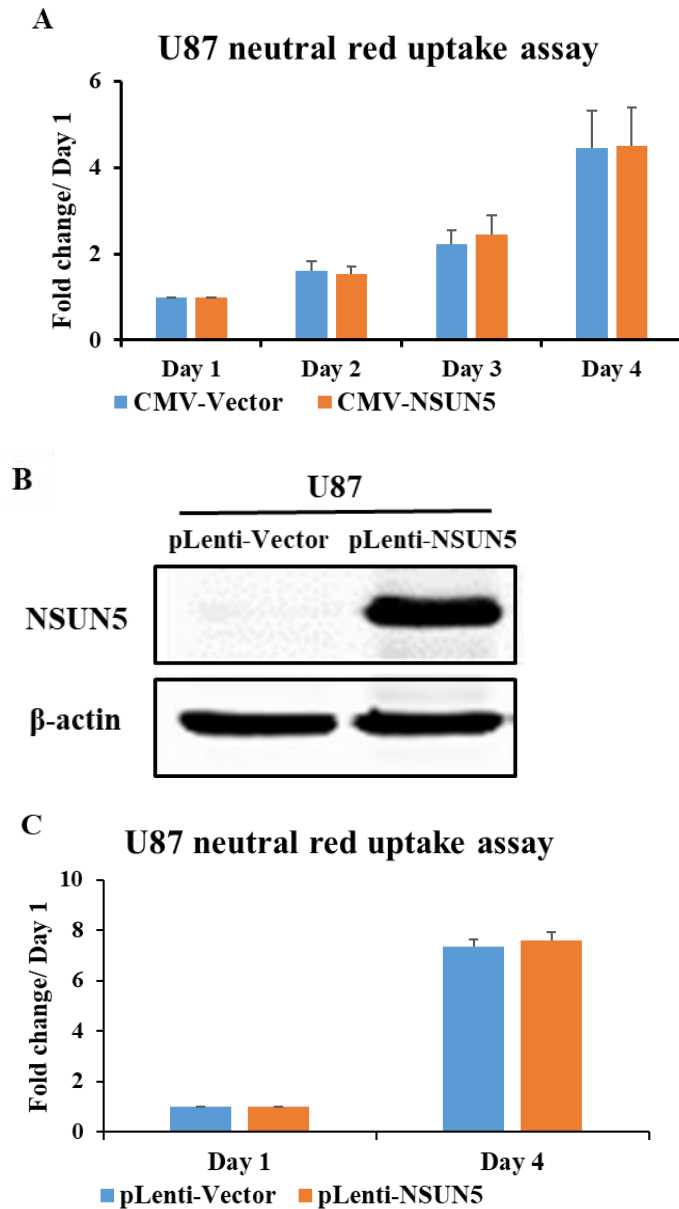


**Figure 4.4 NSUN5 overexpression did not increase the proliferation of U87 cells.**

(A) The proliferation of U87/CMV-Vector and U87/CMV-NSUN5 cells was measured using the neutral red uptake assay and expressed as fold change relative to their respective day 1. There was no difference in proliferation between the two types of cells ( $P = 0.98$ ). Data are mean  $\pm$  SE of

three independent experiments. **(B)** U87 cells were transduced with empty pLenti-Vector or pLenti-NSUN5-FLAG expression plasmids. NSUN5 overexpression was confirmed by Western blotting.  $\beta$ -Actin was the loading control. **(C)** The growth of U87/pLenti-Vector and U87/pLenti-NSUN5 cells was measured using the neutral red uptake assay and expressed as fold change relative to their respective day 1. There was no difference in proliferation between control and NSUN5-expressing U87 cells ( $P = 0.49$ ). Data are mean  $\pm$  SE of three independent experiments.

Taken together, using loss- and gain-of-function approaches, we found that NSUN5 is required for the proliferation of glioblastoma cells that express endogenous NSUN5, but overexpression of NSUN5 does not increase the proliferation of the glioblastoma cells that do not normally express NSUN5. However, the mechanisms underlying the discrepancy between NSUN5 overexpression and knockdown models need to be further studied.

#### **4.1.2 NSUN5 regulates the sphere forming ability of glioblastoma cells.**

In 2003 and 2004, Canadian scientists discovered the existence of glioblastoma cancer stem cells that have the ability to renew themselves and initiate tumors, as well as to differentiate into different lineages of cancer cells [94, 95]. Glioblastoma cancer stem cells are a main cause of tumor recurrence, treatment resistance, and poor survival [96, 98, 396]. NSUN proteins, as cytosine RNA methyltransferases, have been shown to play a role in stem cells [331, 397, 398]. For instance, NSUN2 regulates the balance of neuroepithelial and epidermal stem cells and differentiated cells through regulation of certain tRNA methylations causing tRNA cleavage and degradation [397, 398]. Similarly, NSUN3 regulates embryonic stem cell differentiation through regulation of cytosine methylation in mitochondrial RNA [331]. We have confirmed that NSUN5 methylates cytosine 3782 of 28S rRNA in glioblastoma cells. We speculate that high levels of

NSUN5 alter the structure and/or activity of ribosomes and thereby favor mRNA translation of the genes associated with stem cells, thereby promoting the stem cell phenotype in glioblastoma.

#### **4.1.2.1 Knockdown of NSUN5 decreases the sphere forming ability of glioblastoma cells.**

To determine whether NSUN5 regulates the stem cell phenotype, we performed sphere formation assay (an *in vitro* assay to measure the self-renewal capacity of cancer cells) [399]. First, we investigated whether knockdown of NSUN5 would decrease sphere formation in U251 cells. Indeed, the sphere formation assay showed that NSUN5 knockdown decreases the sphere-forming ability of U251 cells. Compared to U251/shRandom cells, U251/shNSUN5 #3 and U251/shNSUN5 #4 formed 28% and 38% fewer spheres, respectively (**Figure 4.5A**). Interestingly, NSUN5 knockdown in U251 cells also resulted in smaller spheres compared to U251/shRandom cells (**Figure 4.5B**). Of note, U251/shNSUN5 #4 cells, which had a much better NSUN5 knockdown efficiency than U251/shNSUN5 #3 (**Figure 4.2C**), formed fewer and smaller spheres compared to U251/shNSUN5 #3 (**Figure 4.5**). Next, we determined whether knockdown of NSUN5 would decrease sphere formation in A4-012 cells (one of the patient-derived cell line maintained as neurospheres). The knockdown efficiency of NSUN5 in A4-012 cells was confirmed by Western blotting, and the NSUN5 expression levels for A4-012/shNSUN5 #3 and A4-012/shNSUN5 #4 cells were about 74% and 18% of A4-012/shRandom, respectively (**Figure 4.6A**). Similar to U251 cells, knockdown of NSUN5 by shNSUN5 #3 and shNSUN5 #4 decreased sphere numbers by 46% and 80%, respectively, when compared to A4-012/shRandom cells (**Figure 4.6B**). Similarly, A4-012/shNSUN5 #3 and A4-012/shNSUN5 #4 formed smaller spheres compared to A4-012/shRandom cells. In keeping with the extent of NSUN5 knockdown efficiency, A4-012/shNSUN5 #4 cells formed fewer and smaller spheres than A4-012/shNSUN5 #3 cells (**Figures 4.6C**). Intriguingly, knockdown of NSUN5 by shNSUN5 #4 had more dramatic effect

on sphere forming ability in A4-012 than in U251 cells, suggesting that the patient-derived neurosphere cultures are more sensitive to reduced expression of NSUN5 than established cell lines.

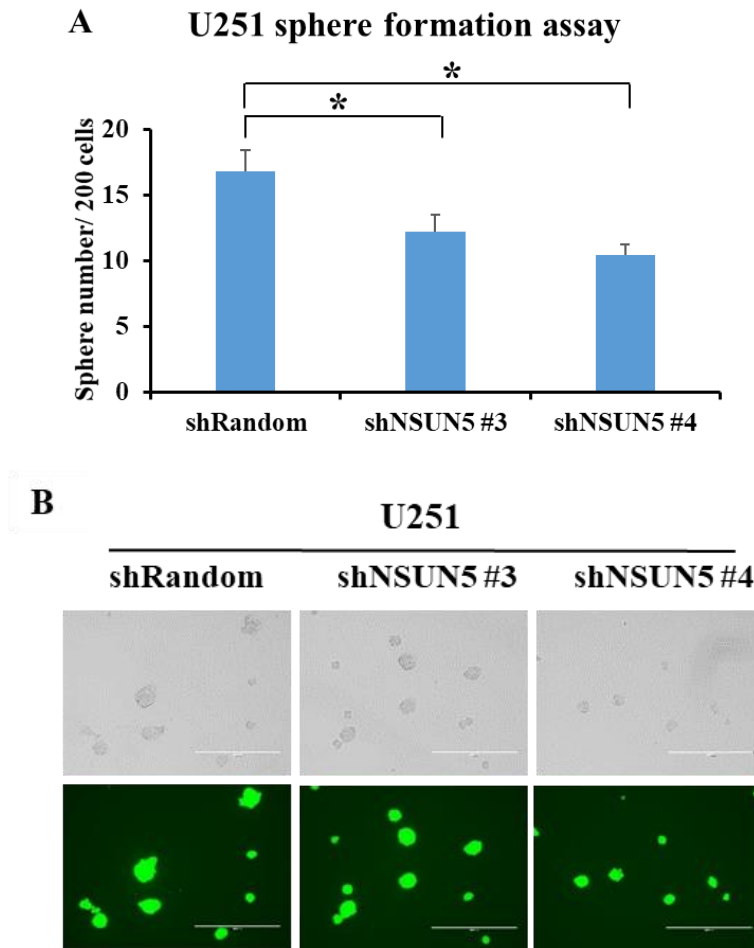


**Figure 4.5 Knockdown of NSUN5 decreases sphere formation in U251 cells.**

(A) Sphere formation assays were performed by seeding 200 U251/shRandom, U251/shNSUN5 #3, or U251/shNSUN5 #4 cells. Data are mean  $\pm$  SE of four independent experiments, with P values of 0.0027 for shRandom vs. shNSUN5 #3 and 7.6e-06 for shRandom vs. shNSUN5 #4. (B) U251/shNSUN5 #3 and U251/shNSUN5 #4 cells formed smaller spheres than U251/shRandom cells. Images of the spheres were taken using a 10X objective under transmitted light and GFP channel, with the scale bar = 400  $\mu$ m. As the NSUN5 shRNAs were in a lentiviral GFP vector and

the transfection efficiency were about 100%, the transfected U251 cells expressed GFP (green color under GFP channel of fluorescence microscope).

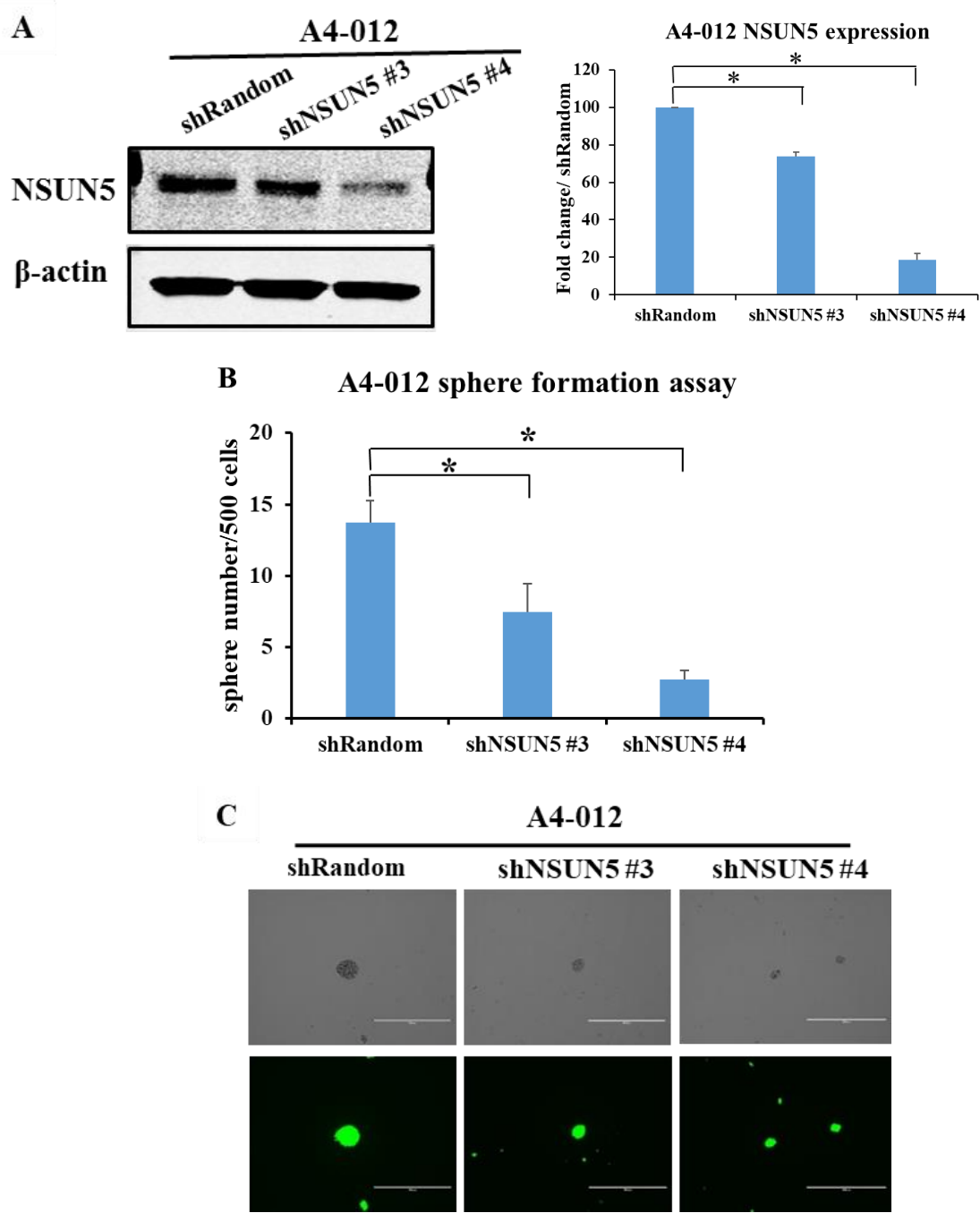
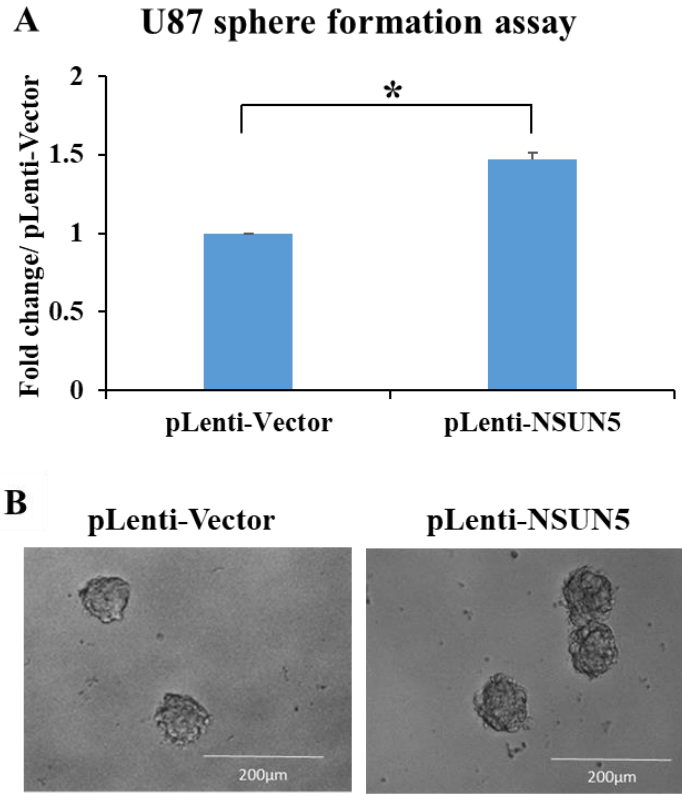


**Figure 4.6 Knockdown of NSUN5 decreases sphere formation in A4-012 cells.**

(A) Western blotting results showing the levels of NSUN5 in A4-012/shRandom, A4-012/shNSUN5 #3, and A4-012/shNSUN5 #4 cells.  $\beta$ -Actin was the loading control. The P values for A4-012/shRandom versus A4-012/shNSUN5 #3, and A4-012/shRandom versus A4-012/shNSUN5 #4, were 4.898e-05 and 3.604e-06, respectively. Data are mean  $\pm$  SE of three independent experiments. (B) Sphere formation assays were performed by seeding 500 cells per well. Data are mean  $\pm$  SE of three independent experiments, with P values of 0.009 for shRandom vs. shNSUN5 #3 and 7.3e-06 for shRandom vs. shNSUN5 #4. (C) A4-012/shNSUN5 #3 and A4-012/shNSUN5 #4 cells formed smaller spheres compared to A4-012/shRandom cells. Images of spheres were taken using a 10X objective under transmitted light and GFP channel, with the scale bar = 400  $\mu$ m. The backbone for the NSUN5 shRNA constructs is the lentiviral GFP vector. The transfection efficiency was about 100%. The transfected A4-012 cells express GFP and show up as green under the GFP channel of the fluorescence microscope.

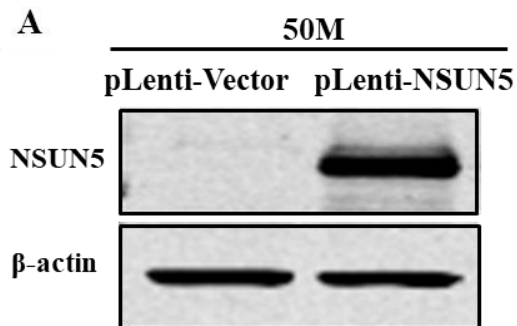
#### 4.1.2.2 Overexpression of NSUN5 increases the sphere forming ability of glioblastoma cells.

We also performed the sphere formation assay in U87/pLenti-Vector and U87/pLenti-NSUN5 cells. U87/pLenti-NSUN5 cells formed about 46% more spheres than U87/pLenti-Vector cells (**Figures 4.7**). We also examined the effect of overexpression of NSUN5 on sphere-forming ability of 50M glioblastoma cells, a patient-derived neurosphere culture that does not express endogenous NSUN5. We overexpressed NSUN5 in 50M cells to generate 50M/pLenti-NSUN5 and 50M/pLenti-vector cells. Overexpression of NSUN5 in 50M/pLenti-NSUN5 was confirmed by Western blotting (**Figure 4.8A**). 50M/pLenti-NSUN5 cells formed about 89% more spheres than 50M/plenti-vector cells (**Figure 4.8B and C**). Our results show that overexpression of NSUN5 increases the sphere-forming ability of glioblastoma cells. This finding is intriguing since NSUN5 overexpression in U87 cells failed to increase their growth/proliferation. Together, these results suggest that overexpression of NSUN5 may specifically regulate the events associated with stemness, but not proliferation, in the overexpression model.



**Figure 4.7 Overexpression of NSUN5 increases sphere formation in U87 cells.**

(A) Sphere formation assays were performed by seeding 100 cells per well. Data are mean  $\pm$  SE of three independent experiments. \*Significant ( $p = 1.0e-3$ ). (B) Images of spheres formed by U87/pLenti-vector and U87/pLenti-NSUN5 were taken using a 20X objective.



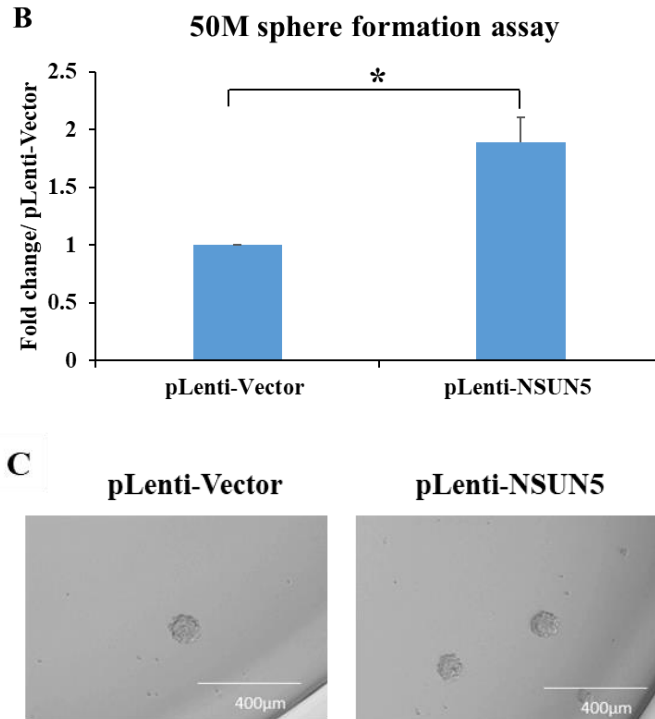


**Figure 4.8 Overexpression of NSUN5 increases sphere formation in 50M cells.**

(A) 50M cells were stably transduced with an empty pLenti-Vector or pLenti-NSUN5-FLAG vector. NSUN5 overexpression was confirmed by Western blotting.  $\beta$ -Actin was the loading control. (B) Sphere formation assays were performed by seeding 200 cells in each well. Data are mean  $\pm$  SE of six replicates in three independent experiments ( $P=0.003878$ ). (C) Images of the spheres formed by 50M/pLenti-vector and 50M/pLenti-NSUN5 were captured using a 10X objective.

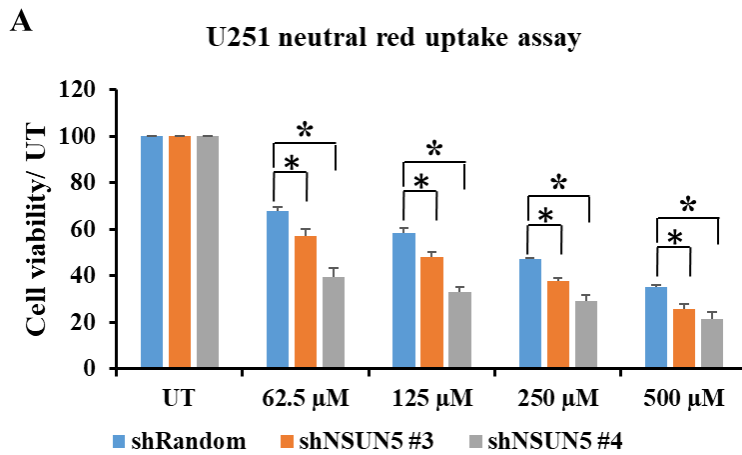
Taken together, our finding that overexpression of NSUN5 increases the number of spheres and knockdown of NSUN5 decreases both the number and size of spheres formed by glioblastoma cells suggest that NSUN5 promotes self-renewal and the stem cell phenotype in glioblastoma.

## 4.2 Knockdown of NSUN5 renders U251 and T98 cells more sensitive to temozolomide

In a yeast study, Rcm1 (the yeast homologue of NSUN5) was shown to regulate the translation of oxidative stress-response mRNAs and the stress response [312]. However, whether NSUN5 is also associated with stress response in glioblastoma cells is unknown. Since radiation therapy and chemotherapy with temozolomide are the standard of care for glioblastoma patients, radiation and chemotherapy are the two most common external stressors for glioblastoma cells [96, 98, 396]. In the clinic, chemotherapy resistance is one of the main causes of poor treatment outcome [96, 98, 396]. Therefore, it is important to investigate whether NSUN5 regulates stress response to chemotherapy and contributes to treatment resistance in glioblastoma.

Temozolomide is an alkylating agent that induces cytotoxicity by methylating the O<sup>6</sup> position of guanine resulting in DNA damage [26]. It is the first line chemotherapy drug for the standard care of glioblastoma patients [25]. According to published studies, the half maximal inhibitory concentration (IC<sub>50</sub>) for temozolomide in U251 cells is approximately 100 to 250 μM, and the *MGMT* promoter of U251 cells is methylated [75, 400-402]. To determine whether NSUN5 regulates stress response to temozolomide treatment in glioblastoma, we performed dose response experiments using U251/shRandom, U251/shNSUN5 #3, and U251/shNSUN5 #4 cells. The neutral red uptake assay showed that U251/shNSUN5 #3 and U251/shNSUN5 #4 cells were more sensitive to temozolomide treatment than U251/shRandom cells (**Figure 4.9A**). The half maximal inhibitory concentrations (IC<sub>50</sub>) for temozolomide were 204.4 μM in U251/shRandom, 109.4 μM in U251/shNSUN5 #3 cells, and 47.83 μM in U251/shNSUN5 #4 (**Figure 4.9B**). Moreover, combination of NSUN5 knockdown and temozolomide treatment markedly decreased the number of viable cells in U251 cells compared to either NSUN5 knockdown or temozolomide alone (**Figure 4.10**). Specifically, the viability of U251/shNSUN5 #4 cells treated with temozolomide

was 54%, 64%, and 76% lower compared to U251/shRandom cells treated with temozolomide, U251/shNSUN5 #4 cells or U251/shRandom cells treated with DMSO, respectively. In addition, we performed the dose response experiments on T98 cells (T98/shRandom, T98/shNSUN5 #3, and T98/shNSUN5 #4 cells) that has unmethylated *MGMT* promoter and is resistant to temozolomide treatment [402, 403]. We found that NSUN5-depleted T98 cells were more sensitive to temozolomide treatment than control cells (**Figure 4.11A**). The half maximal inhibitory concentrations ( $IC_{50}$ ) for temozolomide were 623.3  $\mu$ M in T98/shRandom, 512.3  $\mu$ M in T98/shNSUN5 #3 cells, and 457.6  $\mu$ M in T98/shNSUN5 #4 (**Figure 4.11B**).



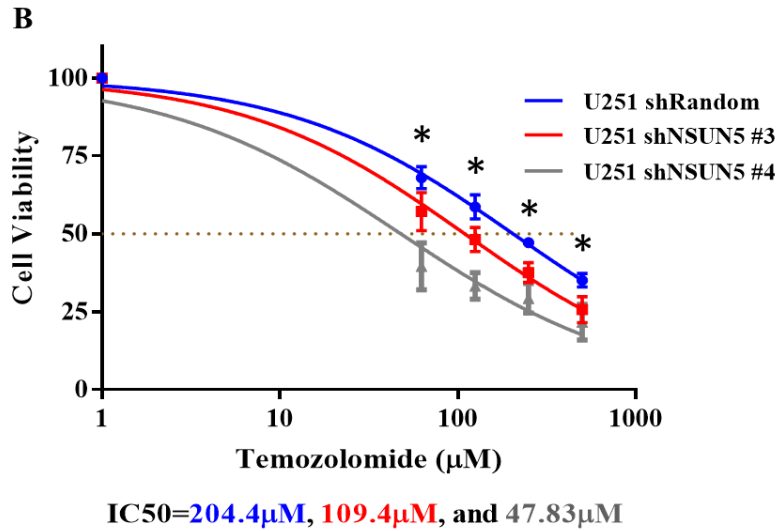


**Figure 4.9 NSUN5 knockdown sensitizes U251 cells to temozolomide treatment.**

**(A)** Dose response to temozolomide was measured in U251/shRandom, U251/shNSUN5 #3, and U251/shNSUN5 #4 cells by the neutral red uptake assay. Cells were treated with 0, 62.5, 125, 250, and 500  $\mu\text{M}$  temozolomide. U251/shNSUN5 #3 and U251/shNSUN5 #4 cells were more sensitive than U251/shRandom when treated with 62.5  $\mu\text{M}$ , 125  $\mu\text{M}$ , 250  $\mu\text{M}$ , and 500  $\mu\text{M}$  of temozolomide.

**(B)** The IC<sub>50</sub> of temozolomide based on the neutral red uptake assay was 204.4, 109.4, and 47.83  $\mu\text{M}$  for U251/shRandom, U251/shNSUN5 #3, and U251/shNSUN5 #4 cells, respectively. Data are presented as the mean of four independent experiments, \* = P < 0.05.

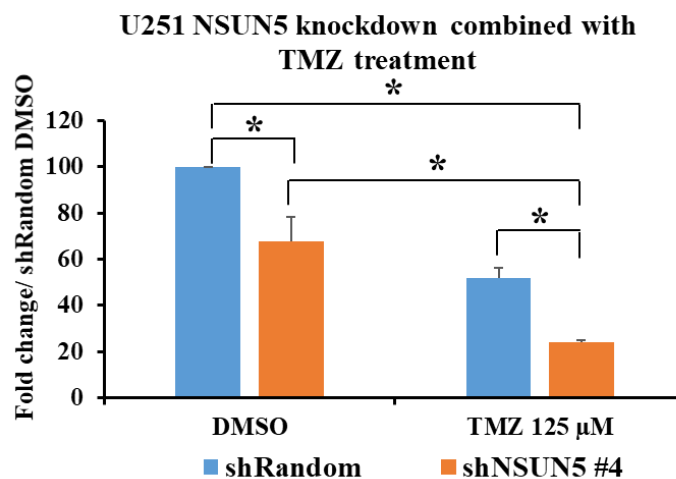


**Figure 4.10 Combination of NSUN5 knockdown with temozolomide treatment markedly decreases cell viability of U251 cells.**

U251/shRandom and U251/shNSUN5 #4 cells were treated with an equal volume of DMSO (vehicle control) or 125  $\mu\text{M}$  temozolomide. Cell viability was measured using the neutral red uptake assay. Data are mean  $\pm$  SE of four independent experiments. \* =  $P < 0.05$ .

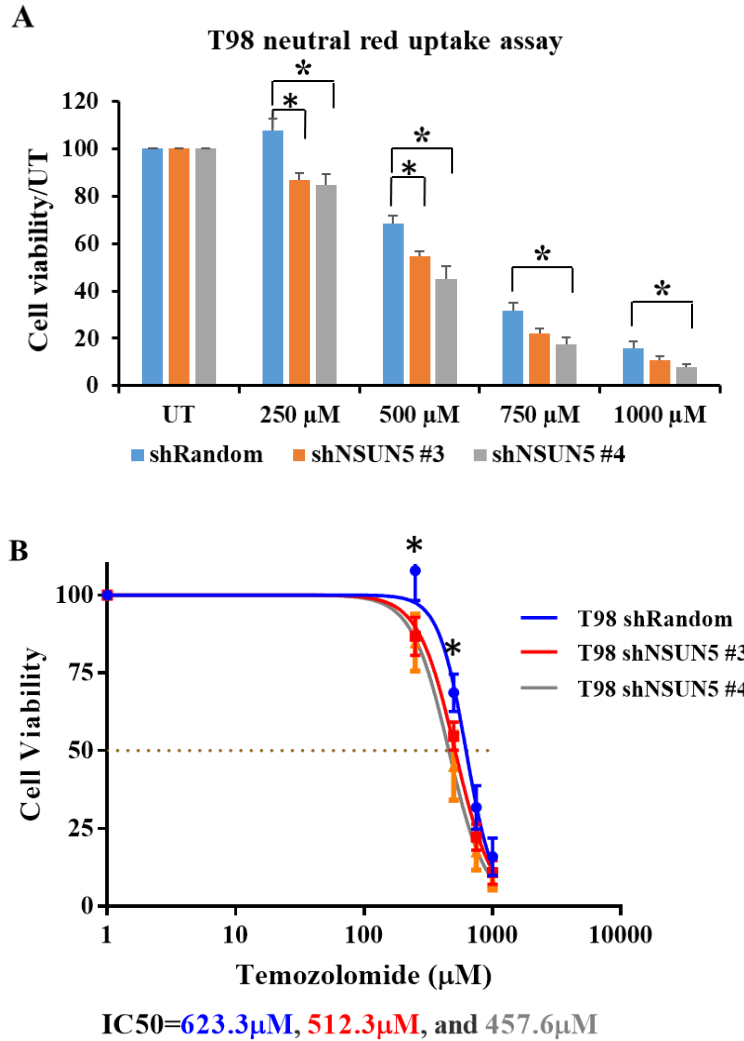


**Figure 4.11 NSUN5 knockdown sensitizes T98 cells to temozolomide treatment.**

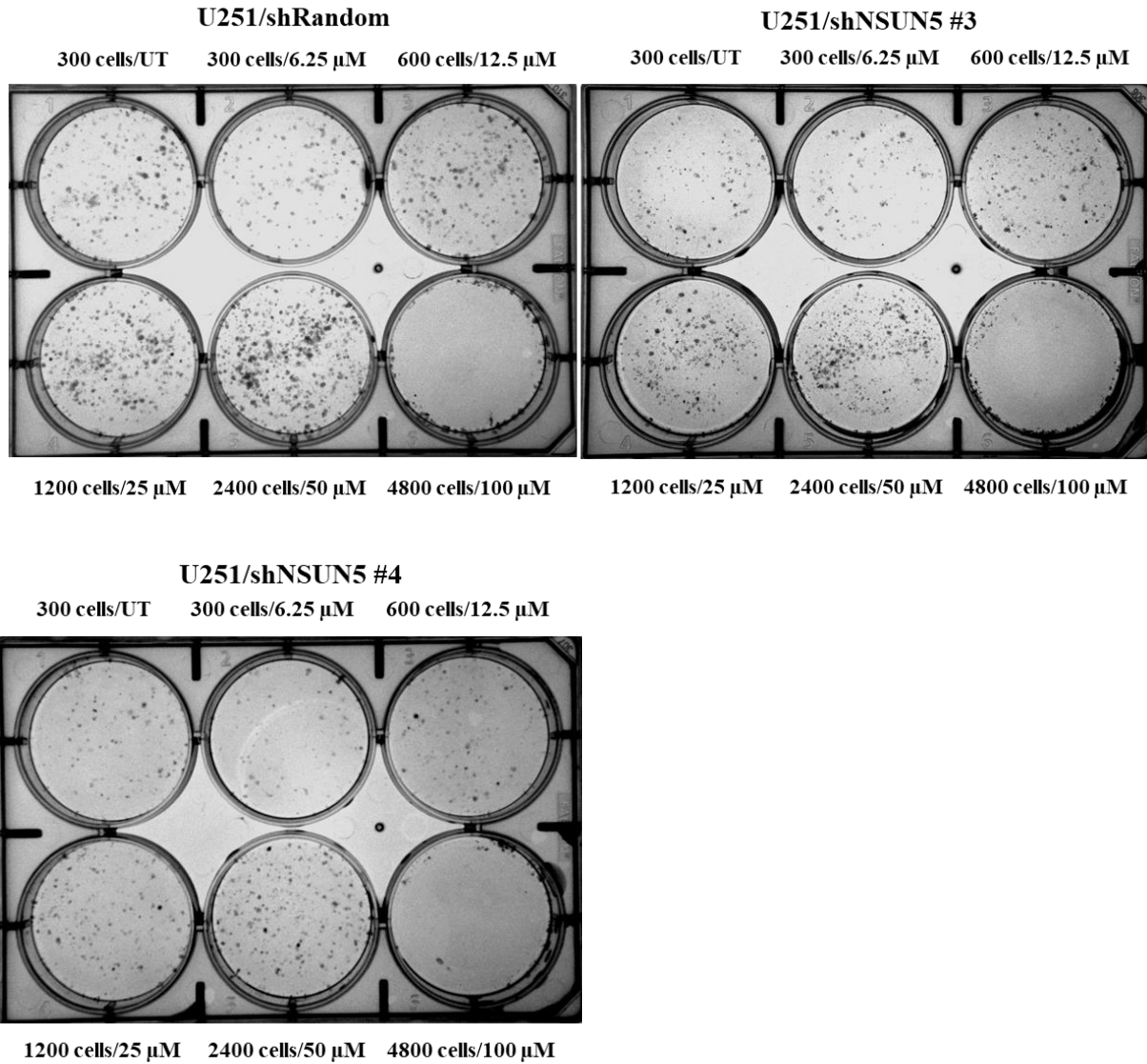
(A) Dose response to temozolomide was measured in T98/shRandom, T98/shNSUN5 #3, and T98/shNSUN5 #4 cells by the neutral red uptake assay. Cells were treated with 0, 250, 500, 750, and 1000  $\mu\text{M}$  temozolomide. T98/shNSUN5 #3 and T98/shNSUN5 #4 cells were more sensitive than T98/shRandom when treated with 250  $\mu\text{M}$ , 500  $\mu\text{M}$ , 750  $\mu\text{M}$ , and 1000  $\mu\text{M}$  of temozolomide.

**(B)** The IC<sub>50</sub> of temozolomide based on the neutral red uptake assay was 623.3, 512.3, and 457.6 μM for T98/shRandom, T98/shNSUN5 #3, and T98/shNSUN5 #4 cells, respectively. Data are presented as the mean of four independent experiments, \* = P < 0.05.

Next, we performed the clonogenic survival assay which more accurately measures the proliferation and survival of cells treated with drugs [367-370]. In keeping with the neutral red uptake assay results, the clonogenic survival assay showed that U251/shNSUN5 #3 and U251/shNSUN5 #4 cells formed fewer colonies and were more sensitive to temozolomide treatment, compared to U251/shRandom cells (**Figure 4.12A**). Specifically, the surviving fractions were 29.2%, 35.6%, 38.3%, and 41.6% lower in U251/shNSUN5 #3 cells, and 30.9%, 40.7%, 45.8%, and 67.1% lower in U251/shNSUN5 #4 cells, compared to U251/shRandom cells upon treatment with 6.25, 12.5, 25, and 50 μM of temozolomide, respectively (**Figure 4.12B**). The IC<sub>50</sub> for temozolomide was 20.15 μM in U251/shRandom, 13.12 μM in U251/shNSUN5 #3, and 12.64 μM in U251/shNSUN5 #4 cells (**Figure 4.12C**). Moreover, we performed the clonogenic survival assay on T98 cells that has unmethylated *MGMT* promoter and is resistant to temozolomide treatment [402, 403]. We found that NSUN5-depleted T98 cells were more sensitive to temozolomide treatment than control cells (**Figure 4.13A**). Specifically, the surviving fractions were 24.2%, 18.4%, 31.3%, and 38.6% lower in T98/shNSUN5 #3 cells, and 23.5%, 24.2%, 27.1%, and 49.2% lower in T98/shNSUN5 #4 cells, compared to T98/shRandom cells upon treatment with 62.5, 125, 250, and 500 μM of temozolomide, respectively (**Figure 4.13B**). The IC<sub>50</sub> for temozolomide was 378.2 μM in T98/shRandom cells, 266.1 μM in T98/shNSUN5 #3 cells, and 264.4 μM in T98/shNSUN5 #4 cells (**Figure 4.13C**). Taken together, the results from the neutral

red uptake and clonogenic assays clearly demonstrate that knockdown of NSUN5 renders U251 and T98 cells more sensitive to temozolomide.

A



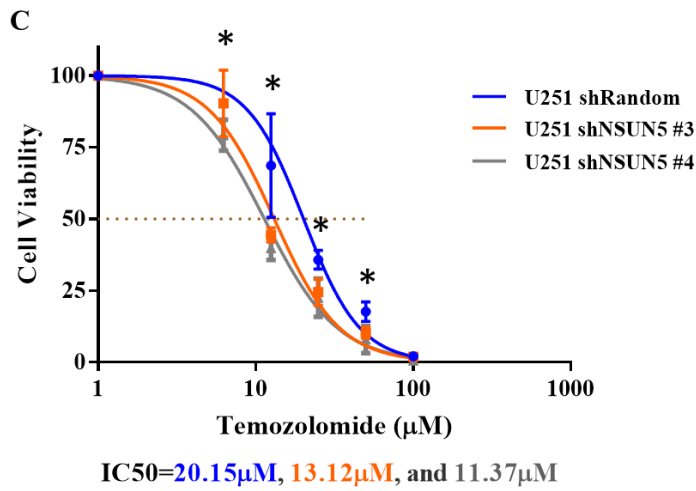
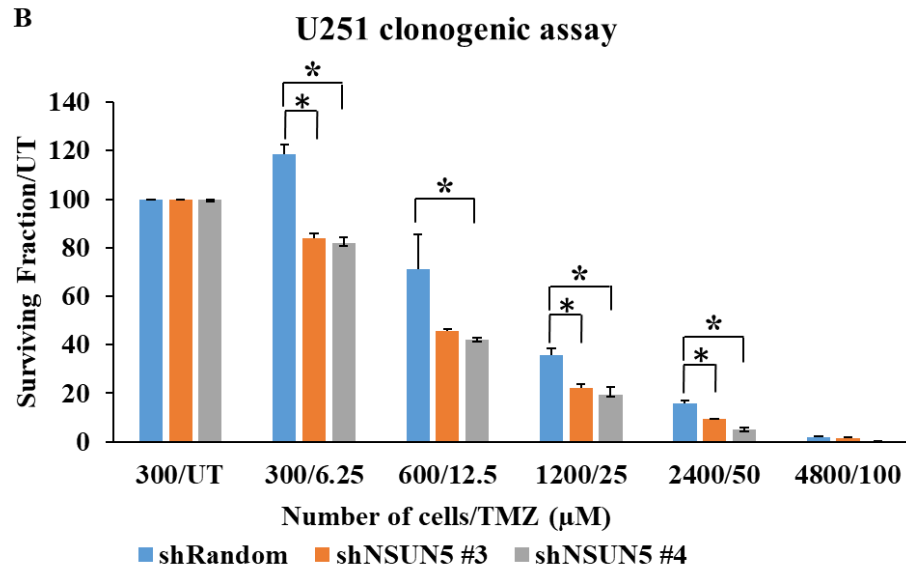
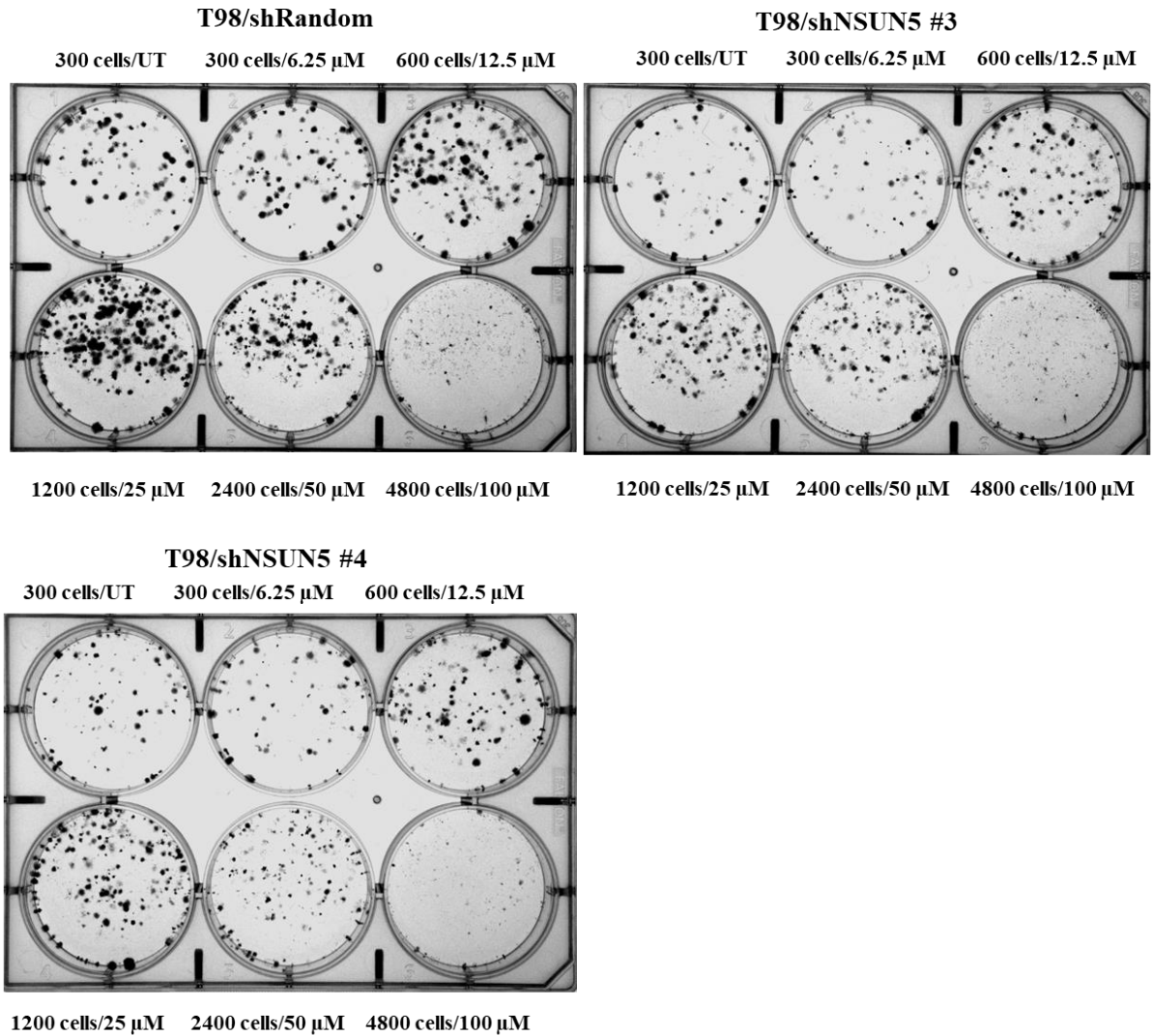


**Figure 4.12 NSUN5 knockdown renders U251 cells more sensitive to temozolomide treatment.**

The clonogenic assay was performed to determine the dose response to temozolomide in U251/shRandom, U251/shNSUN5 #3, and U251/shNSUN5 #4 cells. Cells were seeded at 300, 300, 600, 1200, 2400, and 4800 cells per well and treated with 0, 6.25, 12.5, 25, 50, and 100 µM temozolomide, respectively. (A and B) U251/shNSUN5 #3 and U251/shNSUN5 #4 cells formed fewer colonies than U251/shRandom cells when treated with 6.25, 12.5, 25, or 50 µM temozolomide. (C) The survival curves show that IC<sub>50</sub> for temozolomide was 20.15 µM in

U251/shRandom, 13.12  $\mu$ M in U251/shNSUN5 #3, and 12.64  $\mu$ M in U251/shNSUN5 #4 cells.  
Data are mean  $\pm$  SE of three independent experiments, \* =  $P < 0.05$ .

**A**



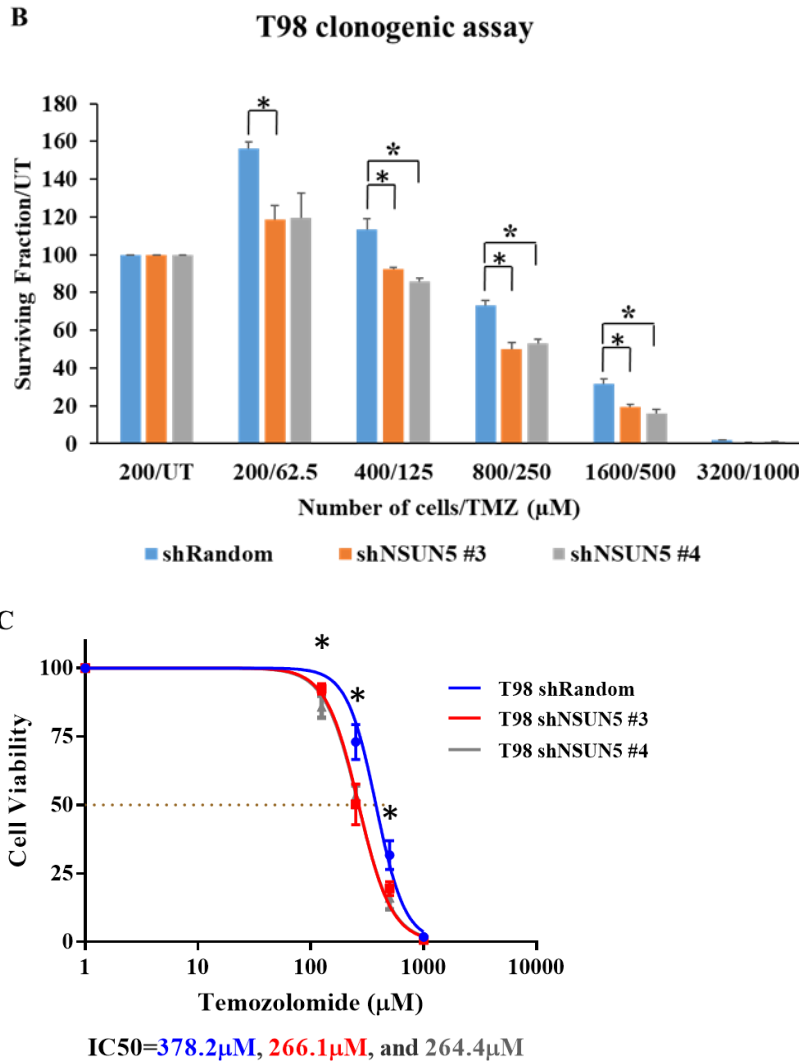


**Figure 4.13 NSUN5 knockdown renders T98 cells more sensitive to temozolomide treatment.**

The clonogenic assay was performed to determine the dose response to temozolomide in T98/shRandom, T98/shNSUN5 #3, and T98/shNSUN5 #4 cells. Cells were seeded at 200, 200, 400, 800, 1600, and 3200 cells per well and treated with 0, 62.5, 125, 250, 500, and 1000 µM temozolomide, respectively. (A and B) T98/shNSUN5 #3 and T98/shNSUN5 #4 cells formed fewer colonies than T98/shRandom cells, especially in the cells treated with 62.5, 125, 250, or 500 µM of temozolomide. (C) The survival curves show that IC<sub>50</sub> for temozolomide was 378.2 µM in T98/shRandom cells, 266.1 µM in T98/shNSUN5 #3 cells, and 264.4 µM in T98/shNSUN5 #4 cells. Data are mean ± SE of three independent experiments, \* = P < 0.05.

### 4.3 Knockdown of NSUN5 prolonged survival of mice bearing U251 intracranial tumors.

Compared with *in vitro* functional assays, mouse xenograft models retain the physiological microenvironment and more accurately mimic tumor growth *in vivo*. Mouse intracranial xenograft tumor models are commonly used for glioblastoma studies which is indispensable to our understanding of the complexity of glioblastoma tumor formation. U251 cells formed tumors in mouse models [404, 405]. U251/WTA1 vs. U251/KOB1, U251/shRandom vs. U251/shNSUN5 #4 cells, were selected for our *in vivo* study.

We first injected 50,000 U251/WTA1 or U251/KOB1 cells in 5 NSG mice each. None of the mice showed signs of weight loss or distress after 3 months. The experiment was terminated at three months and mice were sacrificed. Tumors were not detected in any of these mice. As U251/WTA1 and U251/KOB1 cells are clonal populations, it is possible that the number of tumor cells injected was too low to form tumors. To address this problem, we decided to inject a bulk population of NSUN5-depleted U251 cells into the brains of NSG mice. The firefly luciferase gene-encoding lentivirus plasmid was stably transfected into U251/shRandom and U251/shNSUN5 #4 cells. 250,000 of U251/shRandom-luciferase (U251/shRandom-luc) or U251/shNSUN5#4-luciferase (U251/shNSUN5#4-luc) cells were then injected into mice. Mice were monitored weekly and scored for body weight loss and development of neurological symptoms. Mice were monitored more frequently when the score was close to the endpoint (loss of 20% of body weight) and euthanized when the endpoint was reached. The time between tumor cell injection and euthanasia was recorded as the survival time of the mice. Tumor formation and progression were also measured by weekly bioluminescence imaging after injection of glioblastoma cells.

Three experiments were carried out with U251/shRandom-luc and U251/shNSUN5#4-luc cells. In the first experiment, U251/shRandom-luc and U251/shNSUN5#4-luc cells were injected into one mouse for each cell type as a pilot experiment. Tumor formation and progression was monitored by bioluminescence imaging for 14 weeks, at which time the mice were euthanized. As shown in **Figure 4.14A**, both U251/shRandom-luc and U251/shNSUN5#4 cells formed intracranial tumors. In the second experiment, we injected U251/shRandom-luc and U251/shNSUN5#4-luc cells into five mice for each cell type. All mice formed tumors as shown by the bioluminescence imaging (**Figure 4.14A**). The shNSUN5#4 mice showed longer overall survival compared with the shRandom mice, with the median survival times of 120 days and 89 days ( $P = 0.009$ ), respectively (**Figure 4.14B**). In the third experiment, U251/shRandom-luc or U251/shNSUN5#4-luc cells were injected into five and seven mice, respectively. All mice formed tumors as shown by bioluminescence imaging (**Figure 4.14A**). The shNSUN5#4 mice showed longer overall survival compared with the shRandom mice, with median survival times of 134 days and 106 days ( $P = 0.013$ ), respectively (**Figure 4.14C**). There was no difference in the radiance of tumors from shRandom mice and shNSUN5 #4 mice based on bioluminescence imaging (**Figure 4.14D**), and the survival times did not appear to be associated with the intensity of the imaging signal.

**A**

**The first experiment**

**shRandom Mice**

**shNSUN5#4 Mice**

**B2**

**B3**

**Day 21**



**The second experiment**

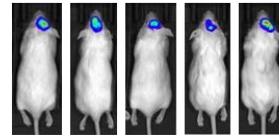
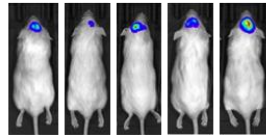
**shRandom Mice**

**shNSUN5 #4 Mice**

**D1 D3 E2 F1 F3**

**D2 E1 E3 F2 F4**

**Day 21**



**The third experiment**

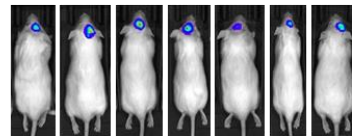
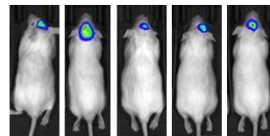
**shRandom Mice**

**shNSUN5 #4 Mice**

**G3 G5 H1 H3 I2**

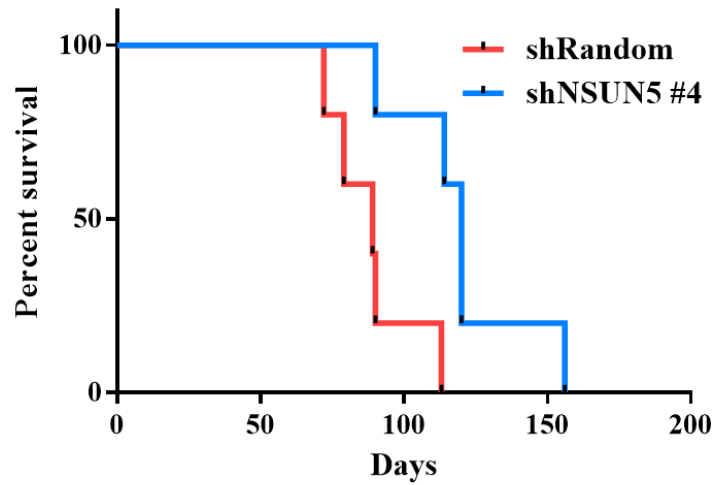
**G2 G4 H2 H4 H5 I1 I3**

**Day 21**



**B**

**U251 intracranial injection mice survival**



**C U251 intracranial injection mice survival**

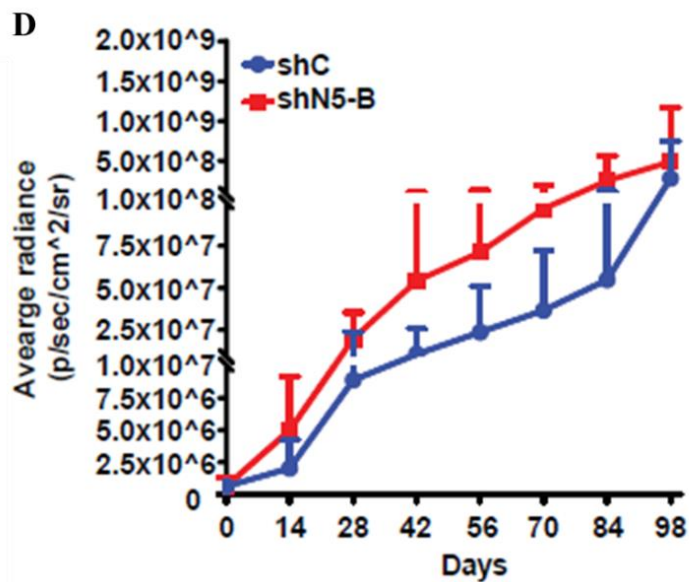
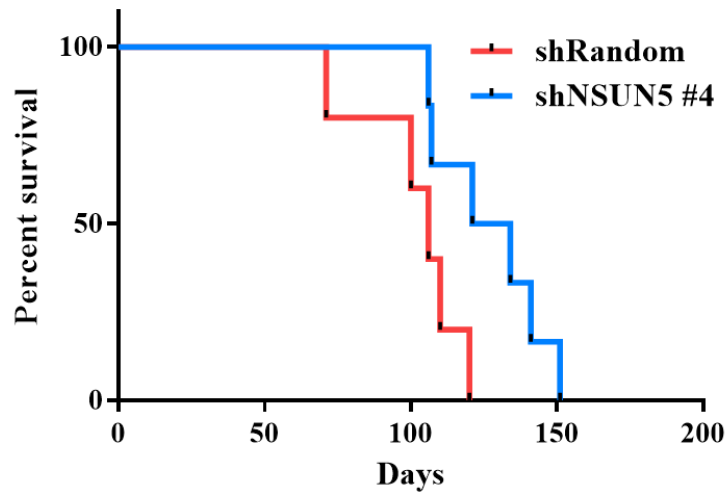
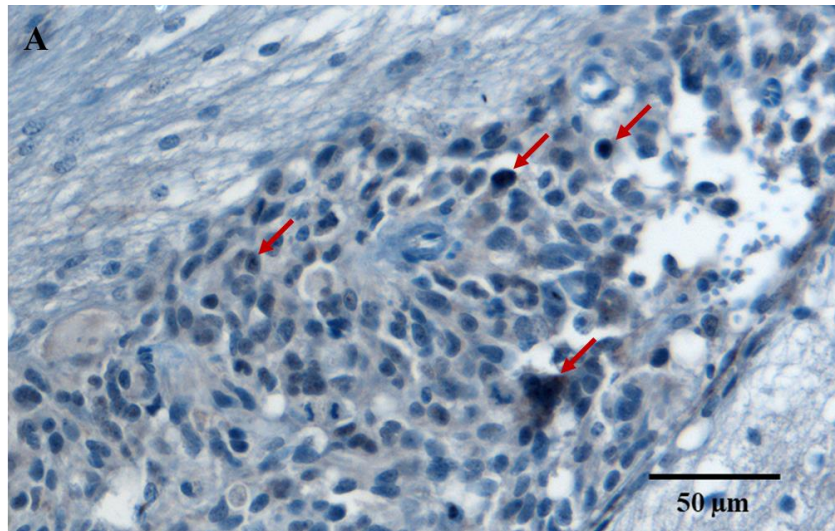


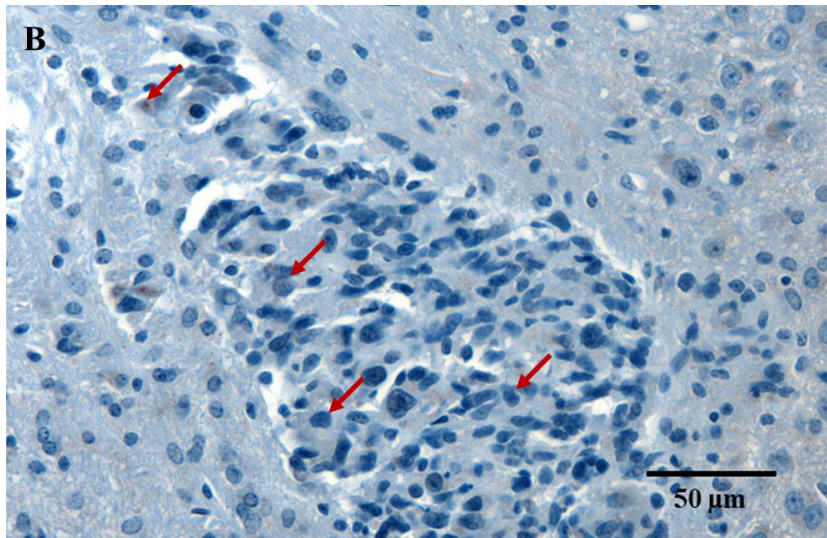
**Figure 4.14 Knockdown of NSUN5 in U251 cells prolongs the survival time of mice bearing U251 tumors.**

(A) U251/shRandom-luc and U251/shNSUN5#4-luc cells were intracranally injected into NSG mice and tumor growth monitored by bioluminescence imaging. In the first (pilot) experiment, we injected one mouse with U251/shRandom-luc and one mouse with U251/shNSUN4-luc. In the second experiment, five mice were injected with U251/shRandom-luc and five mice with U251/shNSUN5#4-luc. In the third experiment, five mice were injected with U251/shRandom-luc and

seven mice were injected with U251/shNSUN5#4-luc. **(B and C)** In the second and third experiments, the shNSUN5#4-injected mice showed a longer overall survival compared with the shRandom-injected mice. Data were analysed by Log-rank (Mantel-Cox) test using GraphPad Prism. **(D)** Bioluminescence imaging analysis of the third experiment showed that the radiance of tumors was not different between shRandom mice and shNSUN5 #4 mice.

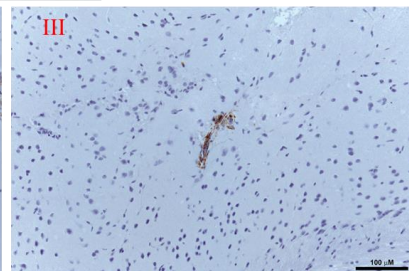
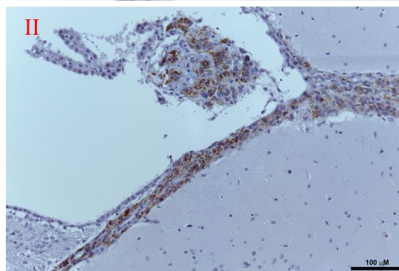
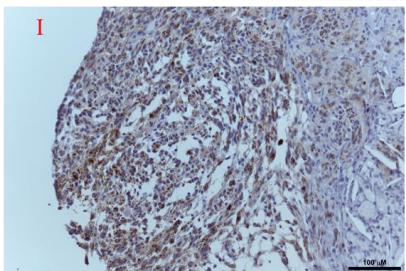
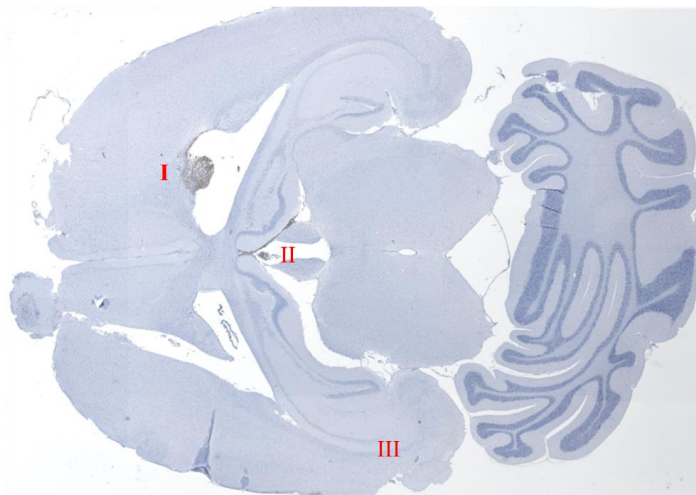
We confirmed the expression of NSUN5 in the tumors of shRandom mice and shNSUN5#4 mice by IHC (**Figure 4.15A and B**). IHC staining using an antibody against a human mitochondrial protein showed that tumors formed by U251/shRandom migrated to the subependymal layer at multiple sites in the brain through the CSF circulation and the ventricular system (**Figure 4.15C**). This type of metastasis is called leptomeningeal metastases, which occurs in 4.7% to 25% of glioblastoma patients [406-409]. By contrast, tumors formed by U251/shNSUN5 cells were more localized in the brain parenchyma which may explain the longer survival of mice with U251/shNSUN5 tumors compared to mice with U251/shRandom tumors (**Figure 4.15C**).





**C**

**shRandom  
tumors**



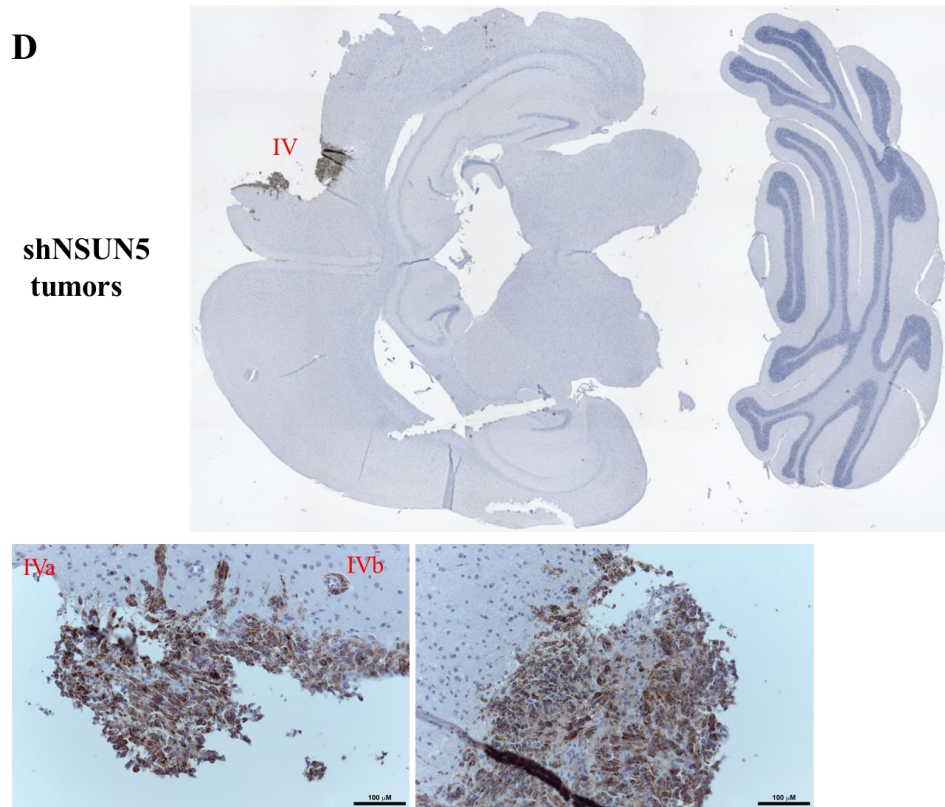


**Figure 4.15 Immunostaining of NSUN5 and tumor cells in U251 xenografts.**

**(A)** IHC staining shows the expression of NSUN5 in U251 shRandom tumors. NSUN5-positive regions are indicated by the brown stain (red arrows), with most of the signal found in the nuclei of tumor cells. **(B)** IHC staining shows low expression of NSUN5 in U251 shNSUN5 #4 tumors. Weakly positive signals are indicated by the brown stain (red arrows). **(A, B)** Nuclei were counterstained with hematoxylin. Images were taken with a 20X objective. **(C)** IHC shows that the shRandom tumors migrate to the subependymal layer at multiple sites in the brain. I, tumor cells located in the ependymal layer of the right frontal horn of the lateral ventricle; II, tumor cells located in the ependymal layer of the third ventricle; III, tumor cells located close to the subependymal area of the left ventral horn of the lateral ventricle. **(D)** shNSUN5 tumors were more localized in the mouse brain. IV, tumor cells located in the parenchyma of the right frontal lobe. Tumor cells were immunostained with an antibody to human mitochondrial protein (HuMito). A positive signal is indicated by the brown stain. The scale bar equals 100 μm.

One interesting observation is that eight out of eleven shRandom mice, but only two out of thirteen shNSUN5#4 mice, in the combined three experiments displayed spinal metastasis (**Figure 4.16**). Most of the spinal metastases was detected approximately 2 months (average 8.8 weeks) after intracranial tumor cell injections (**Table 4.1**). These results are in agreement with the U251/shRandom-luc cells being more infiltrative, and able to migrate to the spine through the CSF circulation and the ventricular system. Even though glioblastoma spinal metastasis has been rarely reported in the literature, two post-mortem autopsy studies revealed spinal metastasis in 15.3% to 25% of glioblastoma patients [409, 410]. However, U251 spinal metastasis has not been reported previously. These results will be further discussed in the discussion chapter.

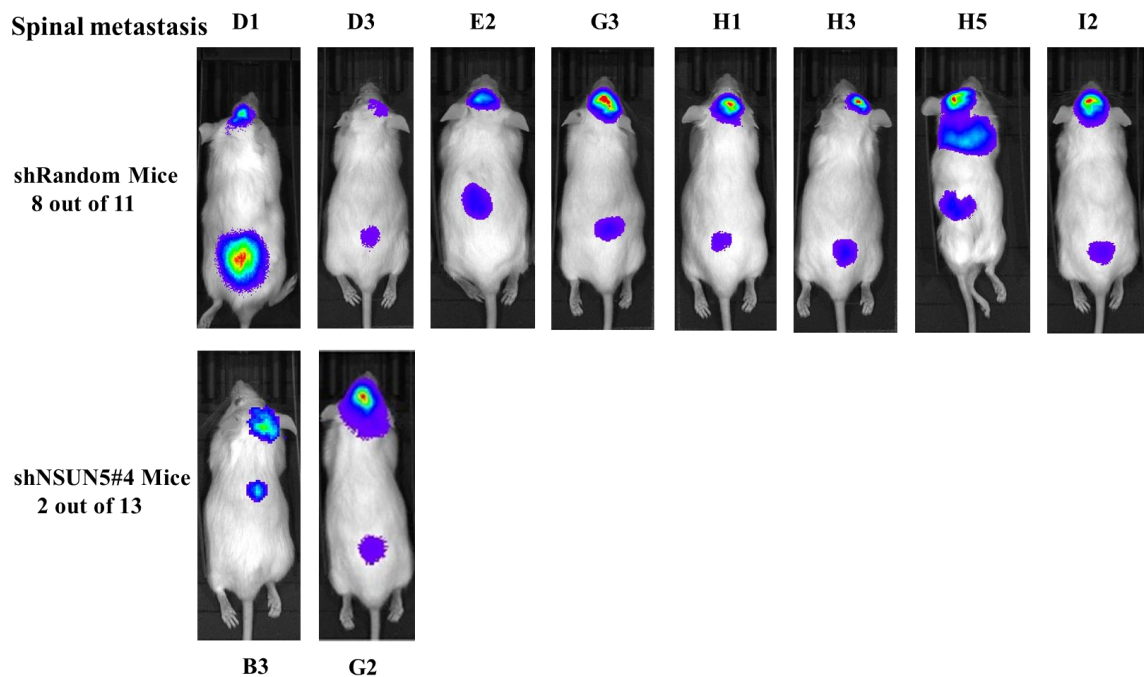


**Figure 4.16 Knockdown of NSUN5 reduces spinal metastasis of intracranial U251 tumors.**

Eight out of eleven shRandom mice and two out of thirteen shNSUN5#4 mice in the three experiments displayed spinal metastasis.

**Table 4.1 The survival times of mice intracranially injected with U251 cells and the time of appearance of spinal metastasis.**

<b>U251 intracranial injection mice</b>	<b>Survival time (days)</b>	<b>Spinal metastasis (weeks)</b>
<b>shRandom-luc mice (Eleven)</b>		
<b>B2</b>	<b>N/A</b>	<b>None</b>
<b>D1</b>	<b>90</b>	<b>9</b>
<b>D3</b>	<b>72</b>	<b>8</b>
<b>E2</b>	<b>79</b>	<b>7</b>
<b>F1</b>	<b>89</b>	<b>None</b>
<b>F3</b>	<b>113</b>	<b>None</b>
<b>G3</b>	<b>100</b>	<b>5</b>
<b>H1</b>	<b>106</b>	<b>10</b>
<b>H3</b>	<b>110</b>	<b>9</b>
<b>H5</b>	<b>71</b>	<b>10</b>
<b>I2</b>	<b>120</b>	<b>11</b>
<b>shNSUN5#4-luc mice (Thirteen)</b>		
<b>B3</b>	<b>N/A</b>	<b>7</b>
<b>D2</b>	<b>156</b>	<b>None</b>
<b>E1</b>	<b>90</b>	<b>None</b>
<b>E3</b>	<b>114</b>	<b>None</b>
<b>F2</b>	<b>120</b>	<b>None</b>
<b>F4</b>	<b>120</b>	<b>None</b>
<b>G2</b>	<b>141</b>	<b>11</b>
<b>G4</b>	<b>107</b>	<b>None</b>
<b>G5</b>	<b>121</b>	<b>None</b>
<b>H2</b>	<b>106</b>	<b>None</b>
<b>H4</b>	<b>134</b>	<b>None</b>
<b>I1</b>	<b>N/A</b>	<b>None</b>
<b>I3</b>	<b>151</b>	<b>None</b>

The survival times of the eleven shRandom mice and thirteen shNSUN5#4 mice are shown in the table. The average time of the spinal metastases was 8.8 weeks after intracranial tumor cell injection. There was no correlation between the spinal metastasis and survival of mice bearing the tumors.

To conclude, knockdown of NSUN5 in U251 cells inhibited tumor metastasis and prolonged survival of mice bearing U251 tumors in the glioblastoma intracranial mouse models.

**Chapter 5 Regulation of global protein synthesis and proteome by NSUN5 in glioblastoma**

## **5.1 NSUN5 regulates global protein synthesis in glioblastoma cells.**

C3782 is located close to the peptidyl transferase center (PTC) of 28S rRNA [238, 312]. The methylation of nucleotides within the PTC of bacteria 23S rRNA has been shown to regulate translation rate and antibiotic resistance [411-418]. In yeast, deletion of Rcm1 (the yeast homologue of NSUN5) alters the structure of 25S rRNA, favoring the translation of oxidative stress response mRNAs [312]. Therefore, it would be interesting to investigate whether methylation of C3782 by NSUN5 affects global protein synthesis rate.

We used the puromycin labelling assay to examine the effect of NSUN5 depletion on protein synthesis rate. Puromycin is an aminonucleoside antibiotic and a protein synthesis inhibitor. Puromycin mimics the 3' end of the aminoacylated tRNA and is incorporated into the nascent peptide chain, which results in termination of translation and the release of puromycin-containing translating peptides [377, 378]. After puromycin treatment, the newly-synthesized peptide chains containing puromycin can be visualized by Western blotting using an anti-puromycin antibody [377, 378]. A stronger signal intensity on Western blots reflects increased nascent peptide synthesis caused by a faster protein synthesis [377, 378].

### **5.1.1 Knockdown of NSUN5 decreases the global protein synthesis rate in U251 cells.**

U251/shRandom and U251/shNSUN5 #4 cells were treated with 10 µg/ml puromycin for 15 minutes and puromycin-labeled proteins detected by Western blotting. Quantification of bands showed that NSUN5 knockdown decreased the protein synthesis in U251 cells. As shown in **Figure 5.1**, the intensity of the puromycin-labelled proteins in U251/shNSUN5 #4 was 60.5% lower compared to U251/shRandom cells, suggesting a lower protein synthesis rate in U251/shNSUN5 cells. Ponceau S staining of the proteins on the membranes indicated even loading of the protein samples (**Figure 5.1A**).

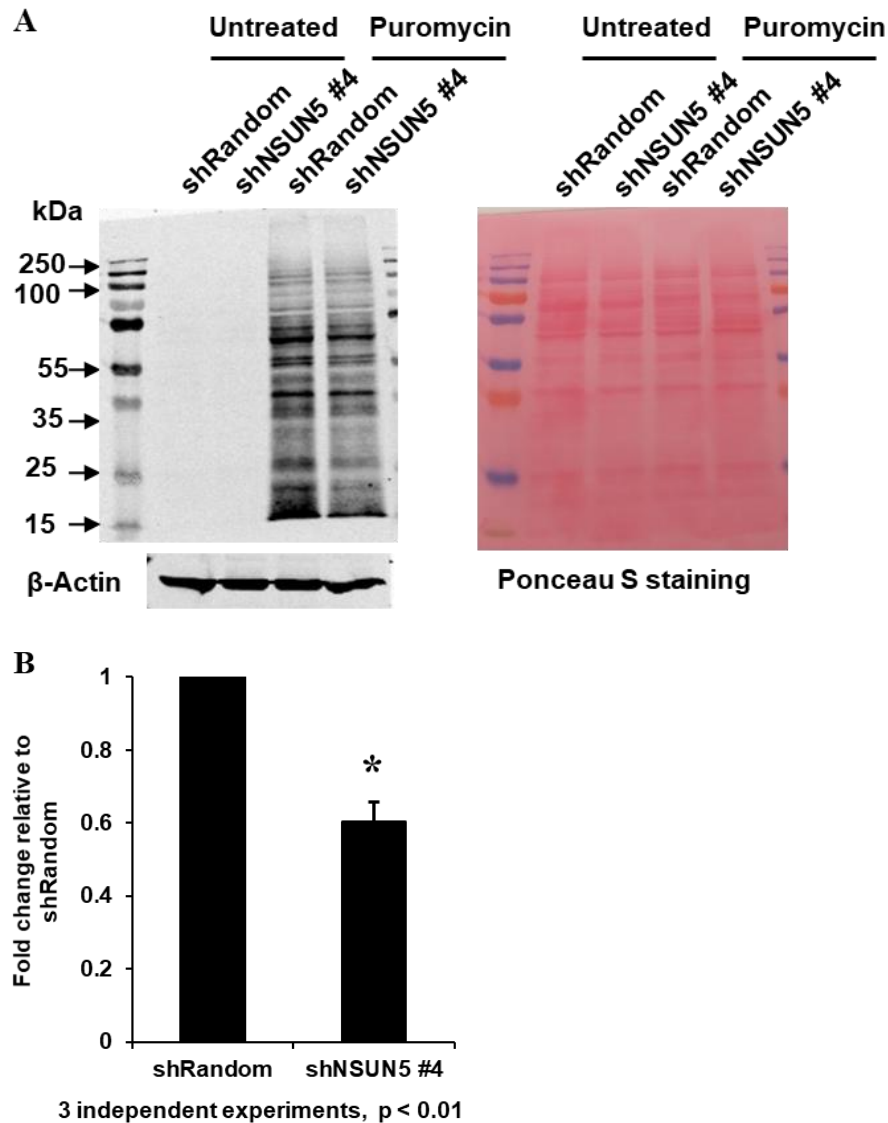


**Figure 5.1 NSUN5 knockdown decreases protein synthesis rate in U251 cells.**

U251/shRandom and U251/shNSUN5 #4 cells were treated with 10  $\mu\text{g/ml}$  puromycin for 15 minutes. **(A)** Western blotting using an anti-puromycin antibody showed that U251/shNSUN5 #4 had fewer and weaker puromycin-labelled protein bands than U251/shRandom cells.  $\beta$ -Actin was the loading control. Ponceau S staining of the proteins on the membranes indicated an even loading of the protein samples. **(B)** Quantification of the Western blotting results showed that U251/shNSUN5 #4 has a lower protein synthesis rate than U251/shRandom cells. Densitometry

analyses were performed using Li-Cor Odyssey imager software.  $\beta$ -Actin was used as a control for quantification experiments. Data are mean  $\pm$  SE of three experiments,  $P = 0.003193$ .

### **5.1.2 Overexpression of NSUN5 increases the global protein synthesis rate of glioblastoma cells.**

U87/pLenti-vector versus U87/pLenti-NSUN5 cells, and 50M/pLenti-vector versus 50M/pLenti-NSUN5 cells were treated with 10  $\mu\text{g/ml}$  puromycin for 15 minutes and puromycin-labeled proteins quantitated. As shown in **Figure 5.2**, the intensity of the puromycin-labelled proteins in U87/pLenti-NSUN5 was 1.7-fold higher compared to U87/pLenti-Vector cells, suggesting that U87/pLenti-NSUN5 had a higher protein synthesis rate than U87/pLenti-Vector. Ponceau S staining of the proteins on the membranes indicated an even loading of the protein samples (**Figure 5.2A**). Moreover, using the puromycin labelling assay we also found that 50M/pLenti-NSUN5 cells had a 2.5-fold higher protein synthesis rate than 50M/pLenti-Vector cells (**Figure 5.3 A, B**), which is consistent with the results obtained in U87 cells.

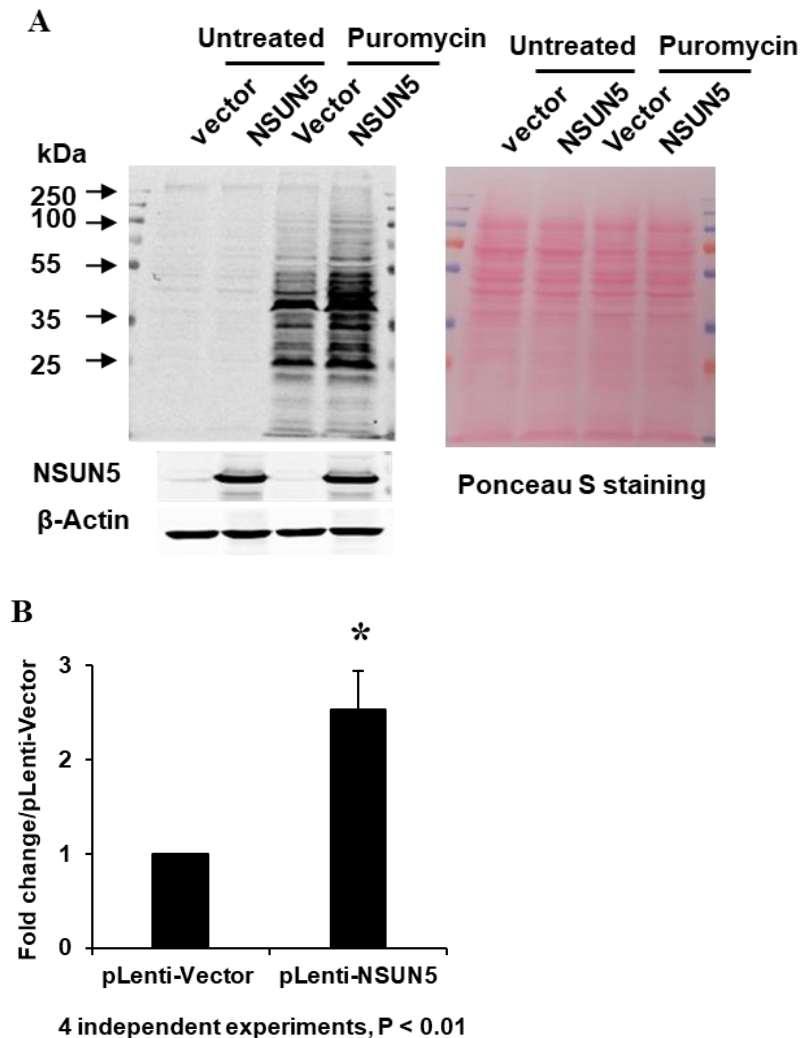


**Figure 5.2 NSUN5 overexpression increases protein synthesis in U87 cells.**

U87/pLenti-NSUN5 and U87/pLenti-vector cells were treated with 10 µg/ml puromycin for 15 minutes. **(A)** Western blotting using an anti-puromycin antibody showed that U87/pLenti-NSUN5 cells had more and stronger puromycin-labelled protein bands than U87/pLenti-Vector cells. NSUN5 expression in the U87/pLenti-NSUN5 was confirmed by Western blotting using an anti-NSUN5 antibody. β-Actin was the loading control. Ponceau S staining of the proteins on the membranes indicated an even loading of the protein samples. **(B)** Quantification of the Western blotting results showed a higher protein synthesis rate in U87/pLenti-NSUN5 cells compared to U87/pLenti-Vector cells. Densitometry analyses were performed using Li-Cor Odyssey imager

software, and quantitation is the ratio of puromycin-labelled proteins/ $\beta$ -Actin between the Vector and NSUN5 cells. Data are mean  $\pm$  SE of four independent experiments,  $P=0.000503$ .

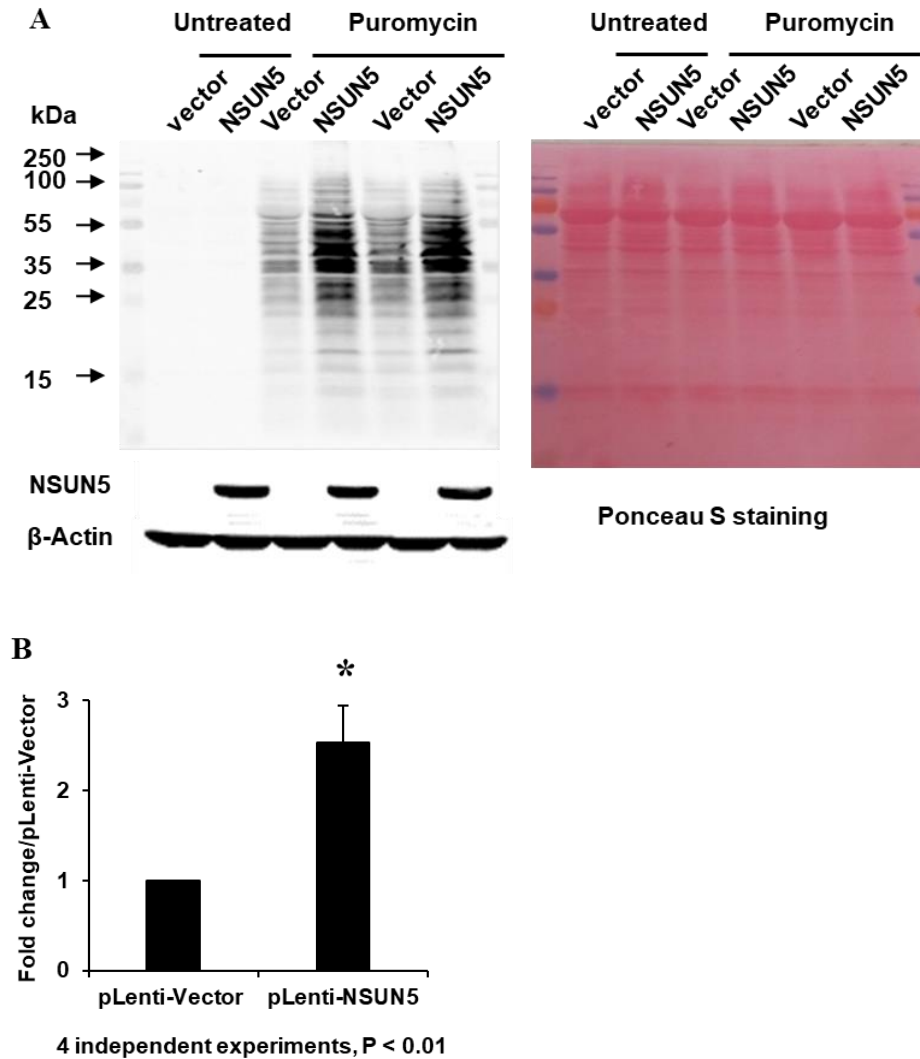


**Figure 5.3 NSUN5 overexpression increases protein synthesis in 50M cells.**

50M/pLenti-NSUN5 and 50M/pLenti-vector cells were treated with 10  $\mu$ g/ml puromycin for 15 minutes. **(A)** Western blotting using an anti-puromycin antibody showed that 50M/pLenti-NSUN5 cells had more and stronger puromycin-labelled protein bands than 50M/pLenti-Vector cells. NSUN5 expression in 50M/pLenti-NSUN5 cells was confirmed by Western blotting using an anti-NSUN5 antibody.  $\beta$ -Actin was the loading control. Ponceau S staining of the proteins on the membranes indicated an even loading of the protein samples. **(B)** Quantification of the Western

blotting results showed a higher protein synthesis rate in 50M/pLenti-NSUN5 cells compared to 50M/pLenti-Vector cells. Densitometry analyses were performed using Li-Cor Odyssey imager software, and quantitation is the ratio of puromycin-labelled proteins/ $\beta$ -Actin between the Vector and NSUN5 cells. Data are mean  $\pm$  SE of four independent experiments, P = 0.00990.

In summary, NSUN5 knockdown decreased protein synthesis rate in U251 cells, whereas NSUN5 overexpression increased protein synthesis in U87 and 50M cells.

## 5.2 NSUN5 regulates the proteome of glioblastoma cells.

In the functional studies described in Chapter 4, we found that overexpression of NSUN5 increased the sphere forming ability of U87 and 50M cells, whereas knockdown of NSUN5 decreased cell proliferation and sphere forming ability in U251 and A4-012 cells and prolonged the survival of mice bearing U251 tumors. In this Chapter, using the puromycin-labelling assay, we demonstrated that NSUN5 regulates global protein synthesis rate in glioblastoma cells. Since deletion of Rcm1 (the yeast homologue of NSUN5) has been shown to alter rRNA structure, which favors the translation of oxidative stress response mRNAs [312], it is important to investigate whether NSUN5 can also selectively regulate the expression of certain groups of proteins that are associated with cell proliferation, stem cell phenotype, treatment resistance, and/or tumor progression.

To determine whether NSUN5 regulates the proteome, we performed liquid chromatography and tandem mass spectrometry (LC-MS/MS) [419]. Three cell lysate replicates (R1, R2, R3) prepared from U251/shRandom and U251/shNSUN5 #4 cells, as well as from 50M/pLenti-Vector and 50M/pLenti-NSUN5 cells, were analysed by LC-MS/MS (performed by Dr. Dylan Dieters in the Postovit lab). A heat map was used to provide an overview of the trend of all the clusters identified in U251/shRandom vs. U251/shNSUN5 #4 cells [420]. Clustering of the three U251/shRandom replicates was observed, although clustering with shRandom R3 was not as tight as with the other two replicates (**Figure 5.4**). The clustering of U251/shNSUN5 #4 cells was similar among the three replicates (**Figure 5.4**) and the clustering of U251/shRandom was different from that of U251/shNSUN5 #4 (**Figure 5.4**). Statistical analysis of shRandom R1, R2, and R3 vs. shNSUN5 #4 R1, R2, and R3 using Student's t-test showed that 1203 out of 6526 proteins were significantly different between shRandom and shNSUN5 #4 cells ( $P < 0.05$ ). Among these

differentially expressed proteins, 60 proteins were downregulated, and 40 proteins were upregulated by  $\geq 2$ -fold in U251/shNSUN5 #4 cells (**Tables 5.1 and 5.2**). In addition, a volcano plot was used to illustrate the difference in protein levels between U251/shRandom and U251/shNSUN5 #4 and to highlight the proteins that were different by  $>2$ -fold (Student's t-test,  $P < 0.05$ ;  $\log_2(\text{difference}) > 1$ ) (**Figure 5.5**).

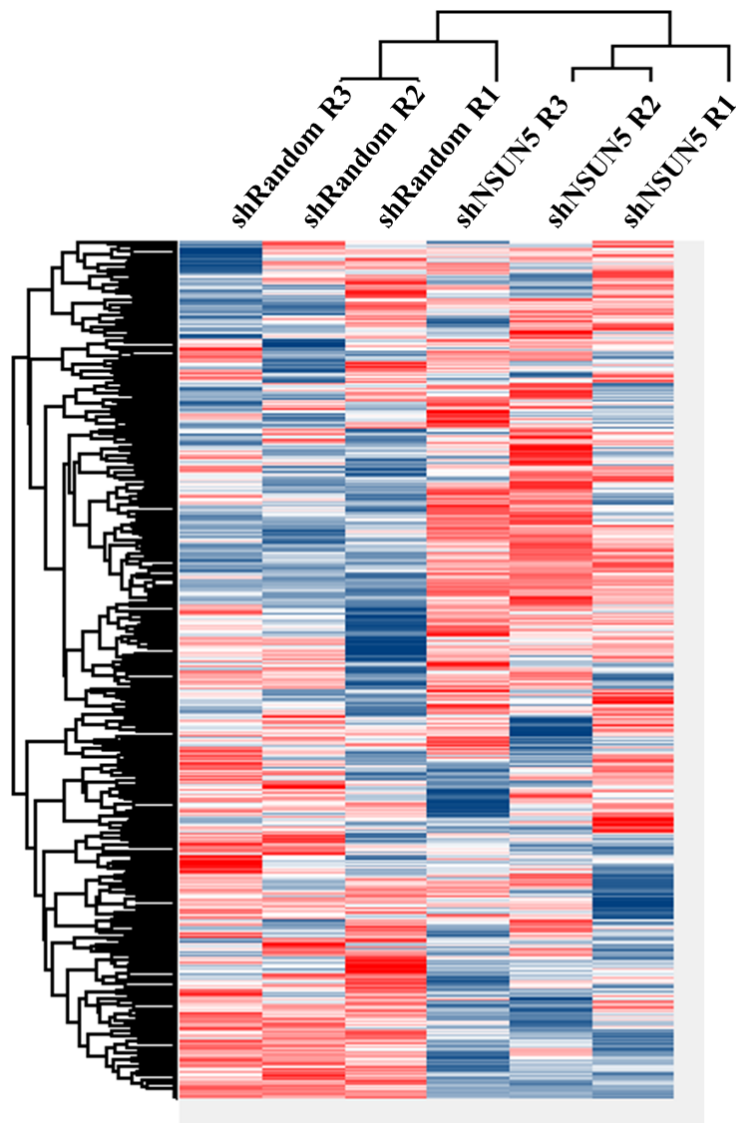


**Figure 5.4 Heat map showing differences in global protein expression patterns in U251/shRandom vs. U251/shNSUN5 #4.**

Heat map of LC-MS/MS results obtained from cell lysates prepared from U251/shRandom (R1, R2, and R3) and U251/shNSUN5 #4 (R1, R2, and R3) cells. The heat map shows the trend for all the identified clusters. The clustering of the three U251/shRandom replicates R1, R2 and R3 was reasonably close, even though shRandom R3 did not cluster tightly with the other two replicates. The clustering of U251/shNSUN5 #4 replicates R1, R2 and R3 was also reasonably close. The clustering of U251/shRandom replicates was different from that of U251/shNSUN5#4 replicates.

**Table 5.1 Proteins that are downregulated in U251/shNSUN5 cells.**

	Gene names	Protein names	-Log Student's T-test p-value	P-value	Fold change
1	STAT3	Signal transducer and activator of transcription 3	5.38223	0.000004	2.4
2	NSUN2	tRNA cytosine methyltransferase	5.16468	0.000007	2.0
3	FAF2	FAS-associated factor 2	5.13964	0.000007	3.3
4	NES	Nestin	4.47511	0.000033	2.3
5	VSNL1	Visinin-like protein 1	4.25795	0.000055	3.1
6	FABP7	Fatty acid-binding protein, brain	3.68596	0.000206	2.0
7	EEF1A2	Elongation factor 1-alpha 2	3.37094	0.000426	2.4
8	OAS3	2-5-oligoadenylate synthase 3	3.33688	0.000460	6.1
9	PLEKHG1	Pleckstrin homology domain-containing family G member 1	3.22637	0.000594	2.3
10	CRYAB	Alpha-crystallin B chain	3.20967	0.000617	3.1
11	AKR1C3	Aldo-keto reductase family 1 member C3	3.16222	0.000688	2.0
12	UNC5C	Netrin receptor UNC5C	3.03357	0.000926	3.6
14	FAM65B	Protein FAM65B	2.84661	0.001424	20.6
15	PDGFRA	Platelet-derived growth factor receptor alpha	2.73423	0.001844	8.4

16	NUDT4	Diphosphoinositol polyphosphate phosphohydrolase 2	2.63764	0.002303	2.2
17	AK4	Adenylate kinase 4, mitochondrial	2.55266	0.002801	3.5
18	SESN3	Sestrin-3	2.4589	0.003476	2.4
19	NEDD9	Enhancer of filamentation 1; Enhancer of filamentation 1 p55	2.44906	0.003556	2.7
20	ARMCX1	Armadillo repeat-containing X-linked protein 1	2.37647	0.004203	4.0
21	MAP2K4	Dual specificity mitogen-activated protein kinase kinase 4	2.35618	0.004404	2.3
22	FNBP1L	Formin-binding protein 1-like	2.33932	0.004578	2.1
23	TMEM2	Transmembrane protein 2	2.32849	0.004694	2.2
24	SGCE	Epsilon-sarcoglycan	2.31792	0.004809	2.0
25	COL14A1	Collagen alpha 1(XIV) chain	2.08988	0.008131	4.1
26	ELMOD2	ELMO domain-containing protein 2	2.06993	0.008513	2.0
27	PEMT	Phosphatidylethanolamine N-methyltransferase	1.96143	0.010929	2.4
28	MPP2	MAGUK p55 subfamily member 2	1.95683	0.011045	2.3
29	CNTNAP1	Contactin-associated protein 1	1.94323	0.011396	3.6
30	RHBDD2	Rhomboid domain-containing protein 2	1.93391	0.011644	2.3
31	VAT1L	Synaptic vesicle membrane protein VAT-1 homolog-like	1.89539	0.012724	2.0
32	RABEPK	Rab9 effector protein with kelch motifs	1.85256	0.014042	4.6
33	NUDT14	Uridine diphosphate glucose pyrophosphatase	1.80574	0.015641	2.3
34	SEPW1	Selenoprotein W	1.75769	0.017471	2.1
35	PTPRG	Receptor-type tyrosine-protein phosphatase gamma	1.70611	0.019674	2.1
36	SYNGR2	Synaptogyrin-2	1.69321	0.020267	2.1
37	NEFL	Neurofilament light polypeptide	1.6771	0.021033	4.4

38	SLC7A11	Cystine/glutamate transporter	1.67507	0.021131	2.6
39	YAF2	YY1-associated factor 2	1.62697	0.023606	2.8
40	SPIN2B; SPIN2A	Spindlin-2B; Spindlin-2A	1.62405	0.023766	4.9
41	PCYT1B	Choline-phosphate cytidyltransferase B	1.61673	0.024170	2.3
42	RILPL1	RILP-like protein 1	1.54888	0.028257	2.4
43	S100A9	Protein S100-A9	1.54738	0.028354	4.2
44	SBF1	Myotubularin-related protein 5	1.528	0.029648	2.4
45	PKN1	Serine/threonine-protein kinase N1	1.49235	0.032185	3.2
46	GPRIN1	G protein-regulated inducer of neurite outgrowth 1	1.44385	0.035987	3.5
47	RAB9A	Ras-related protein Rab-9A	1.42787	0.037336	5.7
48	BCR	Breakpoint cluster region protein	1.42013	0.038008	2.7
49	CBS	Cystathionine beta-synthase	1.41951	0.038062	6.2
50	FAM20B	Glycosaminoglycan xylosylkinase	1.40334	0.039506	2.6
51	FRMD4A	FERM domain-containing protein 4A	1.39811	0.039984	2.0
52	SFN	14-3-3 protein sigma	1.36856	0.042800	15.7
53	ZEB1	Zinc finger E-box-binding homeobox 1	1.36652	0.043001	1.9
54	RAB3D	Ras-related protein Rab-3D	1.3624	0.043411	4.3
55	GGT7	Gamma-glutamyltransferase 7; Gamma-glutamyltransferase 7 heavy chain; Gamma- glutamyltransferase 7 light chain	1.3506	0.044607	3.7
56	DSCC1	Sister chromatid cohesion protein DCC1	1.33215	0.046543	3.7
57	TXLNB	Beta-taxilin	1.32241	0.047598	3.3
58	ZCCHC3	Zinc finger CCHC domain- containing protein 3	1.31813	0.048070	2.4
59	S100B	Protein S100-B	1.31661	0.048238	3.8

60	TUBAL3	Tubulin alpha chain-like 3	1.30781	0.049225	2.0
----	--------	----------------------------	---------	----------	-----

Table 5.1: Differences in the LC-MS/MS results obtained for U251/shNSUN5 #4 and U251/shRandom cells were analyzed using the Student's T-test. 60 proteins were downregulated by  $\geq 2$ -fold when NSUN5 was knocked down in U251 cells. “-log Student's T-test p-value” for all these proteins was greater than 1.30103, which is equal to  $P < 0.05$ .

**Table 5.2 Proteins that are upregulated in U251/shNSUN5#4 cells.**

	Gene names	Protein names	-Log Student's T-test p-value	P-value	Fold change
1	ZNF318	Zinc finger protein 318	5.14211	0.000007	3.6
2	HLA-B	HLA class I histocompatibility antigen, B-14 alpha chain;HLA class I histocompatibility antigen, B-37 alpha chain;HLA class I histocompatibility antigen, B-82 alpha chain	4.9714	0.000011	2.8
3	ALDH1A3	Aldehyde dehydrogenase family 1 member A3	4.86236	0.000014	2.2
4	HLA-B	HLA class I histocompatibility antigen, B-18 alpha chain	4.50092	0.000032	2.6
5	TGM2	Protein-glutamine gamma-glutamyltransferase 2	4.17749	0.000066	2.7
6	UCHL3	Ubiquitin carboxyl-terminal hydrolase isozyme L3	4.0876	0.000082	2.4
7	HLA-A	HLA class I histocompatibility antigen, A-69 alpha chain;HLA class I histocompatibility antigen, A-68 alpha chain	3.86043	0.000138	2.8
8	HLA-A	HLA class I histocompatibility antigen, A-34 alpha chain;HLA	3.39568	0.000402	3.2

		class I histocompatibility antigen, A-66 alpha chain;HLA class I histocompatibility antigen, A-26 alpha chain;HLA class I histocompatibility antigen, A-25 alpha chain;HLA class I histocompatibility antigen, A-43 alpha chain			
9	HDHD1	Pseudouridine-5-phosphatase	3.31822	0.000481	2.4
10	KCT2	Keratinocyte-associated transmembrane protein 2	3.0102	0.000977	7.3
11	ARHGDI1	Rho GDP-dissociation inhibitor 2	2.81424	0.001534	2.1
12	MSI1	RNA-binding protein Musashi homolog 1	2.7234	0.001891	3.5
13	IL6ST	Interleukin-6 receptor subunit beta	2.54241	0.002868	4.2
14	PNPLA2	Patatin-like phospholipase domain-containing protein 2	2.50958	0.003093	2.4
15	PSMB9	Proteasome subunit beta type 9	2.48664	0.003261	2.5
16	HLA-C	HLA class I histocompatibility antigen, Cw-8 alpha chain	2.42499	0.003758	1.9
17	AXL	Tyrosine-protein kinase receptor UFO	2.2988	0.005026	2.9
18	HMGCR	3-hydroxy-3-methylglutaryl-coenzyme A reductase	2.10474	0.007857	4.1
19	NFIA	Nuclear factor 1 A-type	2.09188	0.008093	4.2
20	SLC25A16	Graves' disease carrier protein	2.00252	0.009942	2.0
21	FBXO4	F-box only protein 4	1.94282	0.011407	3.5
22	DICER1	Endoribonuclease Dicer	1.94158	0.011440	2.9
23	CCDC91	Coiled-coil domain-containing protein 91	1.94129	0.011447	2.7

24	CKMT1A	Creatine kinase U-type, mitochondrial	1.92098	0.011996	6.3
25	DAB2	Disabled homolog 2	1.85227	0.014052	2.1
26	IFT27	Intraflagellar transport protein 27 homolog	1.82889	0.014829	2.4
27	ACTN2	Alpha-actinin-2	1.81492	0.015314	2.4
28	CPA4	Carboxypeptidase A4	1.69029	0.020404	2.0
29	PINX1	PIN2/TERF1-interacting telomerase inhibitor 1	1.67766	0.021006	4.2
30	CCDC86	Coiled-coil domain-containing protein 86	1.64626	0.022581	3.5
31	QPCTL	Glutaminy-peptide cyclotransferase-like protein	1.54787	0.028322	2.0
32	PRKD3	Serine/threonine-protein kinase D3	1.53197	0.029379	8.4
33	LPL	Lipoprotein lipase	1.46561	0.034229	4.3
34	REXO2	Oligoribonuclease, mitochondrial	1.45729	0.034891	2.0
35	SIL1	Nucleotide exchange factor SIL1	1.4521	0.035310	2.0
36	APOBEC3G	DNA dC->dU-editing enzyme APOBEC-3G	1.43953	0.036347	3.2
37	C2CD2L	C2 domain-containing protein 2-like	1.41529	0.038434	2.0
38	ACAP3	Arf-GAP with coiled-coil, ANK repeat and PH domain- containing protein 3	1.4146	0.038495	2.1
39	SUCO	SUN domain-containing ossification factor	1.34148	0.045553	3.0
40	CHD6	Chromodomain-helicase-DNA- binding protein 6	1.3099	0.048989	7.5

Table 5.2: The LC-MS/MS results for U251/shNSUN5#4 versus U251/shRandom were analyzed using the Student's T-test. 40 proteins were upregulated by  $\geq 2$ -fold when NSUN5 was knocked down in U251 cells. “-log Student's T-test p-value” for all these proteins more than was greater than 1.30103, which is equal to  $P < 0.05$ .

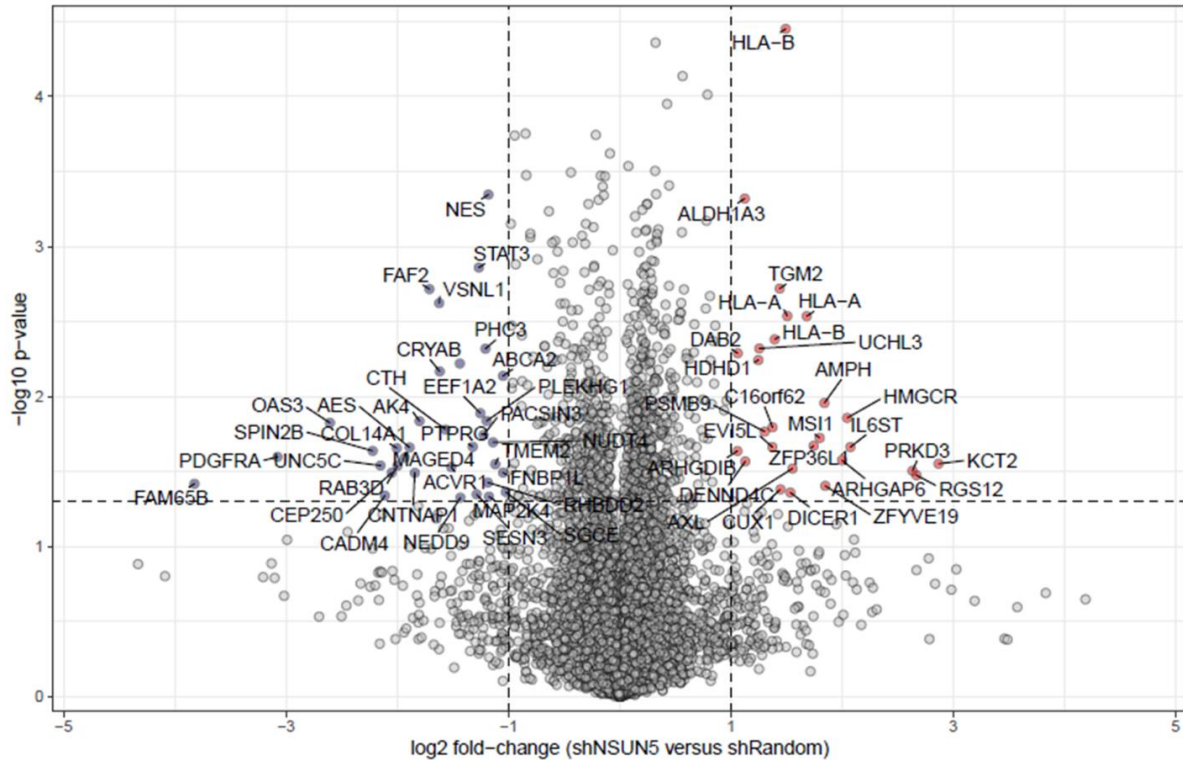


**Figure 5.5** Volcano plot highlighting proteins whose levels are increased or decreased as the result of NSUN5 knockdown in U251 cells.

LC-MS/MS results for U251/shNSUN5 #4 versus U251/shRandom were analyzed using the Student's T-test. A volcano plot is used to illustrate the differences in protein expression between U251/shRandom and U251/shNSUN5 #4 and to highlight the proteins that are more than 2-fold different ( $-\log_{10} p\text{-value} > 1.30103 = P < 0.05$ );  $\log_2$  fold change  $> 1$  or  $< -1$  is equal to  $> 2$ -fold change). Red dots at the top right corner represent proteins that are upregulated by NSUN5 knockdown. Grey dots at the top left corner represent proteins that are downregulated by NSUN5 knockdown.

For the LC-MS/MS results of 50M cells, the heat map showed that the clustering of the R3 replicate of 50M/pLenti-Vector was quite different from the clustering of the R1 and R2 replicates. And the R1, R2, and R3 replicates of 50M/pLenti-NSUN5 did not cluster very tightly with each other (**Figure 5.6**). There were still several hundred proteins that were differentially expressed between 50M/pLenti-Vector and 50M/pLenti-NSUN5 replicates. Student's t-test analysis of 50M/pLenti-Vector R1, R2, and R3 vs. 50M/pLenti-NSUN5 R1, R2, and R3 showed that 450 out of 6800 proteins were significantly different ( $P < 0.05$ ). NSUN5 expression in the 50M/pLenti-NSUN5 replicates was about 250-fold higher compared to the 50M/pLenti-Vector replicates. However, there were only 87 proteins that were different (higher or lower) by  $\geq 1.5$ -fold and 37 proteins that were different by  $\geq 2$ -fold. Among these differentially expressed proteins, 21 proteins were upregulated, and 16 proteins were downregulated by  $\geq 2$ -fold in 50M/pLenti-NSUN5 cells (**Tables 5.3 and 5.4**). A volcano plot was used to illustrate the difference between 50M/pLenti-Vector and 50M/pLenti-NSUN5 and highlight the proteins that are differentially expressed (higher or lower) by more than 2-fold ( $P > 1.30103 = -\log_{10}(0.05)$ , difference  $> 1 = \log_2(2)$ ) (**Figure 5.7**).

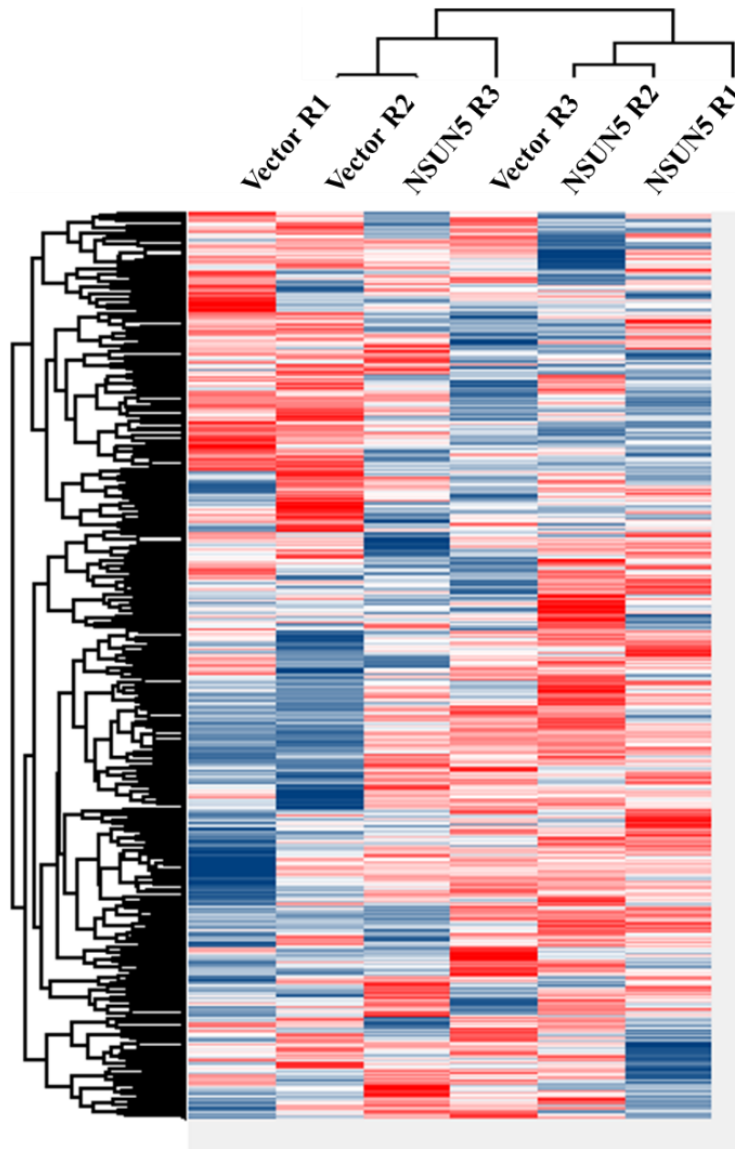


**Figure 5.6 Global protein expression in 50M/pLenti-Vector is different from that of 50M/pLenti-NSUN5 cells.**

Heat map of the LC-MS/MS results for 50M cells showed that the clustering of R3 of 50M/pLenti-Vector was quite different from the clustering of R1 and R2. Furthermore, R1, R2, and R3 of 50M/pLenti-NSUN5 did not cluster very tightly with each other. Several proteins were differentially expressed between 50M/pLenti-Vector replicates and 50M/pLenti-NSUN5 replicates.

**Table 5.3 Proteins that are upregulated in 50M/pLenti-NSUN5 cells.**

	Gene names	Protein names	-Log Student's T- test p-value	P- value	Fold change
1	NSUN5	Probable 28S rRNA (cytosine-C (5))- methyltransferase	3.560	0.0003	251.9
2	ABAT	4-aminobutyrate aminotransferase, mitochondrial	2.596	0.0025	2.1
3	CHCHD4	Mitochondrial intermembrane space import and assembly protein 40	2.473	0.0034	5.1
4	WIPF2	WAS/WASL-interacting protein family member 2	2.322	0.0048	2.7
5	FBXO3	F-box only protein 3	2.135	0.0073	3.1
6	TDRD3	Tudor domain-containing protein 3	2.126	0.0075	2.1
7	SALL3	Sal-like protein 3	2.028	0.0094	3.5
8	SLC11A2	Natural resistance-associated macrophage protein 2	1.840	0.0144	2.5
9	BUB1	Mitotic checkpoint serine/threonine- protein kinase BUB1	1.800	0.0158	6.0
10	PCDHGB2; PCDHGB1	Protocadherin gamma-B2; Protocadherin gamma-B1	1.743	0.0181	2.1
11	P4HA2	Prolyl 4-hydroxylase subunit alpha-2	1.738	0.0183	5.0
12	MATN2	Matrilin-2	1.711	0.0194	2.3
13	RANBP10	Ran-binding protein 10	1.593	0.0255	2.1

14	DUS3L	tRNA-dihydrouridine (47) synthase [NAD(P)(+)]-like	1.463	0.0344	2.3
15	RDH14	Retinol dehydrogenase 14	1.434	0.0368	2.0
16	KANK2	KN motif and ankyrin repeat domain- containing protein 2	1.425	0.0375	3.1
17	HLTF	Helicase-like transcription factor	1.398	0.0400	2.6
18	PEX6	Peroxisome assembly factor 2	1.390	0.0407	2.3
19	TTC3	E3 ubiquitin-protein ligase TTC3	1.380	0.0417	2.6
20	AGGF1	Angiogenic factor with G patch and FHA domains 1	1.343	0.0454	3.4
21	PDCD2L	Programmed cell death protein 2-like	1.327	0.0471	2.3

Table 5.3: The LC-MS/MS results for 50M/pLenti-NSUN5 versus 50M/pLenti-Vector replicates were analyzed using the Student's T-test. 21 proteins were upregulated by  $\geq 2$ -fold when NSUN5 was overexpressed in 50M cells. “-log Student's T-test p-value” for all these proteins more than was greater than 1.30103, which is equal to  $P < 0.05$ .

**Table 5.4 Proteins that are downregulated in 50M/pLenti-NSUN5 cells.**

	Gene names	Protein names	-Log Student's T- test p-value	P- value	Fold change
1	PRKCD	Protein kinase C delta type;Protein kinase C delta type regulatory subunit;Protein kinase C delta type catalytic subunit	3.412	0.0004	17.8

2	VPS54	Vacuolar protein sorting-associated protein 54	3.169	0.0007	3.2
3	B2M	Beta-2-microglobulin; Beta-2-microglobulin form pI 5.3	2.653	0.0022	8.9
4	MAGEC1	Melanoma-associated antigen C1	2.325	0.0047	2.3
5	AP4B1	AP-4 complex subunit beta-1	1.709	0.0196	5.5
6	SFN	14-3-3 protein sigma	1.659	0.0219	55.6
7	SUMO4	Small ubiquitin-related modifier 4	1.639	0.0229	20.1
8	TRIP6	Thyroid receptor-interacting protein 6	1.503	0.0314	4.2
9	DPP7	Dipeptidyl peptidase 2	1.502	0.0315	2.1
10	IL13RA2	Interleukin-13 receptor subunit alpha-2	1.500	0.0317	2.3
11	MON1B	Vacuolar fusion protein MON1 homolog B	1.443	0.0361	3.4
12	SERF2	Small EDRK-rich factor 2	1.427	0.0374	18.9
13	FILIP1L	Filamin A-interacting protein 1-like	1.412	0.0388	2.7
14	LAMTOR4	Regulator complex protein LAMTOR4; Regulator complex protein LAMTOR4, N-terminally processed	1.343	0.0454	4.5
15	ANKRD40	Ankyrin repeat domain-containing protein 40	1.311	0.0488	4.5
16	EMILIN1	EMILIN-1	1.306	0.0494	2.3

Table 5.4: The LC-MS/MS results for 50M/pLenti-NSUN5 versus 50M/pLenti-Vector replicates were analyzed using the Student's T-test. 16 proteins were downregulated by  $\geq 2$ -fold when NSUN5 was overexpressed in 50M cells. “-log Student's T-test p-value” for all these proteins more than was greater than 1.30103, which is equal to  $P < 0.05$ .

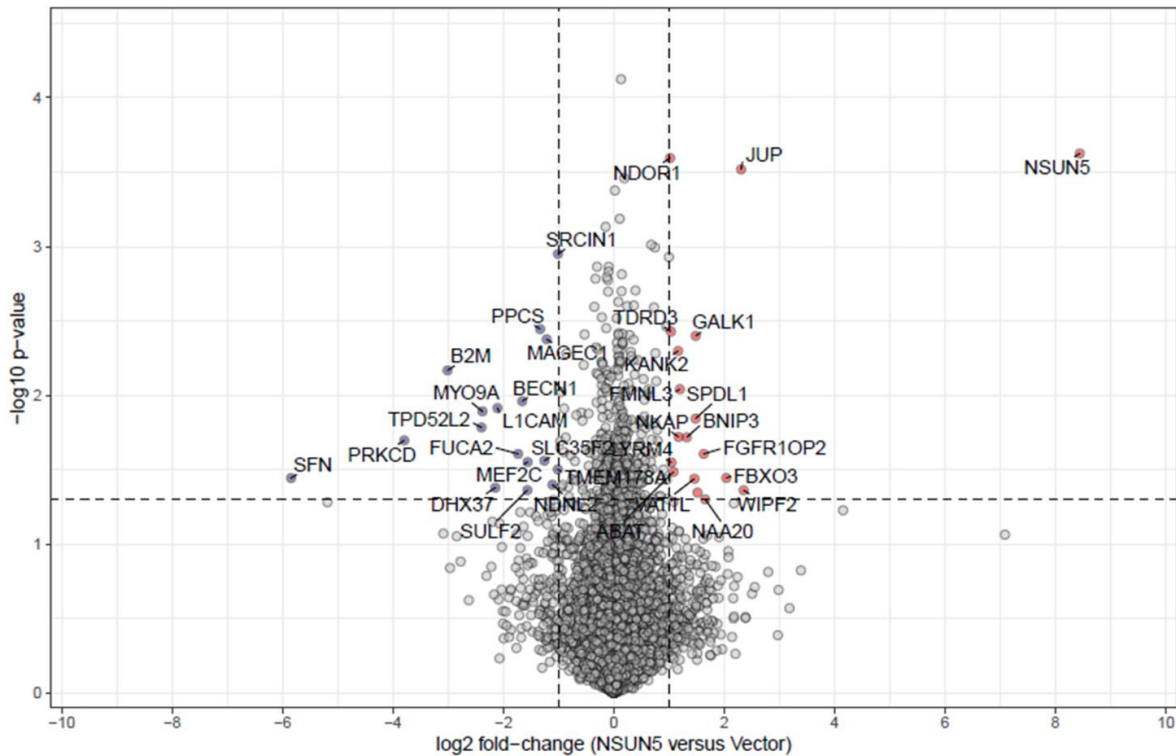


**Figure 5.7 Volcano plot highlighting proteins whose levels are either increased or decreased by more than 2-fold when NSUN5 is overexpressed in 50M cells.**

The LC-MS/MS results of 50M/pLenti-NSUN5 versus 50M/pLenti-Vector were analyzed using the Student's T-test. A volcano plot is used to illustrate the differences in protein expression between 50M/pLenti-NSUN5 and 50M/pLenti-Vector and to highlight the proteins that were different by more than 2-fold ( $-\log_{10} p\text{-value} > 1.30103 = P < 0.05$ ),  $\log_2$  fold change  $> 1$  or  $< -1$  is equal to  $> 2$ -fold change). Red dots in the top right corner indicate proteins upregulated by NSUN5 overexpression. Grey dots in the top left corner indicate proteins downregulated by NSUN5 overexpression.

From the list of differentially expressed proteins between U251/shRandom and U251/shNSUN5 #4, we selected STAT3 and NSUN2 for validation by Western blotting. We found that STAT3 protein levels were decreased by 31.0% and 58.8% and NSUN2 protein levels were decreased by 25.0% and 34.0% in U251/shNSUN5 #3 and U251/shNSUN5 #4 cells respectively, compared to U251/shRandom cells (**Figure 5.8**). These results are consistent with the LC-MS/MS results. Additional proteins (e.g., FABP7, ZEB1, HLA-A, HLA-B, HLA-C, ALDH1A3, and NFIA) still need to be validated in order to reach conclusions about our data. Moreover, to address how STAT3 and NSUN2 protein levels are regulated, we examined the mRNA levels of *STAT3* and *NSUN2* in U251/shRandom and U251/shNSUN5 #4 cells. We found that the mRNA levels of *STAT3* were decreased by 25.2% and 53.6% and the mRNA levels of *NSUN2* were decreased by 28.0% and 58.2% in U251/shNSUN5 #3 and U251/shNSUN5 #4 cells, respectively, compared to U251/shRandom cells (**Figure 5.9**). These results suggest that the decrease in STAT3 and NSUN2 observed upon NSUN5 knockdown occurs at the mRNA level (e.g., transcriptional, or post-transcriptional mechanisms), but not at the translational level. The levels of STAT3 and NSUN2 protein and mRNA levels were also examined in T98/shRandom, T98/shNSUN5 #3, and T98/shNSUN5 #4 cells. We found that STAT3 protein levels were decreased by 11.1% and 33.1% and NSUN2 protein levels were decreased by 29.9% and 51.8% in T98/shNSUN5 #3 and T98/shNSUN5 #4 cells, respectively, compared to T98/shRandom cells (**Figure 5.10**). Consistent with U251 cells, the mRNA levels of *STAT3* were decreased by 8.1% and 36.0% and the mRNA levels of *NSUN2* were decreased by 30.3% and 57.2% in the T98/shNSUN5 #3 and T98/shNSUN5 #4 cells, respectively (**Figure 5.11**). These results suggest that the decrease in STAT3 and NSUN2 observed upon NSUN5 knockdown could be a secondary effect of NSUN5 knockdown or could

be due to direct post transcriptional regulation of their mRNAs (e.g., with loss of their mRNA methylation leading to instability). Potential mechanisms will be discussed in the last chapter.

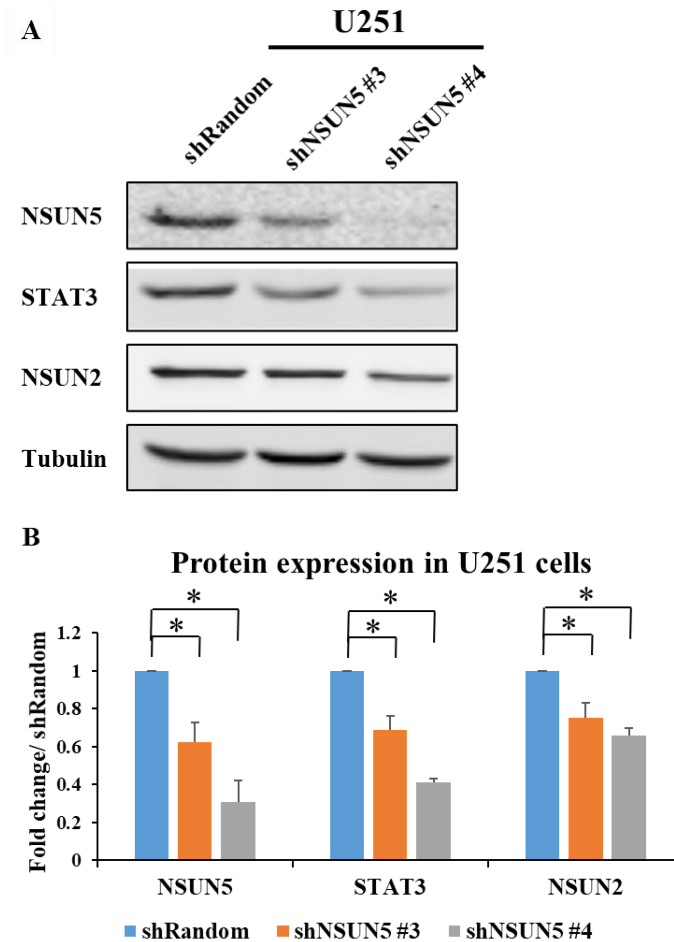


**Figure 5.8 Knockdown of NSUN5 decreases STAT3 and NSUN2 protein levels in U251 cells.** (A) Western blotting showed a decrease in STAT3 and NSUN2 protein levels upon knockdown of NSUN5 in U251/shNSUN5 #3 and U251/shNSUN5 #4 cells. Tubulin was the loading control. (B) Quantification of Western blotting results. \*  $P < 0.05$ . Data are shown as mean  $\pm$  SE of three independent experiments.

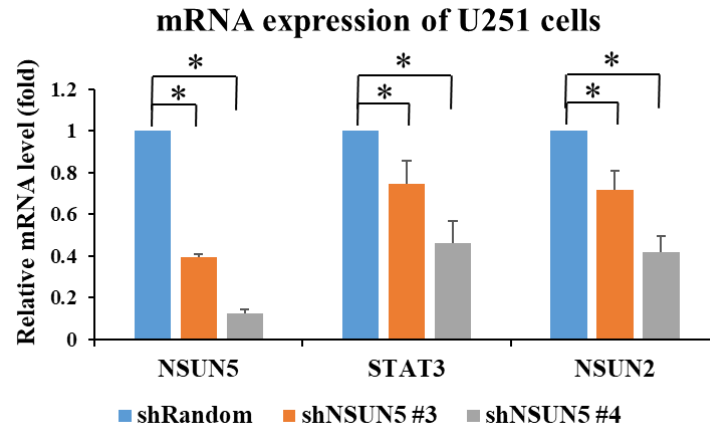


**Figure 5.9 Knockdown of NSUN5 decreases *STAT3* and *NSUN2* mRNA levels in U251 cells.** RT-qPCR shows a decrease of *NSUN5*, *STAT3*, and *NSUN2* mRNA levels upon knockdown of NSUN5 in U251/shNSUN5 #3 and U251/shNSUN5 #4 cells. \*  $P < 0.05$ . Data are shown as mean  $\pm$  SE of three independent experiments.

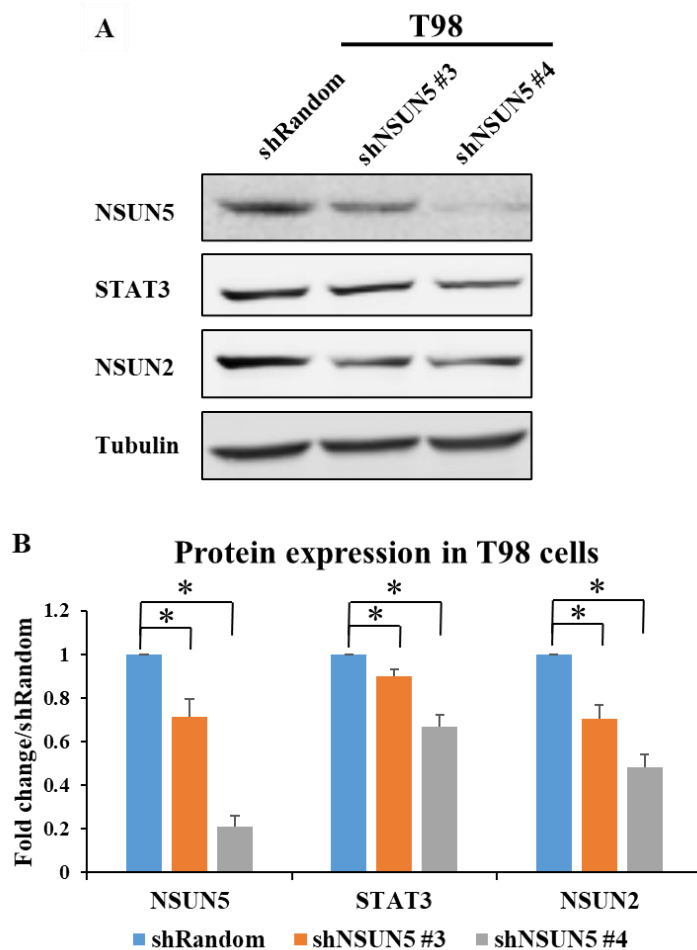


**Figure 5.10 Knockdown of NSUN5 decreases STAT3 and NSUN2 protein levels in T98 cells.**

(A) Western blotting showed a decrease in STAT3 and NSUN2 protein levels upon knockdown of NSUN5 in T98/shNSUN5 #3 and T98/shNSUN5 #4 cells. Tubulin was the loading control. (B) Quantification of Western blotting results. \*  $P < 0.05$ . Data are shown as mean  $\pm$  SE of three independent experiments.

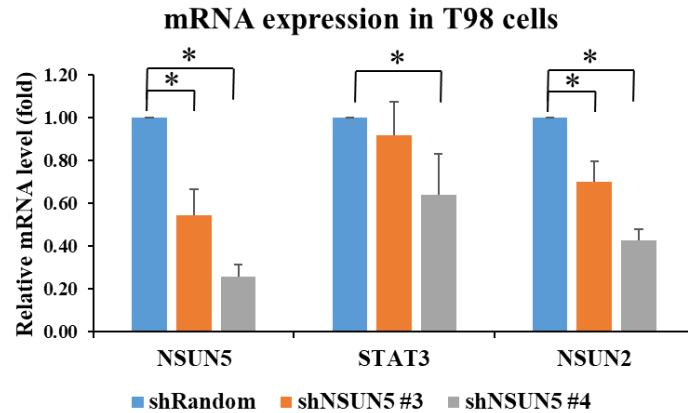


**Figure 5.11 Knockdown of NSUN5 decreases *STAT3* and *NSUN2* mRNA levels in T98 cells.**

RT-qPCR shows a decrease of *NSUN5*, *STAT3*, and *NSUN2* mRNA levels upon knockdown of NSUN5 in T98/shNSUN5 #3 and T98/shNSUN5 #4 cells. \*  $P < 0.05$ . Data are shown as mean  $\pm$  SE of three independent experiments.

In conclusion, the puromycin labelling assay clearly showed that knockdown of NSUN5 decreased protein synthesis in U251 cells and overexpression of NSUN5 increased protein synthesis in 50M cells. LC-MS/MS identified differentially expressed proteins in U251/shRandom vs. U251/shNSUN5 #4 cells. Western blotting validation of STAT3 and NSUN2, the most down-regulated proteins identified by MS, confirmed that they were indeed decreased in NSUN5 knockdown U251 and T98 cells. Because their mRNA levels are also decreased to a similar extent, it is unlikely that the decrease of STAT3 and NSUN2 proteins is due to reduced translation of their mRNAs. We also found that overexpression of NSUN5 in 50M neurosphere cultures increased protein synthesis based on the puromycin labelling assay; however, LC-MS/MS did not identify many proteins altered by NSUN5 overexpression in 50M cells, suggesting that NSUN5 increases protein synthesis through globally increased mRNA translation, as opposed to the translation of

specific mRNAs in 50M cells. Thus, methylation of 28S rRNA by NSUN5 may alter the structure and/or activity of the ribosomes in such a way as to increase the translation of global mRNAs.

## **Chapter 6 Discussion, Future directions, and Conclusions**

## 6.1 Discussion

We and others have confirmed that NSUN5 functions as an RNA cytosine methyltransferase, and NSUN5-mediated RNA methylation is conserved from yeast to humans [387, 421]. Furthermore, we found that high mRNA expression of *NSUN5* is associated with shorter survival of glioblastoma patients through TCGA dataset analysis [346]. However, its biochemical and biological functions in humans, as well as its roles in cancer remains unclear. In this study, we have demonstrated that NSUN5: (1) methylates cytosine 3782 of human 28S rRNA; (2) regulates protein synthesis in glioblastoma cells; and (3) promotes the tumorigenic phenotypes of glioblastoma *in vitro* and *in vivo*. Moreover, we demonstrated that the expression of NSUN5 alters the proteome in glioblastoma cells, modulating the expression of STAT3 and NSUN2. Furthermore, we confirmed that cysteines 308 and 359 are the key catalytic cysteines required for the RNA methyltransferase activity of NSUN5 in humans.

Thus far, only a few laboratories in the world study NSUN5 in cancer. After I started writing my thesis, three studies exploring NSUN5 function in cancer were published by three different groups [387, 421, 422]. In the study by Jiang et al., the authors showed that NSUN5 knockdown decreased the cell proliferation and tumor growth of colorectal cancer [422]. The study conducted by Heissenberger et al. also showed that NSUN5 knockdown decreased the rate of protein synthesis and proliferation of mouse embryonic fibroblasts and HeLa cells [387]. Moreover, they confirmed the cytosine target on ribosome and the catalytic cysteines of NSUN5 in human and mouse [387]. These results are consistent with our findings.

In the study by Janin et al., the authors concluded that loss of NSUN5 depleted overall protein synthesis and was a hallmark of long-term survival for glioblastoma cells [421]. Specifically, they showed that NSUN5 expression increased the rate of protein synthesis under

various stress conditions including oxidative stress via H<sub>2</sub>O<sub>2</sub> treatment and nutrient deprivation in glioblastoma cells [421]. In addition, high NSUN5 promoter methylation (which leads to the silencing of NSUN5 expression) was demonstrated to be associated with better survival of glioma patients [421]. These results are also consistent with our findings. However, in contrast to their glioblastoma patient data analysis showing inverse correlation between NSUN5 expression and patient survival and our *in vivo* results, they showed that NSUN5 overexpression decreased, while knockdown of NSUN5 increased tumor volume and weight *in vivo* [421]. To address the discrepancy in the *in vivo* results, we used IHC to show that control shRandom U251-bearing tumors are more infiltrative than tumors derived from U251 shNSUN5 knockdown cells. Moreover, our *in vivo* work is consistent with our *in vitro* work which included both NSUN5 overexpression and NSUN5 knockdown glioblastoma cell lines using multiple assays including cell viability, sphere forming, migration, and TMZ resistance survival assays.

In the Discussion section of this thesis, I will interpret our results in relation to the results obtained by other investigators working on NSUN5, with a special focus on the differences obtained between our group and Janin and colleagues. I will also discuss the biological and biochemical roles of NSUN5 in glioblastoma, along with potential mechanisms for regulation of the proteome and the expression of STAT3 and NSUN2 as the regulation of STAT3 and NSUN2 could be a molecular mechanism for NSUN5 to regulate the biological behavior of glioblastoma cells.

### **6.1.1 NSUN5 expression in glioblastoma and the key cysteines of NSUN5**

Using a TCGA dataset, we found that both high *NSUN5* mRNA and low *NSUN5* DNA promoter methylation is strongly associated with poor survival of glioblastoma patients, which is

consistent with the report by Janin et al. [421]. (Pre-)/transcriptional regulation includes epigenetic DNA methylation, histone modification, and transcriptional factor regulation. The hypermethylation of CpG islands in the promoter area to silence the expression of certain genes (especially tumor suppressor genes) is commonly found in cancer cells [423-429]. The survival analysis results suggest that the *NSUN5* mRNA levels in glioblastoma cells could be regulated by the methylation of the CpG islands on *NSUN5* promoter. Indeed, Janin et al. showed that expression of *NSUN5* in some glioma cell lines could be increased upon treatment with 5-azacytidine to prevent methylation of nascent gene promoters [421].

Using site-directed mutagenesis, we identified two catalytic cysteines (C308 and C359) that are required for the methylation of C3872 in 28S rRNA in glioblastoma cells. Using overexpression cell models, we found that, unlike wild-type *NSUN5*, overexpression of *NSUN5* C308A, *NSUN5* C359A or *NSUN5* C308A/C359A failed to induce methylation of C3782 in 28S rRNA in U87 cells, indicating that C308 and C359 are two key cysteines for the RNA methyltransferase activity of *NSUN5*. Moreover, overexpression of *NSUN5* C308A, but not that of *NSUN5* C359A or *NSUN5* C308A/C359A caused cell death. The identification of the two catalytic cysteines is consistent with Heissenberger et al.'s study. However, the latter showed that overexpression of *NSUN5* C359S, but not that of *NSUN5* C308S led to cell death. Our finding is consistent with the study in yeast *NSUN5* showing that cysteine 404 in motif IV of Rcm1 (homologous to C359 in *NSUN5*) catalyzes the methylation of target cytosines, whereas cysteine 330 in motif VI of Rcm1 (homologous to C308 in *NSUN5*) assists in the separation of Rcm1 from the cytosine target [238]. Mutation of C330 leads to failure of Rcm1 to release from its target and thus causes the death of yeast cells [238]. Moreover, in the study of yeast *NSUN1* (Nop2), cysteine 478 in motif IV catalyzed the methylation of target cytosine, whereas cysteine 424 in motif VI

helped to release NSUN1 from target RNA after cysteine methylation [238]. Similarly, in the study of human NSUN2, cysteine 321 in motif IV catalyzed the methylation of target cytosine, whereas cysteine 271 in motif VI helped to release NSUN2 from its target RNA after methylation [292, 342]. Hence, despite the discrepancy between our finding and the report by Heissenberger et al., we believe that C308 is responsible for the release of NSUN5 from its RNA target(s).

### **6.1.2 Methylation target(s) of NSUN5 in glioblastoma cells**

NSUN5 is an RNA cytosine methyltransferase based on the study of RCM1 in yeast and the fact that it methylates C2278 in yeast 25S rRNA [238, 312]. In my thesis, using RNA bisulfite sequencing, we confirmed that NSUN5 indeed methylates 28S rRNA at C3872 in human 293T and glioblastoma cells. Our results were also confirmed by two NSUN5 papers using HeLa cells and glioblastoma cell lines [387, 421]. In addition, we observed a partial methylation of C3872 in U87/CMV-NSUN5 cells (40% NSUN5 positive cells) and 100% methylation in U87/pLenti-NSUN5 (100% NSUN5 positive cells), highlighting the dependence of C3872 on NSUN5 expression in glioblastoma cells. In the two NSUN5 papers by Janin et al. and Heissenberger et al. in cancer, they reported that the single cytosine C3782 methylation by NSUN5 contributed to the functional changes in protein synthesis, tumor proliferation and development in glioblastoma and HeLa cells [387, 421]. However, whether NSUN5 has mRNA targets or whether NSUN5 has methyltransferase independent functions were not explored.

There are 5063 m<sup>5</sup>C sites on 1995 mRNAs identified in HeLa cells, and m<sup>5</sup>C hypermethylation was found on 50 representative tumor associated mRNAs in bladder cancer tissues [292, 301]. Amongst the mRNAs identified in HeLa cells, there are 2016 m<sup>5</sup>C sites on 1,158 mRNAs catalyzed by NSUN2, and knockdown of NSUN2 resulted in a decrease of approximately 40% of the total

m<sup>5</sup>C methylation [292]. Whether NSUN5 has cytosine targets on mRNAs could be determined by high throughput RNA bisulfite sequencing on NSUN5 knockdown and control cells. Transcriptome-wide m<sup>5</sup>C analyses could also be performed using a new approach named 5-azacytidine-mediated RNA immunoprecipitation (5-Aza-IP) coupled with RNA sequencing [309]. We found that knockdown of NSUN5 decreased the expression of NSUN2 and STAT3 at both the mRNA and protein levels in U251 and T98 cells. There are 4 m<sup>5</sup>C sites on *NSUN2* mRNAs, and 5 m<sup>5</sup>C sites on *STAT3* mRNAs in the HeLa cells [292]. Furthermore, a recent study reported that NSUN5 methylates cytosine sites at the 5'UTR of ferritin heavy chain 1 (FTH1) mRNA and the 3'UTR of ferritin light chain (FTL) mRNAs in rat bone marrow-derived mesenchymal stem cells [430], suggesting that NSUN5 may have other RNA targets, including mRNAs. It remains to be determined whether NSUN5 regulates the expression of *NSUN2* and *STAT3* mRNAs through methylation of the target cytosines. *In vitro* methylation assays could be used to confirm the presence of m<sup>5</sup>C on mRNA targets [307, 318, 431]. In addition, research has shown that m<sup>5</sup>C on mRNAs can be recognised by m<sup>5</sup>C reader proteins such as ALYREF and YBX1, and the recognition was found to promote tumorigenesis in multiple cancers [292, 300, 301]. Therefore, after the identification of mRNA targets, whether m<sup>5</sup>C by NSUN5 is required for the recognition of mRNAs by ALYREF and YBX1 could be further examined.

Another member of the NSUN protein family, NSUN4 has been shown to have dual functions in mitochondrial rRNA biogenesis [332-335]. NSUN4 methylates C911 in 12S mitochondrial rRNA and forms a complex with mitochondrial transcription termination factor 4 (MTERF4) and thereby plays an essential role in monosome assembly, with the latter being independent of C911 methylation [332-335]. A recent paper showed that NSUN5 plays an RNA methyltransferase independent role in the defense of RNA virus infection and replication in 293T cells and mouse

lungs [432]. Binding of NSUN5 with the retinoic acid-inducible gene I (RIG-I) was found to be required in order for RIG-I to recognize RNA viruses and activate the antiviral immune system to inhibit the RNA virus infection [432]. In future experiments, our NSUN5 cysteine mutants could be used to further determine if the biological functions of NSUN5 we have identified (protein synthesis, cell growth, sphere formation, and tumor formation) depend on methylation of C3872 or other RNA targets.

In addition, deletion of *Rcm1* in yeast (the yeast homologue of NSUN5) led to the loss of methylation of C2278 in 25S rRNA, altering the composition and activity of ribosomes and mRNA translation [312]. Dysregulated ribosome biogenesis is commonly found in cancer, and ribosome heterogeneity plays an important role in cancer initiation and progression [239, 433]. Therefore, it will be interesting to determine whether U251 (NSUN5 positive) and U87 (NSUN5 negative) cells have differential ribosomal composition and/or activity. Currently, it is not clear whether NSUN5-mediated C3782 methylation will alter rRNA structures and ribosomal protein composition in glioblastoma cells. This will be addressed in future experiments by ribosome isolation combined with LC-MS/MS, as well as Cryo-electron microscopy techniques.

### **6.1.3 NSUN5 regulates the behaviour of glioblastoma cells *in vitro***

NSUN5 knockdown in U251 and T98 cells decreased cell proliferation based on the neutral red uptake assay and clonogenic assay. These results suggest that loss of NSUN5 inhibits the proliferation in glioblastoma cells. Consistent with our results, Heissenberger et al. found that knockout of NSUN5 decreased the proliferation and size of HeLa cells [387]. However, we found that ectopic expression of NSUN5 in U87 cells had no effect on cell proliferation. U87 is an established cell line that does not express endogenous NSUN5, thus it is well-adapted to grow

without NSUN5. It is possible that this cell line has evolved to become independent of NSUN5, and the addition of NSUN5 does not change the biological processes associated with proliferation under adherent culture conditions. Additional cell lines that do not express endogenous NSUN5 (both established cell lines and glioblastoma tumor initiating cells) will be tested to confirm the proliferation results.

Overexpression of NSUN5 in U87 and 50M cells increased, whereas knockdown of NSUN5 in U251 and A4-012 cells decreased, sphere formation. The sphere formation assay measures the self-renewal ability of cells in an anchorage-independent setting. These self-renewal cells are considered as GSCs, and they account for a large fraction of cells in the sphere [94, 95]. Moreover, as 50M and A4-012 are maintained as neurospheres, the change in the number or size of the spheres could be caused by cell proliferation, in addition to stemness of the cells. The molecular mechanisms underlying NSUN5 regulation of proliferation and stemness are still unclear. Possibilities include regulation of global protein synthesis or/and regulation of the expression of specific genes such as *STAT3* or *NSUN2*. *STAT3* is an important signal transducer and activator for growth factors, cytokines and signaling pathways, and is a key transcription factor for tumor proliferation, invasion, stemness, and treatment resistance in glioblastoma cells [434-441]. *NSUN2* promotes the migration and proliferation of glioblastoma cells and other tumors [184, 321, 442]. The absence of *NSUN2* decreases global protein synthesis, and the expression of *NSUN2* is required for c-Myc induced tumor proliferation [184]. Whether NSUN5 regulates the behavior of glioblastoma through the regulation of *STAT3* and *NSUN2* needs to be further studied.

Temozolomide treatment is the standard care for glioblastoma, but the effectiveness is not optimal. We found that NSUN5 knockdown increased sensitivity to temozolomide treatment in U251 and T98 cells. Generally, cancer cells develop chemotherapy resistance mainly by reducing

drug accumulation, increasing DNA damage repair, and decreasing apoptosis [443]. GSCs have been shown to contribute to temozolomide treatment resistance in glioblastoma [18, 99]. For instance, breast cancer resistance protein 1 (BCRP1) that pumps out chemotherapeutic drugs, and MGMT that repairs DNA damage caused by temozolomide, are highly expressed in GSCs [18, 99]. Moreover, apoptosis activation by temozolomide is decreased in GSCs as these cells often exist in a quiescent state. As NSUN5 knockdown decreased sphere formation in glioblastoma cells, this could be the underlying reason for increased sensitivity to temozolomide treatment [444]. At the molecular level, STAT3 not only plays a role in GSC stemness, but is also involved in the survival of glioblastoma cells treated with temozolomide [444, 445]. For instance, it has been reported that STAT3 knockdown increases the expression of MGMT and leads to respiratory chain dysfunction, and thereby increases the temozolomide efficacy in glioblastomas [445, 446]. In another study, STAT3 knockdown was found to decrease the expression of anti-apoptotic proteins, such as Bcl-XL, Bcl-2, Mcl-1, and survivin, leading to increased apoptosis of glioblastoma cells [444]. Therefore, down-regulation of STAT3 could be a potential molecular mechanism that increases the sensitivity of NSUN5 knockdown cells to temozolomide treatment. In the future, expression of apoptosis associated proteins will be further examined in NSUN5 knockdown cells.

#### **6.1.4 NSUN5 regulates the behaviour of glioblastoma cells *in vivo***

In Janin et al.'s NSUN5 paper, they found that overexpression of NSUN5 in A172 and LN229 cells decreased, whereas knockdown of NSUN5 in DBTRG-05MG cells increased tumor luminescence intensity (based on bioluminescence imaging) in a murine intracranial injection model, as well as increased tumor volume and weight in a murine subcutaneous injection model [421]. However, in our *in vivo* study, we found that mice bearing U251/shNSUN5 tumors survived

longer as compared to mice bearing U251/shRandom tumors. In two independent experiments, the median survival times for U251/shRandom mice were 120 and 127.5 days, respectively, whereas that of the U251/shNSUN5#4 mice were 106 and 89 days, respectively. In our study, we monitored the U251 tumors weekly by bioluminescence imaging, but we did not see differences in luminescence intensities between U251/shRandom and U251/shNSUN5#4 mice. Moreover, the luminescence intensities were not associated with the survival time of mice in shRandom and shNSUN5#4 mice. We did not have statistics comparing tumor weight, as glioblastoma cells invasively grow in the brain, and it is difficult to isolate tumors from surrounding brain tissues.

To address the discrepancy between our results and Janin et al.'s results, we have IHC data, as well as comprehensive *in vitro* work that supports our *in vivo* work. First, we found that U251/shRandom tumor cells are more infiltrative than shNSUN5 tumor cells. We observed that U251/shRandom tumors tend to migrate to the subarachnoid space in multiple sites of the brain through the CSF circulation and the ventricular system. Moreover, eight out of twelve mice bearing U251/shRandom tumors, but only two out of thirteen mice bearing U251/shNSUN5#4 tumors displayed spinal metastasis. Although spinal metastasis of intracranial U251 tumors has not been reported previously, glioblastoma leptomeningeal and spinal metastases are not uncommon in the clinic as they have been reported in 4% to 25% of glioblastoma patients [406-409]. For example, in 1978, spinal cords were autopsied at post-mortem examination in 20 glioblastoma patients, resulting in the identification of 5 patients (25%) with glioblastoma spinal metastases [409]. Similarly, in another autopsy examination of 52 malignant glioma patients, 8 patients (15.3%) were found to have spinal metastases [410]. The conclusion from these studies is that the occurrence of spinal metastases of glioblastoma is common [409, 410]. In the clinical research setting, spinal metastases are catalogued as leptomeningeal metastases [406, 408]. The tumor cells

can migrate from the superior temporal and central sulcus, the transverse and cortical fissures, and the lateral ventricle to the cerebrospinal fluid (CSF) and the spine to form metastases [406]. However, due to lack of spinal cord MRI imaging and low sensitivity of CSF examination, only 50% of leptomeningeal metastases have been documented as showing positive CSF spreading, and only 15% of leptomeningeal metastases with spinal metastasis can be identified by MRI imaging [406]. With the increased frequency in examining spinal cord by MRI and nuclear imaging, the incidence of spinal metastasis will likely increase and the treatment of this complication will receive more attention [447]. In our study, even though U251/shRandom cells appear to have more infiltrative growth with increased migration, we did not find any association between spinal metastases and the overall survival of mice. Similarly, spinal metastases did not associate with overall survival of glioblastoma patients [406, 408, 410, 447]. This observation may be due to the rapid progression of glioblastoma in the brain, and the poor overall survival of glioblastoma patients [447].

Finally, our *in vivo* work is consistent with our *in vitro* work multiple NSUN5 overexpression and NSUN5 knockdown glioblastoma cell lines using cell viability, sphere forming, migration, and survival assays. NSUN5 knockdown decreased the proliferation, the number and size of spheres, and TMZ resistant behavior in both U251 and T98 cells in our *in vitro* study. In contrast, overexpression of NSUN5 increased the number of spheres formed by U87 and 50M cells.

### **6.1.5 NSUN5 increases protein synthesis in glioblastoma cells**

rRNA methylation alters ribosome structure and protein synthesis and is involved in cancer biology [256, 448, 449]. Consistent with the two published papers, we found that overexpression of NSUN5 increases, whereas NSUN5 knockdown decreases protein synthesis in glioblastoma

cells [387, 421]. These results suggest a role for NSUN5 in mRNA translation. However, the underlying molecular mechanisms of NSUN5 in mRNA translation need to be further studied. NSUN5 could be involved in protein synthesis through three different mechanisms. First, NSUN5-induced C3782 methylation of 28S rRNA could alter the ribosomal conformation in translation processes. C3782 is located in the middle of helix 69 and helix 71 of domain IV of 28S rRNA, which is at the intersubunit bridge and the decoding center of ribosomes [226-228]. The structure of helix 69 to helix 71 interacts with tRNAs at both the A- and P-sites, which assists in the correct binding of tRNAs at the peptidyl transferase center (PTC) [352, 450]. Moreover, helix 69 is required for both the release of initiation factor 3 and start codon selection, and deletion of helix 69 decreases the rate of the translation initiation by 20-fold [229]. In bacterial rRNA studies, the methyl group of m<sup>5</sup>C1942, homologous to C3782 in humans, was found to enhance the stacking interactions with C1942 and U1943 and interact with tRNA at the A site [234, 451]. In Janin et al.'s paper, their computer simulation showed that the methyl group of C3782 could stabilize methyl- $\pi$  interaction with C3781, which allows C3781 to pair with G3810, which indirectly influences the binding of C3809 with a small hairpin (nucleotides 3742–3778) at the P-site, consequently influencing the binding of P-site tRNAs and global protein translation [421]. This evidence suggests that C3782 methylation could directly alter ribosomal conformation in translation processes.

Second, NSUN5-induced C3782 methylation could alter the functionality of helix 69 of 28S rRNA, which in turn alters the stability of the ribosome and translation. Ali et al. have shown that the deletion of helix 69 or helix 70 leads to defective association between 50S and 30S subunits of the ribosome [228, 452]. Moreover, mutation of a single nucleotide A1916 on helix 69 or U1940 on helix 70 led to defects in ribosome assembly, and strongly inhibited translation [452-454].

Similarly, deletion of 3 to 5 nucleotides in helix 69 of 25S rRNAs in bacteria caused instability and increased turnover of ribosomes [227]. As a result, the protein synthesis rate and cell growth were decreased by 50%, and the cells were more sensitive to temperature and antibiotics [227, 353]. Whether C3782 methylation affects the assembly and stability of ribosomes could be investigated using ribosomal fractions analysis in normal and stress conditions [227].

Third, NSUN5 could have methylation-independent functions in ribosome biogenesis. Another member of the NSUN protein family, NSUN4 has been shown to have dual functions in mitochondrial rRNA biogenesis [332-335]. The NSUN4/MTERF4 complex is required for LSU and SSU assembly, and the deletion of NSUN4 impairs mitochondrial translation [334]. The interaction of NSUN4 with MTERF4 is cytosine methylation independent [334]. Whether NSUN5 has methylation-independent functions in ribosome biogenesis could be investigated using the catalytic inactive mutant NSUN5 (NSUN5/C308A and NSUN5/C359A that I have generated) in protein synthesis assays.

In addition, we observed a correlation between decreased protein synthesis and decreased cell growth in U251 and T98 cells upon NSUN5 knockdown. A large increase in global protein synthesis to fulfill abnormal growth demands is commonly observed in cancer cells [108, 247]. However, we did not observe a difference in proliferation between U87/vector and U87/NSUN5 cells using the neutral red assay. Although the exact reason remains unclear, there are two possible explanations for the discrepancies observed using the NSUN5 overexpression cell model. First, NSUN5 expression regulates the size of glioblastoma cells. We found that NSUN5 expression increases the size of U87 cells (data not shown). Similarly, in Heissenberger et al.'s paper, they found that NSUN5 knockout decreased the size of HeLa cells [387]. Second, the increase in protein synthesis observed using the puromycin labelling assay over a period of 15 minutes captures a

snapshot of protein synthesis which could be eventually balanced out via increased protein degradation in U87 cells.

#### **6.1.6 NSUN5 alters the proteome of glioblastoma cells**

Our LC-MS/MS results showed that NSUN5 knockdown in U251 cells decreased the expression of proteins that promote tumorigenic phenotypes in glioblastoma, such as STAT3, NSUN2, Nestin, FABP7, and ZEB1 [436, 438, 442, 455-457]. The decrease in STAT3 and NSUN2 levels in U251/shNSUN5#4 cells was validated by Western blotting and real time-PCR. A 58.8% reduction in STAT3 protein levels and a 37.66% reduction in NSUN2 protein levels were confirmed by Western blotting. A 40% reduction in *STAT3* mRNA levels and a 50% reduction in *NSUN2* mRNA levels were found through RT-qPCR. Furthermore, STAT3 and NSUN2 decreases in T98/shNSUN5#4 cells were confirmed at both the protein and mRNA levels. There are several potential mechanisms by which NSUN5 may regulate *STAT3* and *NSUN2* mRNA levels.

First, NSUN5 may directly methylate *STAT3* and *NSUN2* mRNAs, which increase their stability in glioblastoma. A recent NSUN5 study published by Liu et al. showed that NSUN5 methylates cytosine sites at the 5'UTR of *FTH1* mRNA and the 3'UTR of *FTL* mRNAs in rat bone marrow-derived mesenchymal stem cells [430], suggesting that NSUN5 may have mRNA targets. There are 5063 to 8495 m<sup>5</sup>C sites on more than 1995 mRNAs found in Hela cells, and more than four m<sup>5</sup>C sites were identified on *NSUN2* and *STAT3* mRNAs [292, 301]. Moreover, Chen et al. found that m<sup>5</sup>C on mRNAs affects the stability and translation efficiency of mRNAs [301]. It was also shown that m<sup>5</sup>C on mRNAs can be recognised by Y-box binding protein 1 (YBX1), and YBX1 further recruits ELAVL1 that stabilizes and promotes the translation of mRNAs [300, 301]. Hypermethylated m<sup>5</sup>C sites on oncogenic mRNAs are stabilized by YBX1, allowing YBX1 to

promote formation of multiple cancers [301]. Whether *NSUN2* and *STAT3* mRNAs are methylated by NSUN5 could be determined using the  $^3\text{H}$ -SAM *in vitro* methylation assay [307, 318, 431]. In this assay, mRNAs that are methylated are labeled by  $^3\text{H}$  on their targeted cytosines and measured by autoradiography [307, 318, 431]. Second, as knockdown of NSUN5 decreased global protein synthesis, NSUN5 may indirectly regulate the expression of *STAT3* and *NSUN2*. For instance, knockdown of NSUN5 may decrease protein levels, such as those of transcription factors that are involved in regulating the expression of *STAT3* and *NSUN2* at the transcriptional level. Thus, the decrease in mRNA levels of *STAT3* and *NSUN2* may be a secondary effect of NSUN5 knockdown.

*STAT3* is an important transcription factor, and plays a key role in proliferation, invasion, tumorigenesis, survival under hypoxic conditions, and resistance to chemotherapeutic drugs in glioblastoma [434-441]. NSUN2 has been shown to be associated with progression of glioblastoma and other tumors [184, 321, 442]. Whether NSUN5 regulates the behavior of glioblastoma through the regulation of *STAT3* and *NSUN2* needs to be further studied. Identification of NSUN5-regulated proteins may help elucidate the molecular mechanism of NSUN5 function in GBM cells.

In addition, we have found that knockdown of NSUN5 decreased temozolomide resistance of U251 cells. However, our LC-MS/MS results for U251/Random vs. U251/shNSUN5#4 cells do not address the mechanism of treatment resistance as cells were not treated with temozolomide. In the future, we could repeat the LC-MS/MS experiments using lysates of U251/Random and U251/shNSUN5#4 cells with/without temozolomide treatment. We expect that multiple proteins involved in DNA damage and chemotherapy resistance would be identified using this approach.

In the future, RNA sequencing could be performed to help identify gene expression profiles in NSUN5 knockdown cells. Comparing the RNA sequencing data with the MS/MS data may help identify the proteins whose overall expression is controlled by NSUN5 at the translational level.

In addition, NSUN5 increased protein synthesis (puromycin labelling assay), but LC-MS/MS did not identify many proteins altered by NSUN5 overexpression in 50M cells, suggesting that NSUN5 increases global protein synthesis (mRNA translation), not the translation of specific mRNAs. Thus, it is possible that methylation of 28S rRNA by NSUN5 alters the structure and/or activity of the ribosomes to increase the translation of global mRNAs, rather than specific mRNAs.

## **6.2 Future directions**

Despite these intriguing findings, there are several overarching questions that need to be addressed in order to fully elucidate the function of NSUN5 in glioblastoma. First, does NSUN5 promote the tumorigenic phenotypes of glioblastoma by increasing overall protein synthesis or by altering mRNA translation of cancer-associated genes? Second, does NSUN5 expression alter the composition of ribosomes? Third, does NSUN5 have novel RNA targets other than 28S rRNA or non-canonical functions independent of its RNA methyltransferase activity?

### **6.2.1 To determine whether NSUN5 reprograms the translome in glioblastoma cells**

Deletion of Rcm1 in yeast causes an alteration in the ribosomal profile and translome, including increasing the translation of stress response genes but decreasing the translation of RNA maturation associated genes [312]. Moreover, we have confirmed that NSUN5 is responsible for the methylation of C3782 on 28S rRNA. It will be interesting to investigate whether NSUN5 expression and the subsequent methylation at C3782 will alter the conformation and/or activity of ribosomes, leading to altered translomes. This can be determined by both ribosome profiling coupled with RNA sequencing and polysome profiling coupled with RNA sequencing in NSUN5 overexpression and knockdown glioblastoma cells [458-460]. The transcriptome of each sample will also be determined by total mRNA sequencing, and the translation efficiency (the ratio of the expression of a specific gene in the translome versus the transcriptome) will be determined.

Polysome profiling and ribosome profiling are two important techniques in studying the translome [458-460]. Polysome profiling is a method used to sequence polysome-bound mRNAs, and all these bound mRNAs are considered as the translome. Since the transcripts obtained from polysome profiling have both untranslated and translated regions, this technique can be used for

the study of the untranslated regions of mRNAs. Ribosome profiling allows sequencing of the ribosome-protected mRNA fragments, and all these fragments are considered as the translome. Only mRNA fragments (about 30 nucleotides) bound inside the ribosome can be protected from digestion, when RNAs are treated with RNase I. These ribosome-protected mRNA fragments are termed ribosome footprints. More footprints on a transcript means higher translation rate of the transcript. In addition, from the position of the footprints, it is possible to determine whether a transcript has an upstream open reading frame (uORF) or a stop codon read-through translation. This information will address whether NSUN5 changes the ribosome structure and thus affects uORF binding and stop codon read-through translation.

In future experiments, U251/shRandom vs U251/shNSUN5 #4 cells, as well as primary glioblastoma cells with or without NSUN5 overexpression/knockdown will be used to examine the effect of NSUN5 on the translome. Ribosome profiling will be performed to identify the whole ribosome protected mRNA sequences (translatome 1). Polysome profiling will be performed to identify the whole polysome-bound mRNA sequences (translatome 2). Total mRNA will be sequenced to identify the transcriptome. The top-ranked differentially expressed mRNAs will be validated by RT-qPCR and Western blotting to confirm the gene expression results obtained by RNA sequencing. The top differentially expressed genes in canonical pathways (especially those that are associated with functional roles in proliferation, stemness and tumor formation) will be further studied.

## **6.2.2 To determine whether NSUN5 regulates the composition of ribosomal proteins in glioblastoma cells**

Ribosomal protein composition heterogeneity was observed in different tissues, cell lines, and cancer cells, contributing to functional specialization in protein synthesis [433, 461, 462]. For instance, RPL10A, RPL38, RPS7, and RPS25 are depleted in the ribosomes of mouse embryonic stem cells [272]. RPL10A and RPS25 are located at the mRNA exit tunnel of ribosome, and regulate the translation of specific subgroups of mRNAs in mouse embryonic stem cells [272]. The composition of ribosomal proteins in the whole ribosome is also associated with the modification of rRNAs [275]. A combined loss of cytosine methylation at C2278 and 2'-O methylation at G2288 in helix 71 of domain IV of 28S rRNA causes LSU instability, and decreases the binding of some ribosomal proteins to LSU (e.g. RPL23, PRL24, RPL19, RPL31, RPL38) [275]. C2278 is the methylation target of Rcm1 (the yeast homologue of NSUN5), and RPL23 directly binds to helix 71 of 28S rRNA [275]. In the future, whether loss of methylation at C3782 by NSUN5 knockout will affect the binding of ribosomal proteins in glioblastoma will be investigated. Sucrose density gradients will be used to isolate SSU, LSU and monosomes in U251/shRandom vs. U251/shNSUN5 #4 cells. The isolated ribosomes will be analyzed using LC-MS/MS to identify the composition of ribosomal proteins. In addition, the atomic structure of ribosomes in control and NSUN5 knockdown cells could be further examined using cryogenic electron microscopy (cryo-EM), which could better illustrate the conformation of rRNA and ribosomal proteins [461].

### **6.2.3 To determine whether NSUN5 has other RNA targets and whether *STAT3* and *NSUN2* are the targets of NSUN5**

mRNA modifications are abundantly found in cancer cells, which often functions to regulate the rate of translation. For instance, m<sup>5</sup>C sites were identified on 1995 mRNAs in HeLa cells, and m<sup>5</sup>C on mRNAs played a role in the stability and translation efficiency of mRNAs [292, 301]. In a recent study of NSUN5 by Liu et al. they found that NSUN5 methylates cytosine sites at the 5'UTR of *FTH1* mRNA and the 3'UTR of *FTL* mRNAs [430], suggesting that NSUN5 could have mRNA targets. Moreover, four m<sup>5</sup>C sites on *NSUN2* mRNAs, and 5 m<sup>5</sup>C sites on *STAT3* mRNAs were identified in HeLa cells [292]. Whether *NSUN2* and *STAT3* mRNAs are the targets of NSUN5 could be determined through <sup>3</sup>H-SAM *in vitro* methylation assay [307, 318, 431]. Briefly, NSUN5 protein, *STAT3* or *NSUN2* mRNAs transcripts will be incubated with <sup>3</sup>H-labeled SAM (Hartmann) and methylation associated buffer. Under such conditions, NSUN5 will methylate and label <sup>3</sup>H on its targeted cytosines [307, 318, 431]. Native NSUN5 protein will be prepared through the overexpression of His-tagged NSUN5 in *E. coli* cells and the purification of His-tagged NSUN5 using Ni-NTA Agarose (Qiagen) [320, 431]. *STAT3* or *NSUN2* mRNAs transcripts will be amplified by PCR with primers containing T7 promoter sequences and transcribed by T7 polymerase [320, 431]. The mRNAs will be isolated in 12% denaturing polyacrylamide gel, stained with ethidium bromide, and exposed to X-ray film [320, 431]. Moreover, the location of potential cytosine targets can be further identified by using mRNA fragments and Sanger bisulfite sequencing [318].

NSUN2 has been found to have multiple cytosine targets, including cytosines at the variable loop of most of tRNAs, at C92 on 5S rRNA and at 1158 different mRNAs [292, 344, 463]. However, how many cytosine targets are methylated by NSUN5 in human RNA remains unknown.

More importantly, whether high expression of NSUN5 causes the dysregulation of RNA methylations (other than 28S rRNA) in glioblastoma is also unknown. The difficulty in answering these questions is partly due to the complexity of the technique used for the detection of RNA cytosine methylation sites. High throughput RNA bisulfite sequencing can detect differences in m<sup>5</sup>C methylation, but it does not identify the methylated mRNA targets of NSUN5, because NSUN5 regulates the expression of NSUN2, which prevents us from distinguishing cytosines directly methylated by NSUN2 from cytosines directly methylated by NSUN5. 5-Aza-IP coupled with RNA sequencing is a novel and reliable approach to directly detect RNA methylation sites on the whole genome scale [309, 464]. Briefly, 5-azacytidine treatment randomly replaces cytidine in nascent RNAs and locks cytosine methyltransferases to the RNA targets by forming a stable covalent connection between the enzyme and RNA targets. Therefore, immunoprecipitation of RNA methyltransferase pulls down the RNA sequences with its targeted cytosines. Moreover, the release of cytosine methyltransferase from target cytosines causes breakage of the cytosine ring, with the abnormal broken cytosine pairing with cytosine rather than guanine during cDNA synthesis. The methylated cytosine will be recognized as guanine in the sequencing results. In the future, we will perform Aza-IP coupled with RNA sequencing using 50M/pLenti-Vector vs. 50M/pLenti-NSUN5 cells and U251/shRandom vs. U251/shNSUN5 #4 cells to identify novel RNA targets of NSUN5 in glioblastoma cells. In addition, the immunoprecipitation of NSUN5 with mutated releasing cysteine (NSUN5/C308A) coupled with RNA sequencing is another way to directly detect RNA methylation sites [316, 345]. The overexpressed NSUN5/C308A will form an irreversible covalent bond with its target RNAs. The target RNAs will be pulled down by NSUN5 immunoprecipitation and send out for RNA sequencing. This method can be used to confirm the target sites in the 50M/pLenti-NSUN5/C308A cells.

### 6.3 Conclusions

RNA methylation and deregulation of mRNA translation are implicated in multiple processes associated with cancer initiation and progression.  $m^5C$  occurs on all types of RNA and the functions of  $m^5C$  in cell development and cancers have been increasingly studied in recent years. NSUN5, as an RNA cytosine methyltransferase, has been found to play a role in the cytosine methylation on 28S rRNA. Importantly, elevated *NSUN5* levels are associated with poor survival in glioblastoma patients. In this thesis, we demonstrate that NSUN5 methylates cytosine 3782 of human 28S rRNA. Moreover, we found that NSUN5 expression in glioblastoma cells promotes proliferation, sphere formation, resistance to temozolomide, and tumor formation/progression in mice. In addition, we demonstrate that NSUN5 promotes protein synthesis and that expression of NSUN5 alters the proteome in glioblastoma cells, modulating the expression of STAT3 and NSUN2. Despite these intriguing findings, the underlying mechanisms still need to be further addressed. A better understanding of the function of NSUN5, an RNA methyltransferase that regulates protein synthesis, and the mechanisms of its action may help identify a potential therapeutic target for glioblastoma.

## References

1. Ostrom, Q.T., et al., *CBTRUS Statistical Report: Primary Brain and Central Nervous System Tumors Diagnosed in the United States in 2008-2012*. Neuro Oncol, 2015. **17 Suppl 4**: p. iv1-iv62.
2. Stupp, R., et al., *Radiotherapy plus concomitant and adjuvant temozolomide for glioblastoma*. N Engl J Med, 2005. **352**(10): p. 987-96.
3. Stupp, R., et al., *Maintenance Therapy With Tumor-Treating Fields Plus Temozolomide vs Temozolomide Alone for Glioblastoma: A Randomized Clinical Trial*. JAMA, 2015. **314**(23): p. 2535-43.
4. Gilbert, M.R., et al., *Dose-dense temozolomide for newly diagnosed glioblastoma: a randomized phase III clinical trial*. J Clin Oncol, 2013. **31**(32): p. 4085-91.
5. Nakazato, Y., [*The 4th Edition of WHO Classification of Tumours of the Central Nervous System published in 2007*]. No Shinkei Geka, 2008. **36**(6): p. 473-91.
6. Louis, D.N., et al., *The 2007 WHO classification of tumours of the central nervous system*. Acta Neuropathol, 2007. **114**(2): p. 97-109.
7. Ostrom, Q.T., et al., *CBTRUS Statistical Report: Primary Brain and Other Central Nervous System Tumors Diagnosed in the United States in 2014-2018*. Neuro Oncol, 2021. **23**(Supplement\_3): p. iii1-iii105.
8. Reifenberger, G., et al., *Advances in the molecular genetics of gliomas - implications for classification and therapy*. Nat Rev Clin Oncol, 2017. **14**(7): p. 434-452.
9. Ostrom, Q.T., et al., *CBTRUS statistical report: Primary brain and central nervous system tumors diagnosed in the United States in 2006-2010*. Neuro Oncol, 2013. **15 Suppl 2**: p. ii1-56.
10. Verhaak, R.G., et al., *Integrated genomic analysis identifies clinically relevant subtypes of glioblastoma characterized by abnormalities in PDGFRA, IDH1, EGFR, and NF1*. Cancer Cell, 2010. **17**(1): p. 98-110.
11. Cancer Genome Atlas Research, N., *Comprehensive genomic characterization defines human glioblastoma genes and core pathways*. Nature, 2008. **455**(7216): p. 1061-8.
12. Wang, Q., et al., *Tumor Evolution of Glioma-Intrinsic Gene Expression Subtypes Associates with Immunological Changes in the Microenvironment*. Cancer Cell, 2017. **32**(1): p. 42-56 e6.
13. Dang, L., et al., *Cancer-associated IDH1 mutations produce 2-hydroxyglutarate*. Nature, 2009. **462**(7274): p. 739-44.
14. Yan, H., et al., *IDH1 and IDH2 mutations in gliomas*. N Engl J Med, 2009. **360**(8): p. 765-73.
15. Choi, C., et al., *2-hydroxyglutarate detection by magnetic resonance spectroscopy in IDH-mutated patients with gliomas*. Nat Med, 2012. **18**(4): p. 624-9.
16. Singh, S.K., et al., *A complex of nuclear factor I-X3 and STAT3 regulates astrocyte and glioma migration through the secreted glycoprotein YKL-40*. J Biol Chem, 2011. **286**(46): p. 39893-903.
17. Francescone, R.A., et al., *Role of YKL-40 in the angiogenesis, radioresistance, and progression of glioblastoma*. J Biol Chem, 2011. **286**(17): p. 15332-43.
18. Hegi, M.E., et al., *MGMT gene silencing and benefit from temozolomide in glioblastoma*. N Engl J Med, 2005. **352**(10): p. 997-1003.
19. Nobusawa, S., et al., *IDH1 mutations as molecular signature and predictive factor of secondary glioblastomas*. Clin Cancer Res, 2009. **15**(19): p. 6002-7.
20. Yabroff, K.R., et al., *Patterns of care and survival for patients with glioblastoma multiforme diagnosed during 2006*. Neuro Oncol, 2012. **14**(3): p. 351-9.
21. Brodbelt, A., et al., *Glioblastoma in England: 2007-2011*. Eur J Cancer, 2015. **51**(4): p. 533-42.
22. Kreth, F.W., et al., *Surgical resection and radiation therapy versus biopsy and radiation therapy in the treatment of glioblastoma multiforme*. J Neurosurg, 1993. **78**(5): p. 762-6.

23. Laws, E.R., et al., *Survival following surgery and prognostic factors for recently diagnosed malignant glioma: data from the Glioma Outcomes Project*. J Neurosurg, 2003. **99**(3): p. 467-73.
24. Walker, M.D., T.A. Strike, and G.E. Sheline, *An analysis of dose-effect relationship in the radiotherapy of malignant gliomas*. Int J Radiat Oncol Biol Phys, 1979. **5**(10): p. 1725-31.
25. Sasmita, A.O., Y.P. Wong, and A.P.K. Ling, *Biomarkers and therapeutic advances in glioblastoma multiforme*. Asia Pac J Clin Oncol, 2018. **14**(1): p. 40-51.
26. Jacinto, F.V. and M. Esteller, *MGMT hypermethylation: a prognostic foe, a predictive friend*. DNA Repair (Amst), 2007. **6**(8): p. 1155-60.
27. Brennan, C.W., et al., *The somatic genomic landscape of glioblastoma*. Cell, 2013. **155**(2): p. 462-77.
28. Cloughesy, T.F., W.K. Cavenee, and P.S. Mischel, *Glioblastoma: from molecular pathology to targeted treatment*. Annu Rev Pathol, 2014. **9**: p. 1-25.
29. Furnari, F.B., et al., *Heterogeneity of epidermal growth factor receptor signalling networks in glioblastoma*. Nat Rev Cancer, 2015. **15**(5): p. 302-10.
30. Clarke, J.L., et al., *A single-institution phase II trial of radiation, temozolomide, erlotinib, and bevacizumab for initial treatment of glioblastoma*. Neuro Oncol, 2014. **16**(7): p. 984-90.
31. Liu, S., et al., *Inhibition of Rb and mTOR signaling associates with synergistic anticancer effect of palbociclib and erlotinib in glioblastoma cells*. Invest New Drugs, 2018. **36**(6): p. 961-969.
32. Goodwin, C.R., et al., *Crizotinib and erlotinib inhibits growth of c-Met(+)/EGFRvIII(+) primary human glioblastoma xenografts*. Clin Neurol Neurosurg, 2018. **171**: p. 26-33.
33. Wick, W., *TFields: where does all the skepticism come from?* Neuro Oncol, 2016. **18**(3): p. 303-5.
34. Sampson, J.H. and D.A. Mitchell, *Vaccination strategies for neuro-oncology*. Neuro Oncol, 2015. **17 Suppl 7**: p. vii15-vii25.
35. Mitchell, D.A., et al., *Tetanus toxoid and CCL3 improve dendritic cell vaccines in mice and glioblastoma patients*. Nature, 2015. **519**(7543): p. 366-9.
36. Batick, K.A., et al., *Long-term Survival in Glioblastoma with Cytomegalovirus pp65-Targeted Vaccination*. Clin Cancer Res, 2017. **23**(8): p. 1898-1909.
37. Yu, J.S., et al., *Vaccination with tumor lysate-pulsed dendritic cells elicits antigen-specific, cytotoxic T-cells in patients with malignant glioma*. Cancer Res, 2004. **64**(14): p. 4973-9.
38. Phuphanich, S., et al., *Phase I trial of a multi-epitope-pulsed dendritic cell vaccine for patients with newly diagnosed glioblastoma*. Cancer Immunol Immunother, 2013. **62**(1): p. 125-35.
39. Sampson, J.H., et al., *Immunologic escape after prolonged progression-free survival with epidermal growth factor receptor variant III peptide vaccination in patients with newly diagnosed glioblastoma*. J Clin Oncol, 2010. **28**(31): p. 4722-9.
40. Heimberger, A.B. and J.H. Sampson, *The PEPvIII-KLH (CDX-110) vaccine in glioblastoma multiforme patients*. Expert Opin Biol Ther, 2009. **9**(8): p. 1087-98.
41. Barbee, M.S., et al., *Current status and future directions of the immune checkpoint inhibitors ipilimumab, pembrolizumab, and nivolumab in oncology*. Ann Pharmacother, 2015. **49**(8): p. 907-37.
42. Shu, C.A. and N.A. Rizvi, *Into the Clinic With Nivolumab and Pembrolizumab*. Oncologist, 2016.
43. Vlahovic, G., et al., *Programmed death ligand 1 (PD-L1) as an immunotherapy target in patients with glioblastoma*. Neuro Oncol, 2015. **17**(8): p. 1043-5.
44. Cloughesy, T.F., et al., *Neoadjuvant anti-PD-1 immunotherapy promotes a survival benefit with intratumoral and systemic immune responses in recurrent glioblastoma*. Nat Med, 2019. **25**(3): p. 477-486.
45. Filley, A.C., M. Henriquez, and M. Dey, *Recurrent glioma clinical trial, CheckMate-143: the game is not over yet*. Oncotarget, 2017. **8**(53): p. 91779-91794.

46. Jue, T.R. and K.L. McDonald, *The challenges associated with molecular targeted therapies for glioblastoma*. J Neurooncol, 2016. **127**(3): p. 427-34.
47. Huse, J.T. and E.C. Holland, *Targeting brain cancer: advances in the molecular pathology of malignant glioma and medulloblastoma*. Nat Rev Cancer, 2010. **10**(5): p. 319-31.
48. Alshehri, M.M., S.M. Robbins, and D.L. Senger, *The Role of Neurotrophin Signaling in Gliomagenesis: A Focus on the p75 Neurotrophin Receptor (p75(NTR)/CD271)*. Vitam Horm, 2017. **104**: p. 367-404.
49. Kelly, P.J., et al., *Imaging-based stereotaxic serial biopsies in untreated intracranial glial neoplasms*. J Neurosurg, 1987. **66**(6): p. 865-74.
50. Freije, W.A., et al., *Gene expression profiling of gliomas strongly predicts survival*. Cancer Res, 2004. **64**(18): p. 6503-10.
51. Phillips, H.S., et al., *Molecular subclasses of high-grade glioma predict prognosis, delineate a pattern of disease progression, and resemble stages in neurogenesis*. Cancer Cell, 2006. **9**(3): p. 157-73.
52. Lei, Y., et al., *The brain interstitial system: Anatomy, modeling, in vivo measurement, and applications*. Prog Neurobiol, 2017. **157**: p. 230-246.
53. Zimmermann, D.R. and M.T. Dours-Zimmermann, *Extracellular matrix of the central nervous system: from neglect to challenge*. Histochem Cell Biol, 2008. **130**(4): p. 635-53.
54. Maeda, N., *Proteoglycans and neuronal migration in the cerebral cortex during development and disease*. Front Neurosci, 2015. **9**: p. 98.
55. Gingras, M.C., et al., *Comparison of cell adhesion molecule expression between glioblastoma multiforme and autologous normal brain tissue*. J Neuroimmunol, 1995. **57**(1-2): p. 143-53.
56. Cheresch, D.A., *Human endothelial cells synthesize and express an Arg-Gly-Asp-directed adhesion receptor involved in attachment to fibrinogen and von Willebrand factor*. Proc Natl Acad Sci U S A, 1987. **84**(18): p. 6471-5.
57. Brooks, P.C., R.A. Clark, and D.A. Cheresch, *Requirement of vascular integrin alpha v beta 3 for angiogenesis*. Science, 1994. **264**(5158): p. 569-71.
58. Friedlander, M., et al., *Definition of two angiogenic pathways by distinct alpha v integrins*. Science, 1995. **270**(5241): p. 1500-2.
59. Seker, A., et al., *Expression of integrins in cerebral arteriovenous and cavernous malformations*. Neurosurgery, 2006. **58**(1): p. 159-68; discussion 159-68.
60. Kwiatkowska, A. and M. Symons, *Signaling determinants of glioma cell invasion*. Adv Exp Med Biol, 2013. **986**: p. 121-41.
61. Shishido, S., H. Bonig, and Y.M. Kim, *Role of integrin alpha4 in drug resistance of leukemia*. Front Oncol, 2014. **4**: p. 99.
62. Gritsenko, P.G., O. Ilina, and P. Friedl, *Interstitial guidance of cancer invasion*. J Pathol, 2012. **226**(2): p. 185-99.
63. Zhang, H., et al., *Expression of a cleaved brain-specific extracellular matrix protein mediates glioma cell invasion In vivo*. J Neurosci, 1998. **18**(7): p. 2370-6.
64. Brosicke, N., et al., *Tenascin-C is expressed by human glioma in vivo and shows a strong association with tumor blood vessels*. Cell Tissue Res, 2013. **354**(2): p. 409-30.
65. Martina, E., et al., *Tenascin-W is a specific marker of glioma-associated blood vessels and stimulates angiogenesis in vitro*. FASEB J, 2010. **24**(3): p. 778-87.
66. Cuddapah, V.A., et al., *A neurocentric perspective on glioma invasion*. Nat Rev Neurosci, 2014. **15**(7): p. 455-65.
67. Hirata, E., et al., *Endogenous tenascin-C enhances glioblastoma invasion with reactive change of surrounding brain tissue*. Cancer Sci, 2009. **100**(8): p. 1451-9.

68. Sarkar, S., et al., *Tenascin-C stimulates glioma cell invasion through matrix metalloproteinase-12*. Cancer Res, 2006. **66**(24): p. 11771-80.
69. Sarkar, S., et al., *Activation of NOTCH Signaling by Tenascin-C Promotes Growth of Human Brain Tumor-Initiating Cells*. Cancer Res, 2017. **77**(12): p. 3231-3243.
70. Sivasankaran, B., et al., *Tenascin-C is a novel RBPJkappa-induced target gene for Notch signaling in gliomas*. Cancer Res, 2009. **69**(2): p. 458-65.
71. Jones, P.L., et al., *Induction of vascular smooth muscle cell tenascin-C gene expression by denatured type I collagen is dependent upon a beta3 integrin-mediated mitogen-activated protein kinase pathway and a 122-base pair promoter element*. J Cell Sci, 1999. **112 ( Pt 4)**: p. 435-45.
72. Jinnin, M., et al., *Upregulation of tenascin-C expression by IL-13 in human dermal fibroblasts via the phosphoinositide 3-kinase/Akt and the protein kinase C signaling pathways*. J Invest Dermatol, 2006. **126**(3): p. 551-60.
73. Treere, D., et al., *Nucleolar size and activity are related to pRb and p53 status in human breast cancer*. J Histochem Cytochem, 2004. **52**(12): p. 1601-7.
74. Monteiro, A.R., et al., *The Role of Hypoxia in Glioblastoma Invasion*. Cells, 2017. **6**(4).
75. Hsieh, C.H., et al., *Livin contributes to tumor hypoxia-induced resistance to cytotoxic therapies in glioblastoma multiforme*. Clin Cancer Res, 2015. **21**(2): p. 460-70.
76. Spence, A.M., et al., *Regional hypoxia in glioblastoma multiforme quantified with [18F]fluoromisonidazole positron emission tomography before radiotherapy: correlation with time to progression and survival*. Clin Cancer Res, 2008. **14**(9): p. 2623-30.
77. Mongiardi, M.P., *Angiogenesis and hypoxia in glioblastoma: a focus on cancer stem cells*. CNS Neurol Disord Drug Targets, 2012. **11**(7): p. 878-83.
78. Jensen, R.L., et al., *Preoperative dynamic contrast-enhanced MRI correlates with molecular markers of hypoxia and vascularity in specific areas of intratumoral microenvironment and is predictive of patient outcome*. Neuro Oncol, 2014. **16**(2): p. 280-91.
79. Rong, Y., et al., *'Pseudopalisading' necrosis in glioblastoma: a familiar morphologic feature that links vascular pathology, hypoxia, and angiogenesis*. J Neuropathol Exp Neurol, 2006. **65**(6): p. 529-39.
80. Lee, G., R.R. Hall, 3rd, and A.U. Ahmed, *Cancer Stem Cells: Cellular Plasticity, Niche, and its Clinical Relevance*. J Stem Cell Res Ther, 2016. **6**(10).
81. Persano, L., et al., *The three-layer concentric model of glioblastoma: cancer stem cells, microenvironmental regulation, and therapeutic implications*. ScientificWorldJournal, 2011. **11**: p. 1829-41.
82. Iwadate, Y., *Epithelial-mesenchymal transition in glioblastoma progression*. Oncol Lett, 2016. **11**(3): p. 1615-1620.
83. Mahabir, R., et al., *Sustained elevation of Snail promotes glial-mesenchymal transition after irradiation in malignant glioma*. Neuro Oncol, 2014. **16**(5): p. 671-85.
84. Yang, H.W., et al., *SNAI2/Slug promotes growth and invasion in human gliomas*. BMC Cancer, 2010. **10**: p. 301.
85. Yang, M.H., et al., *Direct regulation of TWIST by HIF-1alpha promotes metastasis*. Nat Cell Biol, 2008. **10**(3): p. 295-305.
86. Ye, X.Z., et al., *Tumor-associated microglia/macrophages enhance the invasion of glioma stem-like cells via TGF-beta1 signaling pathway*. J Immunol, 2012. **189**(1): p. 444-53.
87. Piao, Y., et al., *Glioblastoma resistance to anti-VEGF therapy is associated with myeloid cell infiltration, stem cell accumulation, and a mesenchymal phenotype*. Neuro Oncol, 2012. **14**(11): p. 1379-92.
88. Bazzoni, R. and A. Bentivegna, *Role of Notch Signaling Pathway in Glioblastoma Pathogenesis*. Cancers (Basel), 2019. **11**(3).

89. Stockhausen, M.T., K. Kristoffersen, and H.S. Poulsen, *Notch signaling and brain tumors*. Adv Exp Med Biol, 2012. **727**: p. 289-304.
90. Teodorczyk, M. and M.H.H. Schmidt, *Notching on Cancer's Door: Notch Signaling in Brain Tumors*. Front Oncol, 2014. **4**: p. 341.
91. Paul, I., et al., *Current Understanding on EGFR and Wnt/beta-Catenin Signaling in Glioma and Their Possible Crosstalk*. Genes Cancer, 2013. **4**(11-12): p. 427-46.
92. Charles, N.A., et al., *The brain tumor microenvironment*. Glia, 2012. **60**(3): p. 502-14.
93. Mentlein, R., K. Hattermann, and J. Held-Feindt, *Lost in disruption: role of proteases in glioma invasion and progression*. Biochim Biophys Acta, 2012. **1825**(2): p. 178-85.
94. Singh, S.K., et al., *Identification of a cancer stem cell in human brain tumors*. Cancer Res, 2003. **63**(18): p. 5821-8.
95. Singh, S.K., et al., *Identification of human brain tumour initiating cells*. Nature, 2004. **432**(7015): p. 396-401.
96. Bao, S., et al., *Glioma stem cells promote radioresistance by preferential activation of the DNA damage response*. Nature, 2006. **444**(7120): p. 756-60.
97. Seymour, T., A. Nowak, and F. Kakulas, *Targeting Aggressive Cancer Stem Cells in Glioblastoma*. Front Oncol, 2015. **5**: p. 159.
98. Bleau, A.M., et al., *PTEN/PI3K/Akt pathway regulates the side population phenotype and ABCG2 activity in glioma tumor stem-like cells*. Cell Stem Cell, 2009. **4**(3): p. 226-35.
99. Liu, G., et al., *Analysis of gene expression and chemoresistance of CD133+ cancer stem cells in glioblastoma*. Mol Cancer, 2006. **5**: p. 67.
100. Chen, J., et al., *A restricted cell population propagates glioblastoma growth after chemotherapy*. Nature, 2012. **488**(7412): p. 522-6.
101. Olmez, I., et al., *Dedifferentiation of patient-derived glioblastoma multiforme cell lines results in a cancer stem cell-like state with mitogen-independent growth*. J Cell Mol Med, 2015. **19**(6): p. 1262-72.
102. Nakayama, M., et al., *Side population cell fractions from hepatocellular carcinoma cell lines increased with tumor dedifferentiation, but lack characteristic features of cancer stem cells*. J Gastroenterol Hepatol, 2014. **29**(5): p. 1092-101.
103. Nakano, M., et al., *Dedifferentiation process driven by TGF-beta signaling enhances stem cell properties in human colorectal cancer*. Oncogene, 2019. **38**(6): p. 780-793.
104. Oren, O. and B.D. Smith, *Eliminating Cancer Stem Cells by Targeting Embryonic Signaling Pathways*. Stem Cell Rev, 2017. **13**(1): p. 17-23.
105. Koury, J., L. Zhong, and J. Hao, *Targeting Signaling Pathways in Cancer Stem Cells for Cancer Treatment*. Stem Cells Int, 2017. **2017**: p. 2925869.
106. Dreesen, O. and A.H. Brivanlou, *Signaling pathways in cancer and embryonic stem cells*. Stem Cell Rev, 2007. **3**(1): p. 7-17.
107. Hu, Y.Y., et al., *Hif-1alpha and Hif-2alpha differentially regulate Notch signaling through competitive interaction with the intracellular domain of Notch receptors in glioma stem cells*. Cancer Lett, 2014. **349**(1): p. 67-76.
108. Ruggero, D., *Translational control in cancer etiology*. Cold Spring Harb Perspect Biol, 2013. **5**(2).
109. Xue, S. and M. Barna, *Specialized ribosomes: a new frontier in gene regulation and organismal biology*. Nat Rev Mol Cell Biol, 2012. **13**(6): p. 355-69.
110. Truitt, M.L. and D. Ruggero, *New frontiers in translational control of the cancer genome*. Nat Rev Cancer, 2016. **16**(5): p. 288-304.

111. Bhat, M., et al., *Targeting the translation machinery in cancer*. Nat Rev Drug Discov, 2015. **14**(4): p. 261-78.
112. Lacerda, R., J. Menezes, and L. Romao, *More than just scanning: the importance of cap-independent mRNA translation initiation for cellular stress response and cancer*. Cell Mol Life Sci, 2017. **74**(9): p. 1659-1680.
113. Weingarten-Gabbay, S., et al., *Comparative genetics. Systematic discovery of cap-independent translation sequences in human and viral genomes*. Science, 2016. **351**(6270).
114. Pelletier, J. and N. Sonenberg, *Internal initiation of translation of eukaryotic mRNA directed by a sequence derived from poliovirus RNA*. Nature, 1988. **334**(6180): p. 320-5.
115. Hellen, C.U., *IRES-induced conformational changes in the ribosome and the mechanism of translation initiation by internal ribosomal entry*. Biochim Biophys Acta, 2009. **1789**(9-10): p. 558-70.
116. King, H.A., L.C. Cobbold, and A.E. Willis, *The role of IRES trans-acting factors in regulating translation initiation*. Biochem Soc Trans, 2010. **38**(6): p. 1581-6.
117. Spriggs, K.A., M. Bushell, and A.E. Willis, *Translational regulation of gene expression during conditions of cell stress*. Mol Cell, 2010. **40**(2): p. 228-37.
118. Jackson, R.J., C.U. Hellen, and T.V. Pestova, *The mechanism of eukaryotic translation initiation and principles of its regulation*. Nat Rev Mol Cell Biol, 2010. **11**(2): p. 113-27.
119. Browne, G.J. and C.G. Proud, *A novel mTOR-regulated phosphorylation site in elongation factor 2 kinase modulates the activity of the kinase and its binding to calmodulin*. Mol Cell Biol, 2004. **24**(7): p. 2986-97.
120. Das, F., et al., *TGFbeta enforces activation of eukaryotic elongation factor-2 (eEF2) via inactivation of eEF2 kinase by p90 ribosomal S6 kinase (p90Rsk) to induce mesangial cell hypertrophy*. FEBS Lett, 2010. **584**(19): p. 4268-72.
121. Marintchev, A., *Fidelity and quality control in gene expression. Preface*. Adv Protein Chem Struct Biol, 2012. **86**: p. ix.
122. Rau, M., et al., *A reevaluation of the cap-binding protein, eIF4E, as a rate-limiting factor for initiation of translation in reticulocyte lysate*. J Biol Chem, 1996. **271**(15): p. 8983-90.
123. Haghightat, A., et al., *Repression of cap-dependent translation by 4E-binding protein 1: competition with p220 for binding to eukaryotic initiation factor-4E*. EMBO J, 1995. **14**(22): p. 5701-9.
124. Waskiewicz, A.J., et al., *Phosphorylation of the cap-binding protein eukaryotic translation initiation factor 4E by protein kinase Mnk1 in vivo*. Mol Cell Biol, 1999. **19**(3): p. 1871-80.
125. Minich, W.B., et al., *Chromatographic resolution of in vivo phosphorylated and nonphosphorylated eukaryotic translation initiation factor eIF-4E: increased cap affinity of the phosphorylated form*. Proc Natl Acad Sci U S A, 1994. **91**(16): p. 7668-72.
126. Wang, X., et al., *The phosphorylation of eukaryotic initiation factor eIF4E in response to phorbol esters, cell stresses, and cytokines is mediated by distinct MAP kinase pathways*. J Biol Chem, 1998. **273**(16): p. 9373-7.
127. Fukunaga, R. and T. Hunter, *MNK1, a new MAP kinase-activated protein kinase, isolated by a novel expression screening method for identifying protein kinase substrates*. EMBO J, 1997. **16**(8): p. 1921-33.
128. Wheeler, M.J., P.W. Johnson, and J.P. Blaydes, *The role of MNK proteins and eIF4E phosphorylation in breast cancer cell proliferation and survival*. Cancer Biol Ther, 2010. **10**(7): p. 728-35.
129. D'Abronzio, L.S. and P.M. Ghosh, *eIF4E Phosphorylation in Prostate Cancer*. Neoplasia, 2018. **20**(6): p. 563-573.
130. Furic, L., et al., *eIF4E phosphorylation promotes tumorigenesis and is associated with prostate cancer progression*. Proc Natl Acad Sci U S A, 2010. **107**(32): p. 14134-9.

131. Yoshizawa, A., et al., *Overexpression of phospho-eIF4E is associated with survival through AKT pathway in non-small cell lung cancer*. Clin Cancer Res, 2010. **16**(1): p. 240-8.
132. Pettersson, F., et al., *Genetic and pharmacologic inhibition of eIF4E reduces breast cancer cell migration, invasion, and metastasis*. Cancer Res, 2015. **75**(6): p. 1102-12.
133. Robichaud, N., et al., *Phosphorylation of eIF4E promotes EMT and metastasis via translational control of SNAIL and MMP-3*. Oncogene, 2015. **34**(16): p. 2032-42.
134. Bianchini, A., et al., *Phosphorylation of eIF4E by MNKs supports protein synthesis, cell cycle progression and proliferation in prostate cancer cells*. Carcinogenesis, 2008. **29**(12): p. 2279-88.
135. Jones, R.M., et al., *An essential E box in the promoter of the gene encoding the mRNA cap-binding protein (eukaryotic initiation factor 4E) is a target for activation by c-myc*. Mol Cell Biol, 1996. **16**(9): p. 4754-64.
136. Lin, C.J., et al., *c-Myc and eIF4F are components of a feedforward loop that links transcription and translation*. Cancer Res, 2008. **68**(13): p. 5326-34.
137. Rosenwald, I.B., et al., *Increased expression of eukaryotic translation initiation factors eIF-4E and eIF-2 alpha in response to growth induction by c-myc*. Proc Natl Acad Sci U S A, 1993. **90**(13): p. 6175-8.
138. Choi, K.M., L.P. McMahon, and J.C. Lawrence, Jr., *Two motifs in the translational repressor PHAS-I required for efficient phosphorylation by mammalian target of rapamycin and for recognition by raptor*. J Biol Chem, 2003. **278**(22): p. 19667-73.
139. Brunn, G.J., et al., *Phosphorylation of the translational repressor PHAS-I by the mammalian target of rapamycin*. Science, 1997. **277**(5322): p. 99-101.
140. Jiang, H., et al., *Expression of constitutively active 4EBP-1 enhances p27Kip1 expression and inhibits proliferation of MCF7 breast cancer cells*. Cancer Cell Int, 2003. **3**(1): p. 2.
141. Hsieh, A.C., et al., *Genetic dissection of the oncogenic mTOR pathway reveals druggable addiction to translational control via 4EBP-eIF4E*. Cancer Cell, 2010. **17**(3): p. 249-61.
142. Rogers, G.W., Jr., N.J. Richter, and W.C. Merrick, *Biochemical and kinetic characterization of the RNA helicase activity of eukaryotic initiation factor 4A*. J Biol Chem, 1999. **274**(18): p. 12236-44.
143. Bi, X. and D.J. Goss, *Wheat germ poly(A)-binding protein increases the ATPase and the RNA helicase activity of translation initiation factors eIF4A, eIF4B, and eIF-iso4F*. J Biol Chem, 2000. **275**(23): p. 17740-6.
144. Raught, B., et al., *Phosphorylation of eucaryotic translation initiation factor 4B Ser422 is modulated by S6 kinases*. EMBO J, 2004. **23**(8): p. 1761-9.
145. Shahbazian, D., et al., *The mTOR/PI3K and MAPK pathways converge on eIF4B to control its phosphorylation and activity*. EMBO J, 2006. **25**(12): p. 2781-91.
146. Wolfe, A.L., et al., *RNA G-quadruplexes cause eIF4A-dependent oncogene translation in cancer*. Nature, 2014. **513**(7516): p. 65-70.
147. Tsai, B.P., et al., *A novel Bcr-Abl-mTOR-eIF4A axis regulates IRES-mediated translation of LEF-1*. Open Biol, 2014. **4**(11): p. 140180.
148. Wang, X., et al., *Regulation of elongation factor 2 kinase by p90(RSK1) and p70 S6 kinase*. EMBO J, 2001. **20**(16): p. 4370-9.
149. Smith, E.M. and C.G. Proud, *cdc2-cyclin B regulates eEF2 kinase activity in a cell cycle- and amino acid-dependent manner*. EMBO J, 2008. **27**(7): p. 1005-16.
150. Hizli, A.A., et al., *Phosphorylation of eukaryotic elongation factor 2 (eEF2) by cyclin A-cyclin-dependent kinase 2 regulates its inhibition by eEF2 kinase*. Mol Cell Biol, 2013. **33**(3): p. 596-604.
151. Leprivier, G., et al., *The eEF2 kinase confers resistance to nutrient deprivation by blocking translation elongation*. Cell, 2013. **153**(5): p. 1064-79.

152. Price, N.T. and C.G. Proud, *Phosphorylation of protein synthesis initiation factor-2. Identification of the site in the alpha-subunit phosphorylated in reticulocyte lysates*. *Biochim Biophys Acta*, 1990. **1054**(1): p. 83-8.
153. Pathak, V.K., D. Schindler, and J.W. Hershey, *Generation of a mutant form of protein synthesis initiation factor eIF-2 lacking the site of phosphorylation by eIF-2 kinases*. *Mol Cell Biol*, 1988. **8**(2): p. 993-5.
154. Walters, B. and S.R. Thompson, *Cap-Independent Translational Control of Carcinogenesis*. *Front Oncol*, 2016. **6**: p. 128.
155. Spriggs, K.A., et al., *Re-programming of translation following cell stress allows IRES-mediated translation to predominate*. *Biol Cell*, 2008. **100**(1): p. 27-38.
156. Stoneley, M., et al., *C-Myc 5' untranslated region contains an internal ribosome entry segment*. *Oncogene*, 1998. **16**(3): p. 423-8.
157. Paulin, F.E., et al., *Aberrant translational control of the c-myc gene in multiple myeloma*. *Oncogene*, 1996. **13**(3): p. 505-13.
158. Paulin, F.E., S.A. Chappell, and A.E. Willis, *A single nucleotide change in the c-myc internal ribosome entry segment leads to enhanced binding of a group of protein factors*. *Nucleic Acids Res*, 1998. **26**(13): p. 3097-103.
159. Chappell, S.A., et al., *A mutation in the c-myc-IRES leads to enhanced internal ribosome entry in multiple myeloma: a novel mechanism of oncogene de-regulation*. *Oncogene*, 2000. **19**(38): p. 4437-40.
160. Lang, K.J., A. Kappel, and G.J. Goodall, *Hypoxia-inducible factor-1alpha mRNA contains an internal ribosome entry site that allows efficient translation during normoxia and hypoxia*. *Mol Biol Cell*, 2002. **13**(5): p. 1792-801.
161. Kumari, S., et al., *An RNA G-quadruplex in the 5' UTR of the NRAS proto-oncogene modulates translation*. *Nat Chem Biol*, 2007. **3**(4): p. 218-21.
162. Shahid, R., A. Bugaut, and S. Balasubramanian, *The BCL-2 5' untranslated region contains an RNA G-quadruplex-forming motif that modulates protein expression*. *Biochemistry*, 2010. **49**(38): p. 8300-6.
163. Morris, M.J., et al., *An RNA G-quadruplex is essential for cap-independent translation initiation in human VEGF IRES*. *J Am Chem Soc*, 2010. **132**(50): p. 17831-9.
164. Webb, T.E., et al., *An internal ribosome entry site in the 5' untranslated region of epidermal growth factor receptor allows hypoxic expression*. *Oncogenesis*, 2015. **4**: p. e134.
165. Perry, R.P., et al., *The methylated constituents of L cell messenger RNA: evidence for an unusual cluster at the 5' terminus*. *Cell*, 1975. **4**(4): p. 387-94.
166. Liu, N., et al., *Probing N6-methyladenosine RNA modification status at single nucleotide resolution in mRNA and long noncoding RNA*. *RNA*, 2013. **19**(12): p. 1848-56.
167. Wei, C.M., A. Gershowitz, and B. Moss, *Methylated nucleotides block 5' terminus of HeLa cell messenger RNA*. *Cell*, 1975. **4**(4): p. 379-86.
168. Visvanathan, A., et al., *Essential role of METTL3-mediated m(6)A modification in glioma stem-like cells maintenance and radioresistance*. *Oncogene*, 2018. **37**(4): p. 522-533.
169. Liu, J., et al., *A METTL3-METTL14 complex mediates mammalian nuclear RNA N6-adenosine methylation*. *Nat Chem Biol*, 2014. **10**(2): p. 93-5.
170. Wang, X., et al., *N6-methyladenosine-dependent regulation of messenger RNA stability*. *Nature*, 2014. **505**(7481): p. 117-20.
171. Jia, G., et al., *N6-methyladenosine in nuclear RNA is a major substrate of the obesity-associated FTO*. *Nat Chem Biol*, 2011. **7**(12): p. 885-7.

172. Zhang, S., et al., *m(6)A Demethylase ALKBH5 Maintains Tumorigenicity of Glioblastoma Stem-like Cells by Sustaining FOXM1 Expression and Cell Proliferation Program*. *Cancer Cell*, 2017. **31**(4): p. 591-606 e6.
173. Tang, C., et al., *ALKBH5-dependent m6A demethylation controls splicing and stability of long 3'-UTR mRNAs in male germ cells*. *Proc Natl Acad Sci U S A*, 2018. **115**(2): p. E325-E333.
174. Yang, S., et al., *m(6)A mRNA demethylase FTO regulates melanoma tumorigenicity and response to anti-PD-1 blockade*. *Nat Commun*, 2019. **10**(1): p. 2782.
175. Morris, D.R. and A.P. Geballe, *Upstream open reading frames as regulators of mRNA translation*. *Mol Cell Biol*, 2000. **20**(23): p. 8635-42.
176. Lohmer, S., et al., *Translation of the mRNA of the maize transcriptional activator Opaque-2 is inhibited by upstream open reading frames present in the leader sequence*. *Plant Cell*, 1993. **5**(1): p. 65-73.
177. Barbosa, C., I. Peixeiro, and L. Romao, *Gene expression regulation by upstream open reading frames and human disease*. *PLoS Genet*, 2013. **9**(8): p. e1003529.
178. Schuster, S.L. and A.C. Hsieh, *The Untranslated Regions of mRNAs in Cancer*. *Trends Cancer*, 2019. **5**(4): p. 245-262.
179. Pavon-Eternod, M., et al., *tRNA over-expression in breast cancer and functional consequences*. *Nucleic Acids Res*, 2009. **37**(21): p. 7268-80.
180. Wellman, T.L., et al., *Threonyl-tRNA synthetase overexpression correlates with angiogenic markers and progression of human ovarian cancer*. *BMC Cancer*, 2014. **14**: p. 620.
181. Thompson, D.M. and R. Parker, *Stressing out over tRNA cleavage*. *Cell*, 2009. **138**(2): p. 215-9.
182. Goodarzi, H., et al., *Endogenous tRNA-Derived Fragments Suppress Breast Cancer Progression via YBX1 Displacement*. *Cell*, 2015. **161**(4): p. 790-802.
183. Blanco, S., et al., *Aberrant methylation of tRNAs links cellular stress to neuro-developmental disorders*. *EMBO J*, 2014. **33**(18): p. 2020-39.
184. Frye, M. and F.M. Watt, *The RNA methyltransferase Misu (NSun2) mediates Myc-induced proliferation and is upregulated in tumors*. *Curr Biol*, 2006. **16**(10): p. 971-81.
185. Henderson, A.S., D. Warburton, and K.C. Atwood, *Location of ribosomal DNA in the human chromosome complement*. *Proc Natl Acad Sci U S A*, 1972. **69**(11): p. 3394-8.
186. Birch, J.L. and J.C. Zomerdijk, *Structure and function of ribosomal RNA gene chromatin*. *Biochem Soc Trans*, 2008. **36**(Pt 4): p. 619-24.
187. Schmickel, R.D., *Quantitation of human ribosomal DNA: hybridization of human DNA with ribosomal RNA for quantitation and fractionation*. *Pediatr Res*, 1973. **7**(1): p. 5-12.
188. Gibbons, J.G., et al., *Ribosomal DNA copy number is coupled with gene expression variation and mitochondrial abundance in humans*. *Nat Commun*, 2014. **5**: p. 4850.
189. O'Sullivan, J.M., et al., *The nucleolus: a raft adrift in the nuclear sea or the keystone in nuclear structure?* *Biomol Concepts*, 2013. **4**(3): p. 277-86.
190. Andersen, J.S., et al., *Nucleolar proteome dynamics*. *Nature*, 2005. **433**(7021): p. 77-83.
191. Gonzalez, I.L. and J.E. Sylvester, *Complete sequence of the 43-kb human ribosomal DNA repeat: analysis of the intergenic spacer*. *Genomics*, 1995. **27**(2): p. 320-8.
192. McStay, B. and I. Grummt, *The epigenetics of rRNA genes: from molecular to chromosome biology*. *Annu Rev Cell Dev Biol*, 2008. **24**: p. 131-57.
193. Zentner, G.E., et al., *Integrative genomic analysis of human ribosomal DNA*. *Nucleic Acids Res*, 2011. **39**(12): p. 4949-60.
194. Friedrich, J.K., et al., *TBP-TAF complex SL1 directs RNA polymerase I pre-initiation complex formation and stabilizes upstream binding factor at the rDNA promoter*. *J Biol Chem*, 2005. **280**(33): p. 29551-8.

195. Murano, K., et al., *Reconstitution of human rRNA gene transcription in mouse cells by a complete SL1 complex*. J Cell Sci, 2014. **127**(Pt 15): p. 3309-19.
196. Lin, C.Y., et al., *CK2-mediated stimulation of Pol I transcription by stabilization of UBF-SL1 interaction*. Nucleic Acids Res, 2006. **34**(17): p. 4752-66.
197. Zhai, W. and L. Comai, *A kinase activity associated with simian virus 40 large T antigen phosphorylates upstream binding factor (UBF) and promotes formation of a stable initiation complex between UBF and SL1*. Mol Cell Biol, 1999. **19**(4): p. 2791-802.
198. Stefanovsky, V.Y., et al., *ERK modulates DNA bending and enhances some structure by phosphorylating HMG1-boxes 1 and 2 of the RNA polymerase I transcription factor UBF*. Biochemistry, 2006. **45**(11): p. 3626-34.
199. Stefanovsky, V.Y. and T. Moss, *The splice variants of UBF differentially regulate RNA polymerase I transcription elongation in response to ERK phosphorylation*. Nucleic Acids Res, 2008. **36**(15): p. 5093-101.
200. Stefanovsky, V.Y., et al., *An immediate response of ribosomal transcription to growth factor stimulation in mammals is mediated by ERK phosphorylation of UBF*. Mol Cell, 2001. **8**(5): p. 1063-73.
201. Hannan, K.M., et al., *mTOR-dependent regulation of ribosomal gene transcription requires S6K1 and is mediated by phosphorylation of the carboxy-terminal activation domain of the nucleolar transcription factor UBF*. Mol Cell Biol, 2003. **23**(23): p. 8862-77.
202. Clos, J., D. Buttgerit, and I. Grummt, *A purified transcription factor (TIF-IB) binds to essential sequences of the mouse rDNA promoter*. Proc Natl Acad Sci U S A, 1986. **83**(3): p. 604-8.
203. Zhang, C., L. Comai, and D.L. Johnson, *PTEN represses RNA Polymerase I transcription by disrupting the SL1 complex*. Mol Cell Biol, 2005. **25**(16): p. 6899-911.
204. Chen, C., et al., *High frequency trans-splicing in a cell line producing spliced and polyadenylated RNA polymerase I transcripts from an rDNA-myc chimeric gene*. Nucleic Acids Res, 2005. **33**(7): p. 2332-42.
205. Li, Z. and S.R. Hann, *Nucleophosmin is essential for c-Myc nucleolar localization and c-Myc-mediated rDNA transcription*. Oncogene, 2013. **32**(15): p. 1988-94.
206. Liao, P., et al., *A positive feedback loop between EBP2 and c-Myc regulates rDNA transcription, cell proliferation, and tumorigenesis*. Cell Death Dis, 2014. **5**: p. e1032.
207. Shiue, C.N., R.G. Berkson, and A.P. Wright, *c-Myc induces changes in higher order rDNA structure on stimulation of quiescent cells*. Oncogene, 2009. **28**(16): p. 1833-42.
208. Grandori, C., et al., *c-Myc binds to human ribosomal DNA and stimulates transcription of rRNA genes by RNA polymerase I*. Nat Cell Biol, 2005. **7**(3): p. 311-8.
209. Jung, J.H., et al., *Melatonin Suppresses the Expression of 45S Preribosomal RNA and Upstream Binding Factor and Enhances the Antitumor Activity of Puromycin in MDA-MB-231 Breast Cancer Cells*. Evid Based Complement Alternat Med, 2013. **2013**: p. 879746.
210. Huang, R., et al., *Upstream binding factor up-regulated in hepatocellular carcinoma is related to the survival and cisplatin-sensitivity of cancer cells*. FASEB J, 2002. **16**(3): p. 293-301.
211. Poortinga, G., et al., *MAD1 and c-MYC regulate UBF and rDNA transcription during granulocyte differentiation*. EMBO J, 2004. **23**(16): p. 3325-35.
212. Lackmann, F., et al., *Maturation of the 90S pre-ribosome requires Mrd1 dependent U3 snoRNA and 35S pre-rRNA structural rearrangements*. Nucleic Acids Res, 2018. **46**(7): p. 3692-3706.
213. Padilla, P.I., et al., *Association of guanine nucleotide-exchange protein BIG1 in HepG2 cell nuclei with nucleolin, U3 snoRNA, and fibrillarin*. Proc Natl Acad Sci U S A, 2008. **105**(9): p. 3357-61.
214. Brule, F., et al., *The yeast Hansenula wingei U3 snoRNA gene contains an intron and its coding sequence co-evolved with the 5' ETS region of the pre-ribosomal RNA*. RNA, 1996. **2**(2): p. 183-97.

215. Michot, B., et al., *Evolutionarily conserved structural features in the ITS2 of mammalian pre-rRNAs and potential interactions with the snoRNA U8 detected by comparative analysis of new mouse sequences*. Nucleic Acids Res, 1999. **27**(11): p. 2271-82.
216. Tomasevic, N. and B. Peculis, *Identification of a U8 snoRNA-specific binding protein*. J Biol Chem, 1999. **274**(50): p. 35914-20.
217. Dunbar, D.A. and S.J. Baserga, *The U14 snoRNA is required for 2'-O-methylation of the pre-18S rRNA in Xenopus oocytes*. RNA, 1998. **4**(2): p. 195-204.
218. Decatur, W.A. and M.J. Fournier, *rRNA modifications and ribosome function*. Trends Biochem Sci, 2002. **27**(7): p. 344-51.
219. Maden, B.E., et al., *Classical and novel approaches to the detection and localization of the numerous modified nucleotides in eukaryotic ribosomal RNA*. Biochimie, 1995. **77**(1-2): p. 22-9.
220. Taoka, M., et al., *Landscape of the complete RNA chemical modifications in the human 80S ribosome*. Nucleic Acids Res, 2018. **46**(18): p. 9289-9298.
221. Bachellerie, J.P., J. Cavaille, and A. Huttenhofer, *The expanding snoRNA world*. Biochimie, 2002. **84**(8): p. 775-90.
222. Samarsky, D.A., et al., *The snoRNA box C/D motif directs nucleolar targeting and also couples snoRNA synthesis and localization*. EMBO J, 1998. **17**(13): p. 3747-57.
223. Speckmann, W.A., R.M. Terns, and M.P. Terns, *The box C/D motif directs snoRNA 5'-cap hypermethylation*. Nucleic Acids Res, 2000. **28**(22): p. 4467-73.
224. Ganot, P., M. Caizergues-Ferrer, and T. Kiss, *The family of box ACA small nucleolar RNAs is defined by an evolutionarily conserved secondary structure and ubiquitous sequence elements essential for RNA accumulation*. Genes Dev, 1997. **11**(7): p. 941-56.
225. Henras, A.K., et al., *An overview of pre-ribosomal RNA processing in eukaryotes*. Wiley Interdiscip Rev RNA, 2015. **6**(2): p. 225-42.
226. Charette, M. and M.W. Gray, *Pseudouridine in RNA: what, where, how, and why*. IUBMB Life, 2000. **49**(5): p. 341-51.
227. Liang, X.H., Q. Liu, and M.J. Fournier, *rRNA modifications in an intersubunit bridge of the ribosome strongly affect both ribosome biogenesis and activity*. Mol Cell, 2007. **28**(6): p. 965-77.
228. Ali, I.K., et al., *Deletion of a conserved, central ribosomal intersubunit RNA bridge*. Mol Cell, 2006. **23**(6): p. 865-74.
229. Liu, Q. and K. Fredrick, *Roles of helix H69 of 23S rRNA in translation initiation*. Proc Natl Acad Sci U S A, 2015. **112**(37): p. 11559-64.
230. King, T.H., et al., *Ribosome structure and activity are altered in cells lacking snoRNPs that form pseudouridines in the peptidyl transferase center*. Mol Cell, 2003. **11**(2): p. 425-35.
231. Ofengand, J., *Ribosomal RNA pseudouridines and pseudouridine synthases*. FEBS Lett, 2002. **514**(1): p. 17-25.
232. Liang, X.H., Q. Liu, and M.J. Fournier, *Loss of rRNA modifications in the decoding center of the ribosome impairs translation and strongly delays pre-rRNA processing*. RNA, 2009. **15**(9): p. 1716-28.
233. Kawai, G., et al., *Conformational rigidity of specific pyrimidine residues in tRNA arises from posttranscriptional modifications that enhance steric interaction between the base and the 2'-hydroxyl group*. Biochemistry, 1992. **31**(4): p. 1040-6.
234. Polikanov, Y.S., et al., *Structural insights into the role of rRNA modifications in protein synthesis and ribosome assembly*. Nat Struct Mol Biol, 2015. **22**(4): p. 342-344.
235. Esguerra, J., J. Warringer, and A. Blomberg, *Functional importance of individual rRNA 2'-O-ribose methylations revealed by high-resolution phenotyping*. RNA, 2008. **14**(4): p. 649-56.

236. Ignatova, V.V., et al., *The rRNA m(6)A methyltransferase METTL5 is involved in pluripotency and developmental programs*. *Genes Dev*, 2020. **34**(9-10): p. 715-729.
237. van Tran, N., et al., *The human 18S rRNA m6A methyltransferase METTL5 is stabilized by TRMT112*. *Nucleic Acids Res*, 2019. **47**(15): p. 7719-7733.
238. Sharma, S., et al., *Yeast Nop2 and Rcm1 methylate C2870 and C2278 of the 25S rRNA, respectively*. *Nucleic Acids Res*, 2013. **41**(19): p. 9062-76.
239. Pelletier, J., G. Thomas, and S. Volarevic, *Ribosome biogenesis in cancer: new players and therapeutic avenues*. *Nat Rev Cancer*, 2018. **18**(1): p. 51-63.
240. Drygin, D., W.G. Rice, and I. Grummt, *The RNA polymerase I transcription machinery: an emerging target for the treatment of cancer*. *Annu Rev Pharmacol Toxicol*, 2010. **50**: p. 131-56.
241. Zhao, J., et al., *ERK-dependent phosphorylation of the transcription initiation factor TIF-IA is required for RNA polymerase I transcription and cell growth*. *Mol Cell*, 2003. **11**(2): p. 405-13.
242. Voit, R., M. Hoffmann, and I. Grummt, *Phosphorylation by G1-specific cdk-cyclin complexes activates the nucleolar transcription factor UBF*. *EMBO J*, 1999. **18**(7): p. 1891-9.
243. Voit, R. and I. Grummt, *Phosphorylation of UBF at serine 388 is required for interaction with RNA polymerase I and activation of rDNA transcription*. *Proc Natl Acad Sci U S A*, 2001. **98**(24): p. 13631-6.
244. Panov, K.I., J.K. Friedrich, and J.C. Zomerdijs, *A step subsequent to preinitiation complex assembly at the ribosomal RNA gene promoter is rate limiting for human RNA polymerase I-dependent transcription*. *Mol Cell Biol*, 2001. **21**(8): p. 2641-9.
245. Arabi, A., et al., *c-Myc associates with ribosomal DNA and activates RNA polymerase I transcription*. *Nat Cell Biol*, 2005. **7**(3): p. 303-10.
246. Poortinga, G., L.M. Quinn, and R.D. Hannan, *Targeting RNA polymerase I to treat MYC-driven cancer*. *Oncogene*, 2015. **34**(4): p. 403-12.
247. Ruggero, D., *The role of Myc-induced protein synthesis in cancer*. *Cancer Res*, 2009. **69**(23): p. 8839-43.
248. Heix, J., et al., *Mitotic silencing of human rRNA synthesis: inactivation of the promoter selectivity factor SL1 by cdc2/cyclin B-mediated phosphorylation*. *EMBO J*, 1998. **17**(24): p. 7373-81.
249. Zhai, W. and L. Comai, *Repression of RNA polymerase I transcription by the tumor suppressor p53*. *Mol Cell Biol*, 2000. **20**(16): p. 5930-8.
250. Budde, A. and I. Grummt, *p53 represses ribosomal gene transcription*. *Oncogene*, 1999. **18**(4): p. 1119-24.
251. Feng, L., et al., *Ribosomal DNA copy number is associated with P53 status and levels of heavy metals in gastrectomy specimens from gastric cancer patients*. *Environ Int*, 2020. **138**: p. 105593.
252. Jayaraman, S., et al., *The nuclear mitotic apparatus protein NuMA controls rDNA transcription and mediates the nucleolar stress response in a p53-independent manner*. *Nucleic Acids Res*, 2017. **45**(20): p. 11725-11742.
253. Su, H., et al., *Elevated snoRNA biogenesis is essential in breast cancer*. *Oncogene*, 2014. **33**(11): p. 1348-58.
254. Koh, C.M., et al., *Alterations in nucleolar structure and gene expression programs in prostatic neoplasia are driven by the MYC oncogene*. *Am J Pathol*, 2011. **178**(4): p. 1824-34.
255. Choi, Y.W., et al., *Identification of differentially expressed genes using annealing control primer-based GeneFishing in human squamous cell cervical carcinoma*. *Clin Oncol (R Coll Radiol)*, 2007. **19**(5): p. 308-18.
256. Marcel, V., et al., *p53 acts as a safeguard of translational control by regulating fibrillarin and rRNA methylation in cancer*. *Cancer Cell*, 2013. **24**(3): p. 318-30.

257. Eralles, J., et al., *Evidence for rRNA 2'-O-methylation plasticity: Control of intrinsic translational capabilities of human ribosomes*. Proc Natl Acad Sci U S A, 2017. **114**(49): p. 12934-12939.
258. Barna, M., et al., *Suppression of Myc oncogenic activity by ribosomal protein haploinsufficiency*. Nature, 2008. **456**(7224): p. 971-5.
259. Hou, P., et al., *DKC1 enhances angiogenesis by promoting HIF-1alpha transcription and facilitates metastasis in colorectal cancer*. Br J Cancer, 2020. **122**(5): p. 668-679.
260. Miao, F.A., et al., *Increased DKC1 expression in glioma and its significance in tumor cell proliferation, migration and invasion*. Invest New Drugs, 2019. **37**(6): p. 1177-1186.
261. Yoon, A., et al., *Impaired control of IRES-mediated translation in X-linked dyskeratosis congenita*. Science, 2006. **312**(5775): p. 902-6.
262. Ruggero, D., et al., *Dyskeratosis congenita and cancer in mice deficient in ribosomal RNA modification*. Science, 2003. **299**(5604): p. 259-62.
263. Montanaro, L., et al., *Novel dyskerin-mediated mechanism of p53 inactivation through defective mRNA translation*. Cancer Res, 2010. **70**(11): p. 4767-77.
264. Alawi, F. and M.N. Lee, *DKC1 is a direct and conserved transcriptional target of c-MYC*. Biochem Biophys Res Commun, 2007. **362**(4): p. 893-8.
265. Ge, J., et al., *Dyskerin ablation in mouse liver inhibits rRNA processing and cell division*. Mol Cell Biol, 2010. **30**(2): p. 413-22.
266. Liang, J., et al., *Knockdown of ribosomal protein S15A inhibits human kidney cancer cell growth in vitro and in vivo*. Mol Med Rep, 2019. **19**(2): p. 1117-1127.
267. Yang, M., et al., *Down-regulation of ribosomal protein L22 in non-small cell lung cancer*. Med Oncol, 2013. **30**(3): p. 646.
268. Huang, C.J., et al., *Faecal ribosomal protein L19 is a genetic prognostic factor for survival in colorectal cancer*. J Cell Mol Med, 2008. **12**(5B): p. 1936-43.
269. Kobayashi, T., et al., *Activation of the ribosomal protein L13 gene in human gastrointestinal cancer*. Int J Mol Med, 2006. **18**(1): p. 161-70.
270. Wang, H., et al., *Overexpression of ribosomal protein L15 is associated with cell proliferation in gastric cancer*. BMC Cancer, 2006. **6**: p. 91.
271. Hong, M., H. Kim, and I. Kim, *Ribosomal protein L19 overexpression activates the unfolded protein response and sensitizes MCF7 breast cancer cells to endoplasmic reticulum stress-induced cell death*. Biochem Biophys Res Commun, 2014. **450**(1): p. 673-8.
272. Shi, Z., et al., *Heterogeneous Ribosomes Preferentially Translate Distinct Subpools of mRNAs Genome-wide*. Mol Cell, 2017. **67**(1): p. 71-83 e7.
273. Holmberg Olausson, K., M. Nister, and M.S. Lindstrom, *p53 -Dependent and -Independent Nucleolar Stress Responses*. Cells, 2012. **1**(4): p. 774-98.
274. Sasaki, M., et al., *Regulation of the MDM2-P53 pathway and tumor growth by PICT1 via nucleolar RPL11*. Nat Med, 2011. **17**(8): p. 944-51.
275. Gigova, A., et al., *A cluster of methylations in the domain IV of 25S rRNA is required for ribosome stability*. RNA, 2014. **20**(10): p. 1632-44.
276. Boccaletto, P., et al., *MODOMICS: a database of RNA modification pathways. 2017 update*. Nucleic Acids Res, 2018. **46**(D1): p. D303-D307.
277. Delaunay, S. and M. Frye, *RNA modifications regulating cell fate in cancer*. Nat Cell Biol, 2019. **21**(5): p. 552-559.
278. Zaccara, S., R.J. Ries, and S.R. Jaffrey, *Reading, writing and erasing mRNA methylation*. Nat Rev Mol Cell Biol, 2019. **20**(10): p. 608-624.

279. Zhao, B.S., I.A. Roundtree, and C. He, *Post-transcriptional gene regulation by mRNA modifications*. Nat Rev Mol Cell Biol, 2017. **18**(1): p. 31-42.
280. Boriack-Sjodin, P.A., S. Ribich, and R.A. Copeland, *RNA-modifying proteins as anticancer drug targets*. Nat Rev Drug Discov, 2018. **17**(6): p. 435-453.
281. Pan, T., *Modifications and functional genomics of human transfer RNA*. Cell Res, 2018. **28**(4): p. 395-404.
282. Cantara, W.A., et al., *The RNA Modification Database, RNAMDB: 2011 update*. Nucleic Acids Res, 2011. **39**(Database issue): p. D195-201.
283. Rezgui, V.A., et al., *tRNA tKUUU, tQUUG, and tEUUC wobble position modifications fine-tune protein translation by promoting ribosome A-site binding*. Proc Natl Acad Sci U S A, 2013. **110**(30): p. 12289-94.
284. Nakano, S., et al., *NSUN3 methylase initiates 5-formylcytidine biogenesis in human mitochondrial tRNA(Met)*. Nat Chem Biol, 2016. **12**(7): p. 546-51.
285. Tsutsumi, S., et al., *Wobble inosine tRNA modification is essential to cell cycle progression in G(1)/S and G(2)/M transitions in fission yeast*. J Biol Chem, 2007. **282**(46): p. 33459-33465.
286. Lamichhane, T.N., et al., *Lack of tRNA modification isopentenyl-A37 alters mRNA decoding and causes metabolic deficiencies in fission yeast*. Mol Cell Biol, 2013. **33**(15): p. 2918-29.
287. Tuorto, F., et al., *The tRNA methyltransferase Dnmt2 is required for accurate polypeptide synthesis during haematopoiesis*. EMBO J, 2015. **34**(18): p. 2350-62.
288. Arluison, V., M. Buckle, and H. Grosjean, *Pseudouridine synthetase Pus1 of Saccharomyces cerevisiae: kinetic characterisation, tRNA structural requirement and real-time analysis of its complex with tRNA*. J Mol Biol, 1999. **289**(3): p. 491-502.
289. Simos, G., et al., *Nuclear pore proteins are involved in the biogenesis of functional tRNA*. EMBO J, 1996. **15**(9): p. 2270-84.
290. Grosshans, H., et al., *Pus1p-dependent tRNA pseudouridylation becomes essential when tRNA biogenesis is compromised in yeast*. J Biol Chem, 2001. **276**(49): p. 46333-9.
291. Carlile, T.M., et al., *Pseudouridine profiling reveals regulated mRNA pseudouridylation in yeast and human cells*. Nature, 2014. **515**(7525): p. 143-6.
292. Yang, X., et al., *5-methylcytosine promotes mRNA export - NSUN2 as the methyltransferase and ALYREF as an m(5)C reader*. Cell Res, 2017. **27**(5): p. 606-625.
293. Mauer, J., et al., *Reversible methylation of m(6)Am in the 5' cap controls mRNA stability*. Nature, 2017. **541**(7637): p. 371-375.
294. Safra, M., et al., *The m1A landscape on cytosolic and mitochondrial mRNA at single-base resolution*. Nature, 2017. **551**(7679): p. 251-255.
295. Mao, Y., et al., *m(6)A in mRNA coding regions promotes translation via the RNA helicase-containing YTHDC2*. Nat Commun, 2019. **10**(1): p. 5332.
296. Ping, X.L., et al., *Mammalian WTAP is a regulatory subunit of the RNA N6-methyladenosine methyltransferase*. Cell Res, 2014. **24**(2): p. 177-89.
297. Patil, D.P., et al., *m(6)A RNA methylation promotes XIST-mediated transcriptional repression*. Nature, 2016. **537**(7620): p. 369-373.
298. Wang, X., et al., *N(6)-methyladenosine Modulates Messenger RNA Translation Efficiency*. Cell, 2015. **161**(6): p. 1388-99.
299. Kretschmer, J., et al., *The m(6)A reader protein YTHDC2 interacts with the small ribosomal subunit and the 5'-3' exoribonuclease XRN1*. RNA, 2018. **24**(10): p. 1339-1350.

300. Zou, F., et al., *Drosophila YBX1 homolog YPS promotes ovarian germ line stem cell development by preferentially recognizing 5-methylcytosine RNAs*. Proc Natl Acad Sci U S A, 2020. **117**(7): p. 3603-3609.
301. Chen, X., et al., *5-methylcytosine promotes pathogenesis of bladder cancer through stabilizing mRNAs*. Nat Cell Biol, 2019. **21**(8): p. 978-990.
302. Levy, N.S., et al., *Hypoxic stabilization of vascular endothelial growth factor mRNA by the RNA-binding protein HuR*. J Biol Chem, 1998. **273**(11): p. 6417-23.
303. Schwartz, S., et al., *Transcriptome-wide mapping reveals widespread dynamic-regulated pseudouridylation of ncRNA and mRNA*. Cell, 2014. **159**(1): p. 148-162.
304. Ma, H., et al., *N(6-Methyladenosine methyltransferase ZCCHC4 mediates ribosomal RNA methylation*. Nat Chem Biol, 2019. **15**(1): p. 88-94.
305. Roundtree, I.A., et al., *Dynamic RNA Modifications in Gene Expression Regulation*. Cell, 2017. **169**(7): p. 1187-1200.
306. Khoddami, V., A. Yerra, and B.R. Cairns, *Experimental Approaches for Target Profiling of RNA Cytosine Methyltransferases*. Methods Enzymol, 2015. **560**: p. 273-96.
307. Haag, S., et al., *NSUN6 is a human RNA methyltransferase that catalyzes formation of m5C72 in specific tRNAs*. RNA, 2015. **21**(9): p. 1532-43.
308. Van Haute, L., et al., *Deficient methylation and formylation of mt-tRNA(Met) wobble cytosine in a patient carrying mutations in NSUN3*. Nat Commun, 2016. **7**: p. 12039.
309. Khoddami, V. and B.R. Cairns, *Identification of direct targets and modified bases of RNA cytosine methyltransferases*. Nat Biotechnol, 2013. **31**(5): p. 458-64.
310. Squires, J.E., et al., *Widespread occurrence of 5-methylcytosine in human coding and non-coding RNA*. Nucleic Acids Res, 2012. **40**(11): p. 5023-33.
311. Motorin, Y., F. Lyko, and M. Helm, *5-methylcytosine in RNA: detection, enzymatic formation and biological functions*. Nucleic Acids Res, 2010. **38**(5): p. 1415-30.
312. Schosserer, M., et al., *Methylation of ribosomal RNA by NSUN5 is a conserved mechanism modulating organismal lifespan*. Nat Commun, 2015. **6**: p. 6158.
313. Haag, S., et al., *NSUN3 and ABH1 modify the wobble position of mt-tRNA<sup>Met</sup> to expand codon recognition in mitochondrial translation*. EMBO J, 2016. **35**(19): p. 2104-2119.
314. Popis, M.C., S. Blanco, and M. Frye, *Posttranscriptional methylation of transfer and ribosomal RNA in stress response pathways, cell differentiation, and cancer*. Curr Opin Oncol, 2016. **28**(1): p. 65-71.
315. Penzo, M., et al., *The importance of being (slightly) modified: The role of rRNA editing on gene expression control and its connections with cancer*. Biochim Biophys Acta, 2016. **1866**(2): p. 330-338.
316. Xue, C., Y. Zhao, and L. Li, *Advances in RNA cytosine-5 methylation: detection, regulatory mechanisms, biological functions and links to cancer*. Biomark Res, 2020. **8**: p. 43.
317. Blanco, S. and M. Frye, *Role of RNA methyltransferases in tissue renewal and pathology*. Curr Opin Cell Biol, 2014. **31**: p. 1-7.
318. Tang, H., et al., *NSun2 delays replicative senescence by repressing p27 (KIP1) translation and elevating CDK1 translation*. Aging (Albany NY), 2015. **7**(12): p. 1143-58.
319. Xing, J., et al., *NSun2 Promotes Cell Growth via Elevating Cyclin-Dependent Kinase 1 Translation*. Mol Cell Biol, 2015. **35**(23): p. 4043-52.
320. Zhang, X., et al., *The tRNA methyltransferase NSun2 stabilizes p16<sup>INK4</sup> mRNA by methylating the 3'-untranslated region of p16*. Nat Commun, 2012. **3**: p. 712.
321. Okamoto, M., et al., *Frequent increased gene copy number and high protein expression of tRNA (cytosine-5-)-methyltransferase (NSUN2) in human cancers*. DNA Cell Biol, 2012. **31**(5): p. 660-71.

322. Frye, M., et al., *Genomic gain of 5p15 leads to over-expression of Misu (NSUN2) in breast cancer.* Cancer Lett, 2010. **289**(1): p. 71-80.
323. Sun, Z., et al., *Aberrant NSUN2-mediated m(5)C modification of H19 lncRNA is associated with poor differentiation of hepatocellular carcinoma.* Oncogene, 2020. **39**(45): p. 6906-6919.
324. Diril, M.K., et al., *Cyclin-dependent kinase 1 (Cdk1) is essential for cell division and suppression of DNA re-replication but not for liver regeneration.* Proc Natl Acad Sci U S A, 2012. **109**(10): p. 3826-31.
325. Hussain, S., et al., *The nucleolar RNA methyltransferase Misu (NSun2) is required for mitotic spindle stability.* J Cell Biol, 2009. **186**(1): p. 27-40.
326. de Beus, E., et al., *Yeast NOP2 encodes an essential nucleolar protein with homology to a human proliferation marker.* J Cell Biol, 1994. **127**(6 Pt 2): p. 1799-813.
327. Kosi, N., et al., *Nop2 is expressed during proliferation of neural stem cells and in adult mouse and human brain.* Brain Res, 2015. **1597**: p. 65-76.
328. Wang, F., et al., *Oncofetal long noncoding RNA PVT1 promotes proliferation and stem cell-like property of hepatocellular carcinoma cells by stabilizing NOP2.* Hepatology, 2014. **60**(4): p. 1278-90.
329. Kong, W., et al., *Nucleolar protein NOP2/NSUN1 suppresses HIV-1 transcription and promotes viral latency by competing with Tat for TAR binding and methylation.* PLoS Pathog, 2020. **16**(3): p. e1008430.
330. Paramasivam, A., et al., *Novel Biallelic NSUN3 Variants Cause Early-Onset Mitochondrial Encephalomyopathy and Seizures.* J Mol Neurosci, 2020.
331. Trixl, L., et al., *RNA cytosine methyltransferase Nsun3 regulates embryonic stem cell differentiation by promoting mitochondrial activity.* Cell Mol Life Sci, 2018. **75**(8): p. 1483-1497.
332. Yakubovskaya, E., et al., *Structure of the essential MTERF4:NSUN4 protein complex reveals how an MTERF protein collaborates to facilitate rRNA modification.* Structure, 2012. **20**(11): p. 1940-7.
333. Spahr, H., et al., *Structure of the human MTERF4-NSUN4 protein complex that regulates mitochondrial ribosome biogenesis.* Proc Natl Acad Sci U S A, 2012. **109**(38): p. 15253-8.
334. Metodiev, M.D., et al., *NSUN4 is a dual function mitochondrial protein required for both methylation of 12S rRNA and coordination of mitoribosomal assembly.* PLoS Genet, 2014. **10**(2): p. e1004110.
335. Camara, Y., et al., *MTERF4 regulates translation by targeting the methyltransferase NSUN4 to the mammalian mitochondrial ribosome.* Cell Metab, 2011. **13**(5): p. 527-39.
336. Long, T., et al., *Sequence-specific and Shape-selective RNA Recognition by the Human RNA 5-Methylcytosine Methyltransferase NSun6.* J Biol Chem, 2016. **291**(46): p. 24293-24303.
337. Liu, R.J., et al., *Structural basis for substrate binding and catalytic mechanism of a human RNA:m5C methyltransferase NSun6.* Nucleic Acids Res, 2017. **45**(11): p. 6684-6697.
338. Ren, H.Y., et al., *Investigation of polymorphisms in exon7 of the NSUN7 gene among Chinese Han men with asthenospermia.* Genet Mol Res, 2015. **14**(3): p. 9261-8.
339. Khosronezhad, N., A. Hosseinzadeh Colagar, and S.M. Mortazavi, *The Nsun7 (A11337)-deletion mutation, causes reduction of its protein rate and associated with sperm motility defect in infertile men.* J Assist Reprod Genet, 2015. **32**(5): p. 807-15.
340. Khosronezhad, N., A.H. Colagar, and S.G. Jorsarayi, *T26248G-transversion mutation in exon7 of the putative methyltransferase Nsun7 gene causes a change in protein folding associated with reduced sperm motility in asthenospermic men.* Reprod Fertil Dev, 2015. **27**(3): p. 471-80.
341. Harris, T., et al., *Sperm motility defects and infertility in male mice with a mutation in Nsun7, a member of the Sun domain-containing family of putative RNA methyltransferases.* Biol Reprod, 2007. **77**(2): p. 376-82.
342. King, M.Y. and K.L. Redman, *RNA methyltransferases utilize two cysteine residues in the formation of 5-methylcytosine.* Biochemistry, 2002. **41**(37): p. 11218-25.

343. Li, Q., et al., *NSUN2-Mediated m5C Methylation and METTL3/METTL14-Mediated m6A Methylation Cooperatively Enhance p21 Translation*. J Cell Biochem, 2017. **118**(9): p. 2587-2598.
344. Tuorto, F., et al., *RNA cytosine methylation by Dnmt2 and NSun2 promotes tRNA stability and protein synthesis*. Nat Struct Mol Biol, 2012. **19**(9): p. 900-5.
345. Hussain, S., et al., *NSun2-mediated cytosine-5 methylation of vault noncoding RNA determines its processing into regulatory small RNAs*. Cell Rep, 2013. **4**(2): p. 255-61.
346. Kim, Y.W., et al., *Identification of prognostic gene signatures of glioblastoma: a study based on TCGA data analysis*. Neuro Oncol, 2013. **15**(7): p. 829-39.
347. Doll, A. and K.H. Grzeschik, *Characterization of two novel genes, WBSCR20 and WBSCR22, deleted in Williams-Beuren syndrome*. Cytogenet Cell Genet, 2001. **95**(1-2): p. 20-7.
348. Zhang, T., et al., *Cognitive deficits in mice lacking Nsun5, a cytosine-5 RNA methyltransferase, with impairment of oligodendrocyte precursor cells*. Glia, 2019. **67**(4): p. 688-702.
349. Yuan, Z., et al., *Agensis and Hypomyelination of Corpus Callosum in Mice Lacking Nsun5, an RNA Methyltransferase*. Cells, 2019. **8**(6).
350. Maden, B.E., *Locations of methyl groups in 28 S rRNA of Xenopus laevis and man. Clustering in the conserved core of molecule*. J Mol Biol, 1988. **201**(2): p. 289-314.
351. Liu, Q. and K. Fredrick, *Intersubunit Bridges of the Bacterial Ribosome*. J Mol Biol, 2016. **428**(10 Pt B): p. 2146-64.
352. Valle, M., et al., *Incorporation of aminoacyl-tRNA into the ribosome as seen by cryo-electron microscopy*. Nat Struct Biol, 2003. **10**(11): p. 899-906.
353. Wang, L., et al., *Allosteric control of the ribosome by small-molecule antibiotics*. Nat Struct Mol Biol, 2012. **19**(9): p. 957-63.
354. Gravendeel, L.A., et al., *Intrinsic gene expression profiles of gliomas are a better predictor of survival than histology*. Cancer Res, 2009. **69**(23): p. 9065-72.
355. Elsherbiny, M.E., et al., *omega-3 and omega-6 Fatty Acids Modulate Conventional and Atypical Protein Kinase C Activities in a Brain Fatty Acid Binding Protein Dependent Manner in Glioblastoma Multiforme*. Nutrients, 2018. **10**(4).
356. Bisgrove, D.A., et al., *Regulation of brain fatty acid-binding protein expression by differential phosphorylation of nuclear factor I in malignant glioma cell lines*. J Biol Chem, 2000. **275**(39): p. 30668-76.
357. Mita, R., et al., *B-FABP-expressing radial glial cells: the malignant glioma cell of origin?* Neoplasia, 2007. **9**(9): p. 734-44.
358. Kelly, J.J., et al., *Proliferation of human glioblastoma stem cells occurs independently of exogenous mitogens*. Stem Cells, 2009. **27**(8): p. 1722-33.
359. Cusulin, C., et al., *Precursor States of Brain Tumor Initiating Cell Lines Are Predictive of Survival in Xenografts and Associated with Glioblastoma Subtypes*. Stem Cell Reports, 2015. **5**(1): p. 1-9.
360. Zhou, J., et al., *Notch and TGFbeta form a positive regulatory loop and regulate EMT in epithelial ovarian cancer cells*. Cell Signal, 2016. **28**(8): p. 838-49.
361. Findlay, S.D., et al., *A Digital PCR-Based Method for Efficient and Highly Specific Screening of Genome Edited Cells*. PLoS One, 2016. **11**(4): p. e0153901.
362. Corpet, F., *Multiple sequence alignment with hierarchical clustering*. Nucleic Acids Res, 1988. **16**(22): p. 10881-90.
363. Sambrook, J. and D.W. Russell, *Calcium-phosphate-mediated Transfection of Eukaryotic Cells with Plasmid DNAs*. CSH Protoc, 2006. **2006**(1).
364. Li, L., et al., *DEAD Box 1 Facilitates Removal of RNA and Homologous Recombination at DNA Double-Strand Breaks*. Mol Cell Biol, 2016. **36**(22): p. 2794-2810.

365. Ates, G., et al., *Assaying Cellular Viability Using the Neutral Red Uptake Assay*. Methods Mol Biol, 2017. **1601**: p. 19-26.
366. Repetto, G., A. del Peso, and J.L. Zurita, *Neutral red uptake assay for the estimation of cell viability/cytotoxicity*. Nat Protoc, 2008. **3**(7): p. 1125-31.
367. Franken, N.A., et al., *Clonogenic assay of cells in vitro*. Nat Protoc, 2006. **1**(5): p. 2315-9.
368. Alberts, D.S., et al., *In-vitro clonogenic assay for predicting response of ovarian cancer to chemotherapy*. Lancet, 1980. **2**(8190): p. 340-2.
369. Shimizu, E., et al., *Correlation between drug sensitivity determined by clonogenic cell assay and clinical effect of chemotherapy in patients with primary lung cancer*. Gan, 1984. **75**(11): p. 1030-5.
370. Strayer, D.R. and S.B. Kahn, *Cancer chemotherapy using a clonogenic cell assay*. Am Fam Physician, 1983. **27**(4): p. 223-5.
371. Johnson, S., H. Chen, and P.K. Lo, *In vitro Tumorsphere Formation Assays*. Bio Protoc, 2013. **3**(3).
372. Jacobs, V.L., et al., *Current review of in vivo GBM rodent models: emphasis on the CNS-1 tumour model*. ASN Neuro, 2011. **3**(3): p. e00063.
373. Baumann, B.C., et al., *Stereotactic intracranial implantation and in vivo bioluminescent imaging of tumor xenografts in a mouse model system of glioblastoma multiforme*. J Vis Exp, 2012(67).
374. Wilcox, M.E., et al., *Reovirus as an oncolytic agent against experimental human malignant gliomas*. J Natl Cancer Inst, 2001. **93**(12): p. 903-12.
375. De Boeck, A., et al., *Glioma-derived IL-33 orchestrates an inflammatory brain tumor microenvironment that accelerates glioma progression*. Nat Commun, 2020. **11**(1): p. 4997.
376. Brun, M., et al., *Calcineurin regulates nuclear factor I dephosphorylation and activity in malignant glioma cell lines*. J Biol Chem, 2013. **288**(33): p. 24104-15.
377. Deliu, L.P., A. Ghosh, and S.S. Grewal, *Investigation of protein synthesis in Drosophila larvae using puromycin labelling*. Biol Open, 2017. **6**(8): p. 1229-1234.
378. Aviner, R., T. Geiger, and O. Elroy-Stein, *Genome-wide identification and quantification of protein synthesis in cultured cells and whole tissues by puromycin-associated nascent chain proteomics (PUNCH-P)*. Nat Protoc, 2014. **9**(4): p. 751-60.
379. Dieters-Castator, D.Z., et al., *Proteomics-Derived Biomarker Panel Improves Diagnostic Precision to Classify Endometrioid and High-grade Serous Ovarian Carcinoma*. Clin Cancer Res, 2019. **25**(14): p. 4309-4319.
380. Wessel, D. and U.I. Flugge, *A method for the quantitative recovery of protein in dilute solution in the presence of detergents and lipids*. Anal Biochem, 1984. **138**(1): p. 141-3.
381. Duan, X., et al., *A straightforward and highly efficient precipitation/on-pellet digestion procedure coupled with a long gradient nano-LC separation and Orbitrap mass spectrometry for label-free expression profiling of the swine heart mitochondrial proteome*. J Proteome Res, 2009. **8**(6): p. 2838-50.
382. UniProt, C., *UniProt: a hub for protein information*. Nucleic Acids Res, 2015. **43**(Database issue): p. D204-12.
383. Cox, J. and M. Mann, *MaxQuant enables high peptide identification rates, individualized p.p.b. -range mass accuracies and proteome-wide protein quantification*. Nat Biotechnol, 2008. **26**(12): p. 1367-72.
384. Lee, J., et al., *Tumor stem cells derived from glioblastomas cultured in bFGF and EGF more closely mirror the phenotype and genotype of primary tumors than do serum-cultured cell lines*. Cancer Cell, 2006. **9**(5): p. 391-403.
385. Allen, M., et al., *Origin of the U87MG glioma cell line: Good news and bad news*. Sci Transl Med, 2016. **8**(354): p. 354re3.

386. Serikawa, T., et al., *Comprehensive identification of proteins binding to RNA G-quadruplex motifs in the 5' UTR of tumor-associated mRNAs*. *Biochimie*, 2018. **144**: p. 169-184.
387. Heissenberger, C., et al., *Loss of the ribosomal RNA methyltransferase NSUN5 impairs global protein synthesis and normal growth*. *Nucleic Acids Res*, 2019. **47**(22): p. 11807-11825.
388. Filipowicz, W., et al., *Structure and biogenesis of small nucleolar RNAs acting as guides for ribosomal RNA modification*. *Acta Biochim Pol*, 1999. **46**(2): p. 377-89.
389. Watkins, N.J. and M.T. Bohnsack, *The box C/D and H/ACA snoRNPs: key players in the modification, processing and the dynamic folding of ribosomal RNA*. *Wiley Interdiscip Rev RNA*, 2012. **3**(3): p. 397-414.
390. Yang, J., et al., *Mapping of Complete Set of Ribose and Base Modifications of Yeast rRNA by RP-HPLC and Mung Bean Nuclease Assay*. *PLoS One*, 2016. **11**(12): p. e0168873.
391. Chi, L. and P. Delgado-Olguin, *Expression of NOL1/NOP2/sun domain (Nsun) RNA methyltransferase family genes in early mouse embryogenesis*. *Gene Expr Patterns*, 2013. **13**(8): p. 319-27.
392. Yuan, S., et al., *Methylation by NSun2 represses the levels and function of microRNA 125b*. *Mol Cell Biol*, 2014. **34**(19): p. 3630-41.
393. Walker, M.D., et al., *Randomized comparisons of radiotherapy and nitrosoureas for the treatment of malignant glioma after surgery*. *N Engl J Med*, 1980. **303**(23): p. 1323-9.
394. Hanahan, D. and R.A. Weinberg, *Hallmarks of cancer: the next generation*. *Cell*, 2011. **144**(5): p. 646-74.
395. Hanahan, D. and R.A. Weinberg, *The hallmarks of cancer*. *Cell*, 2000. **100**(1): p. 57-70.
396. Colak, S. and J.P. Medema, *Cancer stem cells--important players in tumor therapy resistance*. *FEBS J*, 2014. **281**(21): p. 4779-91.
397. Blanco, S., et al., *The RNA-methyltransferase Misu (NSun2) poises epidermal stem cells to differentiate*. *PLoS Genet*, 2011. **7**(12): p. e1002403.
398. Flores, J.V., et al., *Cytosine-5 RNA Methylation Regulates Neural Stem Cell Differentiation and Motility*. *Stem Cell Reports*, 2017. **8**(1): p. 112-124.
399. Rota, L.M., et al., *Determining mammosphere-forming potential: application of the limiting dilution analysis*. *J Mammary Gland Biol Neoplasia*, 2012. **17**(2): p. 119-23.
400. Ryu, C.H., et al., *Valproic acid downregulates the expression of MGMT and sensitizes temozolomide-resistant glioma cells*. *J Biomed Biotechnol*, 2012. **2012**: p. 987495.
401. Towner, R.A., et al., *OKN-007 Increases temozolomide (TMZ) Sensitivity and Suppresses TMZ-Resistant Glioblastoma (GBM) Tumor Growth*. *Transl Oncol*, 2019. **12**(2): p. 320-335.
402. van Nifterik, K.A., et al., *Absence of the MGMT protein as well as methylation of the MGMT promoter predict the sensitivity for temozolomide*. *Br J Cancer*, 2010. **103**(1): p. 29-35.
403. Balvers, R.K., et al., *ABT-888 enhances cytotoxic effects of temozolomide independent of MGMT status in serum free cultured glioma cells*. *J Transl Med*, 2015. **13**: p. 74.
404. Advani, S.J., et al., *Preferential replication of systemically delivered oncolytic vaccinia virus in focally irradiated glioma xenografts*. *Clin Cancer Res*, 2012. **18**(9): p. 2579-90.
405. Hu, Y., et al., *Cell context-dependent dual effects of EFEMP1 stabilizes subpopulation equilibrium in responding to changes of in vivo growth environment*. *Oncotarget*, 2015. **6**(31): p. 30762-72.
406. Dardis, C., et al., *Leptomeningeal metastases in high-grade adult glioma: development, diagnosis, management, and outcomes in a series of 34 patients*. *Front Neurol*, 2014. **5**: p. 220.
407. Andersen, B.M., et al., *Leptomeningeal metastases in glioma: The Memorial Sloan Kettering Cancer Center experience*. *Neurology*, 2019. **92**(21): p. e2483-e2491.
408. Arita, N., M. Taneda, and T. Hayakawa, *Leptomeningeal dissemination of malignant gliomas. Incidence, diagnosis and outcome*. *Acta Neurochir (Wien)*, 1994. **126**(2-4): p. 84-92.

409. Erlich, S.S. and R.L. Davis, *Spinal subarachnoid metastasis from primary intracranial glioblastoma multiforme*. Cancer, 1978. **42**(6): p. 2854-64.
410. Yung, W.A., B.C. Horten, and W.R. Shapiro, *Meningeal gliomatosis: a review of 12 cases*. Ann Neurol, 1980. **8**(6): p. 605-8.
411. Maini, R., et al., *Incorporation of beta-amino acids into dihydrofolate reductase by ribosomes having modifications in the peptidyltransferase center*. Bioorg Med Chem, 2013. **21**(5): p. 1088-96.
412. McCusker, K.P. and D.G. Fujimori, *The chemistry of peptidyltransferase center-targeted antibiotics: enzymatic resistance and approaches to countering resistance*. ACS Chem Biol, 2012. **7**(1): p. 64-72.
413. Rakauskaitė, R. and J.D. Dinman, *Mutations of highly conserved bases in the peptidyltransferase center induce compensatory rearrangements in yeast ribosomes*. RNA, 2011. **17**(5): p. 855-64.
414. Rakauskaitė, R. and J.D. Dinman, *rRNA mutants in the yeast peptidyltransferase center reveal allosteric information networks and mechanisms of drug resistance*. Nucleic Acids Res, 2008. **36**(5): p. 1497-507.
415. Zeng, F. and H. Jin, *Conformation of methylated GGQ in the Peptidyl Transferase Center during Translation Termination*. Sci Rep, 2018. **8**(1): p. 2349.
416. Marks, J., et al., *Context-specific inhibition of translation by ribosomal antibiotics targeting the peptidyl transferase center*. Proc Natl Acad Sci U S A, 2016. **113**(43): p. 12150-12155.
417. Tan, G.T., A. DeBlasio, and A.S. Mankin, *Mutations in the peptidyl transferase center of 23 S rRNA reveal the site of action of sparsomycin, a universal inhibitor of translation*. J Mol Biol, 1996. **261**(2): p. 222-30.
418. Torres de Farias, S., T. Gaudencio Rego, and M.V. Jose, *Peptidyl Transferase Center and the Emergence of the Translation System*. Life (Basel), 2017. **7**(2).
419. Pitt, J.J., *Principles and applications of liquid chromatography-mass spectrometry in clinical biochemistry*. Clin Biochem Rev, 2009. **30**(1): p. 19-34.
420. Key, M., *A tutorial in displaying mass spectrometry-based proteomic data using heat maps*. BMC Bioinformatics, 2012. **13 Suppl 16**: p. S10.
421. Janin, M., et al., *Epigenetic loss of RNA-methyltransferase NSUN5 in glioma targets ribosomes to drive a stress adaptive translational program*. Acta Neuropathol, 2019. **138**(6): p. 1053-1074.
422. Jiang, Z., et al., *High expression of NSUN5 promotes cell proliferation via cell cycle regulation in colorectal cancer*. Am J Transl Res, 2020. **12**(7): p. 3858-3870.
423. Zhao, H., et al., *CpG methylation at promoter site -140 inactivates TGFbeta2 receptor gene in prostate cancer*. Cancer, 2005. **104**(1): p. 44-52.
424. Suter, C.M., et al., *CpG island methylation is a common finding in colorectal cancer cell lines*. Br J Cancer, 2003. **88**(3): p. 413-9.
425. Rhee, I., et al., *CpG methylation is maintained in human cancer cells lacking DNMT1*. Nature, 2000. **404**(6781): p. 1003-7.
426. Jair, K.W., et al., *De novo CpG island methylation in human cancer cells*. Cancer Res, 2006. **66**(2): p. 682-92.
427. Gebhard, C., et al., *General transcription factor binding at CpG islands in normal cells correlates with resistance to de novo DNA methylation in cancer cells*. Cancer Res, 2010. **70**(4): p. 1398-407.
428. Draht, M.X., et al., *Promoter CpG island methylation of RET predicts poor prognosis in stage II colorectal cancer patients*. Mol Oncol, 2014. **8**(3): p. 679-88.
429. Tran, A., et al., *In Silico Enhanced Restriction Enzyme Based Methylation Analysis of the Human Glioblastoma Genome Using Agilent 244K CpG Island Microarrays*. Front Neurosci, 2009. **3**: p. 57.
430. Liu, J., et al., *The NSUN5-FTH1/FTL pathway mediates ferroptosis in bone marrow-derived mesenchymal stem cells*. Cell Death Discov, 2022. **8**(1): p. 99.

431. Muller, S., et al., *Target recognition, RNA methylation activity and transcriptional regulation of the Dictyostelium discoideum Dnmt2-homologue (DnmA)*. Nucleic Acids Res, 2013. **41**(18): p. 8615-27.
432. Sun, B., et al., *NSUN5 Facilitates Viral RNA Recognition by RIG-I Receptor*. J Immunol, 2020. **205**(12): p. 3408-3418.
433. Genuth, N.R. and M. Barna, *The Discovery of Ribosome Heterogeneity and Its Implications for Gene Regulation and Organismal Life*. Mol Cell, 2018. **71**(3): p. 364-374.
434. Fan, Q.W., et al., *EGFR phosphorylates tumor-derived EGFRvIII driving STAT3/5 and progression in glioblastoma*. Cancer Cell, 2013. **24**(4): p. 438-49.
435. Guryanova, O.A., et al., *Nonreceptor tyrosine kinase BMX maintains self-renewal and tumorigenic potential of glioblastoma stem cells by activating STAT3*. Cancer Cell, 2011. **19**(4): p. 498-511.
436. Kang, S.H., et al., *Activated STAT3 regulates hypoxia-induced angiogenesis and cell migration in human glioblastoma*. Neurosurgery, 2010. **67**(5): p. 1386-95; discussion 1395.
437. Kim, E., et al., *Phosphorylation of EZH2 activates STAT3 signaling via STAT3 methylation and promotes tumorigenicity of glioblastoma stem-like cells*. Cancer Cell, 2013. **23**(6): p. 839-52.
438. Kim, J.E., et al., *STAT3 Activation in Glioblastoma: Biochemical and Therapeutic Implications*. Cancers (Basel), 2014. **6**(1): p. 376-95.
439. Peixoto, P., et al., *HDAC7 inhibition resets STAT3 tumorigenic activity in human glioblastoma independently of EGFR and PTEN: new opportunities for selected targeted therapies*. Oncogene, 2016. **35**(34): p. 4481-94.
440. Rahaman, S.O., et al., *Inhibition of constitutively active Stat3 suppresses proliferation and induces apoptosis in glioblastoma multiforme cells*. Oncogene, 2002. **21**(55): p. 8404-13.
441. Sherry, M.M., et al., *STAT3 is required for proliferation and maintenance of multipotency in glioblastoma stem cells*. Stem Cells, 2009. **27**(10): p. 2383-92.
442. Xu, X., et al., *NSun2 promotes cell migration through methylating autotaxin mRNA*. J Biol Chem, 2020. **295**(52): p. 18134-18147.
443. Pan, S.T., et al., *Molecular mechanisms for tumour resistance to chemotherapy*. Clin Exp Pharmacol Physiol, 2016. **43**(8): p. 723-37.
444. Wu, N., et al., *Cardamonin induces apoptosis by suppressing STAT3 signaling pathway in glioblastoma stem cells*. Tumour Biol, 2015. **36**(12): p. 9667-76.
445. Kohsaka, S., et al., *STAT3 inhibition overcomes temozolomide resistance in glioblastoma by downregulating MGMT expression*. Mol Cancer Ther, 2012. **11**(6): p. 1289-99.
446. Cui, P., et al., *STAT3 inhibition induced temozolomide-resistant glioblastoma apoptosis via triggering mitochondrial STAT3 translocation and respiratory chain dysfunction*. Cell Signal, 2020. **71**: p. 109598.
447. Birzu, C., et al., *Leptomeningeal Spread in Glioblastoma: Diagnostic and Therapeutic Challenges*. Oncologist, 2020. **25**(11): p. e1763-e1776.
448. Liu, B., et al., *Mis-targeted methylation in rRNA can severely impair ribosome synthesis and activity*. RNA Biol, 2008. **5**(4): p. 249-54.
449. Iyer-Bierhoff, A., et al., *SIRT7-Dependent Deacetylation of Fibrillarin Controls Histone H2A Methylation and rRNA Synthesis during the Cell Cycle*. Cell Rep, 2018. **25**(11): p. 2946-2954 e5.
450. Wilson, D.N., et al., *X-ray crystallography study on ribosome recycling: the mechanism of binding and action of RRF on the 50S ribosomal subunit*. EMBO J, 2005. **24**(2): p. 251-60.
451. Larsen, L.H., et al., *Identification and characterization of the Thermus thermophilus 5-methylcytidine (m5C) methyltransferase modifying 23 S ribosomal RNA (rRNA) base C1942*. J Biol Chem, 2012. **287**(33): p. 27593-600.
452. Schifano, J.M., et al., *Mycobacterial toxin MazF-mt6 inhibits translation through cleavage of 23S rRNA at the ribosomal A site*. Proc Natl Acad Sci U S A, 2013. **110**(21): p. 8501-6.

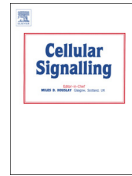
453. Liiv, A., et al., *Analysis of the function of E. coli 23S rRNA helix-loop 69 by mutagenesis*. BMC Mol Biol, 2005. **6**: p. 18.
454. Leviev, I., S. Levieva, and R.A. Garrett, *Role for the highly conserved region of domain IV of 23S-like rRNA in subunit-subunit interactions at the peptidyl transferase centre*. Nucleic Acids Res, 1995. **23**(9): p. 1512-7.
455. Liu, R.Z., E.A. Monckton, and R. Godbout, *Regulation of the FABP7 gene by PAX6 in malignant glioma cells*. Biochem Biophys Res Commun, 2012. **422**(3): p. 482-7.
456. Siebzehnruhl, F.A., et al., *The ZEB1 pathway links glioblastoma initiation, invasion and chemoresistance*. EMBO Mol Med, 2013. **5**(8): p. 1196-212.
457. Kahlert, U.D., et al., *Activation of canonical WNT/beta-catenin signaling enhances in vitro motility of glioblastoma cells by activation of ZEB1 and other activators of epithelial-to-mesenchymal transition*. Cancer Lett, 2012. **325**(1): p. 42-53.
458. Gandin, V., et al., *Polysome fractionation and analysis of mammalian translates on a genome-wide scale*. J Vis Exp, 2014(87).
459. Andreev, D.E., et al., *Insights into the mechanisms of eukaryotic translation gained with ribosome profiling*. Nucleic Acids Res, 2017. **45**(2): p. 513-526.
460. Brar, G.A. and J.S. Weissman, *Ribosome profiling reveals the what, when, where and how of protein synthesis*. Nat Rev Mol Cell Biol, 2015. **16**(11): p. 651-64.
461. Poitevin, F., et al., *Structural Heterogeneities of the Ribosome: New Frontiers and Opportunities for Cryo-EM*. Molecules, 2020. **25**(18).
462. Sauert, M., H. Temmel, and I. Moll, *Heterogeneity of the translational machinery: Variations on a common theme*. Biochimie, 2015. **114**: p. 39-47.
463. Muller, M., et al., *Division of labour: tRNA methylation by the NSun2 tRNA methyltransferases Trm4a and Trm4b in fission yeast*. RNA Biol, 2019. **16**(3): p. 249-256.
464. Khoddami, V. and B.R. Cairns, *Transcriptome-wide target profiling of RNA cytosine methyltransferases using the mechanism-based enrichment procedure Aza-IP*. Nat Protoc, 2014. **9**(2): p. 337-61.

## **Appendix I: Notch and TGF $\beta$ form a positive regulatory loop and regulate EMT in epithelial ovarian cancer cells**

Jiesi Zhou, Saket Jain, Abul K Azad, Xia Xu, Hai Chuan Yu, Zhihua Xu, Roseline Godbout, YangXin Fu. Cellular Signalling, Volume 28, Issue 8, August 2016, Pages 838-849.

**Abstract:** Epithelial-mesenchymal transition (EMT) plays a critical role in the progression of epithelial ovarian cancer (EOC). However, the mechanisms that regulate EMT in EOC are not fully understood. Here, we report that activation of Notch1 induces EMT in EOC cells as evidenced by downregulation of E-cadherin and cytokeratins, upregulation of Slug and Snail, as well as morphological changes. Interestingly, activation of Notch1 increases TGF $\beta$ /Smad signaling by upregulating the expression of TGF $\beta$  and TGF $\beta$  type 1 receptor. Time course experiments demonstrate that inhibition of Notch by DAPT (a  $\gamma$ -secretase inhibitor) decreases TGF $\beta$ -induced phosphorylation of receptor Smads at late, but not at early, timepoints. These results suggest that Notch activation plays a role in sustaining TGF $\beta$ /Smad signaling in EOC cells. Furthermore, inhibition of Notch by DAPT decreases TGF $\beta$  induction of Slug and repression of E-cadherin and knockdown of Notch1 decreases TGF $\beta$ -induced repression of E-cadherin, indicating that Notch is required, at least in part, for TGF $\beta$ -induced EMT in EOC cells. On the other hand, TGF $\beta$  treatment increases the expression of Notch ligand Jagged1 and Notch target gene HES1 in EOC cells. Functionally, the combination of Notch1 activation and TGF $\beta$  treatment is more potent in promoting motility and migration of EOC cells than either stimulation alone. Taken together, our results indicate that Notch and TGF $\beta$  form a reciprocal positive regulatory loop and cooperatively regulate EMT and promote EOC cell motility and migration.

**Keywords:** EMT; Epithelial ovarian cancer; Notch; TGF $\beta$ .



## Notch and TGF $\beta$ form a positive regulatory loop and regulate EMT in epithelial ovarian cancer cells



Jiesi Zhou<sup>a,c</sup>, Saket Jain<sup>a</sup>, Abul K. Azad<sup>a</sup>, Xia Xu<sup>a</sup>, Hai Chuan Yu<sup>a</sup>, Zhihua Xu<sup>a</sup>,  
Roseline Godbout<sup>a</sup>, YangXin Fu<sup>a,b,\*</sup>

<sup>a</sup> Department of Oncology, Faculty of Medicine and Dentistry, University of Alberta, Edmonton, AB, Canada

<sup>b</sup> Department of Obstetrics and Gynecology, Faculty of Medicine and Dentistry, University of Alberta, Edmonton, AB, Canada

<sup>c</sup> The first affiliated hospital, Shantou University Medical College, Shantou, Guangdong Province, China

### ARTICLE INFO

#### Article history:

Received 11 October 2015  
Received in revised form 31 March 2016  
Accepted 31 March 2016  
Available online 10 April 2016

#### Keywords:

Epithelial ovarian cancer  
Notch  
TGF $\beta$   
EMT

### ABSTRACT

Epithelial–mesenchymal transition (EMT) plays a critical role in the progression of epithelial ovarian cancer (EOC). However, the mechanisms that regulate EMT in EOC are not fully understood. Here, we report that activation of Notch1 induces EMT in EOC cells as evidenced by downregulation of E-cadherin and cytokeratins, upregulation of Slug and Snail, as well as morphological changes. Interestingly, activation of Notch1 increases TGF $\beta$ /Smad signaling by upregulating the expression of TGF $\beta$  and TGF $\beta$  type 1 receptor. Time course experiments demonstrate that inhibition of Notch by DAPT (a  $\gamma$ -secretase inhibitor) decreases TGF $\beta$ -induced phosphorylation of receptor Smads at late, but not at early, timepoints. These results suggest that Notch activation plays a role in sustaining TGF $\beta$ /Smad signaling in EOC cells. Furthermore, inhibition of Notch by DAPT decreases TGF $\beta$  induction of Slug and repression of E-cadherin and knockdown of Notch1 decreases TGF $\beta$ -induced repression of E-cadherin, indicating that Notch is required, at least in part, for TGF $\beta$ -induced EMT in EOC cells. On the other hand, TGF $\beta$  treatment increases the expression of Notch ligand Jagged1 and Notch target gene HES1 in EOC cells. Functionally, the combination of Notch1 activation and TGF $\beta$  treatment is more potent in promoting motility and migration of EOC cells than either stimulation alone. Taken together, our results indicate that Notch and TGF $\beta$  form a reciprocal positive regulatory loop and cooperatively regulate EMT and promote EOC cell motility and migration.

© 2016 Elsevier Inc. All rights reserved.

### 1. Introduction

Epithelial–mesenchymal transition (EMT), which is a critical event in tumor progression, can be induced by the tumor microenvironment signals and/or activation of oncogenes that lead to upregulation of EMT transcription factors (EMT-TFs), including the ZEB, Snail and Twist families [1–3]. These EMT transcription factors induce EMT by repressing the expression of cell junction and adhesion molecules, breaking the cell–cell junction and attachment of cells to the extracellular matrix [1–3]. As a result, epithelial cancer cells that have undergone EMT lose expression of adhesion molecule (e.g., E-cadherin), acquire mesenchymal phenotypes, and become more motile and invasive [1–3]. Epithelial ovarian cancer (EOC) is the leading cause of death due to gynecological malignancies. Most EOC patients are diagnosed at the late stages when the disease has spread to other parts of the peritoneal cavity, making the current therapy regimens ineffective. EMT promotes dissemination of EOC cells from the original tumors and survival

of the disseminated cells in ascites, thus playing a critical role in the progression of EOC [4–7]. Because EMT is also associated with acquisition of cancer stem cell properties, resistance to chemotherapy and radiation therapy, and recurrence of cancers [1–3], targeting EMT holds great promise for the treatment of recurrent and resistant EOC. Multiple signaling pathways form a regulatory network to orchestrate EMT [1–3]. A better understanding of the interaction between the signaling pathways in EMT will be critical for developing therapeutic strategies to target EMT and tumor progression.

Our previous studies demonstrate that TGF $\beta$  and Notch3 signaling induce EMT in EOC cells [8,9]. The Notch signaling pathway that regulates multiple cellular processes can be either oncogenic or tumor suppressing depending on the cancer types [10,11]. Notch signaling is initiated through cell–cell contact; the transmembrane Notch ligands bind to the Notch receptors on the neighboring cells, which triggers a series of proteolytic cleavages of the transmembrane Notch receptors [12,13]. The final cleavage is mediated by the  $\gamma$ -secretase complex, which releases the Notch intracellular domain (NICD). The NICD then goes to the nucleus where it interacts with the DNA binding protein CSL (CBF1/Su(H)/Lag-1) and recruits co-activators to regulate gene expression [14,15]. Increasing evidence in the literature demonstrates

\* Corresponding author at: Department of Oncology, University of Alberta, 5142M, Katz Building, 114th St & 87th Ave., Edmonton, AB T6G 2E1, Canada.

E-mail address: [yangxin@ualberta.ca](mailto:yangxin@ualberta.ca) (Y. Fu).

that activation of Notch plays an oncogenic role in EOC; activation of Notch promotes EOC cell proliferation, survival, EMT, resistance to chemotherapy, and tumor formation in mice, as well as angiogenesis in EOC [16–28]. Among the five ligands (Jagged1; Jagged2; and Delta-like

ligands [Dll] 1, 3 and 4) and four receptors (Notch1–4), Jagged1, Notch1 and Notch3 have been shown to be the major Notch components that are elevated in EOC [16–18,26]. Integrated genomic analysis by the Cancer Genome Atlas (TCGA) researchers showed that the

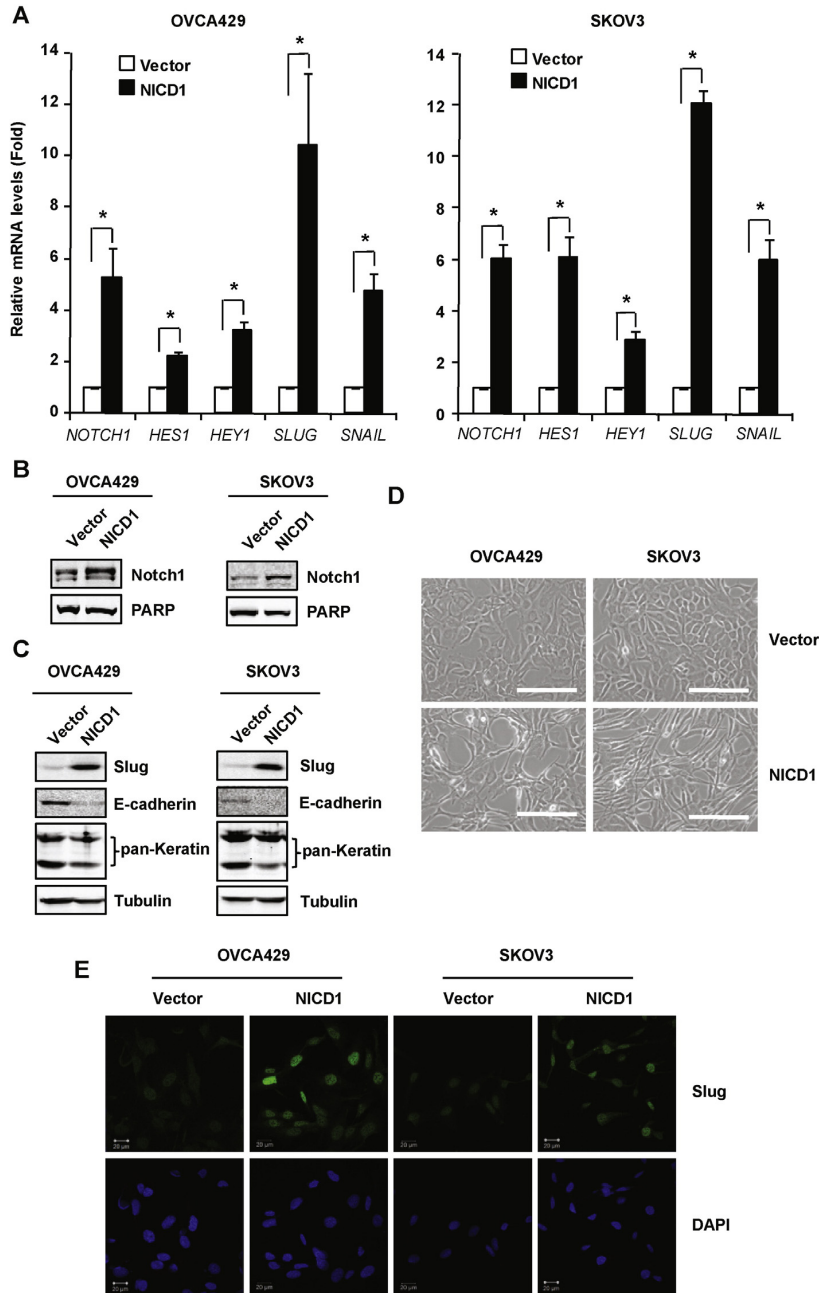


**Fig. 1.** Activation of Notch1 induces EMT in EOC cells. OVCA429 and SKOV3 cells were stably transduced with the intracellular domain of Notch1 (NICD1, the constitutively active form of Notch1) to activate Notch1 in these cells. (A) mRNA levels of Notch1, HES1, HEY1, Slug and Snail were examined by qRT-PCR and expressed as fold change with that in the vector cells designated as 1. Data are shown as mean  $\pm$  SEM of three independent experiments. \*Significantly different ( $P < 0.05$ ). (B) Nuclear Notch1 in the nuclear fractions prepared from the OVCA429 and SKOV3 cells stably transduced with empty vector or NICD1 was examined by subcellular fractionation and Western blotting using anti-Notch1 antibody. Poly(ADP-ribose) polymerase (PARP) was used as the nuclear loading control. (C) Expression of E-cadherin, pan-keratin and Slug in whole cell lysates prepared from the OVCA429 and SKOV3 cells stably transduced with empty vector or NICD1 was examined by Western blotting. Tubulin was used as a loading control. (D) Images of OVCA429 and SKOV3 cells stably transduced with empty vector or NICD1 were captured under phase contrast. Scale bar = 100  $\mu$ m. (E) Slug expression and cellular localization in OVCA429 and SKOV3 cells stably transduced with empty vector or NICD1 were examined by confocal fluorescence microscopy.

Notch signaling pathway is one of the signaling pathways commonly altered in high grade serous EOC (22%) [18]. In particular, Notch3 is amplified/mutated in 11% of high grade serous EOC [18]. Thus far, most functional studies on Notch in EOC have focused on Notch3 [9,16,22,23,26,27]. However, several lines of evidence suggest that other Notch receptors also contribute to tumorigenesis or progression of EOC. First, two recent studies showed that siRNA knockdown of Notch ligand Dll4 or Jagged1 reduces tumor formation of Notch3-negative EOC cell lines (SKOV3ip1 and SKOV3Trip2) in mouse xenograft models [19,20], suggesting that Notch receptors other than Notch3 mediate the tumorigenic effect of Dll4 and Jagged1 in these cells. Second, although most EOC cell lines express Notch1, only a few of them express Notch3 at the mRNA and protein level [19,26,27]. For these reasons, it is important to investigate the function of other Notch receptors in EOC. Notch1 was

selected for this study because it has been shown to be active and promote growth and survival of EOC cells [17,21,28].

TGF $\beta$  is an important cytokine that induces EMT through Smad-dependent and -independent pathways [29–32]. In the Smad-dependent pathway, TGF $\beta$  activates the transmembrane type I and type II serine/threonine kinase TGF $\beta$  receptors (TGFBR1 and TGFBR2) that, in turn, recruit and phosphorylate receptor-activated Smads (R-Smads), including Smad2 and Smad3. The phosphorylated R-Smads then form a complex with a common Smad (Smad4) and translocate to the nucleus. In the nucleus, the Smad complex binds to the promoter of the target genes and interacts with other transcription factors and co-factors to regulate the expression of the target genes [29,33].

In this study, we demonstrate that activation of Notch1 induces EMT in EOC cells. Interestingly, our results suggest that Notch and TGF $\beta$

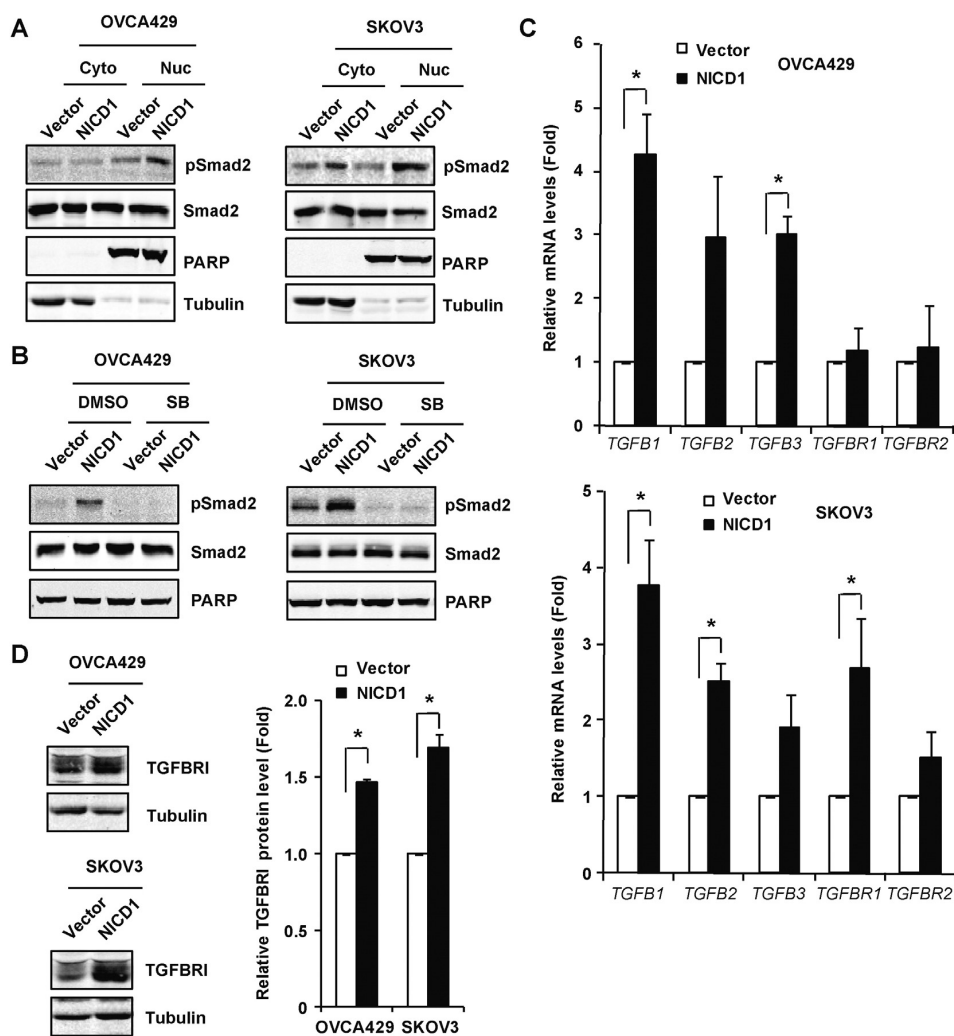


**Fig. 2.** Activation of Notch1 increases TGF $\beta$ /Smad signaling in EOC cells. OVCA429 and SKOV3 cells were stably transduced with NICD1 to activate Notch1 in these cells. (A) Cytosolic and nuclear fractions were prepared from OVCA429 and SKOV3 cells stably transduced with empty vector or NICD1. Phosphorylated and total Smad2 in cytosolic and nuclear fractions were examined by Western blotting. PARP and tubulin were used as loading controls for nuclear and cytosolic fraction, respectively. (B) OVCA429 and SKOV3 cells stably transduced with empty vector or NICD1 were treated with 10  $\mu$ M SB431542 or an equal volume of DMSO (vehicle control) overnight. Phosphorylated and total Smad2 in the nuclear fractions were measured by Western blotting. PARP was used as the nuclear loading control. (C) mRNA levels of TGF $\beta$ 1 and TGF $\beta$  receptors in OVCA429 and SKOV3 cells stably transduced with empty vector or NICD1 were measured by qRT-PCR and expressed as fold change with that in the vector cells designated as 1. Data are shown as mean  $\pm$  SEM of three independent experiments. \*Significantly different ( $P < 0.05$ ). (D) Protein expression of TGFBR1 in whole cell lysates was analyzed in OVCA429 and SKOV3 cells stably transduced with empty vector or NICD1 by Western blotting. Tubulin was used as the loading control. TGFBR1 protein levels were quantified using Odyssey imaging software. The density of the TGFBR1 bands was normalized to that of tubulin and expressed as fold change with that in the vector control designated as 1. Data are shown as mean  $\pm$  SEM of three independent experiments. \*Significantly different ( $P < 0.05$ ).

signaling form a positive regulatory loop and cooperatively regulate EMT and promote EOC cell motility and migration.

**2. Materials and methods**

**2.1. Reagents and antibodies**

Human recombinant TGFβ1 was purchased from R&D Systems Inc. SB431542 (a TGFβRI inhibitor) was purchased from Cell Signaling Technology. DAPT (γ-secretase inhibitor IX) was purchased from Calbiochem. The following antibodies were purchased from Cell Signaling Technology: Smad2 (#5339), phospho-Smad2 (#3018), Smad3 (#9523), phospho-Smad3 (#9520), Slug (#9585), E-cadherin (#3195), Jagged1 (#2620), Notch1 (#3439) and pan-keratin (#4545). The pan-keratin antibody recognizes cytokeratins 4, 5, 6, 8, 10, 13 and 18. Antibodies for tubulin (ab59680) and TGFβRI (sc-398) were purchased from Abcam and Santa Cruz Biotechnology, respectively. Secondary antibodies IRDye 800CW conjugates of donkey anti-rabbit-IgG and anti-mouse IgG were purchased from LI-COR Biosciences.

**2.2. Cell culture and treatment**

Human EOC cell lines OVCA429 and SKOV3 were cultured in RPMI 1640 medium and DMEM/F12, respectively, supplemented with 10% FBS, 100 U/ml penicillin and 100 μg/ml streptomycin. For TGFβ treatment, cells were serum starved in medium containing 0.2% FBS overnight prior to the treatment of 1 ng/ml TGFβ1 for various durations. For DAPT treatment, cells were pre-treated with 10 μM DAPT or an equal volume of DMSO (the vehicle control) overnight prior to TGFβ treatment in the presence of DAPT or DMSO. For SB431542 treatment, cells were treated with 10 μM SB431542 or an equal volume of DMSO (the vehicle control) overnight.

**2.3. Overexpression of the intracellular domain of Notch1 and knockdown of Notch1**

OVCA429 and SKOV3 cells were stably transduced with the intracellular domain of Notch1 (NICD1) using retroviral vector pLNC-NICD1 (provided by Dr. Aly Karsan) and selected in 1 mg/ml G418. Overexpression of NICD1 was confirmed by RT-PCR and Western blotting. Notch1 in OVCA429 and SKOV3 cells was stably knocked down using a lentivirus-delivered shRNA approach as previously described [34]. Two shRNA constructs targeting two different sequences in human Notch1 were used for these experiments: shNotch1-A (5'GGAGCATGTGTAACATCAACA3') and shNotch1-B (5'GCATGGTGCCGAACCAATAC A3'). A shRNA targeted against a random sequence (shRandom: 5' GTTGCTTGCCACGTCCTAGAT3') was used as a negative control [34]. Knockdown of Notch1 in these cells was confirmed by Western blotting.

**2.4. RNA isolation and quantitative reverse transcription-PCR (qRT-PCR)**

RNA isolation, reverse transcription (RT) and quantitative RT-PCR were performed as described previously [35]. Briefly, RNA was extracted from cells using TRIzol reagent (Invitrogen) following the manufacturer's instructions. The cDNAs were synthesized using SuperScript II reverse transcriptase reagent (Invitrogen) in the presence of RNase inhibitor. qRT-PCR was carried out using the Eppendorf Mastercycler ep realplex. PCR primer sequences are listed in Supplementary Table 1.

**2.5. Preparation of whole cell lysates and cytosolic and nuclear fractions, and Western blotting**

Whole cell lysates were prepared using modified radioimmuno-precipitation assay (RIPA) buffer as described previously [36]. Cytosolic and nuclear fractions were prepared as previously described [35]. Protein concentration was quantified using the DC protein assay (Bio-Rad) and an equal amount of proteins was used for Western blotting.

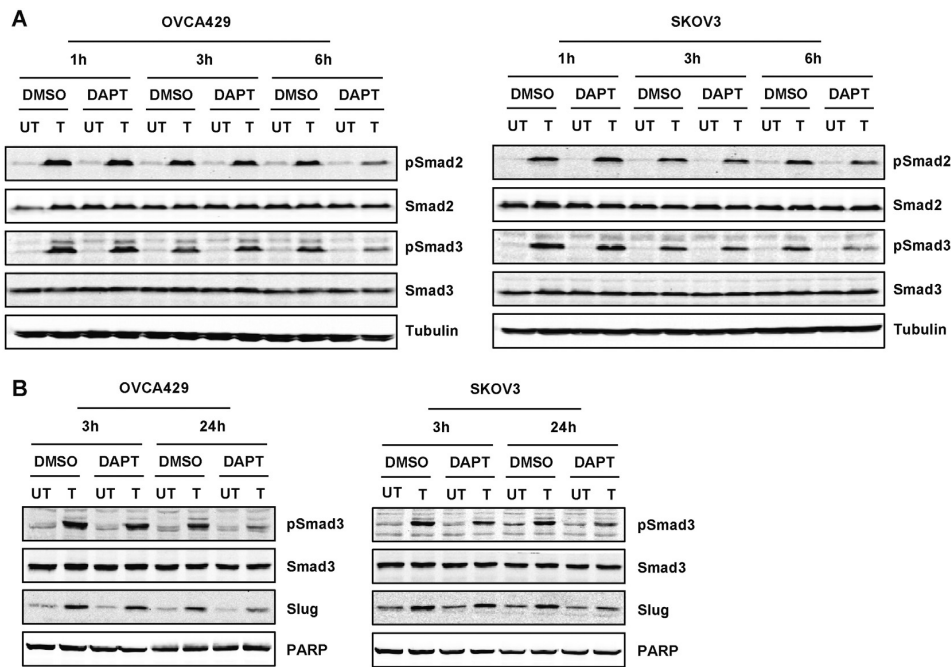


**Fig. 3.** Activation of Notch sustains TGFβ/Smad signaling in EOC cells. OVCA429 and SKOV3 cells were pre-treated with 10 μM DAPT or an equal volume of DMSO (vehicle control) overnight and then left untreated or treated with 1 ng/ml TGFβ1 for the indicated periods of time. (A) Phosphorylated and total Smad2 and Smad3 in the whole cell lysates were measured by Western blotting. Tubulin was used as the loading control. (B) Phosphorylated and total Smad3 and Slug in the nuclear fractions were analyzed by Western blotting. PARP was used as the nuclear loading control.

All antibodies were used at 1:1000 dilution. IRDye 800CW secondary antibodies were used. Membranes were scanned and analyzed using an Odyssey® IR scanner and Odyssey® imaging software 3.0.

## 2.6. Immunocytochemistry

Immunocytochemistry was performed as previously described [37]. Briefly, cells growing on coverslips were fixed in 2% paraformaldehyde

in phosphate-buffered saline for 10 min and permeabilized in 0.25% Triton X-100 for 5 min. The cells were incubated with affinity-purified rabbit anti-Slug antibody (1:200 dilution) followed by Alexa-488 donkey anti-rabbit secondary antibody (1:400 dilution) (Molecular Probes). Coverslips were mounted onto slides with polyvinyl alcohol containing 1 µg/ml 4',6-diamidino-2-phenylindole (DAPI). Images were captured on a Zeiss (Oberkochen, Germany) LSM510 confocal microscope with a 40×/1.3 oil immersion lens.

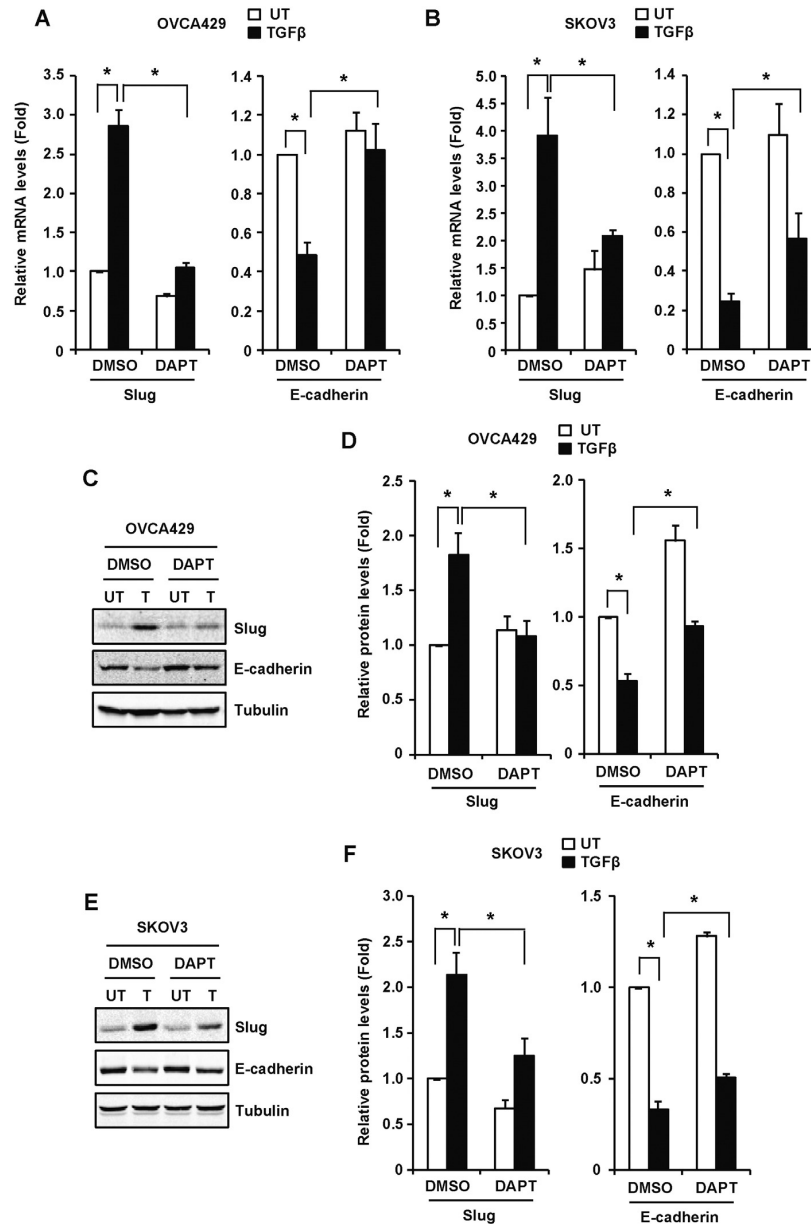


**Fig. 4.** Activation of Notch is partially required for TGF $\beta$ -induced EMT in EOC cells. (A and B) OVCA429 and SKOV3 cells were pre-treated with 10 µM DAPT or an equal volume of DMSO (vehicle control) overnight and then left untreated or treated with 1 ng/ml TGF $\beta$ 1 for 4 h (for Slug expression) or 24 h (for E-cadherin). mRNA levels of Slug and E-cadherin were measured by qRT-PCR and expressed as fold change relative to DMSO/UT (untreated) cells which were designated as 1. Data are shown as mean  $\pm$  SEM of three independent experiments. \*Significantly different ( $P < 0.05$ ). (C to F) OVCA429 and SKOV3 cells were pre-treated with 10 µM DAPT or an equal volume of DMSO (vehicle control) overnight and then left untreated or treated with 1 ng/ml TGF $\beta$ 1 for 24 h. Slug and E-cadherin protein expression of in whole cell lysates was analyzed by Western blotting. Tubulin was used as the loading control. Slug and E-cadherin protein levels were quantified using Odyssey imaging software. The density of the Slug and E-cadherin bands was normalized to that of tubulin and expressed as fold change relative to that of DMSO/UT cells which was designated as 1. Data are shown as mean  $\pm$  SEM of three independent experiments. \*Significantly different ( $P < 0.05$ ).

### 2.7. Scratch assay

OVCA429 and SKOV3 cells stably transduced with empty vector or NICD1 were seeded in 12-well plates in triplicate. When cells formed a monolayer, they were serum starved in DMEM medium supplemented with 0.2% FBS overnight. A scratch was then made in the center of the wells using a P200 pipette tip. The medium was removed and cells were washed with PBS to remove cell debris. Cells were cultured in DMEM medium containing 0.2% FBS with or without 1 ng/ml TGF $\beta$ 1. Cells were imaged using a digital imaging microscope (Axiovert 200 M, Zeiss) with an incubator enclosure as they migrated to fill the scratch. Images were captured at 2 positions in each well using a phase contrast lens (Plan-NEOFLUAR Ph-1) at 10 $\times$  magnification. In total, 6 positions were imaged for each experimental group for statistical analysis. Metamorph imaging software (Version 7.8.8.0, Molecular Devices) was used to capture a total of 97 images at each position at 15 minute intervals over a period of 24 h. Images were then analyzed using the TScratch software to measure the area occupied by the cells at different time points. The open area of each scratch at 0 h was set as 100% to nullify the effects of minor differences of the scratch size in different wells. The open area at subsequent time points was expressed as percentage relative to their respective 0 h.

### 2.8. Migration assay

Directional cell migration was measured using the Transwell migration assay in HTS 24-Multiwell Insert plates (BD Falcon Labware, Bedford, MA) as we previously described with minor modifications [38]. Cells were cultured in DMEM/F12 medium containing 0.2% FBS, with or without 1 ng/ml TGF $\beta$ 1, for 24 h prior to seeding the cells for the migration assay. Cells were added to the top chamber (25,000 cells for OVCA429; 50,000 cells for SKOV3) in DMEM/F12 medium with no serum. Cells were allowed to migrate through an 8  $\mu$ m polyethylene terephthalate (PET) membrane towards a chemoattractant (DMEM/F12 + 10% FBS) in the bottom chamber for 20 h. Cells were then fixed with 100% cold methanol and stained with 1% crystal violet in 20% methanol. Migrated cells were imaged using a Zeiss Axioskop2 plus

microscope. For counting migrated cells, Transwells were imaged using a 4 $\times$  lens on a High Content microscope and four frames were combined to reconstruct the entire well. Cell counting was carried out using Meta express imaging software.

### 2.9. Statistical analysis

Statistical significance between two groups was determined by one-way ANOVA and defined as  $P < 0.05$ . Statistical analysis was performed using GraphPad Prism5.

## 3. Results

### 3.1. Activation of Notch1 induces EMT in EOC cells

Among the four Notch receptors, Notch1 and Notch3 have been shown to be elevated in EOC [16–18,26]. Interestingly, while most EOC cell lines express Notch1, only a few EOC cell lines express Notch3 at the protein level [19,26,27]. We have previously shown that OVCA429 and SKOV3 cells express Notch1, but not Notch3, at the protein level [39] and that overexpression of the intracellular domain of Notch3 (the constitutively active form of Notch3) induces EMT in OVCA429 cells [9]. However, whether Notch1 activation induces EMT in EOC cells has not been determined. To address this question, we stably transduced OVCA429 and SKOV3 cells with the intracellular domain of Notch1 (NICD1) to activate Notch1 in these cells. Overexpression of NICD1 was confirmed by increased mRNA levels of Notch1 and its target genes HES1 and HEY1 as determined by qRT-PCR (Fig. 1A) and by the increased NICD1 in the nucleus as shown by Western blotting (Fig. 1B). Notch activation increased mRNA levels of Slug and Snail (two EMT-TFs) (Fig. 1A). Western blotting showed that Notch1 activation increased Slug expression, but decreased E-cadherin and cytokeratin expression at the protein level (Fig. 1C), which is concordant with changes in the morphology of the cells to a more spindle and fibroblast-like shape (Fig. 1D). We further confirmed the induction of Slug by Notch1 activation and nuclear localization of Slug in both cell lines using immunocytochemistry (Fig. 1E). Our results thus

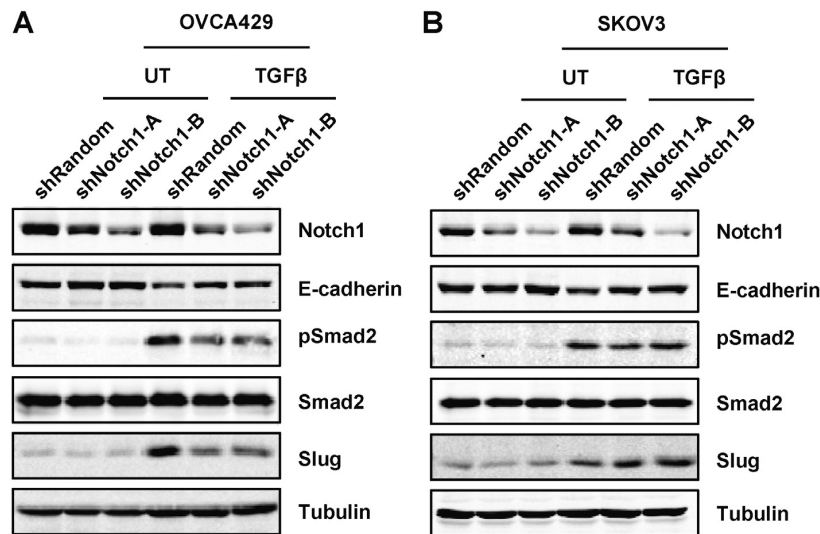


**Fig. 5.** Activation of Notch is partially required for TGF $\beta$  repression of E-cadherin in EOC cells. Notch1 in OVCA429 (A) and SKOV3 (B) cells was stably knocked down using two different shRNAs (shNotch1-A and shNotch1-B). Cells were serum starved overnight and then left untreated or treated with 1 ng/ml TGF $\beta$ 1 for 24 h. Expression of Notch1, E-cadherin, and Slug as well as Smad2 phosphorylation in whole cell lysates was analyzed by Western blotting. Tubulin was used as the loading control.

indicate that, similar to Notch3 [9], Notch1 activation induces EMT in EOC cells.

### 3.2. Activation of Notch1 increases TGF $\beta$ /Smad signaling via upregulation of TGF $\beta$ and TGFBR1 in EOC cells

Our previous study demonstrated that TGF $\beta$  induces EMT in EOC cells [8]. To determine whether Notch and TGF $\beta$  signaling pathways interact in the context of EMT in EOC, we isolated the cytosolic and nuclear fractions from OVCA429 and SKOV3 cells that were stably transduced with empty vector or NICD1 and examined phosphorylation of Smad2 as readout of TGF $\beta$ /Smad signaling activation. Western blotting showed that Notch1 activation increased the levels of phosphorylated Smad2 in the nuclear fraction of OVCA429 and SKOV3 cells (Fig. 2A), indicating that Notch1 activation increases TGF $\beta$ /Smad signaling in these cells. The basal and Notch1-induced Smad2 phosphorylation was completely abolished by TGF $\beta$  type I receptor (TGFBR1) kinase inhibitor SB431542, indicating that Notch1-induced Smad2 phosphorylation is TGFBR1-dependent (Fig. 2B). To determine the mechanism underlying the activation of TGF $\beta$ /Smad signaling by Notch1, we measured the expression of TGF $\beta$  and TGF $\beta$  receptors in OVCA429 and SKOV3 cells with or without Notch1 activation. qRT-PCR results showed that Notch1 activation upregulated the expression of TGF $\beta$  in both OVCA429 and SKOV3 cells (Fig. 2C). Among the three isoforms of TGF $\beta$ , TGF $\beta$ 1 was the most abundant in both cell lines. Specifically, our qRT-PCR results showed that TGF $\beta$ 1 mRNA levels were 81-fold and 137-fold higher than those of TGF $\beta$ 2 and TGF $\beta$ 3, respectively, in OVCA429 cells, and 63-fold and 461-fold higher than those of TGF $\beta$ 2 and TGF $\beta$ 3, respectively, in SKOV3 cells. Notch activation also upregulated the mRNA expression of TGFBR1 in SKOV3 cells, but not in OVCA429 cells (Fig. 2C). Interestingly, however, Western blotting showed that activation of Notch1 increased TGFBR1 protein level by 1.5-fold in OVCA429 and 1.7-fold in SKOV3 cells (Fig. 2D). Taken together, our results indicate that activation of Notch1 increases TGF $\beta$ /Smad signaling by upregulating the expression of TGF $\beta$  and TGFBR1 in EOC cells.

### 3.3. Notch activation sustains TGF $\beta$ /Smad signaling in EOC cells

To further investigate the effect of Notch activation on TGF $\beta$ /Smad signaling in EOC cells, we pre-treated OVCA429 and SKOV3 cells with DAPT (a  $\gamma$ -secretase inhibitor to inactivate Notch) or an equal volume of DMSO (the vehicle control) overnight and then treated the cells with TGF $\beta$  in the presence of DMSO or DAPT for 1 to 6 h. TGF $\beta$ -induced Smad2 and Smad3 phosphorylation was measured to determine the activation of TGF $\beta$ /Smad signaling. Western blotting showed that inhibition of Notch by DAPT did not affect TGF $\beta$ -induced phosphorylation of Smad2 and Smad3 at 1 h and 3 h in both cell lines (Fig. 3A). However, TGF $\beta$ -induced phosphorylation of Smad2 and Smad3 was markedly decreased by DAPT at 6 h in both cell lines (Fig. 3A). These results suggest that Notch activation is not required for the initiation of TGF $\beta$ /Smad signaling, but may play a role in sustaining the TGF $\beta$ /Smad signaling in EOC cells. Upon phosphorylation, Smad2 and Smad3 form a complex with Smad4 and translocate to the nucleus where they interact with other transcription factors to regulate the expression of their target genes, including Slug [8]. To confirm the effect of Notch activation in sustaining the TGF $\beta$ /Smad signaling, we treated OVCA429 and SKOV3 cells with TGF $\beta$  for 3 or 24 h with or without Notch inhibition by DAPT and analyzed phosphorylated Smad3 and Slug in the nuclear fractions by Western blotting. As shown in Fig. 3B, TGF $\beta$ -induced expression of phosphorylated Smad3 and Slug in the nucleus was decreased by DAPT and the inhibition was more pronounced at 24 h compared to 3 h. Taken together, these results suggest that Notch activation has a minimal effect on the initial activation of the TGF $\beta$ /Smad signaling but sustains the TGF $\beta$ /Smad signaling in EOC cells.

### 3.4. Activation of Notch is partially required for TGF $\beta$ -induced EMT in EOC cells

Our previous study demonstrated that TGF $\beta$  induces EMT in EOC cells [8]. To determine whether Notch activation is required for TGF $\beta$ -induced EMT in EOC cells, we pre-treated OVCA429 and SKOV3 cells with DAPT or an equal volume of DMSO overnight and then treated the cells with TGF $\beta$  for 24 h in the presence of DMSO or DAPT. We measured the expression of Slug and E-cadherin as EMT markers at mRNA and protein levels. qRT-PCR results showed that TGF $\beta$  induced mRNA expression of Slug, but decreased that of E-cadherin in both cell lines (Fig. 4A and B). DAPT inhibited Slug induction and E-cadherin repression by TGF $\beta$  (Fig. 4A and B). Specifically, DAPT decreased TGF $\beta$ -induced mRNA expression of Slug by 63.2% in OVCA429 and 46.8% in SKOV3 cells, but increased E-cadherin mRNA levels in TGF $\beta$ -treated cells by 110.1% in OVCA429 and 132.6% in SKOV3 cells (Fig. 4A and B). The inhibitory effect of DAPT on TGF $\beta$  induction of Slug and repression

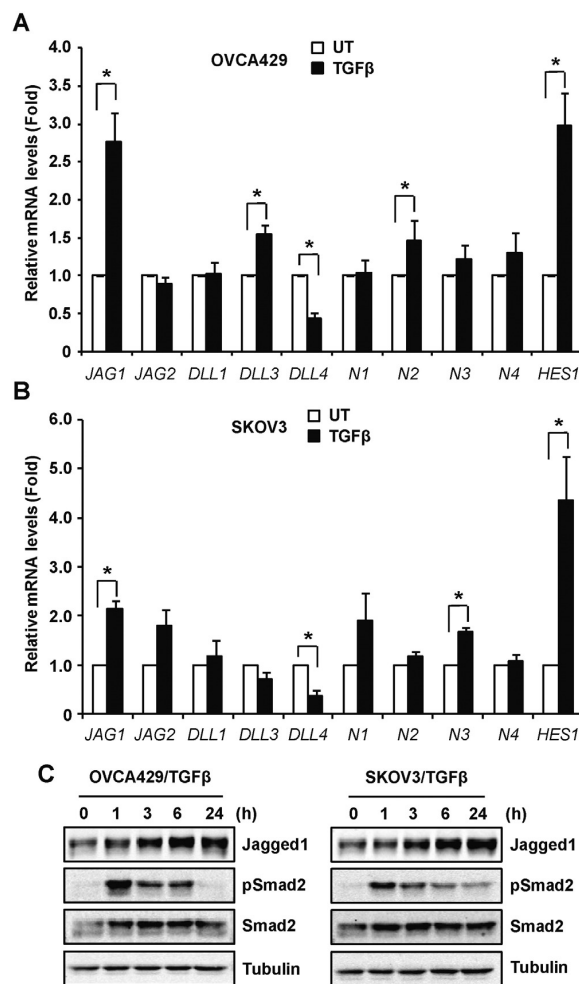


**Fig. 6.** TGF $\beta$  increases Notch ligand Jagged1 and target gene HES1 expression in EOC cells. (A and B) OVCA429 and SKOV3 cells were left untreated or treated with 1 ng/ml TGF $\beta$ 1 for 4 h. mRNA expression of Notch ligands, receptors and target gene was examined by qRT-PCR and expressed as fold change relative to UT (untreated) cells which were designated as 1. Data are shown as mean  $\pm$  SEM of three independent experiments. \*Significantly different ( $P < 0.05$ ). JAG1: Jagged1; JAG2: Jagged1; N1: Notch1; N2: Notch2; N3: Notch3; N4: Notch4. (C) OVCA429 and SKOV3 cells were left untreated or treated with 1 ng/ml TGF $\beta$ 1 for various periods of time. Expression of Jagged1 in whole cell lysates was examined by Western blotting. Tubulin was used as the loading control.

of E-cadherin was confirmed at the protein level (Fig. 4C to F). Quantification of the Western blotting results showed that DAPT decreased TGFβ-induced Slug protein levels by 40.4% in OVCA429 and 53.1% in SKOV3 cells, but increased the E-cadherin protein levels in TGFβ-treated cells by 40.4% in OVCA429 and by 41.5% in SKOV3 cells (Fig. 4D and F). To determine whether Notch1 is required for TGFβ-induced EMT in EOC cells, we stably knocked down Notch1 using two shRNA constructs (shNotch1-A and shNotch1-B) in OVCA249 and SKOV3 cells (Fig. 5A and B). As expected, TGFβ-induced repression of E-cadherin was partially restored in both OVCA429 and SKOV3 cells (Fig. 5A and B). However, inconsistent results were observed between the two cell lines for TGFβ-induced Smad2 phosphorylation and Slug expression. Knockdown of Notch1 decreased TGFβ-induced Smad2 phosphorylation and Slug expression in OVCA429 cells, but not in SKOV3 cells. Taken together, these results indicate that activation of Notch is required, at least in part, for TGFβ-induced EMT in EOC cells. However, the molecular mechanisms underlying the effect of Notch1 on TGFβ-induced EMT appear to be different between OVCA429 and SKOV3 cells.

3.5. TGFβ induces Jagged1 and HES1 expression in EOC cells

Having determined the role of Notch activation in TGFβ signaling, we wanted to investigate whether TGFβ affects Notch signaling in EOC cells. We treated OVCA429 and SKOV3 cells with TGFβ for various durations and examined the expression of Notch signaling components (ligands, receptors and target gene *HES1*) in these cells. Our qRT-PCR results showed that TGFβ treatment for 3 h increased Jagged1 mRNA levels, but decreased Dll4 mRNA levels, in OVCA429 (Fig. 6A) and SKOV3 cells (Fig. 6B). The mRNA levels of Dll3 and Notch2 in OVCA429 cells (Fig. 6A) and Notch3 in SKOV3 cells (Fig. 6B) were also increased, but less pronounced compared to the induction of Jagged1. TGFβ increased the expression of HES1 (a classic Notch target gene) in both OVCA429 and SKOV3 cells (Fig. 6A and B). To confirm the induction of Jagged1, we performed a time course experiment of TGFβ treatment and analyzed Jagged1 protein levels by Western blotting. In keeping with mRNA results, an increase in Jagged1 protein level as a function of TGFβ treatment was observed at 3 h, which lasted up to 24 h (Fig. 6C). Phosphorylation of Smad2 was included to confirm the activation of TGFβ/Smad signaling

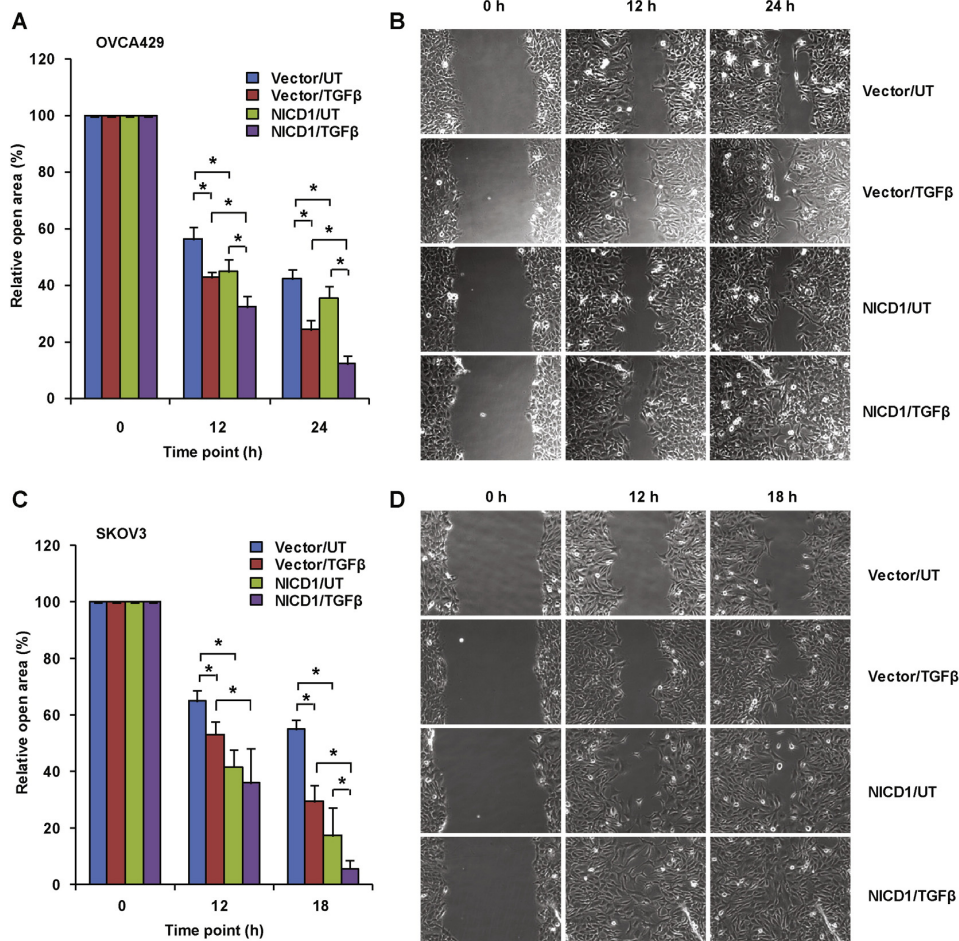


**Fig. 7.** Notch1 activation and TGFβ cooperatively promote motility of EOC cells. OVCA429 and SKOV3 cells stably transduced with empty vector or NICD1 were seeded in 12-well plates in triplicate. After a scratch was made, cells were left untreated or treated with 1 ng/ml TGFβ<sub>31</sub> in DMEM medium supplemented with 0.2% FBS. Cell motility at six positions (two positions per well) was monitored for each cell type using a digital imaging microscope and quantified using the Metamorph imaging software. (A and C) Cell motility was quantified and expressed as relative open areas at the indicated hours with the 0 h designated as 100%. Data are shown as mean ± SD for the six scratch positions. \*Significantly different ( $P < 0.05$ ). A smaller open area indicates that the cells are more motile. (B) Representative cell motility images of OVCA429 cells are shown for 0, 12 and 24 h. (D) Representative cell motility images of SKOV3 cells are shown for 0, 12 and 18 h.

by TGF $\beta$  treatment (Fig. 6C). Taken together, our results indicate that TGF $\beta$  increases the expression of Notch ligand Jagged1 and target gene HES1, suggesting that TGF $\beta$  enhances Notch signaling in EOC cells.

### 3.6. Combined activation of Notch1 and TGF $\beta$ is more potent in promoting EOC cell motility and migration

Cells that have undergone EMT become more motile and migratory. Our finding that both Notch1 and TGF $\beta$  induce EMT in EOC cells suggests that simultaneous activation of Notch1 and TGF $\beta$  can be more potent in promoting the motility or migration of EOC cells than either of them alone. To test this, we first performed a scratch assay using OVCA429 and SKOV3 cells stably transduced with empty vector or NICD1 that were left untreated or treated with TGF $\beta$ . Indeed, the scratch assay showed that activation of Notch1 or TGF $\beta$  treatment alone increased the motility of OVCA429 cells (Fig. 7A and B) and SKOV3 cells (Fig. 7C and D) and a combination of both was more potent in promoting the motility of OVCA29 and SKOV3 cells than Notch activation or TGF $\beta$

treatment alone (Fig. 7A to D). We then measured the effect of activation of Notch1 and TGF $\beta$  on migration of cells towards chemokines. In keeping with the motility results, a combination of Notch activation and TGF $\beta$  treatment was more potent in inducing migration of OVCA429 and SKOV3 cells than either Notch or TGF $\beta$  alone (Fig. 8). Specifically, TGF $\beta$  treatment and Notch activation increased migration of OVCA429 cells by 1.45 and 1.46 fold, respectively, whereas the combination of both increased the migration of OVCA429 cells by 1.82 fold (Fig. 8A and B). Similarly, while TGF $\beta$  treatment and Notch activation increased migration of SKOV3 cells by 2.08 and 2.03 fold, respectively, the combination of both increased the migration of SKOV3 cells by 4.05 fold (Fig. 8C and D). Taken together, these results indicate that Notch and TGF $\beta$  signaling cooperate to promote motility and migration of EOC cells.

## 4. Discussion

EMT has been shown to play a critical role in the progression of EOC [4–7]. A better understanding of the molecular mechanisms that

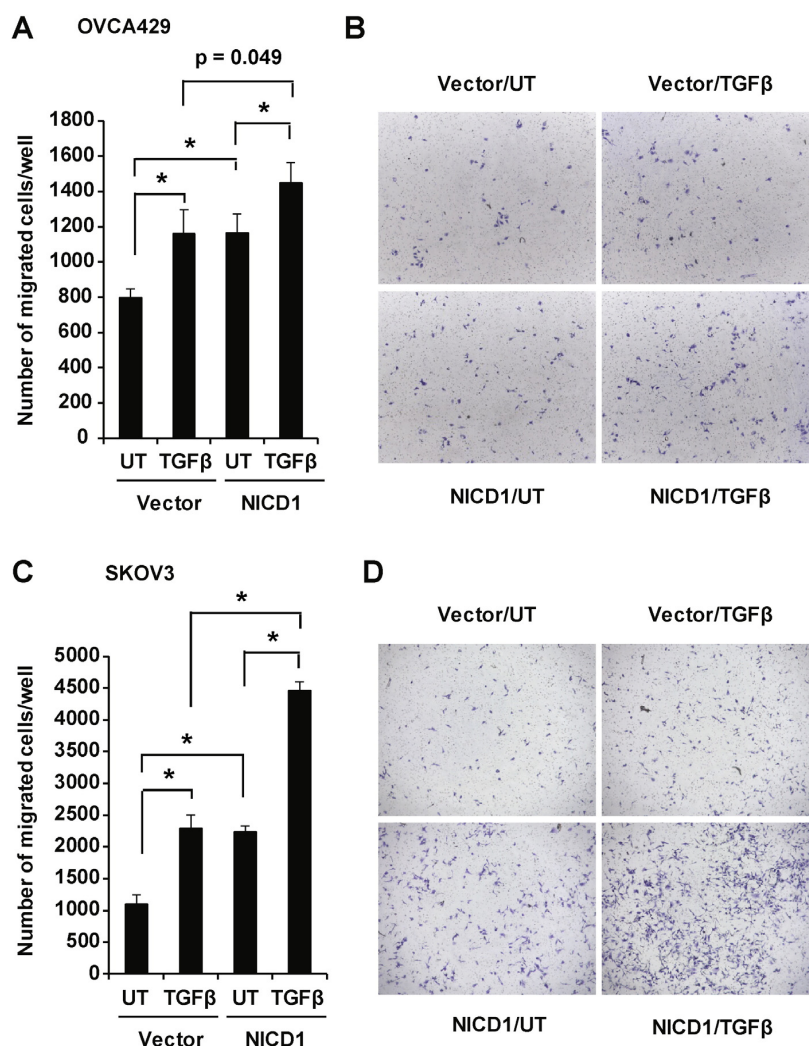


**Fig. 8.** Notch1 activation and TGF $\beta$  promote migration of EOC cells. OVCA429 and SKOV3 cells stably transduced with an empty vector or NICD1 were treated with 1 ng/ml TGF $\beta$ 1 for 24 h prior to seeding the cells to the top chamber in medium with no serum. Cells were allowed to migrate through an 8  $\mu$ m polyethylene terephthalate (PET) membrane towards a chemoattractant (10% FBS) in the bottom chamber for 20 h. Cells were then fixed and stained. Migrated cells were imaged and counted. (A and C) Numbers of migrated cells per well are shown. Data are shown as mean  $\pm$  SD for three replicates. \*Significantly different ( $P < 0.05$ ). (B and D) Representative images of the migrated cells for OVCA429 (B) and SOV3 cells (D) are shown.

regulate EMT in EOC cells will help develop novel therapeutic strategies. A growing body of evidence suggests that activation of Notch plays a tumorigenic role in EOC [16–28], highlighting the importance of further investigating the biological functions of Notch in EOC. We previously demonstrated that activation of Notch3 induces EMT in EOC cells and renders EOC cells more resistant to carboplatin [9]. Two recent studies showed that knockdown of Dll4 or Jagged1 decreased the tumorigenicity of Notch3-negative EOC cells [19,20], indicating that other Notch receptors besides Notch3 also play a role in tumorigenesis of EOC. Indeed, Notch1 has also been shown to play a role in proliferation and survival of EOC cells [17,21,28], indicating that Notch1 is another important Notch receptor in EOC and its role in EOC needs to be further investigated. In this study, we showed that activation of Notch1 induces EMT in EOC cells as evidenced by induction of Slug, repression of E-cadherin and cytokeratin, and cell morphology change. Our findings thus indicate that EMT in EOC cells can be induced by activation of Notch1 or Notch3.

Notch and TGF $\beta$  can be synergistic or antagonistic dependent on cell types. Although Notch activation inhibits TGF $\beta$  anti-growth action in mouse EpH4 and HC-11 mammary epithelial cells and in Mv1Lu mink lung epithelial cells [40–42], it is necessary for TGF $\beta$ -induced growth arrest in human HaCaT keratinocytes and mouse NMuMG mammary epithelial cells [43]. Interestingly Notch and TGF $\beta$  have been shown to cooperatively regulate EMT in various cell types (e.g., HaCaT, NMuMG, human A549 alveolar type II epithelial cells and human HK-2 proximal tubule epithelial cells) [44–46]. Despite the well-documented cooperation between TGF $\beta$  and other signaling pathways in EMT [47], whether Notch and TGF $\beta$  interact in the context of EMT in EOC has not been studied. TGF $\beta$  is highly expressed in EOC tissues and is present at high levels in the plasma and ascites of advanced EOC patients [48–50]. We and others have shown that TGF $\beta$  induces EMT in EOC cells [8,51,52]. Notch signaling is activated and plays a tumorigenic role in EOC [16–28]. Therefore, a better understanding of the interaction of TGF $\beta$  and Notch in EMT in EOC will help identify potential therapeutic targets to treat this deadly disease.

Our results show that activation of Notch1 increases the phosphorylation of Smad2, suggesting that Notch activation enhances TGF $\beta$ /Smad signaling in EOC cells. Further analysis suggests that Notch1-induced Smad2 phosphorylation is TGFBR1-dependent, because inhibition of TGFBR1 kinase activity by its inhibitor SB431542 completely abolished basal and Notch1-induced Smad2 phosphorylation. Mechanistically, Notch1 activation increases the mRNA levels of TGF $\beta$ 1 (the most abundant form of TGF $\beta$ ) in OVCA429 and SKOV3 cells by approximately 4-fold. Additionally, Notch1 activation increases the levels of TGFBR1 mRNA by 2.7-fold in SKOV3 cells and increases the levels of TGFBR1 protein by 1.5- and 1.7-fold in OVCA429 and SKOV3 cells, respectively. TGFBR1 protein levels are regulated through multiple mechanisms, including regulation of expression and turnover of the receptor [53,54]. The effect of Notch on TGFBR1 mRNA versus protein levels in OVCA429 cells suggests that Notch may regulate TGFBR1 protein stability or turnover without affecting the transcription in this cell line. Together, these results indicate that activation of Notch1 enhances the endogenous TGF $\beta$ /Smad signaling by up-regulating the expression of TGF $\beta$  and TGFBR1 in EOC cells.

We also found that Notch activation affects exogenous TGF $\beta$ -induced Smad signaling in EOC cells. Based on time course experiments, inhibition of Notch by DAPT has no effect on TGF $\beta$ -induced phosphorylation of Smad2 and Smad3 at early timepoints, but markedly inhibits Smad2/3 phosphorylation at late timepoints. Furthermore, inhibition of Notch by DAPT decreases TGF $\beta$ -induced Slug expression and E-cadherin repression. These results suggest that Notch activation is not required for the initiation, but is partially required for sustained activity of TGF $\beta$ /Smad signaling and TGF $\beta$ -induced EMT. Notch1 knockdown partially reversed the TGF $\beta$ -dependent repression of E-cadherin observed in OVCA429 and SKOV3 cells, suggesting that activation of Notch1 is partially required for TGF $\beta$ -induced EMT. However, knockdown of Notch1 decreased TGF $\beta$ -induced Slug expression and Smad2

phosphorylation in OVCA429 cells, but not in SKOV3 cells, suggesting these effects are cell-dependent, which is consistent with the heterogeneity of EOC cells. These data also suggest that repression of E-cadherin expression by TGF $\beta$  in SKOV3 cells is likely to be independent of Smad2 phosphorylation and Slug induction. In this regard, it has been well-documented that TGF $\beta$  can induce EMT in both a Smad-dependent and -independent manner [29–32]. Taken together, our results indicate that Notch1 activation contributes to TGF $\beta$ -induced EMT; however, the molecular mechanism underlying this Notch function remains to be determined. In this study, we found that Notch1 activation upregulates the expression of TGF $\beta$  and TGFBR1, suggesting that upregulation of these genes is a potential mechanism for Notch to sustain TGF $\beta$ /Smad signaling in EOC cells.

Having determined that activation of Notch promotes TGF $\beta$ /Smad signaling, we investigated whether TGF $\beta$  affects Notch signaling in EOC cells. Indeed, TGF $\beta$  increases the expression of Notch ligand Jagged1 in EOC cells, which is consistent with previous reports in other cell types [43–46]. Our results demonstrate that Notch and TGF $\beta$  form a reciprocal positive regulatory loop in EOC cells. Our findings have clinical implications. Jagged1 is overexpressed in EOC cells and the Jagged1/Notch signaling pathway contributes to the growth, invasion and tumorigenicity of EOC cells [16,20]. A recent study demonstrated that TGF $\beta$ 1 signaling is activated in omental metastasis of EOC compared to the primary sites and inhibition of TGF $\beta$ 1 signaling decreases the progression of EOC in a mouse xenograft model of EOC [55]. Our data suggest that TGF $\beta$  may be one of the factors that are involved in Jagged1 upregulation and Notch activation in EOC. Furthermore, our results show that combined activation of Notch and TGF $\beta$  signaling is more potent in promoting motility and migration of OVCA429 and SKOV3 cells than either Notch or TGF $\beta$  alone. Our findings thus provide evidence for functional interaction between Notch and TGF $\beta$  in EOC. Taken together, we identify a reciprocal positive regulatory loop between Notch and TGF $\beta$  in EOC, suggesting that simultaneous inhibition of both Notch and TGF $\beta$  signaling may represent a more effective approach to target the progression of EOC.

Our expression data show that Notch ligand Dll4 is downregulated by TGF $\beta$  in OVCA429 and SKOV3 cells. A recent study showed that Dll4 is expressed in both cancer cells and endothelial cells in human EOC tissues and its expression is inversely associated with survival of EOC patients [19]. Functionally, targeting Dll4 in cancer cells and stromal cells decreased tumor formation and angiogenesis of EOC [19], suggesting that Dll4 contributes to progression of EOC. Induction of Jagged1 and downregulation of Dll4 by TGF $\beta$  may result in opposing effect on Notch activation. Our results indicate that TGF $\beta$  treatment increases the expression of the Notch target gene HES1, suggesting that the net effect of TGF $\beta$  on Notch signaling is to enhance Notch activation. This is likely because Jagged1 mRNA levels are much more abundant than Dll4 mRNA levels in both cell lines as determined by qRT-PCR (*data not shown*). However, the significance of downregulation of Dll4 in EOC cells by TGF $\beta$  warrants further investigation.

In summary, this is the first study to demonstrate that activation of Notch1 induces EMT in EOC cells and that Notch and TGF $\beta$  form a reciprocal positive regulatory loop in EOC cells. Notch activation contributes to sustained TGF $\beta$  signaling and TGF $\beta$ -induced EMT in EOC cells. Functionally, activation of both Notch and TGF $\beta$  signaling increases motility and migration of EOC cells to a greater extent than either Notch or TGF $\beta$  alone. Our findings provide insight into the molecular mechanisms underlying the regulation of EMT and the progression of EOC, which may help the development of novel therapeutic approaches for recurrent and resistant EOC.

Supplementary data to this article can be found online at <http://dx.doi.org/10.1016/j.cellsig.2016.03.016>.

#### Conflicts of interest statement

The authors have no conflict of interest to declare.

## Role of the funding source

The study sponsors played no role in any aspect of this study.

## Acknowledgements

This study was generously supported by a start-up fund from the Women and Children's Health Research Institute (WCHRI) with funding donated by the Royal Alexandra Hospital Foundation (RAHF) to Dr. Fu as well as a CIHR grant (funding reference 130314) to Dr. Godbout. Jiesi Zhou was supported by a graduate studentship from the Li Ka Shing Foundation. Xia Xu was supported by a graduate studentship from the Chinese Scholarship Council. Hai Chuan Yu was supported by summer studentships from the Canadian Cancer Society Research Institute and WCHRI. We thank the Cell Imaging and Flow Cytometry Facility of the Oncology Department at the University of Alberta at the Cross Cancer Institute for cell imaging and sorting.

## References

- De Craene, G. B., Bex, Regulatory networks defining EMT during cancer initiation and progression, *Nat. Rev. Cancer* 13 (2013) 97–110.
- K. Polyak, R.A. Weinberg, Transitions between epithelial and mesenchymal states: acquisition of malignant and stem cell traits, *Nat. Rev. Cancer* 9 (2009) 265–273.
- H. Zheng, Y. Kang, Multilayer control of the EMT master regulators, *Oncogene* 33 (2014) 1755–1763.
- D. Vergara, B. Merlot, J.P. Lucot, P. Collinet, D. Vinatier, I. Fournier, M. Salzet, Epithelial–mesenchymal transition in ovarian cancer, *Cancer Lett.* 291 (2010) 59–66.
- N. Ahmed, K. Abubaker, J. Findlay, M. Quinn, Epithelial mesenchymal transition and cancer stem cell-like phenotypes facilitate chemoresistance in recurrent ovarian cancer, *Curr. Cancer Drug Targets* 10 (2010) 268–278.
- N. Ahmed, E.W. Thompson, M.A. Quinn, Epithelial–mesenchymal interconversions in normal ovarian surface epithelium and ovarian carcinomas: an exception to the norm, *J. Cell. Physiol.* 213 (2007) 581–588.
- B. Davidson, C.G. Trope, R. Reich, Epithelial–mesenchymal transition in ovarian carcinoma, *Front. Oncol.* 2 (2012) 33.
- Z. Xu, Y. Jiang, H. Steed, S. Davidge, Y. Fu, TGFbeta and EGF synergistically induce a more invasive phenotype of epithelial ovarian cancer cells, *Biochem. Biophys. Res. Commun.* 401 (2010) 376–381.
- N. Gupta, Z. Xu, A. El-Sehemy, H. Steed, Y. Fu, Notch3 induces epithelial–mesenchymal transition and attenuates carboplatin-induced apoptosis in ovarian cancer cells, *Gynecol. Oncol.* 130 (2013) 200–206.
- M. Roy, W.S. Pear, J.C. Aster, The multifaceted role of Notch in cancer, *Curr. Opin. Genet. Dev.* 17 (2007) 52–59.
- K.G. Leong, A. Karsan, Recent insights into the role of Notch signaling in tumorigenesis, *Blood* 107 (2006) 2223–2233.
- S. Artavanis-Tsakonas, M.D. Rand, R.J. Lake, Notch signaling: cell fate control and signal integration in development, *Science* 284 (1999) 770–776.
- T. Iso, Y. Hamamori, L. Kedes, Notch signaling in vascular development, *Arterioscler. Thromb. Vasc. Biol.* 23 (2003) 543–553.
- Y. Nam, P. Sliz, L. Song, J.C. Aster, S.C. Blacklow, Structural basis for cooperativity in recruitment of MAML coactivators to Notch transcription complexes, *Cell* 124 (2006) 973–983.
- L. Wu, T. Sun, K. Kobayashi, P. Gao, J.D. Griffin, Identification of a family of mastermind-like transcriptional coactivators for mammalian notch receptors, *Mol. Cell. Biol.* 22 (2002) 7688–7700.
- J.H. Choi, J.T. Park, B. Davidson, P.J. Morin, M. Shih Ie, T.L. Wang, Jagged-1 and Notch3 juxtacrine loop regulates ovarian tumor growth and adhesion, *Cancer Res.* 68 (2008) 5716–5723.
- S.L. Rose, M. Kunnimalaiyaan, J. Drenzek, N. Seiler, Notch 1 signaling is active in ovarian cancer, *Gynecol. Oncol.* 117 (2010) 130–133.
- Integrated genomic analyses of ovarian carcinoma, *Nature* 474 (2011) 609–615.
- W. Hu, C. Lu, H.H. Dong, J. Huang, D.Y. Shen, R.L. Stone, A.M. Nick, M.M. Shahzad, E. Mora, N.B. Jennings, S.J. Lee, J.W. Roh, K. Matsuo, M. Nishimura, B.W. Goodman, R.B. Jaffe, R.R. Langley, M.T. Deavers, G. Lopez-Berestein, R.L. Coleman, A.K. Sood, Biological roles of the Delta family Notch ligand Dll4 in tumor and endothelial cells in ovarian cancer, *Cancer Res.* 71 (2011) 6030–6039.
- A.D. Steg, A.A. Katre, B. Goodman, H.D. Han, A.M. Nick, R.L. Stone, R.L. Coleman, R.D. Alvarez, G. Lopez-Berestein, A.K. Sood, C.N. Landen, Targeting the notch ligand JAGGED1 in both tumor cells and stroma in ovarian cancer, *Clin. Cancer Res.* 17 (2011) 5674–5685.
- M. Wang, L. Wu, L. Wang, X. Xin, Down-regulation of Notch1 by gamma-secretase inhibition contributes to cell growth inhibition and apoptosis in ovarian cancer cells A2780, *Biochem. Biophys. Res. Commun.* 393 (2010) 144–149.
- J.T. Park, X. Chen, C.G. Trope, B. Davidson, M. Shih Ie, T.L. Wang, Notch3 overexpression is related to the recurrence of ovarian cancer and confers resistance to carboplatin, *Am. J. Pathol.* 177 (2010) 1087–1094.
- S.G. Jung, Y.D. Kwon, J.A. Song, M.J. Back, S.Y. Lee, C. Lee, Y.Y. Hwang, H.J. An, Prognostic significance of Notch 3 gene expression in ovarian serous carcinoma, *Cancer Sci.* 101 (2010) 1977–1983.
- N. Gupta, Z. Xu, A. El-Sehemy, H. Steed, Y. Fu, Notch3 induces epithelial–mesenchymal transition and attenuates carboplatin-induced apoptosis in ovarian cancer cells, *Gynecol. Oncol.* (2013).
- S.M. McAuliffe, S.L. Morgan, G.A. Wyant, L.T. Tran, K.W. Muto, Y.S. Chen, K.T. Chin, J.C. Partridge, B.B. Poole, K.H. Cheng, J. Daggett Jr., K. Cullen, E. Kantoff, K. Hasselbatt, J. Berkowitz, M.G. Muto, R.S. Berkowitz, J.C. Aster, U.A. Matulonis, D.M. Dinulescu, Targeting Notch, a key pathway for ovarian cancer stem cells, sensitizes tumors to platinum therapy, *Proc. Natl. Acad. Sci. U. S. A.* 109 (2012) E2939–E2948.
- J.T. Park, M. Li, K. Nakayama, T.L. Mao, B. Davidson, Z. Zhang, R.J. Kurman, C.G. Eberhart, M. Shih Ie, T.L. Wang, Notch3 gene amplification in ovarian cancer, *Cancer Res.* 66 (2006) 6312–6318.
- W. Hu, T. Liu, C. Ivan, Y. Sun, J. Huang, L.S. Mangala, T. Miyake, H.J. Dalton, S. Pradeep, R. Rupaimoole, R.A. Previs, H.D. Han, J. Bottsford-Miller, B. Zand, Y. Kang, C.V. Pecot, A.M. Nick, S.Y. Wu, J.S. Lee, V. Sehgal, P. Ram, J. Liu, S.L. Tucker, G. Lopez-Berestein, K.A. Baggerly, R.L. Coleman, A.K. Sood, Notch3 pathway alterations in ovarian cancer, *Cancer Res.* 74 (2014) 3282–3293.
- O. Hopfer, D. Zwhalen, M.F. Fey, S. Aebi, The Notch pathway in ovarian carcinomas and adenomas, *Br. J. Cancer* 93 (2005) 709–718.
- J. Massague, TGFbeta in cancer, *Cell* 134 (2008) 215–230.
- H. Ikushima, K. Miyazono, TGFbeta signalling: a complex web in cancer progression, *Nat. Rev. Cancer* 10 (2010) 415–424.
- Y.E. Zhang, Non-Smad pathways in TGF-beta signaling, *Cell Res.* 19 (2009) 128–139.
- S. Lamouille, J. Xu, R. Derynck, Molecular mechanisms of epithelial–mesenchymal transition, *Nat. Rev. Mol. Cell Biol.* 15 (2014) 178–196.
- L. Attisano, J.L. Wrana, Signal transduction by the TGF-beta superfamily, *Science* 296 (2002) 1646–1647.
- S.H. Barghout, N. Zepeda, K. Vincent, A.K. Azad, Z. Xu, C. Yang, H. Steed, L.M. Postovit, Y. Fu, RUNX3 contributes to carboplatin resistance in epithelial ovarian cancer cells, *Gynecol. Oncol.* 138 (2015) 647–655.
- Y. Fu, A. Chang, L. Chang, K. Niessen, S. Eapen, A. Setiadi, A. Karsan, Differential regulation of transforming growth factor beta signaling pathways by Notch in human endothelial cells, *J. Biol. Chem.* 284 (2009) 19452–19462.
- Y. Fu, H. Sies, X.G. Lei, Opposite roles of selenium-dependent glutathione peroxidase-1 in superoxide generator diquat- and peroxynitrite-induced apoptosis and signaling, *J. Biol. Chem.* 276 (2001) 43004–43009.
- M. Brun, D.D. Glubrecht, S. Baksh, R. Godbout, Calcineurin regulates nuclear factor 1 dephosphorylation and activity in malignant glioma cell lines, *J. Biol. Chem.* 288 (2013) 24104–24115.
- R. Mita, M.J. Beaulieu, C. Field, R. Godbout, Brain fatty acid-binding protein and omega-3/omega-6 fatty acids: mechanistic insight into malignant glioma cell migration, *J. Biol. Chem.* 285 (2010) 37005–37015.
- A. El-Sehemy, A.C. Chang, A.K. Azad, N. Gupta, Z. Xu, H. Steed, A. Karsan, Y. Fu, Notch activation augments nitric oxide/soluble guanylyl cyclase signaling in immortalized ovarian surface epithelial cells and ovarian cancer cells, *Cell. Signal.* 25 (2013) 2780–2787.
- Y. Sun, W. Lowther, K. Kato, C. Bianco, N. Kenney, L. Strizzi, D. Raafat, M. Hirota, N.I. Khan, S. Bargo, B. Jones, D. Salomon, R. Callahan, Notch4 intracellular domain binding to Smad3 and inhibition of the TGF-beta signaling, *Oncogene* 24 (2005) 5365–5374.
- P. Rao, T. Kadesch, The intracellular form of notch blocks transforming growth factor beta-mediated growth arrest in Mv1Lu epithelial cells, *Mol. Cell. Biol.* 23 (2003) 6694–6701.
- S. Masuda, K. Kumano, K. Shimizu, Y. Imai, M. Kurokawa, S. Ogawa, M. Miyagishi, K. Taira, H. Hirai, S. Chiba, Notch1 oncoprotein antagonizes TGF-beta/Smad-mediated cell growth suppression via sequestration of coactivator p300, *Cancer Sci.* 96 (2005) 274–282.
- H. Niimi, K. Pardali, M. Vanlandewijck, C.H. Heldin, A. Moustakas, Notch signaling is necessary for epithelial growth arrest by TGF-beta, *J. Cell Biol.* 176 (2007) 695–707.
- J. Zavadil, L. Cermak, N. Soto-Nieves, E.P. Bottinger, Integration of TGF-beta/Smad and Jagged1/Notch signalling in epithelial-to-mesenchymal transition, *EMBO J.* 23 (2004) 1155–1165.
- Y. Matsuno, A.L. Coelho, G. Jarai, J. Westwick, C.M. Hogaboam, Notch signaling mediates TGF-beta1-induced epithelial–mesenchymal transition through the induction of Snai1, *Int. J. Biochem. Cell Biol.* 44 (2012) 776–789.
- K.C. Nyhan, N. Faherty, G. Murray, L.B. Cooley, C. Godson, J.K. Crean, D.P. Brazil, Jagged/Notch signalling is required for a subset of TGFbeta1 responses in human kidney epithelial cells, *Biochim. Biophys. Acta* 1803 (2010) 1386–1395.
- R. Derynck, B.P. Muthusamy, K.Y. Saeteurn, Signaling pathway cooperation in TGF-beta-induced epithelial–mesenchymal transition, *Curr. Opin. Cell Biol.* 31 (2014) 56–66.
- R. Henriksen, A. Gobl, E. Wilander, K. Oberg, K. Miyazono, K. Funa, Expression and prognostic significance of TGF-beta isoforms, latent TGF-beta 1 binding protein, TGF-beta type I and type II receptors, and endoglin in normal ovary and ovarian neoplasms, *Lab. Invest.* 73 (1995) 213–220.
- T. Higashi, T. Sasagawa, M. Inoue, R. Oka, L. Shuangyong, K. Saijoh, Overexpression of latent transforming growth factor-beta 1 (TGF-beta 1) binding protein 1 (LTBP-1) in association with TGF-beta 1 in ovarian carcinoma, *Jpn. J. Cancer Res.* 92 (2001) 506–515.
- A.D. Santin, S. Bellone, A. Ravaggi, J. Roman, C.V. Smith, S. Pecorelli, M.J. Cannon, G.P. Parham, Increased levels of interleukin-10 and transforming growth factor-beta in the plasma and ascitic fluid of patients with advanced ovarian cancer, *BJOG* 108 (2001) 804–808.
- T.V. Do, L.A. Kubba, H. Du, C.D. Sturgis, T.K. Woodruff, Transforming growth factor-beta1, transforming growth factor-beta2, and transforming growth factor-beta3 enhance ovarian cancer metastatic potential by inducing a Smad3-dependent epithelial-to-mesenchymal transition, *Mol. Cancer Res.* 6 (2008) 695–705.

- [52] L. Cao, M. Shao, J. Schilder, T. Guise, K.S. Mohammad, D. Matei, Tissue transglutaminase links TGF-beta, epithelial to mesenchymal transition and a stem cell phenotype in ovarian cancer, *Oncogene* 31 (2012) 2521–2534.
- [53] A. Moustakas, C.H. Heldin, The regulation of TGFbeta signal transduction, *Development* 136 (2009) 3699–3714.
- [54] G.M. Di Guglielmo, C. Le Roy, A.F. Goodfellow, J.L. Wrana, Distinct endocytic pathways regulate TGF-beta receptor signalling and turnover, *Nat. Cell Biol.* 5 (2003) 410–421.
- [55] S. Yamamura, N. Matsumura, M. Mandai, Z. Huang, T. Oura, T. Baba, J. Hamanishi, K. Yamaguchi, H.S. Kang, T. Okamoto, K. Abiko, S. Mori, S.K. Murphy, I. Konishi, The activated transforming growth factor-beta signaling pathway in peritoneal metastases is a potential therapeutic target in ovarian cancer, *Int. J. Cancer* 130 (2012) 20–28.